Modifying axonal transport as a therapeutic strategy for Amyotrophic Lateral Sclerosis

Katherine Louise Gibbs

Institute of Neurology, University College London
and
Cancer Research UK London Research Institute

Academic Supervisors:
Giampietro Schiavo and Linda Greensmith

Industry Supervisor:
Ceri Davies (GlaxoSmithKline)

A thesis submitted for the degree of
Doctor of Philosophy
University College London
July 2015

Declaration

I, Katherine Louise Gibbs, confirm that the work presented in this thesis is my own. Where information has been derived from other sources, I confirm that this has been indicated in the thesis.

Abstract

Deficits in retrograde axonal transport have been described at a presymptomatic stage in the $SOD1^{G93A}$ mouse model of ALS. The early appearance of transport defects suggests that they may play an important role in disease pathogenesis. However, the causative role of axonal transport deficits in ALS motor neuron degeneration has not yet been demonstrated directly. The goal of my PhD project was to identify pharmacological enhancers of retrograde axonal transport that could be used to prove conclusively whether axonal transport defects play a significant role in ALS pathogenesis.

To this aim, I developed and performed a microscopy-based screen for the identification of pharmacological enhancers of retrograde axonal transport in motor neurons. I was able to demonstrate that the accumulation of α-$p75^{NTR}$ and H_CT in the cell body of mouse ES-derived motor neurons acts as a sensitive read-out of retrograde axonal transport efficiency and using this assay, I identified and validated two compounds (A1 and E4) that were able to accelerate retrograde axonal transport in motor neurons.

Compound A1 was revealed to be an inhibitor of p38 MAPK. Inhibition of p38 MAPK was found to correct deficits in retrograde axonal transport in $SOD1^{G93A}$ motor neurons both *in vitro* and *in vivo*. Using genetic and pharmacological approaches, I was able to demonstrate that p38 MAPKα is responsible for the transport deficits observed. Compound E4 was revealed to be an inhibitor of the IGF1 receptor (IGF1R). It was found to accelerate retrograde axonal transport in both wild type and $SOD1^{G93A}$ motor neurons, but had no effect on anterograde transport speeds.

In conclusion, this thesis work has identified inhibitors of p38 MAPK and IGF1R as novel modifiers of retrograde axonal transport and demonstrated that inhibitors of p38 MAPKα can be used to determine the role of axonal transport defects in ALS pathogenesis.

Acknowledgements

Firstly, I would like to thank my academic supervisors, Gipi and Linda, for giving me the opportunity to work in their labs and for their support and encouragement over the last four years. I would also like to thank Ceri Davies, my industry supervisor, and all the people at GSK who have supported the project throughout and played a key role in its success.

A big thank you to the past and present members of the Schiavo and Greensmith labs, who have made the last four years so enjoyable. Everyone has been so willing to share their skills, knowledge and time, and for that I will always be grateful. Special thanks to Jim for his help with the SOD1 mice and settling in after the lab move; to Bernadett for her invaluable help setting up the *in vivo* imaging protocol; to James whose optimism and encouragement helped me gain confidence in my work; and of course to Nathalie who has shared this PhD journey with me from the start and without whom it would have been nowhere near as fun. I also have to thank Justin, Martina, Eyal, Solène, Martin, Kinga, Todd and Tessa for their friendship and the many hours spent in the pub commiserating over failed experiments.

This work would not have been possible without the funding provided by the BBSRC and GSK. I would also like to thank the Cancer Research UK London Research Institute, where the Schiavo lab was based for the first two and a half years of my PhD, for including me in their PhD programme and allowing me to use their facilities throughout.

Lastly, I would like to thank my family, for their love and support and for inspiring me to always do my best.

Table of Contents

List of figures

List of tables

Movie Legends

Movie 1. *In vitro* axonal transport of $p75^{NTR}$ in primary motor neurons

Wild type primary motor neurons in MatTek dishes were incubated with AlexaFluor-647 labelled α-$p75^{NTR}$ for 25 min at 37°C, 5% CO_2. After 25 min, motor neurons were washed once and then imaged in 2 ml fresh imaging medium. MatTek dishes were then placed in an environmental chamber heated to 37°C and imaged using an invert Zeiss LSM 780 confocal microscope with the 63X oil immersion objective. Images were acquired every 3 s. The video is played at 8 frames/s. The cell body is located out of view to the left. Scale bar, 10 µm.

Movie 2. *In vitro* axonal transport of WGA in primary hippocampal neurons

Primary hippocampal neurons were plated in two compartment microfluidic chambers and quantum dot-labelled WGA was added to the axonal compartment. Hippocampal neurons were incubated at 37°C, 5% CO_2 for 2 hours, then washed with pre-warmed differentiation medium and imaged on an invert fluorescence microscope. Images were acquired every 0.5 s. The video is played at 8 frames/s. Cell bodies are located to the left.

Movie 3. *In vivo* axonal transport of H_CT in the sciatic nerve (63X)

Mice were anaesthetised using isoflurane (National Veterinary Services) and AlexaFluor-555 labelled H_CT (13 µg) and BDNF (50 ng) were injected intramuscularly into the exposed tibialis anterior and gastrocnemius muscles of the right hind leg. The mice were allowed to recover and four hours later were re-anaesthetised and the sciatic nerve of the right leg exposed. The anaesthetised mouse was placed on a heated stage in an environmental chamber (both kept at 37°C) and axonal transport was imaged in the intact sciatic nerve by time-lapse confocal microscopy. Images of axons were acquired every 5 s with an invert Zeiss LSM 780 using a 63X oil immersion objective. The video is played at 8 frames/s. Retrograde carriers are moving from the top right to the bottom left. Scale bar, 20 µm.

Movie 4. *In vivo* axonal transport of H_CT in the sciatic nerve (100X)

Axons were imaged with the 63X objective and a representative area was selected for imaging at 100X. Images of the selected axons were acquired every 3.2 s and the video is played at 8 frames/s. Retrograde carriers are moving to the left. Scale bar, 10 μm.

Abbreviations

AAV	Adeno-associated virus
AD	Alzheimer's disease
ADNP	Activity-dependent neuroprotective peptide
ALCAR	Acetyl-l-carnitine
ALS	Amyotrophic Lateral Sclerosis
APP	Amyloid precursor protein
AR	Androgen receptor
ASK1	Apoptosis signal-regulating kinase 1
ATP	Adenosine triphosphate
BBB	Blood brain barrier
BDNF	Brain derived neurotrophic factor
Cdk5	Cyclin-dependent kinase 5
CMT	Charcot Marie Tooth
CNTF	Ciliary neurotrophic factor
CSF	Cerebrospinal spinal fluid
CTB	Cholera toxin subunit B
DCN	Deep cerebellar nuclei
DIC	Differential interference contrast
DIV	Days *in vitro*
DMSO	Dimethyl sulfoxide
DNA	Deoxyribonucleic acid
DRG	Dorsal root ganglion
EAAT	Excitatory amino-acid transporter
EHNA	Erythro-9-(2-hydroxy-3-nonyl)adenine
ECM	Extracellular matrix
ERKs	Extracellular signal-regulated kinases
ES	Embryonic stem cell
fALS	Familial Amyotrophic Lateral Sclerosis
FDA	Food and Drug Administration
FTD	Frontotemporal dementia
FTDP-17	FTD with parkinsonism-17

FUS	Fused in sarcoma/translocated in liposarcoma
GARP	Golgi-associated retrograde protein
GDNF	Glial derived neurotrophic factor
GEF	Guanine nucleotide exchange factors
GFP	Green fluorescent protein
GSK3	Glycogen synthase kinase 3
HC	Dynein heavy chain
H_CT	Binding fragment of tetanus toxin
HDAC6	Histone deacetylase 6
HEK	Human Embryonic Kidney 293 cells
HRP	Horseradish peroxidase
htt	Huntingtin
i.m.	Intramuscular
i.p.	Intraperitoneal
IC	Dynein intermediate chain
IC_{50}	Half maximal inhibitory concentration
IF	Immunofluorescence
IGF1	Insulin-like growth factor 1
IGF1R	Insulin-like growth factor receptor 1
IGF2	Insulin-like growth factor 2
IGF2R	Insulin-like growth factor receptor 2
IL-1β	Interleukin-1 beta
iPSC	Induced pluripotent stem cell
IRS	Insulin receptor substrates
JNK	c-Jun N-terminal kinases
K_D	Dissociation constant
KIF	Kinesin heavy chain
KLC	Kinesin light chain
Loa	Legs at odd angles
LRRK2	Leucine-rich repeat kinase 2
MAPK	Mitogen-activated protein kinase
MAPKK	Mitogen-activated protein kinase kinase
NAP	Davunetide

NF-H	Neurofilament heavy chain
NF-L	Neurofilament light chain
NF-M	Neurofilament medium chain
NGF	Nerve growth factor
NT-3	Neurotrophin-3
NT-4	Neurotrophin-4
$p75^{NTR}$	p75 neurotrophin receptor
PPP	Picropodophyllotoxin
QD	Quantum dot
RET	Rearranged during transfection
RNA	Ribonucleic acid
ROS	Reactive oxygen species
sALS	Sporadic Amyotrophic Lateral Sclerosis
SBMA	Spinal and bulbar muscular atrophy
SGK	Serum- and glucocorticoid-induced kinase
Shc	Src homology 2
shRNA	Short hairpin RNA
SOD1	Superoxide dismutase 1
STEP	Striatal enriched tyrosine phosphatase
TA	Tibialis anterior
TDP-43	TAR DNA-binding protein 43
TNFR	TNF alpha receptor
TNFα	Tumour necrosis factor alpha
VAMP	Vesicle-associated membrane protein
VCP	Valosin-containing protein
VEGF	Vascular endothelial growth factor receptor
WB	Western blot
WGA	Wheat germ agglutinin
WT	Wild type
YFP	Yellow fluorescent protein

Chapter 1. Introduction

1.1. Amyotrophic Lateral Sclerosis

Amyotrophic lateral sclerosis (ALS) is a fatal neurodegenerative disease caused by the degeneration of upper and lower motor neurons. This degeneration of motor neurons leads to progressive muscle paralysis and ultimately death, usually due to respiratory failure. The incidence of ALS is approximately 2 per 100,000 people per year and the mean age of onset is between 55 and 60 years. However, cases of juvenile ALS have been reported, where disease onset occurs before the age of 25. Patients with ALS typically survive for 2 to 5 years after symptom onset.

1.1.1. Cognitive impairment in ALS

It is now clear that at least 50% of ALS patients have evidence of cognitive decline, with approximately 15% of patients developing features of frontotemporal dementia (FTD) (Ringholz et al., 2005). FTD is characterised by the degeneration of neurons in the frontal and temporal lobes and is the second most common cause of progressive cognitive impairment after Alzheimer's disease. It is thought by some that ALS and FTD may form the two ends of a spectrum of a single neurodegenerative disorder (Swinnen and Robberecht, 2014). This is supported by the overlapping genetics and pathology of the two diseases. Understanding the different forms of ALS and recognising them in patients is a major challenge in the field and will certainly impact the development and success of new therapeutic strategies.

1.2. Genetics of ALS

Although the majority of cases of ALS are reported to be sporadic (sALS), approximately 5-10% of cases are familial (fALS). The majority of these cases are of autosomal dominant inheritance. Clinically, sporadic and familial ALS are indistinguishable, therefore studying fALS-associated genes allows us to investigate the pathological mechanisms underlying both fALS and sALS.

A number of genes have now been unequivocally linked to fALS, the details of which are summarised in Table 1. Mutations in some of these genes have also been found in a small number of apparently sporadic cases of ALS.

Table 1. Genes identified to carry ALS-causing mutations

Gene	Incidence (%)		Putative protein function	Reference
	fALS	sALS		
Chromosome 9 open reading frame 72 (C9orf72)	40	7	DENN Rab GEF	(DeJesus-Hernandez et al., 2011, Renton et al., 2011)
Superoxide dismutase 1 (SOD1)	12	1-2	Superoxide metabolism	(Rosen et al., 1993)
Tar DNA binding protein (TARDBP)	4	1	RNA processing	(Gitcho et al., 2008, Kabashi et al., 2008, Sreedharan et al., 2008)
Fused in sarcoma (FUS)	4	1	RNA processing	(Kwiatkowski et al., 2009, Vance et al., 2009)
Valosin-containing protein (VCP)	1	1	Proteasome, vesicle trafficking, autophagy	(Johnson et al., 2010)
Sequestosome 1 (SQSTM1)	1	<1	Ubiquitination, autophagy	(Fecto et al., 2011)
Optineurin (OPTN)	<1	<1	Membrane trafficking	(Maruyama et al., 2010)
Profilin 1 (PFN1)	<1	<1	Cytoskeleton dynamics	(Wu et al., 2012)
Ubiquilin 2 (UBQLN2)	<1	<1	Autophagy, proteasome	(Deng et al., 2011)

(Modified from Renton et al., 2014)

The mutations that have had the most significant impact on our understanding of ALS are described below.

1.2.1. Superoxide dismutase 1

Superoxide dismutase 1 (SOD1) was the first gene identified as being mutated in ALS (Rosen et al., 1993). Population-based studies estimate that mutations in SOD1 account for approximately 12% of fALS cases and 1-2% of sporadic cases (Chio et al., 2008). SODs are a class of highly conserved enzymes that catalyse the conversion of superoxide into oxygen and H_2O_2. To date, over 180 mutations in the SOD1 gene have been identified in ALS (http://alsod.iop.kcl.ac.uk/als) and the different mutations display considerable phenotypic heterogeneity, particularly in the age of onset and progression of the disease (Andersen et al., 2003). The toxicity of mutant SOD1 in ALS is widely thought to result from a toxic gain of function rather than a loss of function, as a number of fALS-associated SOD1 mutants retain their intrinsic enzymatic activity (Gurney et al., 1994) and no correlation has been found between intrinsic SOD1 activity and clinical severity (Ratovitski et al., 1999). However, measurements in patient samples have revealed that overall SOD1 activity is in fact reduced in the majority of SOD1 fALS cases compared to healthy controls (Saccon et al., 2013). In addition, although mice lacking SOD1 (SOD1-/-) do not develop motor neuron degeneration (Reaume et al., 1996), they do display progressive denervation of hindlimb muscles (Fischer et al., 2011). Furthermore, mice carrying the fALS-associated D83G mutation in the mouse SOD1 gene, which results in a loss of dismutase activity, not only develop the distal axonopathy found in SOD1-/- mice but also develop upper and lower motor neuron degeneration (Joyce et al., 2015). These results raise the possibility that loss of SOD1 activity may contribute to neuromuscular denervation in ALS and that central motor neuron loss and peripheral axonal dysfunction may be mediated by different mechanisms.

Transgenic mouse models expressing ALS-associated mutations in SOD1 have played a key role in furthering our understanding of the disease and will be discussed in detail in Section 1.3.

1.2.2. TDP-43 and FUS

Following the discovery of mutations in SOD1 in 1993, it was another 15 years before the next ALS causative mutation was identified. Fuelled by the observation that TDP-43 is a major component of the ubiquitinated inclusions that are characteristic of ALS (Neumann et al., 2006), mutations in TARDBP (which encodes TDP-43) were soon identified in patients with fALS (Gitcho et al., 2008; Kabashi et al., 2008; Sreedharan et al., 2008). TDP-43 is a ubiquitously expressed RNA-DNA binding protein that has been implicated in transcriptional regulation, alternative splicing and microRNA processing (Xu, 2012). Mutations in TARDBP are thought to account for approximately 4% of fALS cases and a small percentage of sALS cases (Chio et al., 2012). The discovery that TDP-43 is also a component of the ubiquitinated inclusions found in FTD patients (Neumann et al., 2006) provided one of the first indications that ALS and FTD may be part of a continuous spectrum of a single neurodegenerative disorder.

Soon after the discovery of ALS-causing TARDBP mutations, mutations in another RNA binding protein, fused in sarcoma (FUS), were also identified in fALS patients (Kwiatkowski et al., 2009; Vance et al., 2009). FUS has been proposed to play a role in transcriptional regulation, RNA and microRNA processing and mRNA axonal transport (Lagier-Tourenne et al., 2010). Its discovery reinforced the idea that defects in RNA processing may play a role in ALS pathogenesis (discussed in detail in Section 1.5.5).

1.2.3. Hexanucleotide repeat expansion in C9orf72

The most common mutation associated with fALS has been identified as a hexanucleotide repeat expansion (GGGGCC) in a non-coding region of the gene C9orf72 (DeJesus-Hernandez et al., 2011; Renton et al., 2011). This genetic defect has also been implicated in sporadic forms of the disease (Renton et al., 2011) and FTD (DeJesus-Hernandez et al., 2011). Homology searches have shown that C9orf72 encodes a protein that is structurally related to the DENN family of guanine nucleotide exchange factors, which regulate the activity of Rab proteins (Levine et al., 2013). Rab proteins are part of the Ras superfamily of small GTPases and

regulate many aspects of membrane trafficking, including vesicle formation and movement, and membrane fusion. C9orf72 has been found to colocalise with Rab proteins in human spinal cord motor neurons and siRNA-mediated knockdown of C9orf72 in motor neuron cell lines has been shown to disrupt endosomal trafficking (Farg et al., 2014). However, it is currently unclear how the hexanucleotide repeat expansion affects the normal cellular function of C9orf72 and if this contributes to the pathogenic effect of the mutation. It has recently been demonstrated that knocking out C9orf72 in neuronal and glial cells does not cause motor neuron degeneration or motor deficits in mice (Koppers et al., 2015). Other hypotheses have also been proposed to explain the toxicity of the hexanucleotide repeat expansion. It has been proposed that the RNA product of the repeat expansion forms nuclear foci that sequester key RNA-binding proteins, leading to defects in RNA metabolism (Cooper-Knock et al., 2014, Renton et al., 2014). Interestingly, the frequency of RNA splicing errors has recently been shown to correlate with disease severity in C9orf72 ALS patients (Cooper-Knock et al., 2015). Other groups have suggested that the dipeptide repeat proteins, translated from the GGGGCC repeat expansion, form toxic aggregates and contribute to motor neuron degeneration (Mizielinska et al., 2014).

In addition to the genes known to be causative for ALS (summarised in Table 1), mutations in several other genes have also been reported in ALS patients (Table 2, next page). For the majority of these genes, more evidence is still required to support their involvement in ALS pathogenesis.

Furthermore, a number of susceptibility genes have been identified for sALS, for example ITPR2 (van Es et al., 2007) and DPP6 (van Es et al., 2008). It has been proposed that mutations in multiple small effect genes, plus gene–environment interactions, may underlie many cases of apparently sporadic ALS (Simpson and Al-Chalabi, 2006).

Table 2. Additional genes associated with ALS

Gene	Protein function	Reference
Dynactin 1/ p150^{glued} (DCTN1)	Axonal transport	(Puls et al., 2003)
Neurofilament heavy chain (NF-H)	Axonal transport	(Al-Chalabi et al., 1999)
Alsin (ALS2)	Vesicle trafficking	(Hadano et al., 2001)
Charged multivesicular body protein 2B (CHMP2B)	Vesicle trafficking	(Parkinson et al., 2006)
FIG4 phosphoinositide 5-phosphatase (FIG4)	Vesicle trafficking	(Chow et al., 2009)
Vesicle-associated membrane protein B (VAPB)	Vesicle trafficking	(Nishimura et al., 2004)
TANK-binding kinase 1 (TBK1)	Membrane trafficking; inflammatory signalling	(Freischmidt et al., 2015)
Tubulin Alpha 4A (TUBA4A)	Cytoskeleton dynamics	(Smith et al., 2014)
Ataxin-2 (ATXN2)	Endocytosis; RNA translation	(Elden et al., 2010)
Heterogeneous nuclear ribonucleoprotein A1 (HNRNPA1)	RNA metabolism	(Kim et al., 2013)
Heterogeneous nuclear ribonucleoprotein A2B1 (HNRNPA2B1)	RNA metabolism	(Kim et al., 2013)
Senataxin (SETX)	RNA metabolism	(Chen et al., 2004)
Elongator protein 3 (ELP3)	RNA metabolism	(Simpson et al., 2009)
Matrin-3 (MATR3)	RNA metabolism	(Johnson et al., 2014b)
CHCHD10	Mitochondrial function	(Johnson et al., 2014a)
Angiogenin (ANG)	Angiogenesis	(Greenway et al., 2006)
Spastic paraplegia 11 (SPG11)	DNA damage repair	(Orlacchio et al., 2010)

(Modified from Renton et al., 2014)

1.3. Mouse models of ALS

The identification of genetic mutations causative for ALS has been key for the development of rodent models of the disease.

The most commonly used and best-characterised model of ALS is a transgenic mouse overexpressing the human SOD1 gene carrying the G93A mutation (Gurney

et al., 1994). These mice mimic the human disease, showing progressive motor neuron loss accompanied by a loss of motor function (as illustrated in Figure 1.1.)

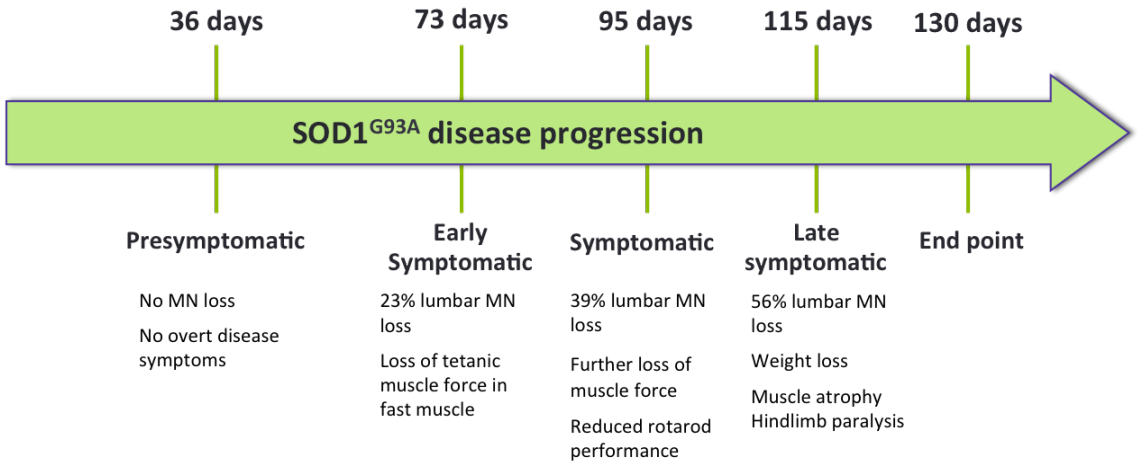

Figure 1.1. Disease progression in the SOD1^{G93A} mouse model of ALS
Schematic representation of the appearance of disease signs and motor neuron pathology in the SOD1^{G93A} mouse model of ALS, as described in Bilsland et al., 2010.

Mice overexpressing fALS-associated G37R and G85R mutant forms of human SOD1 have also been developed and are also widely used in ALS research (Morrison and Morrison, 1999). A significant concern with the majority of transgenic models of the disease is the fact that they overexpress the ALS-associated mutant protein at high levels, for example the SOD1^{G93A} mouse expresses the SOD1 protein at up to 20-fold the endogenous level. In fact, overexpression of wild type SOD1 at a similar level has been shown to cause progressive motor neuron death in transgenic mice (Graffmo et al., 2013). In order to investigate the effects of mutant SOD1 at endogenous levels, Joyce et al. recently identified the SOD1^{D83G} mouse, which carries this fALS-associated mutation in the mouse SOD1 gene (Joyce et al., 2015). The SOD1^{D83G} mouse develops progressive upper and lower motor neuron degeneration between 6 and 15 weeks of age, indicating that fALS-associated mutations in SOD1 are sufficient to elicit motor neuron degeneration when expressed at endogenous levels.

It is important to note that the different mutant SOD1 mouse models show different ages of disease onset and rates of disease progression and the results obtained

from the different models do not always agree. However, this could reflect heterogeneity in the disease caused by different SOD1 mutations rather than a limitation of the mouse models themselves. In addition, the disease phenotype of mutant SOD1 mice can be strongly affected by genetic background (Mancuso et al., 2012).

Mouse models based on the ALS-associated genes TDP-43, FUS and VCP have also been reported, but so far none have been able to recapitulate the ALS phenotype as well as mutant SOD1 transgenic mice (McGoldrick et al., 2013). Recently, a mouse model has been reported that expresses expanded C9orf72 $(GGGGCC)_{66}$ selectively in the central nervous system (Chew et al., 2015). At six months, these mice display cortical neuron and cerebellar Purkinje cell loss, as well as behavioural and motor deficits similar to the clinical symptoms of C9orf72 FTD/ALS patients. However, a detailed longitudinal analysis of motor neuron pathology and motor function has not yet been performed in these mice.

1.4. Cell autonomous versus non-cell autonomous mechanisms

Although ALS is defined as a disease of motor neurons, it is now widely accepted that non-neuronal cells play a key role in disease pathogenesis. Evidence for this comes from cell-type specific expression or deletion of ALS-associated mutant genes.

1.4.1. Motor neurons

It has been demonstrated that expression of mutant SOD1 only in motor neurons is not sufficient to cause degeneration. Clement et al. generated chimeric mice with different contributions of wild type and $SOD1^{G37R}$-expressing cells (Clement et al., 2003). The authors found that mice with mutant $SOD1^{G37R}$ in motor neurons but wild type non-neuronal cells did not develop symptoms of ALS. Looking at different chimeric mice with different contributions of wild type and $SOD1^{G37R}$-expressing non-neuronal cells, they observed that mice with an increasing contribution of wild

type non-neuronal cells survived for longer compared to 100% mutant controls. In addition they found that motor neurons expressing mutant SOD1 were more likely to survive if they were in proximity to wild type glial cells.

However, it is clear that mutant SOD1 expression in motor neurons does play a key role in ALS pathogenesis. By crossing Islet-Cre mice with Lox-SOD1^{G37R} mice, Boillee et al. were able to produce a mouse that expressed mutant SOD1 everywhere except the motor neurons (Boillee et al., 2006). The authors found that loss of SOD1^{G37R} in motor neurons delayed disease onset and slowed disease progression at an early stage, leading to an increase in survival.

These results indicate that expression of mutant SOD1 in motor neurons plays an important role in disease initiation and early progression. However, the fact that loss of mutant SOD1 from motor neurons could not prevent the disease in mice indicates that non-neuronal cells must also play a role in the pathogenesis.

1.4.2. Astrocytes

It has been demonstrated *in vitro* that co-culture of SOD1^{G93A}-expressing astrocytes with wild type mouse embryonic stem cell (ES)-derived motor neurons is neurotoxic (Di Giorgio et al., 2007). Similar results have also been found using patient-derived astrocytes from fALS patients (carrying the SOD1^{A4V} mutation and the C9orf72 expansion repeat) and also sALS patients (Meyer et al., 2014, Haidet-Phillips et al., 2011). However, mice expressing SOD1^{G86R} only in astrocytes (using the GFAP promoter sequence) display normal motor neuron physiology (Gong et al., 2000). This suggests that mutant SOD1-expressing astrocytes alone may not be sufficient to cause motor neuron degeneration *in vivo*.

In order to determine the role of astrocytes in ALS pathogenesis, Yamanaka et al. crossed lox-SOD1^{G37R} mice with cre-GFAP mice, to eliminate expression of mutant SOD1 in astrocytes only (Yamanaka et al., 2008). Loss of mutant SOD1 in astrocytes was found to have no effect on disease onset, but did cause a small slowing of disease progression and an increase in lifespan.

1.4.3. Microglia

Microglia are the innate immune cells of the central nervous system. Boillee et al. generated mice that express mutant SOD1 in all cells except microglia and macrophages (Boillee et al., 2006). The authors found that loss of microglial mutant SOD1 expression had no effect on disease onset or early progression, but did slow the progression of the later phase of the disease and extended survival significantly.

Interestingly, delayed microglial activation has been observed in mice that do not express mutant SOD1 in astrocytes, even though there was no change in mutant SOD1 levels in microglia (Yamanaka et al., 2008). This indicates that there is crosstalk between the cells proposed to be involved in ALS and it is likely that a complex interaction of both neuronal and non-neuronal cells contributes to disease pathogenesis.

1.4.4. Skeletal muscle

There have been conflicting reports on the effect of muscle-specific expression of ALS-associated SOD1 mutants. Dobrowolny et al. demonstrated that selective expression of $SOD1^{G93A}$ in mouse skeletal muscle using the myosin light chain promoter led to progressive muscle atrophy, reduced muscle strength, impaired contractility and mitochondrial dysfunction, but did not cause motor neuron degeneration (Dobrowolny et al., 2008). However, Wong and Martin reported that muscle-specific expression of either $SOD1^{G93A}$ or $SOD1^{G37R}$ using the human skeletal actin promoter resulted in both muscle and motor neuron pathology, similar to that seen in ALS patients (Wong and Martin, 2010), suggesting that defects in skeletal muscle may play a role in motor neuron degeneration in ALS. However, reducing levels of $SOD1^{G93A}$ by over 50% in skeletal muscle has been reported to have no effect on disease progression in $SOD1^{G93A}$ mice (Towne et al., 2008). These studies indicate that mutant SOD1 is toxic to skeletal muscle and likely plays a role in muscle weakness and atrophy in ALS. However, whether skeletal muscle dysfunction also contributes to motor neuron pathology still remains unclear.

1.5. Pathological mechanisms involved in ALS

At present, the precise cause of motor neuron death in ALS is not fully understood and many different mechanisms have been linked to the disease pathogenesis (illustrated in Figure 1.2). Difficulties arise in trying to distinguish which mechanisms play a causative role in disease pathogenesis, and which are simply downstream effects. It is likely that the interaction of multiple pathogenic processes is responsible for the dysfunction and ultimate degeneration of motor neurons in ALS.

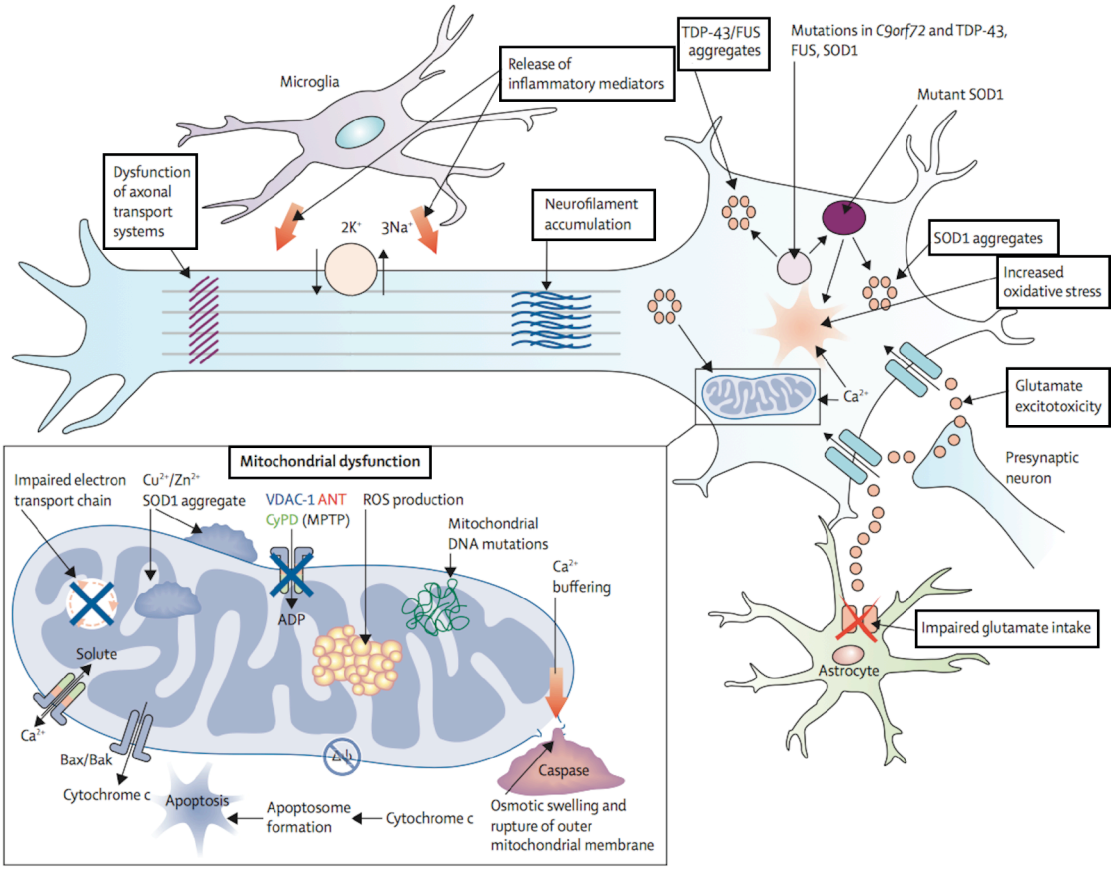

Figure 1.2. Mechanisms proposed to be involved in the pathogenesis of ALS

A wide range of mechanisms have been reported to be defective in ALS motor neurons, based on observations in mouse models of the disease as well as human patient samples. However, their exact role in ALS pathogenesis is poorly understood. Reprinted with permission from Elsevier (Turner et al., 2013).

1.5.1. Oxidative stress

Oxidative stress is caused by the generation and build-up of reactive oxygen species (ROS). ROS cause oxidative damage to proteins, lipids and nucleic acids. There have been a number of reports of increased oxidative stress in both sporadic and familial ALS patients. Increased levels of markers of lipid peroxidation have been found in the cerebrospinal spinal fluid (CSF) and urine of living patients (Smith et al., 1998, Simpson et al., 2004, Mitsumoto et al., 2008). Oxidative damage to proteins, DNA and lipids has also been observed in ALS spinal cords post-mortem (Shaw et al., 1995b, Shibata et al., 2001, Fitzmaurice et al., 1996). In addition, expression of ALS-associated mutant forms of TDP-43 in motor neuron cell lines has been reported to induce oxidative stress (Duan et al., 2010).

Oxidative damage of mRNA has been reported to be present presymptomatically in spinal cords of $SOD1^{G93A}$ mice, whilst damage to proteins, lipids and DNA was not observed until later in the disease progression (Chang et al., 2008). Of the mRNAs reported to be oxidised in this paper, many encoded proteins previously associated with ALS, including SOD1, $p150^{glued}$ (DCTN1) and vesicle-associated membrane protein B (VAPB). The authors were also able to demonstrate that vitamin E, which has been shown to reduce oxidative stress, delayed disease onset and slowed disease progression in $SOD1^{G93A}$ mice. However, vitamin E had no effect on the lifespan of the mice. In addition, when high dose vitamin E was administered to ALS patients in combination with riluzole, no beneficial effect was found compared to riluzole alone (Graf et al., 2005).

1.5.2. Mitochondrial dysfunction

In addition to their role in producing energy for the cell, mitochondria also play a key role in calcium homeostasis and the control of apoptosis. Mitochondrial damage has been observed in the $SOD1^{G93A}$ mouse before the onset of symptoms (Kong and Xu, 1998). The damage observed has been proposed to be a result of mutant SOD1 accumulating in the mitochondria of these mice (Higgins et al., 2002). Mitochondrial accumulation of mutant SOD1 has been reported to impair mitochondrial function by reducing the activity of the electron transport chain

complexes (Ferri et al., 2006). In addition, the calcium buffering capacity of spinal cord mitochondria has also been reported to be defective in presymptomatic $SOD1^{G93A}$ and $SOD1^{G85R}$ mice (Damiano et al., 2006), and may provide a link between mitochondrial dysfunction and calcium-mediated glutamate excitotoxicity, another mechanism proposed to be involved in ALS pathogenesis (described in detail in Section 1.5.3). Furthermore, the axonal transport of mitochondria has been shown to be defective both *in vitro* (De Vos et al., 2007) and *in vivo* (Bilsland et al., 2010) in motor neurons of the $SOD1^{G93A}$ mouse and will be discussed later in Section 1.7.2.6.

Attempts to prevent mitochondrial dysfunction pharmacologically have not shown promising results in ALS patients to date. Olesoxime, a mitochondrial pore modulator that was found to prevent motor neuron death in $SOD1^{G93A}$ mice (Sunyach et al., 2012), failed to show any beneficial effects in Phase III trials (Lenglet et al., 2014). In addition, dexpramipexole, a drug shown to protect motor neurons by stabilising the proton gradients needed for ATP production and preventing mitochondrial-dependent apoptosis (Alavian et al., 2012), failed to improve function or survival in a Phase III study (Cudkowicz et al., 2013).

1.5.3. Glutamate excitotoxicity

Glutamate is the main excitatory neurotransmitter in the central nervous system (CNS). It exerts its effects through both ionotropic and metabotropic glutamate receptors and its excitatory effects are terminated by removal of glutamate from the synapse. Glutamate is removed from the synaptic cleft by astrocytes and presynaptic neurons via glutamate reuptake transporters, EAAT1, EAAT2, and EAAT3 (Arriza et al., 1994). Glutamate excitotoxicity results from excessive stimulation of glutamate receptors, usually due to increased levels of glutamate in the synapse or increased sensitivity of the neuron to glutamate, for example due to increased expression of glutamate receptors. Excessive activation of glutamate receptors leads to disruption of neuronal calcium homeostasis and cellular toxicity. There are numerous reports providing evidence for glutamate excitotoxicity in ALS. Levels of glutamate have been found to be elevated in the CSF of ALS patients

(Rothstein et al., 1990). This could be explained by the post mortem observation that the number of presynaptic glutamate re-uptake sites is reduced in the spinal cord of ALS patients (Shaw et al., 1995a, Rothstein et al., 1995). In addition, electrophysiology studies have revealed hyperexcitability of the motor system before symptom onset in ALS patients (Vucic and Kiernan, 2006).

Riluzole, the only licensed drug available for ALS, acts to reduce glutamate excitotoxicity by a number of mechanisms, including inhibition of repetitive neuronal firing (Doble, 1996), inhibition of glutamate release (Wang et al., 2004) and stimulation of glutamate transporters (Fumagalli et al., 2008). It is able to increase survival of patients by around two months, although it has little effect on slowing functional decline (Miller et al., 2003).

1.5.4. Inflammation

Neuroinflammation is emerging as a common link between many neurodegenerative diseases. In $SOD1^{G93A}$ mice, an increased number of activated microglia is found in the ventral horn at a presymptomatic stage (Tortarolo et al., 2003). When activated, microglia alter their gene expression, leading to the production and release of several inflammatory mediators, including cytokines, chemokines and proteases. Proinflammatory cytokines, such as TNFα and IL-1β, have been implicated to play a role in ALS pathogenesis.

Using microarray techniques to examine mRNA expression in the spinal cord of $SOD1^{G93A}$ mice, TNFα was found to be one of the earliest inflammatory stimuli to be induced (11 weeks, early symptomatic) (Yoshihara et al., 2002). In addition, high levels of TNFα are reported in blood samples from sALS patients (Poloni et al., 2000). However, knocking out TNFα in $SOD1^{G93A}$ mice was found to have no effect on disease onset, progression or survival, nor any influence on motor neuron degeneration (Gowing et al., 2006).

Interleukin 1-beta (IL-1β) has also been reported to be chronically upregulated in mutant $SOD1^{G93A}$ and $SOD1^{G37R}$ transgenic mice (Hensley et al., 2002, Nguyen et

al., 2001). However, knocking out IL-1β in $SOD1^{G37R}$ mice was found to have no effect on either lifespan or motor neuron degeneration (Nguyen et al., 2001).

These results suggest that TNFα and IL-1β do not play a key role in triggering motor neuron death in ALS, but may instead be a consequence of the underlying pathology.

1.5.5. RNA processing

Several genes found to cause fALS encode proteins involved in the regulation of RNA transcription and processing, including TDP-43 and FUS.

TDP-43 is a ubiquitously expressed RNA-DNA binding protein that has been implicated in transcriptional regulation, alternative splicing and microRNA processing. Although normally located in the nucleus, the ALS mutant form is found predominantly in the cytoplasm and has been localised to the ubiquitinated inclusions that are characteristic of ALS (Neumann et al., 2006). Fibroblasts taken from TDP-43-associated ALS patients have been shown to have widespread alterations in RNA splicing, indicating that mutant TDP-43 could cause ALS due to a loss of its normal function (Highley et al., 2010). This is supported by the observation that knocking down TDP-43 in mice leads to progressive motor neuron degeneration, motor dysfunction and ultimately paralysis (Yang et al., 2014).

FUS is another RNA-DNA binding protein that has been identified to be mutated in ALS (Kwiatkowski et al., 2009; Vance et al., 2009). It has been shown to play a role in transcriptional regulation, RNA and microRNA processing and mRNA axonal transport (Lagier-Tourenne et al., 2010). Similarly to TDP-43, the nuclear localisation of FUS is reported to be lost in ALS, with the protein being found in cytoplasmic aggregates in spinal cord motor neurons (Vance et al., 2009). Recent evidence has indicated that mutant FUS may cause neurodegeneration due to a loss of its normal function and also a toxic gain of function. Qiu et al. demonstrated that, in mice expressing FUS carrying the fALS-associated R521C mutation, mutant FUS bound to the wild type form of the protein, preventing its interaction

with its normal partners (Qiu et al., 2014). In addition, mutant FUS was found to form more stable complexes with BDNF RNA and as a result cause BDNF splicing defects and impaired BDNF-TrkB signalling.

1.5.6. Protein aggregation

There are numerous reports of pathological protein aggregates in both mouse models of ALS and in fALS and sALS patient samples. Many proteins previously associated with the disease through genetics have now been shown to be components of these aggregates.

TDP-43 is one of the major protein constituents of the ubiquitin-positive inclusions that have been described in ALS (Neumann et al., 2006). In fact, over 95% of ALS cases are reported to show cytoplasmic aggregation of TDP-43 (Mackenzie et al., 2007) and it has been proposed that TDP-43 could be a point of convergence in ALS pathogenesis, downstream of many different disease-initiating mechanisms. Interestingly, mutant SOD1-associated ALS lacks TDP-43 pathology, suggesting that the pathogenesis of SOD1-associated ALS could be distinct from most other forms of the disease (Mackenzie et al., 2007).

Redistribution of TDP-43 from the nucleus to the cytoplasm is thought to occur at an early stage in ALS pathogenesis (Giordana et al., 2010). However, when synthetic peptides were used to block TDP-43 aggregation, Liu et al. found that the protein could still mediate cell death when overexpressed in HeLa cells (Liu et al., 2013). There are also mouse models expressing mutant TDP-43 that develop adult-onset motor neuron disease but do not exhibit aggregation of the mutant protein (Arnold et al., 2013). These results indicate that aggregation of TDP-43 may not be a key mechanism underlying its pathogenic effect. However, the exact role of macro-aggregates versus micro-aggregates of TDP-43, as well as soluble monomeric and oligomeric forms, still needs to be determined.

ALS-associated SOD1 mutants have also been reported to form aggregates. Aggregates have been observed in human ALS spinal cords (Ince et al., 1998) and

also in the SOD1^{G93A} mouse model, where high molecular weight complexes containing mutant SOD1 appear at an early symptomatic stage and accumulate throughout disease progression (Wang et al., 2002). The authors proposed that mutations in SOD1 destabilise the protein structure and trigger aggregation. Furthermore it has been demonstrated that the propensity of SOD1 to aggregate correlates with the clinical severity of the mutations (Pratt et al., 2014). Interestingly, it has been shown that mutant SOD1 aggregates contain the dynein motor complex and could therefore interfere with retrograde axonal transport (Zhang et al., 2007). The role of defects in axonal transport in ALS pathogenesis will be discussed in Section 1.7.2.6.

The role of protein aggregation in ALS pathogenesis is still not fully understood. Aggregates may act to sequester mutant proteins and limit their deleterious effects. Alternatively, aggregates could form as the cell's protein quality control system is overwhelmed and cannot remove mutant, damaged and/or misfolded proteins quickly enough. Accumulation of aggregated proteins could then induce cellular stress and ultimately contribute to neurodegeneration. This theory is supported by the observation that treatment of early symptomatic SOD1^{G93A} mice with arimoclomol, which acts to enhance the clearance of protein aggregates, significantly improved muscle strength, motor neuron survival and lifespan (Kalmar et al., 2008). Arimoclomol is now in Phase II trials for SOD1-positive fALS (www.clinicaltrials.gov/ct2/show/NCT00706147).

1.5.7. Axonal transport

Defects in both retrograde and anterograde axonal transport have been reported in ALS and will be described in detail in Section 1.7.2.6. Deficits in axonal transport have also been found in many other neurodegenerative diseases, including Huntington's disease, Alzheimer's disease, Parkinson's disease and Charcot Marie Tooth type 2 (Millecamps and Julien, 2013), suggesting that they may be a key pathogenic mechanism in neurodegeneration.

1.6. Axonal transport

Neurons are highly polarised cells, with axons that can extend over a meter away from the cell body in large mammals. This unique morphology makes neurons particularly dependent on active intracellular transport. Axonal transport plays two major roles in neurons:

1) Supply and clearance: delivery of organelles and newly synthesised proteins, lipids and RNA to the axon and distal synapses, and removal of faulty ones to the soma for degradation;
2) Long-distance communication between the axon tip and the soma, including transport of neurotrophic factors and their receptors, which are essential for survival (Chowdary et al., 2012).

Axonal transport can be divided into two classes based on the speed at which cargoes move. Vesicles, organelles and mRNA are transported by fast axonal transport and move at a speed of 50–200 mm per day (0.5-3 μm/s), whilst cytoskeletal proteins, such as neurofilaments and tubulin, and some soluble proteins are transported by slow axonal transport and move at a speed of 0.1–3 mm per day (Maday et al., 2014).

The axonal transport of all cargoes is mediated by two families of ATP-dependent motor proteins, kinesins and cytoplasmic dynein, which carry their cargoes along microtubule tracks that run the length of the axon. Microtubules impart an intrinsic polarity to neurons, with their “plus” ends located at the axon tips and their “minus” ends within the cell body. This polarity confers directionality to axonal transport.

1.6.1. Anterograde axonal transport

Anterograde axonal transport refers to the movement of cargoes from the cell body towards the axon tips and is mediated by the kinesin superfamily of motor proteins. Kinesin is composed of two heavy chains (115–130 kDa) and two light chains (62–70 kDa). Structural studies have revealed that kinesin is a rod-shaped protein, with two globular heads connected to a tail domain by a long stalk (Figure 1.3).

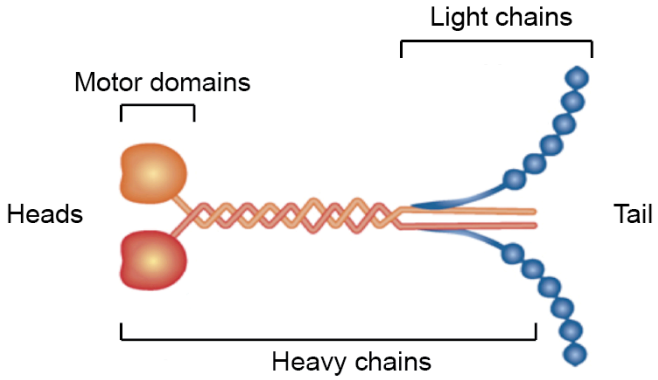

Figure 1.3. The structure of the kinesin-1 motor protein
Kinesin-1 is a tetramer composed of two light chains (blue) and two heavy chains (orange). The motor domains are located in the globular heads at the N terminus of each heavy chain. Modified from (Dodding and Way, 2011). Reprinted with permission from John Wiley and Sons.

The globular heads of the kinesin heavy chains (also known as KIFs) comprise the motor domains and contain both the ATP and microtubule binding motifs. The crystal structure of the motor domain was reported in 1996 (Kull et al., 1996) and it is now clear how small conformational changes in the ATP binding pocket lead to the motor taking a step (termed a powerstroke) (Vale and Milligan, 2000). The tail domains of the KIFs are thought to participate in cargo binding. Kinesin light chains (KLCs) localise to the end of the KIF tail domains and are thought to regulate cargo binding and the motor's autoinhibitory mechanism (Vale, 2003). Kinesin-1, also known as conventional kinesin, is responsible for the fast axonal transport of most vesicles, organelles, proteins and RNA particles and the slow axonal transport of cytoskeletal proteins (Maday et al., 2014). Kinesin-2 and kinesin-3 are also important for neuronal axonal transport. Kinesin-2 motors have been shown to be associated with late endosome-lysosome compartments (Brown et al., 2005), whilst kinesin-3 motors carry synaptic vesicle precursors and dense core vesicles (Okada et al., 1995, Kiris et al., 2011).

1.6.2. Retrograde axonal transport

Retrograde axonal transport refers to the movement of cargoes from the axon tips back towards the cell body and is mediated by cytoplasmic dynein. Cytoplasmic

dynein is composed of two heavy chains (HC) and additional intermediate, light intermediate and light chains (Figure 1.4).

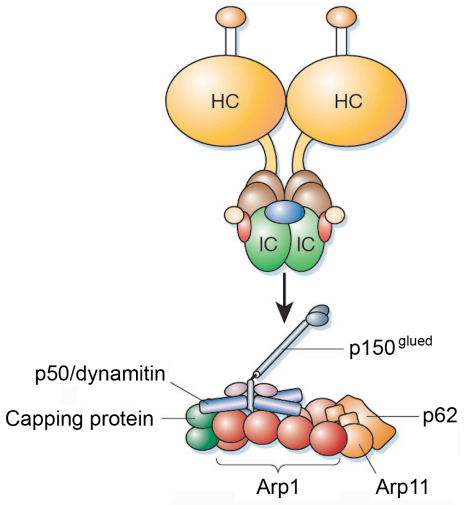

Figure 1.4. Schematic of dynein-dynactin complex
Components of the dynein motor and its cofactor dynactin. Dynein interacts with the dynactin complex via its intermediate chains (IC). Reprinted with permission from Nature Publishing Group (Schliwa and Woehlke, 2003).

The dynein heavy chains contain a carboxy-terminal motor domain, comprising the ATP and microtubule binding motifs. High-resolution crystal structures of the dynein motor domain were reported in 2012 (Kon et al., 2012, Schmidt et al., 2012) and have revealed that the motor uses a different mechanism from kinesin to produce a powerstroke, involving much larger conformational changes. The amino-terminal tails of the heavy chains combine with the additional smaller chains to form the cargo-binding domain. Diversity is achieved in the dynein family through different combinations of heavy, intermediate, light intermediate and light chains and this is thought to underlie the ability of dynein to display cargo-specific transport characteristics.

Dynein function is regulated by a multi-subunit cofactor called dynactin (see Figure 1.4) and consists of eight core subunits: Arp1, Arp11, p62, p150^{Glued}, p50/dynamitin, p24, p25 and p27. Arp1, p25 and p27 subunits have been implicated in the regulation of cargo binding. A dimer of p150^{Glued} subunits forms a bridge between the dynein intermediate chain and microtubules, which is proposed to increase the

processivity of the motor complex. In contrast, dynamitin acts to inhibit dynein-mediated axonal transport by disrupting the dynein-dynactin complex. It is thought to do this by causing the release of the $p150^{Glued}$ and p24 subunits (Melkonian et al., 2007). Dynactin has also been shown to interact with and increase the processivity of kinesin-2 (Berezuk and Schroer, 2007).

1.7. Axonal transport defects and neurodegeneration

Given the key role that axonal transport plays in neurons, it is not surprising that defects in transport are deleterious to the health of neurons and that such defects have been proposed to be involved in the pathogenesis of neurodegenerative diseases.

1.7.1. Genetic evidence

Evidence of a general relationship between axonal transport deficits and neuronal death comes from studies of mice expressing mutations in transport-related genes. In 2003, Hafezparast et al. performed an ENU mutagenesis screen in mice, looking for mutations that caused progressive locomotor disorders (Hafezparast et al., 2003). One of the strains identified, legs at odd angles (Loa), was found to carry a single point mutation in the gene encoding dynein heavy chain 1 and was reported to exhibit a progressive loss of alpha motor neurons. The group were also able to demonstrate that embryonic motor neurons from Loa/Loa mice showed a significant defect in retrograde axonal transport. It was initially assumed that the loss of alpha motor neurons in these mice was responsible for the motor defects observed, however subsequent studies showed that the Loa mice also had a significant sensory neuropathy (Chen et al., 2007b).

Another mouse that presents motor neuron degeneration in combination with axonal transport defects is the Wobbler mouse. Wobbler mice carry a L967Q point mutation in the Vps54 gene, a component of the Golgi-associated retrograde protein (GARP) complex that has been proposed to regulate endosome to trans-Golgi network transport. Wobbler mice were found to mimic several features of

human ALS. Motor neuron death begins at around three weeks of age and is accompanied by a progressive loss of body weight and muscle strength (Moser et al., 2013). Defects in both anterograde and retrograde axonal transport have been described in symptomatic Wobbler mice (Mitsumoto et al., 1993). The L967Q mutation has been proposed to destabilise Vps54 and the entire GARP complex and thereby induce deficits in axonal transport (Karlsson et al., 2013).

Evidence of a link between axonal transport defects and neurodegeneration also comes from human genetic studies. Mutations in the genes encoding the molecular motors have been linked to neurodegenerative diseases. For example, mutations in the dynein heavy chain have been found to cause Charcot Marie Tooth type 2 (CMT2) and spinal muscular atrophy, whilst mutations in kinesin-1 and 3 cause hereditary spastic paraplegia (Maday et al., 2014). In addition, mutations in motor adaptor and regulator proteins has also been linked to neurodegenerative diseases. ALS has been associated with mutations in the $p150^{glued}$ subunit of dynactin (Puls et al., 2003, Munch et al., 2005) and mutations in the late endosomal GTPase Rab7 (Verhoeven et al., 2003) have been found in patients with CMT2B.

1.7.2. Functional studies

The majority of evidence suggesting that axonal transport deficits play an early, possibly causative, role in neurodegenerative diseases comes from functional rather than genetic studies.

1.7.2.1. Huntington's Disease

Huntington's disease is an autosomal dominant neurodegenerative disease associated with a trinucleotide repeat expansion in the gene encoding huntingtin (htt). It has been demonstrated in a number of cellular and animal models of the disease that pathogenic htt causes inhibition of both anterograde and retrograde axonal transport, often before the appearance of other obvious pathological signs (Gunawardena et al., 2003, Trushina et al., 2004). Interestingly, this inhibition shows the same cell-type specificity as the disease: deficits in the axonal transport

of amyloid precursor protein (APP) and brain-derived neurotrophic factor (BDNF) were observed in striatal and hippocampal neurons from a mouse model of Huntington's disease (*Hdh150Q),* but not in the cortical neurons (Her and Goldstein, 2008). Several mechanisms have been proposed to explain this inhibition of axonal transport, including disruption of the huntingtin/HAP1/p150^{glued} complex leading to the release of dynein from the microtubules (Li et al., 1998, Gauthier et al., 2004), physical blockade of transport by htt aggregates (Sinadinos et al., 2009) and htt-mediated activation of JNK3 leading to phosphorylation and inhibition of kinesin (Morfini et al., 2009).

1.7.2.2. Alzheimer's Disease

Alzheimer's disease (AD) has been linked to mutations in the presenilin and APP genes. Mutations in these genes have been reported to alter the proteolytic processing of the APP protein, leading to increased production of the Aβ species (Scheuner et al., 1996). Smith et al. demonstrated in the Tg2576 mouse model, which overexpresses AD-associated mutant APP (K670N/M671L), that axonal transport deficits in olfactory receptor neurons are present early in disease progression, before the appearance of amyloid plaques (Smith et al., 2007). Oligomeric Aβ has been proposed to inhibit fast axonal transport through modulation of a number of kinases, including suppression of Akt (Takach et al., 2015) and activation of casein kinase 2 (Pigino et al., 2009), GSK3β (Vossel et al., 2015) and p38 MAPK (Guo et al., 2013). In fact, correcting fast axonal transport defects by reducing GSK3β activity has been shown to be beneficial in AD experimental models (Shaw and Chang, 2013, Vossel et al., 2015).

AD-associated mutations in presenilin-1 have also been shown to induce defects in anterograde axonal transport through activation of GSK3β (Pigino et al., 2003). Furthermore, the microtubule-associated protein tau, which forms the neurofibrillary tangles observed in AD, has been found to play a key role in Aβ-mediated activation of GSK3β and subsequent axonal transport defects (Vossel et al., 2015).

1.7.2.3. Parkinson's Disease

Axonal transport defects have also been proposed to play a role in Parkinson's disease (PD). The disease is characterised by the loss of the neurotransmitter dopamine and neuronal degeneration in the substantia nigra pars compacta. The most common genetic cause of PD has been shown to be mutations in the leucine-rich repeat kinase 2 gene (LRRK2) (Zimprich et al., 2004, Paisan-Ruiz et al., 2004). Godena et al. recently demonstrated that expression of mutant LRRK2 in rat cortical neurons resulted in defects in both retrograde and anterograde mitochondrial transport (Godena et al., 2014). Similar results were found *in vivo* in the motor neurons of *Drosophila* larvae expressing mutant LRRK2. The authors proposed that the deficits in axonal transport were due to an aberrant interaction between mutant LRRK2 and microtubules. Furthermore, RNAi-mediated knockdown of histone deacetylase 6 (HDAC6) was able to restore axonal transport and rescue defects in locomotion in LRRK2 mutant flies. HDAC6 knockdown leads to increased acetylation of microtubules, allowing for the enhanced recruitment of both dynein and kinesin motors (Dompierre et al., 2007). These results provide exciting evidence that enhancing axonal transport can prevent neurodegeneration and rescue motor phenotypes.

1.7.2.4. Charcot Marie Tooth type 2

Charcot Marie Tooth is the most common inherited disorder of the peripheral nervous system. It is characterised by the degeneration of both motor and sensory neurons. Defects in axonal transport have been described in mouse models of CMT2 that express mutant forms of the heat shock protein Hsp27. Mice carrying the S135F mutation (which is associated with human CMT type 2F) were found to develop a CMT2-like phenotype and were shown to have defects in mitochondrial transport in DRG neurons dissected from symptomatic mice (d'Ydewalle et al., 2011). The authors found that treatment with an HDAC6 inhibitor was able to correct deficits in axonal transport and also rescue the CMT2 phenotype – improving motor performance and reducing denervation in the mice.

1.7.2.5. Spinal and bulbar muscular atrophy

Spinal and bulbar muscular atrophy (SBMA) is a hereditary late-onset neurodegenerative disorder, caused by an expansion of a CAG repeat in the first exon of the androgen receptor (AR). The disease is characterised by selective loss of motor neurons in the spinal cord and bulbar nuclei of the brain stem. Similarly to ALS, the mechanism(s) responsible for motor neuron degeneration are still unclear, and there have been contradicting views on the role of axonal transport defects in disease pathogenesis. In knock-in mice overexpressing the pathogenic form of the AR, Kemp et al. reported reduced retrograde axonal transport of cholera toxin subunit B (CTB)-labelled endosomes in the sciatic nerve (Kemp et al., 2011). However, mice overexpressing wild type AR were also found to exhibit retrograde axonal transport defects (Kemp et al., 2011). Later in the same year it was demonstrated that if the pathogenic form of AR is expressed at endogenous levels, the mice still have significant motor neuron loss but there are no overt retrograde transport deficits (Malik et al., 2011). Such findings raise the possibility that retrograde axonal transport deficits could be unique to ALS among the motor neuron diseases and may therefore have potential as an early biomarker for the disease.

1.7.2.6. Amyotrophic Lateral Sclerosis

There is evidence for both anterograde and retrograde axonal transport defects in ALS motor neurons.

Anterograde axonal transport defects

Defects in the anterograde axonal transport of a number of different cargoes have been reported in ALS model systems. Experiments performed in isolated squid axoplasm have shown that perfusion of fALS-linked SOD1 mutants (G93A, G85R, and H46R) causes a specific inhibition of anterograde axonal transport, with no effect on retrograde speeds (Morfini et al., 2013). However, the particular type of cargo affected was not identified in these studies. In cortical neurons, transfection with SOD1 mutants was found to cause defects in the anterograde axonal transport of mitochondria and APP (De Vos et al., 2007).

Deficits in anterograde axonal transport have also been reported in transgenic mice overexpressing mutant SOD1. *In vivo* axonal transport studies in the $SOD1^{G93A}$ mouse have revealed defects in the anterograde transport of mitochondria in the sciatic nerve at a presymptomatic stage (Bilsland et al., 2010). The authors were able to demonstrate that overexpression of the wild type form of SOD1 had no effect on anterograde axonal transport speeds. Defects in the anterograde axonal transport of mRNA have also been reported. Live imaging of *Drosophila* motor neurons revealed that ALS-associated TDP-43 mutants were not transported efficiently along axons and displayed a less continuous movement than wild type TDP-43 mRNA granules (Alami et al., 2014). Deficits were observed in the anterograde direction only. Similar results were also reported in mouse cortical neurons and induced pluripotent stem cell-derived human motor neurons carrying ALS-causing TDP-43 mutations (Alami et al., 2014).

Retrograde axonal transport defects

Deficits in retrograde axonal transport have been reported both *in vitro* and *in vivo* in ALS model systems. *In vitro,* mutant SOD1 has been shown to induce deficits in the retrograde axonal transport of mitochondria, APP and H_CT (Kieran et al., 2005, De Vos et al., 2007). Bilsland et al. were the first to provide *in vivo* evidence of retrograde axonal transport defects in a mouse model of ALS (Bilsland et al., 2010). Using *in vivo* imaging of the sciatic nerve, they were able to demonstrate a significant inhibition in retrograde axonal transport in adult $SOD1^{G93A}$ mice compared to wild type controls. A similar defect was also seen in the retrograde axonal transport of the p75 neurotrophin receptor ($p75^{NTR}$) and mitochondria. Of particular interest was the observation that retrograde axonal transport defects were found in motor but not sensory neurons and were present at a presymptomatic stage. Importantly, transgenic mice overexpressing the wild type form of SOD1 did not develop defects in retrograde axonal transport.

The early appearance of transport deficits in $SOD1^{G93A}$ mice suggests that they may play a crucial role in triggering motor neuron dysfunction and the subsequent degeneration observed in ALS. However, the work of Bilsland et al. did not directly demonstrate the causal relationship between axonal transport defects and motor neuron degeneration. The importance of axonal transport deficits in ALS

pathogenesis is in fact still a matter of debate. Marinkovic et al. have proposed that axonal transport defects observed in the $SOD1^{G93A}$ mouse are not responsible for the degeneration of motor neurons (Marinkovic et al., 2012). In order to investigate the causative relationship between deficits in axonal transport and neurodegeneration, the group studied transgenic mice expressing the $SOD1^{G85R}$ mutation. $SOD1^{G85R}$ mutant mice exhibit progressive weight loss and muscle weakness at a preterminal stage, associated with significant denervation of muscle fibres. However, analysis of CTB-labelled endosomes in preterminal stage mice did not identify any significant deficits in either retrograde or anterograde axonal transport in either the intercostal or tibialis nerves. The authors concluded that axons are able to degenerate in the absence of axonal transport defects in the $SOD1^{G85R}$ mouse, marking the possible dissociation between transport deficits and motor neuron loss in ALS. However, the $SOD1^{G85R}$ mouse has not been as thoroughly studied as the $SOD1^{G93A}$ model. In addition, the mice demonstrate a variable disease progression suggesting that the $SOD1^{G85R}$ mouse could be a less reliable model of the human disease. Alternatively, axonal transport defects may only play a role in the pathogenesis of specific types of ALS.

These studies highlight the need to demonstrate whether axonal transport defects are a true cause of ALS or simply a consequence of the pathology. Identifying compounds able to enhance retrograde axonal transport will help answer this question and may also shed light on the relative importance of retrograde versus anterograde axonal transport defects in ALS.

1.8. Accelerating axonal transport as a therapeutic strategy for ALS

A limited body of evidence already exists that suggests accelerating axonal transport could be beneficial in ALS.

Inhibitors of HDAC6 have been described to accelerate anterograde and retrograde axonal transport and were mentioned previously in relation to their effects in PD and CMT2 mouse models in Sections 1.7.2.3 and 1.7.2.4. Taes et al. tested the

effect of deleting the HDAC6 gene in the SOD1^{G93A} mouse model (Taes et al., 2013). The authors found that loss of HDAC6 extended survival, but had no effect on disease onset. They also reported modest increases in motor neuron survival and neuromuscular junction innervation. The lack of effect on disease onset and modest beneficial effects reported could be due to the fact that HDAC6 also plays a major role in axonal regeneration and degradation of misfolded proteins (Simoes-Pires et al., 2013). This is supported by the fact that knocking out HDAC6 in cultured cells has been shown to increase mutant SOD1 aggregation (Gal et al., 2013). However, these results still provide promising evidence that accelerating axonal transport could be beneficial in ALS.

Further genetic evidence for the beneficial effects of accelerating axonal transport in ALS comes from crossing SOD1^{G93A} mice with heterozygous Loa mice, which carry a point mutation in the dynein heavy chain (Kieran et al., 2005). Primary motor neurons derived from Loa/SOD1^{G93A} mice show a complete recovery of the retrograde axonal transport defects that are found in SOD1^{G93A} motor neurons. In addition, Loa/SOD1^{G93A} mice display delayed disease progression and an increase in lifespan compared to SOD1^{G93A} controls. The molecular mechanism by which the Loa mutation affects axonal transport in SOD1^{G93A} motor neurons is still unclear; especially as homozygous Loa mice display defects in retrograde axonal transport (Hafezparast et al., 2003). However, these results provide convincing evidence that retrograde axonal transport defects play a critical role in motor neuron degeneration in ALS and indicate that pharmacological enhancement of axonal transport could be beneficial.

There have been very few studies investigating the effect of pharmacological enhancement of axonal transport on ALS pathogenesis. Davunetide (NAP) is an eight amino acid peptide that is derived from activity-dependent neuroprotective peptide (ADNP). Acute treatment of three-month-old SOD1^{G93A} mice with 10 µg NAP was shown to normalise anterograde axonal transport in olfactory neurons to wild type speeds (Jouroukhin et al., 2013). The group reported that chronic treatment of early symptomatic SOD1^{G93A} mice with 10 µg NAP per day significantly increased lifespan compared to saline treated controls (from 129.8 to 134.2 days). However, the evidence for this minimal increase in survival was not

robust, as the gender and control groups used in the study were not balanced (7 NAP treated and 4 saline treated females versus 17 NAP treated and 23 saline treated males) and a mean increase in survival of four days is unlikely to be biologically significant. Furthermore, the therapeutic potential of NAP is limited, as peptides are not suited for use as drugs due to their low bioavailability, metabolic instability and poor membrane permeability. This study highlights the need to identify small molecule drugs able to accelerate axonal transport in motor neurons and test them in well-designed preclinical trials.

A final piece of evidence that suggests pharmacological enhancement of retrograde axonal transport could be beneficial in ALS comes from studies investigating the effects of acetyl-l-carnitine (ALCAR). ALCAR, which we found to accelerate retrograde axonal transport in motor neurons *in vitro* (see Figure 3.5), has been shown to be beneficial in the treatment of ALS patients. In a Phase II trial, patients treated with 100 mg/day riluzole and 3 g/day ALCAR were compared to patients treated with riluzole alone. Addition of ALCAR into the treatment regime was found to cause a slowing of functional decline, especially in the first six months, and was also seen to increase the median survival by 23 months (Beghi et al., 2013). ALCAR has been previously described to be neuroprotective *in vitro*, and this was linked to its ability to potentiate aerobic energy metabolism (Forloni et al., 1994) and enhance glutamate transporter activity, thereby reducing excitotoxicity (Jalal et al., 2010). It could be that ALCAR's enhancing effect on retrograde axonal transport also contributes to its beneficial effects in ALS patients.

Interestingly, it has been suggested that defects in mitochondrial axonal transport may not play a significant role in ALS pathogenesis. Knocking out syntaphilin, a docking receptor for axonal mitochondria, has been shown to increase the number of motile mitochondria without affecting the axonal transport of other cargoes. Zhu and Sheng crossed these syntaphilin knockouts with $SOD1^{G93A}$ mice. Although there was a significant increase in the number of motile mitochondria (shown in DRGs cultured from adult $SOD1^{G93A}$ mice), there was no effect on disease pathogenesis (Zhu and Sheng, 2011). However, the study did not demonstrate whether mitochondrial transport defects in motor neurons had been corrected.

This study highlights the need to consider the role of alterations in the axonal transport of different cargoes individually, rather than considering the process as a whole. This could have important implications when looking to modify axonal transport as a therapeutic strategy for ALS and also other neurodegenerative diseases.

1.9. Aims of this thesis

The aims of this PhD project were to:

i. Develop and validate a screen to identify pharmacological enhancers of retrograde axonal transport in motor neurons

ii. Screen a small library of kinase inhibitors for novel enhancers of retrograde axonal transport

iii. Validate the effects of hit compounds on axonal transport *in vitro* in wild type and $SOD1^{G93A}$ motor neurons

iv. Determine the effect of hit compounds on retrograde axonal transport *in vivo* in early symptomatic $SOD1^{G93A}$ mice

v. Investigate the mechanism of action of hit compounds

Chapter 2. Materials and Methods

2.1. Materials

2.1.1. Reagents and media

Reagents were purchased from Sigma Aldrich unless otherwise stated. Distilled water (dH_2O), phosphate buffered saline (PBS), Hank's, penicillin/streptomycin (Pen/Strep), SOC medium and ethylenediaminetetraacetic acid (EDTA) were provided by Cancer Research UK Laboratory Services. Ciliobrevin A was from InterBioScreen, SB-239063 and SB-203580 were supplied by GlaxoSmithKline, anisomycin was from Cell Signalling, picropodophyllotoxin was from Tocris and the NAP peptide and scrambled control were synthesised by the Cancer Research UK Peptide Synthesis service.

2.1.2. Bacterial Strains

E.coli strain XL1Blue was used for DNA amplification.

2.1.3. Antibodies

Fluorescently conjugated secondary antibodies for immunofluorescence were purchased from Invitrogen and were used at a dilution of 1:400.

HRP-conjugated secondary antibodies for western blotting were from DAKO and were used at a dilution of 1:4000.

The primary antibodies that were used in this thesis are listed in Table 3.

Table 3. Primary antibodies used

Antigen	Antibody Name	Supplier	Dilution
Akt	9272	Cell Signalling	1:1000 WB
p-Akt (Ser473)	D9E	Cell Signalling	1:1000 WB
β-actin	AC40	Sigma	1:2000 WB
β-III-tubulin	Tuj1	Covance	1:1000 IF
ERK1/2	9102	Cell Signalling	1:1000 WB
pERK1/2 (Thr202/Tyr204)	9101	Cell Signalling	1:1000 WB
GAPDH	mab374	Millipore	1:5000 WB
GFP	4E12/8	CRUK monoclonal facility	1:2000 WB
p-IGF1R (Tyr1161/Tyr1165/ Tyr1166)	ABE332	Millipore	1:1000 WB
Pan p38 MAPK	9212	Cell Signalling	1:50 IF 1:1000 WB
p-p38 MAPK (Thr180/Tyr182)	4511	Cell Signalling	1:200 IF 1:800 WB
p38 MAPK alpha	9218	Cell Signalling	1:1000 WB
p38 MAPK beta	PA1-41154	Pierce	1:1000 WB
p38 MAPK gamma	2307	Cell Signalling	1:1000 WB
p38 MAPK delta	2308	Cell Signalling	1:1000 WB
$p75^{NTR}$ CRD (0.8 mg/ml)	5410	Molecular Neuropathobiology Laboratory, CRUK	1:4000 IF
Rab7	sc-376362	Santa Cruz	1:200 IF
SOD1	ab16831	Abcam	1:2000 WB

IF: immunofluorescence, WB: western blot

2.1.4. Primers used

The following primers were used for genotyping mice.

Control	IMR 0042 and IMR 0043
SOD1 mice	IMR 0113 and IMR 0114

Primer sequences:

Name: IMR0042

Sequence: 5'- CTA GGC CAC AGA ATT GAA AGA TCT -3'

Name: IMR0043

Sequence: 5'- GTA GGT GGA AAT TCT AGC ATC ATC -3'

Name: IMR0113

Sequence: 5'- CAT CAG CCC TAA TCC ATC TGA -3'

Name: IMR0114

Sequence: 5'- CGC GAC TAA CAA TCA AAG TGA -3'

2.1.5. Sequences of shRNA used

All shRNA constructs were purchased from GeneCopoeia's OmicsLink library and were expressed using the psi-LVRU6GP vector, under the control of the U6 promoter. The vector map for all shRNA constructs is shown below:

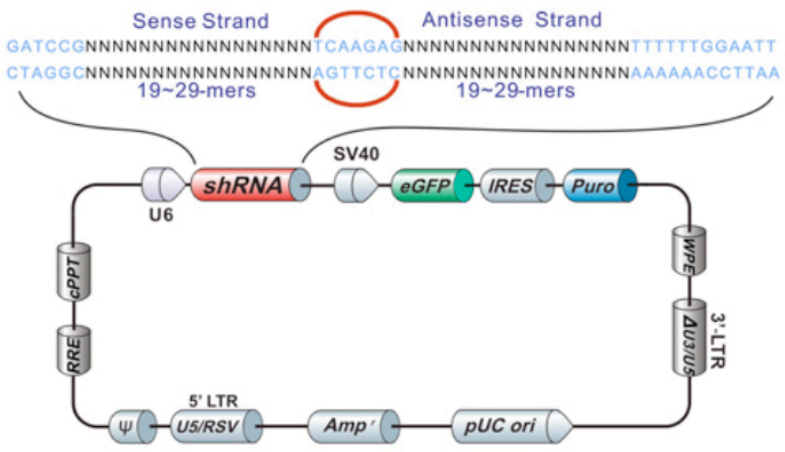

The sequences of individual shRNAs are listed below:

Clone Name	Target	Target Sequence
MSH030694-1-LVRU6GP(OS342165)	MAPK13	agcttccatgatttctacc
MSH030694-2-LVRU6GP(OS342166)	MAPK13	gacagacctacagaagatc
MSH030694-3-LVRU6GP(OS342167)	MAPK13	aggtccagtacttggtgta
MSH030694-4-LVRU6GP(OS342168)	MAPK13	ccagatcctgaaagtgact
MSH030695-1-LVRU6GP(OS303957)	MAPK14	tgaccggaagaacgttgtt
MSH030695-2-LVRU6GP(OS303958)	MAPK14	atgaccagtcctttgaaag
MSH030695-3-LVRU6GP(OS303959)	MAPK14	agagcctgacctatgatga
MSH030695-4-LVRU6GP(OS303960)	MAPK14	ctgcctttaccatatcagt
MSH029442-1-LVRU6GP(OS202113)	IGF1R	tcgagatgaccaatctcaa
MSH029442-2-LVRU6GP(OS300906)	IGF1R	gagaggcaataacattgcc
MSH029442-3-LVRU6GP(OS300907)	IGF1R	gtccggaaagatgtacttt
MSH029442-4-LVRU6GP(OS300908)	IGF1R	caacggattgatcctaatg

2.1.6. Kinase inhibitor libraries

Table 4 and Table 5 report the kinase inhibitors supplied by GlaxoSmithKline for the accumulation assay screen. All compounds were supplied as 10 mM stocks in DMSO and stored at -20°C.

2.1.6.1. Preliminary screen

Table 4. Library of kinase inhibitors used for the preliminary screen

Reference	GSK Reg. No.	Primary Target
2A1	GW693481X	TGFBR
2A2	GW572738X	JNK
3A1	GSK200398A	EGFR/ErbB2
3A2	GW651576X	EGFR/ErbB2
A1	SB-239272	p38 MAPK

A2	GSK248233A	RHO
A3	GW296115X	PDGFR
A4	GW589961A	TIE2/VEGFR2
A5	GW806742X	VEGFR
A6	GSK586581A	IKK
A7	GW410563A	VEGFR
B1	GW801372X	GSK3
B2	SB-772077-B	RHO
B3	SB-400868-A	TGFBR
B4	SB-220025-A	p38 MAPK
B5	GI261520A	EGFR/ErbB2
B6	GW824645A	CDK2
B7	GSK1023156A	PLK
C1	GW679410X	TGFBR
C2	SB-675259-M	GSK3
C3	GW440139A	RET
C4	GW820759X	p38 MAPK
C5	GW642125X	TIE2/VEGFR2
C6	GW275616X	TRKA
C7	GW406731X	RAF
D1	GW549390X	VEGFR
D2	GW561436X	p38 MAPK
D3	GW768505A	TIE2/VEGFR2
D4	GW856804X	TIE2/VEGFR2
D5	GW461104A	EGFR/ErbB2
D6	GSK180736A	RHO
D7	GW559768X	RET
E1	GW575808A	LCK
E2	GSK319347A	IKK
E3	GW743024X	p38 MAPK
E4	GSK1713088A	IGF-1R
E5	GSK1000163A	AKT
E6	GSK237700A	PLK

F1	GW632580X	CSF
F2	GW837331X	PLK
F3	SB-358518	GSK3
F4	GW275944X	CDK2
F5	GSK554170A	AKT
F6	GW513184X	GSK3
G1	GSK317354A	RHO
G2	GW284372X	EGFR/ErbB2
G3	SB-437013	TIE2
G4	GW305074X	RAF
G5	SB-737198	MSK
G6	GSK1173862A	IGF-1R
H1	GW819230X	GSK3
H2	SB-744941	MSK
H3	SB-725317	GSK3
H4	GSK182497A	EGFR/ErbB2
H5	GR105659X	TRKA
H6	GSK953913A	IKK

2.1.6.2. Target Validation Screen

Table 5. Library of kinase inhibitors used for the target validation screen

Reference	GSK Reg. No.	Primary Target
A1	SB-226879	p38 MAPK
A2	GW775608X	p38 MAPK
A3	GW796921X	p38 MAPK
B1	SB-221466	p38 MAPK
B2	GW581744X	p38 MAPK
B3	GSK1511931A	IGF-1R
C1	GSK2186269A	IGF-1R
C2	GW607117X	p38 MAPK
C3	SB-223133	p38 MAPK

D1	GW618013A	p38 MAPK
D2	SB-242719	p38 MAPK
D3	GW434756X	p38 MAPK
E1	GSK1326255A	IGF-1R
E2	GW734508X	p38 MAPK
F1	GSK1220512A	IGF-1R
F2	GSK1819799A	IGF-1R
G1	GW769076X	p38 MAPK
G2	GSK2163632A	IGF-1R
H1	GW569293E	p38 MAPK
H2	GW782907X	p38 MAPK

2.1.7. Eukaryotic cell lines

Mouse neuroblastoma N2A cells and Lenti-X 293T (HEK) cells were maintained in adherent conditions. Hb9-GFP mouse embryonic stem cells were a gift from T.Jessell and H.Wichterle (Columbia University, New York, USA) (Wichterle et al., 2002).

2.1.8. Animals

Transgenic mice carrying a human wild-type SOD1 (B6SJLTg[SOD1]2Gur/J; $SOD1^{WT}$) or mutant $SOD1^{G93A}$ (Tg[SOD1-G93A]1Gur) gene were originally obtained from Jackson Laboratories. Colonies were maintained at the UCL Institute of Neurology Biological Services Unit by breeding male heterozygotes with female (C57BL/6 x SJL) F1 hybrids. Animals were housed in a controlled temperature and humidity environment and maintained on a 12 h light/dark cycle with access to food and water provided *ad libitum*.

All experiments were carried out under license from the UK Home Office in accordance with the Animals (Scientific Procedures) Act 1986 and the GSK Policy on the Care, Welfare and Treatment of Animals and were approved by the Institute of Neurology Ethical Review Committee.

2.2. Methods

2.2.1. Bacterial cultures

2.2.1.1. Preparation of chemically competent bacteria

E.coli XL1Blue were grown in 5 ml Luria Bertani (LB) medium overnight at 37°C, then expanded in an additional 500 ml of LB medium. The bacterial cultures were incubated at 37°C until an optical density (OD_{600}) of 0.35 was achieved. Bacteria were centrifuged at 3000*g* for 15 min at 4°C using a JA-10 rotor (Beckman) and the pellet resuspended in 400 ml ice-cold $MgCl_2$. Cells were harvested by centrifugation at 2000*g* for 15 min at 4°C and the pellet resuspended in 200 ml ice-cold $CaCl_2$. This suspension was incubated on ice for 20 min. The suspension was then centrifuged at 2000*g* for 15 min at 4°C and the pellet resuspended in 40 ml ice-cold 85 mM $CaCl_2$, 15% glycerol and transferred to a 50 ml falcon. Cells were then harvested by centrifugation at 1000*g* for 15 min at 4°C using a GH-3.8 rotor (Beckman) and resuspended in 2 ml ice-cold 85 mM $CaCl_2$, 15% glycerol. The final OD_{600} of the suspension was around 200. Finally the suspension was aliquoted and stored at -80°C.

2.2.1.2. Bacterial transformation

For each construct, 10 µl competent bacteria were diluted in 40 µl 100 mM $CaCl_2$, 20 % glycerol and 1 µl DNA added. The mix was incubated on ice for 30 min and then heat shocked at 42°C for 70 seconds. Bacteria were chilled on ice for 2 min and then 200 µl SOC medium was added. The bacteria were shaken at 37°C for 1 h and 10 µl of the culture plated on a pre-warmed LB agar plate containing ampicillin (100 µg/ml). Bacteria were grown overnight at 37°C and single colonies then picked and expanded in an appropriate volume of LB medium containing 100 µg/ml ampicillin.

2.2.2. Nucleic acid techniques

2.2.2.1. Isolation of plasmid DNA

Plasmid DNA was purified from bacterial cultures using either the QIAprep Spin Mini Prep kit or Maxi Prep kit according to the manufacturer's instructions.

2.2.2.2. Nucleic acid quantification

Isolated DNA was diluted in TE Buffer (10 mM Tris-HCl, pH 8.0; 0.1 mM EDTA) and its optical density at 260 (OD_{260}) measured using a Nanodrop spectrophotometer (Labtech International). 1 unit of OD_{260} corresponds to 50 mg/ml of double-stranded DNA.

2.2.2.3. Extraction of genomic DNA

Adult mouse ear snips and embryo tails were lysed overnight in 120 µl DirectPCR Lysis Reagent (Viagen Biotech) with 0.1 mg/ml Proteinase K in a shaking hot block at 55°C. The reaction was then inactivated at 95°C for 30 min.

2.2.2.4. Genotyping PCR

Genotyping was carried out using MegaMix Blue (Microzone Ltd.), a PCR mastermix containing recombinant Taq polymerase. 15 µl MegaMix Blue, 0.25 µl of each primer pair and 1 µl genomic DNA was used for each PCR reaction. The genotyping PCR programme used is shown below:

Step	Function	Temperature	Time (min)
1	Denaturation	95°C	3:00
2	Denaturation	95°C	0:30
3	Annealing	60°C	0:30
4	Extension	72°C	0:45
5	Repeat steps 2 → 4	35 times	
6	Final extension	72°C	2:00

An example of the PCR products obtained is shown in Figure 2.1.

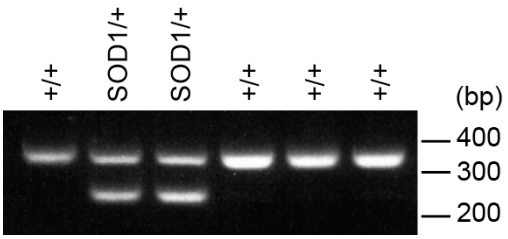

Figure 2.1. Genotyping of SOD1^{G93A} and SOD1^{WT} mice
The presence of the SOD1 gene was detected using IMR0113 and IMR 0114 primers and seen as a product at 236 bp. IMR 0042 and IMR 0043 primers were used as a control for the presence of DNA and yield a band at 324 bp.

2.2.2.5. DNA agarose electrophoresis

Electrophoresis was performed using 2% agarose gels in TBE (90 mM Tris-HCl, 90 mM boric acid, 2 mM EDTA pH 8.0) with ethidium bromide (0.5 µg/ml). Samples were either mixed with 10X DNA loading buffer (10% Ficoll 400, 25% glycerol, 10 mM Tris-HCl pH 7.6, 1 mM EDTA, 0.25% bromophenol blue) or loaded directly (genotyping PCR DNA). Samples were electrophoresed at 150 V for 40 min in TBE buffer.

2.2.3. Cell culture techniques

2.2.3.1. Culture of undifferentiated mouse embryonic stem (ES) cells

Prior to cell plating, tissue culture flasks were coated in 0.2% fish skin gelatin (diluted in distilled water) at room temperature for at least 30 min. Excess gelatin was removed just before plating cells. ES cells were maintained at 37°C and 5% CO_2 in growth medium composed of Glasgow MEM (GMEM), 5% ES-cell tested foetal bovine serum (FBS), 5% knockout serum replacement (Gibco), 1% GlutaMAX, 0.1 mM β-mercaptoethanol and 1000 units/ml leucocyte inhibitory factor (LIF). ES cells were passaged every other day. Growth medium was removed and ES cells were trypsinised with 0.05% trypsin/versene for 1 minute at 37°C. Cells were resuspended in growth medium and pelleted by centrifugation at 1000 rpm for 3 min. The cells were resuspended in growth medium and plated. ES cells were fed on alternate days.

2.2.3.2. Differentiation of mouse ES cells into motor neurons

ES cells were trypsinised, resuspended in growth medium and counted. 1.2 x 10^6 cells were centrifuged at 1000 rpm for 3 min, washed in differentiation medium (DFNK), comprising DMEM/F12, Neurobasal, 10% knockout serum replacement, 1% GlutaMAX and 0.1 mM β-mercaptoethanol, and finally resuspended in 6 ml DFNK. Resuspended cells were plated in 50 mm petri dishes and incubated at 37°C with 5% CO_2.

The day after seeding, the forming embryoid bodies were centrifuged at 1000 rpm for 3 min, resuspended in 10 ml fresh DFNK and plated in a fresh dish. On the following day, embryoid bodies were allowed to settle by gravity and then resuspended in fresh DFNK supplemented with 1 μM all-trans retinoic acid (RA) and 333 nM sonic hedgehog agonist (SAG). DFNK containing RA and SAG was replaced every day until the embryoid bodies were dissociated.

2.2.3.3. Dissociation of embryoid bodies

Embryoid bodies were allowed to settle and were then washed in PBS. Embryoid bodies were resuspended in 1 ml PBS and dissociated by incubation with 10 μl of 2.5% trypsin in PBS (final concentration 0.025%) for 10 min at 37°C, followed by trituration. Once dissociated, the cells were triturated in 1 ml Leibovitz 15 (L-15) medium containing 0.1 mg/ml DNase and 0.4% bovine serum albumin (BSA) and any fragments were allowed to settle. The supernatant was then transferred to 1ml Leibovitz 15 (L-15) medium containing 0.02 mg/ml DNase and 0.4% BSA and triturated further if necessary. A 1.5 ml BSA cushion (4% BSA in L-15) was applied and the cell suspension centrifuged for 5 min at 1000 rpm. The resulting cell pellet was resuspended in 1 ml motor neuron medium (see Section 2.2.3.7) and centrifuged at 1000 rpm for 1 min. The resulting pellet was resuspended in 10 ml motor neuron medium supplemented with 1 μM retinoic acid and the number of cells counted. The cells were then plated on poly-ornithine/laminin coated dishes.

2.2.3.4. N2A and HEK cell culture

N2A and HEK cells were maintained in culture medium (DMEM, 10% horse serum, 2 mM glutamine) at 37°C in a 5% CO_2 incubator. When cells became confluent, the medium was removed, the cells washed once with PBS and then detached using trypsin. Trypsin was inhibited by addition of culture medium. Resuspended cells were centrifuged at 1000 rpm for 3 min at 24°C and then plated in fresh tissue culture flasks.

2.2.3.5. Coating of plates, dishes and coverslips for motor neuron cultures

Plates, dishes and coverslips were coated overnight at 37°C with poly-ornithine (1.5 mg/ml diluted in distilled H_2O). The poly-ornithine was removed, and laminin (3 µg/ml diluted in Neurobasal medium) was added for 4 h at 37°C. Just before plating, the laminin was removed and the dishes/coverslips/plates washed with Neurobasal medium.

2.2.3.6. Isolation of mouse spinal cord motor neurons

Motor neurons were isolated from the spinal cords of E11.5-13.5 mouse embryos (Arce et al., 1999). Embryos were sacrificed and the spinal cords dissected in HBSS containing Penicillin/Streptomycin antibiotics (Pen/Strep). The meninges and dorsal horns were removed and the remaining ventral horns minced and collected in 500 µl HBSS. Ventral horns from each embryo were collected in separate tubes in order to prevent contamination of different genotypes. Ventral horns were dissociated by incubation with 0.025% trypsin in PBS for 10 min at 37°C, followed by trituration. Once dissociated, the cells were triturated in 1 ml Leibovitz 15 (L-15) medium containing 0.1 mg/ml DNase and 0.4% BSA, and then 1ml Leibovitz 15 (L-15) medium containing 0.02 mg/ml DNase and 0.4% BSA was added. A 1 ml BSA cushion (4% BSA in L-15) was applied and the cell suspension centrifuged for 5 min at 1500 rpm. The resulting cell pellet was resuspended in 100 µl L-15. 500 µl motor neuron medium (see Section 2.2.3.7) was then added and the cells immediately plated on poly-ornithine/laminin coated dishes.

2.2.3.7. Maintenance of primary motor neuron cultures

Primary motor neurons were maintained at 37°C and 5% CO_2 in motor neuron medium comprising Neurobasal (Gibco), 2% v/v B27 supplement (Gibco), 2% heat inactivated horse serum, 1% GlutaMAX (Invitrogen), 25 µM β-mercaptoethanol, 10 mg/ml recombinant rat ciliary neurotrophic factor (CNTF; R&D Systems), 100 pg/ml recombinant rat glial derived neurotrophic factor (GNTF; R&D Systems), 1 ng/ml recombinant human brain derived neurotrophic factor (BDNF; R&D Systems) and Pen/Strep. Motor neurons were maintained in culture for 5-8 days.

2.2.3.8. Preparation of microfluidic chambers

Microfluidic chambers were prepared at the Cui laboratory (Stanford, CA), as previously described (Zhang et al., 2010). Briefly, two compartment microfluidic chips were made out of polydimethyl silane (PDMS) and washed with detergent followed by distilled water and then sterilized by autoclaving before use. Microfluidic devices were constructed by pressing the PDMS chips onto the PLL-coated coverslips.

2.2.3.9. Primary hippocampal neuron cultures

Prior to dissection, glass coverslips were coated with 0.2 mg/ml poly-L-lysine (diluted in dH_2O) overnight at 37°C. Coverslips were then washed in distilled H_2O and allowed to dry.

E18 wild type rat embryos were sacrificed and their brains extracted. The meninges were removed, the brain bisected, the cerebellum removed and the hippocampus isolated from each hemisphere of the cerebrum. The hippocampi were collected on ice in HBSS containing Pen/Strep.

Hippocampi were incubated with 0.025% trypsin at 37°C for 8 min. The trypsinised hippocampi were then centrifuged at 1000 rpm for 5 min, and the supernatant removed. The hippocampi were resuspended in hippocampal plating medium (Neurobasal, 2% v/v B27 supplement, 0.5 mM glutamine, 25 µM glutamate,

1 mM HEPES, 10% heat inactivated FBS and Pen/Strep) and mechanically dissociated by trituration. Fragments were allowed to settle, the supernatant transferred to a fresh tube and the neurons plated on the cell body side of microfluidic chambers and incubated at 37°C with 5% CO_2. After 2-4 h the plating medium was replaced with differentiation medium (Neurobasal, 2% v/v B27 supplement, 0.5 mM glutamine, 1 mM HEPEs and Pen/Strep). Once the medium had flowed through the microgrooves, differentiation medium was added to the axonal side. Hippocampal neurons were maintained in culture for 7-10 days.

2.2.3.10. Primary dorsal root ganglion (DRG) cultures

Primary DRG cultures were prepared by James Sleigh (Institute of Neurology, UCL) as previously described (Malin et al., 2007) but with minor alterations. Briefly, ≈20 thoracic and lumbar DRG ganglia were dissected from 3 month-old wild-type mice in Ca^{2+}/Mg^{2+}-free Hank's Balanced Salt Solution (Life Technologies) supplemented with 1% Penicillin-Streptomycin. To produce single cell cultures, DRG were enzymatically digested for 10 min in papain solution (60 U papain [Worthington 3126], 1 mg/ml L-cysteine, and 0.2 mg/ml $NaHCO_3$ in HBSS) followed by 10 min in collagenase/dispase solution (4 mg/ml collagenase type II [Worthington 4176] and 4.67 mg/ml dispase II in HBSS). Cells were plated onto MatTek dishes coated with 20 µg/ml poly-D-lysine (BD Biosciences) overnight at 4°C followed by 20 µg/ml laminin for 4-6 h at 37°C. DRG cultures were maintained for 48 h in F12 media (Life Technologies) supplemented with 10% FBS, 1% Pen/Strep, 20 ng/ml mouse GDNF, and 50 ng/ml mouse nerve growth factor (NGF; Peprotech) before imaging.

2.2.4. Harvesting of mouse tissue

2.2.4.1. Spinal cord collection

Mice were anaesthetised by i.p. injection of Euthatal (150 mg/kg) and transcardially perfused with PBS. Spinal cords were dissected and then snap-frozen in liquid nitrogen and stored at -80°C.

2.2.4.2. Cryosectioning of sciatic nerves

Sciatic nerves from both hind legs were dissected and fixed in 4% paraformaldehyde (PFA) in PBS for 15 min at room temperature. Sciatic nerves were then transferred to 20% sucrose in PBS and incubated overnight at 4°C. Samples were then embedded in OCT tissue freezing medium and 20 µm sections cut on the cryostat. DAPI was applied for 10 min at room temperature and the samples were washed with PBST three times for 5 min each. Samples were then post-fixed in 4% PFA in PBS for 30 min at room temperature and mounted using Dako fluorescent mounting medium.

2.2.5. Protein techniques

2.2.5.1. Cell lysate preparation

Cells were cooled on ice and washed with ice-cold Hanks. Cells were then scraped in RIPA buffer (50 mM Tris pH 7.5, 150 mM NaCl, 1% Triton X-100, 0.5% sodium deoxycholate, 0.1% SDS) containing Halt phosphatase and protease inhibitor cocktail (1:100, Pierce Biotechnology) and the lysate incubated on ice for 20 min. Lysates were then spun at 14000 rpm for 20 min and the pellet discarded.

2.2.5.2. Spinal cord lysate preparation

Spinal cords were defrosted on ice then homogenised in RIPA buffer (50 mM Tris pH 7.5, 150 mM NaCl, 2% NP-40, 0.5% sodium deoxycholate, 0.1% SDS, 2 mM EDTA) containing Halt phosphatase and protease inhibitor cocktail. The lysate was incubated on ice for 20 min and then spun at 14000 rpm for 20 min and the pellet discarded.

2.2.5.3. Protein quantification

The protein content of cell lysates was determined using the Bio-Rad protein assay reagent. Briefly, dilutions of the lysate and BSA standards were made in 200 µl of the assay reagent (dilute 1 to 4 in distilled water) in a 96 well NUNC plate. The

absorption at 595 nm was then measured using a Fluostar Omega plate reader (BMG Labtech). The absorption profile of the BSA standards was used to determine the protein concentration of lysates.

The protein content of the spinal cord lysates was determined using the BCA assay (Pierce Biotechnology) according to the manufacturer's instructions using BSA as standard.

2.2.5.4. SDS-Polyacrylamide Gel Electrophoresis (SDS-PAGE)

Samples were mixed with 5X Laemmli sample buffer (15% SDS, 312.5 mM Tris-HCl pH 6.8, 50% glycerol, 16% β-mercaptoethanol, 0.1% bromophenol blue) and incubated at 100°C for 4 min. SDS-PAGE was performed using 4–12% NuPAGE Bis-Tris gradient gels (Life Technologies) and MOPS buffer (Invitrogen) according to the manufacturer's instructions. Gels were run at 60 V for 10 min then at 200 V for 60 min.

2.2.5.5. Western blotting

Proteins were transferred onto methanol-activated polyvinylidene fluoride (PVDF) membranes (Millipore) in NuPAGE transfer buffer (Invitrogen) containing 10% methanol. Transfers were performed either at room temperature for 3 h at 30V or at 4°C overnight at 15V. Membranes were blocked in 5% BSA dissolved in Tris-buffered saline containing 0.5% Tween-20 (TBST) for 1 h at 4°C and then incubated with primary antibodies either overnight at 4°C or at room temperature for 1 h. Blots were washed 4 times for 5 min each with TBST and then incubated with the appropriate HRP-conjugated secondary antibodies (GE Healthcare) diluted in 5% milk in TBST. Finally blots were washed 4 times for 5 min each with TBST, rinsed once in distilled water and the immunoreactivity detected using Crescendo ECL substrates (Millipore) and Fujifilm X-ray films (Fisher Scientific). Films were scanned and the intensity of bands analysed using ImageJ software.

2.2.5.6. Fluorescent labelling of H_CT with AlexaFluor dyes

1.5 mg H_CT protein was diluted in labelling buffer (10 mM HEPES-NaOH pH 7.4, 250 mM NaCl) containing a 10X molar excess of tris-(2-carboxyethyl)phosphine hydrochloride (TCEP). The reaction mixture was incubated for 30 min at 4°C and then a 25X molar excess of AlexaFluor 647 C2 Maleimide or AlexaFluor 555 C2 Maleimide in DMSO (Invitrogen) was added under stirring. The resulting mixture was incubated at 4°C overnight in the dark with constant agitation. The labelling reaction was stopped by addition of 4 mM reduced glutathione in Tris-HCl (pH 8.0). The labelled protein was isolated from free dye using a PD10 desalting column (GE Healthcare), equilibrated with ice-cold PBS, according to the manufacturer's instructions and then dialysed over three days against ice-cold dialysis buffer (10 mM HEPES-NaOH, 100 mM NaCl, pH 7.4) at 4°C in the dark. Finally the labelled protein was concentrated using an Amicon Ultra-0.5 filter device (EMD Millipore) according to the manufacturer's instructions and then aliquoted, snap frozen in liquid nitrogen and stored at -80°C.

2.2.5.7. Fluorescent labelling of the $p75^{NTR}$ antibody with AlexaFluor dyes

$p75^{NTR}$ antibody (α-$p75^{NTR}$) raised against the extracellular domain of the $p75^{NTR}$ (batch 5410, 0.8 mg/ml) (Deinhardt et al., 2007) was dialysed in PBS at 4°C under stirring for 48 h to remove glycine present in the storage buffer. The antibody was then concentrated using an Amicon Ultra-0.5 filter device (EMD Millipore) according to the manufacturer's instructions until a final concentration of 1 mg/ml was achieved. The antibody was then labelled using the AlexaFluor 647 monoclonal antibody labelling kit (Life Technologies) according to the manufacturer's instructions. The concentration of the labelled antibody was determined using a Nanodrop spectrophotometer (Labtech International) and the antibody then stored at 4°C in the dark.

2.2.6. Cell-based assays

2.2.6.1. H_CT and α-$p75^{NTR}$ binding assay

Motor neurons plated on coverslips were cooled on ice for 2 min, the medium removed and ice-cold motor neuron medium containing 20 nM AlexaFluor 555-conjugated H_CT and 0.2 µg/ml α-$p75^{NTR}$ antibody added. Motor neurons were then incubated at 4°C for 10 min, washed twice with ice-cold Hanks and fixed on ice in 4% PFA in PBS for 15 min. After fixation, motor neurons were washed once with PBS.

2.2.6.2. H_CT and α-$p75^{NTR}$ accumulation assay

For the accumulation assay screening, ES cell-derived motor neurons were plated on poly-ornithine/laminin-coated 24 well glass bottom plates (MatTek Corporation) and the assay was performed 3 days after dissociation of embryoid bodies.

Motor neurons were cooled on ice for 2 min, the medium removed and fresh motor neuron medium containing 20 nM AlexaFluor 555-conjugated H_CT and 0.2 µg/ml α-$p75^{NTR}$ added. Motor neurons were then incubated at 37°C, 5% CO_2 for 2 h.

After 2 h, motor neurons were cooled on ice for 5 min, acid washed on ice with a solution of 100 mM citrate-NaOH, 142 mM NaCl (pH 2.0) for 1.5 min, washed twice with ice-cold Hanks and then fixed with 4% PFA in PBS for 15 min at room temperature. After fixation, motor neurons were washed once with PBS.

2.2.6.3. H_CT and α-$p75^{NTR}$ internalisation assay

Motor neurons were cooled on ice for 2 min, the medium removed and fresh motor neuron medium containing 20 nM AlexaFluor 555-conjugated H_CT and 0.2 µg/ml α-$p75^{NTR}$ added. Motor neurons were then incubated at 37°C, 5% CO_2 for 20 min, to allow for internalisation of the probes but before axonal transport was significant. Motor neurons were then cooled on ice for 5 min, acid washed on ice (as described in Section 2.2.6.2) for 1.5 min, washed twice with ice-cold Hank's and then fixed

with 4% PFA in PBS for 15 min at room temperature. After fixation, motor neurons were washed once with PBS.

2.2.6.4. Transfection of N2A cells with shRNA

N2A cells in 6 well plates were transfected with 2.5 µg DNA using Lipofectamine 3000 according to the manufacturer's instructions. N2A cells were incubated overnight with the transfection mix and then fresh medium was applied. Cells were assayed after 3 days.

2.2.6.5. Production of lentiviral shRNA particles

shRNA constructs directed against p38 MAPKα and δ and scrambled controls were purchased from the GeneCopoeia OmicsLink™ shRNA clone collection (all constructs were in psi-LVRU6GP plasmids with an eGFP reporter gene). HEK239 cells were co-transfected with shRNA, packaging, and envelope plasmid vectors using Lipofectamine 3000 (Life Technologies) according to the manufacturer's instructions. Medium containing lentiviral particles was collected every day for 3 days after transfection. Medium containing viral particles was then concentrated using LentiX Concentrator (ClonTech) according to the manufacturer's instructions and the concentrated lentiviral particles resuspended in complete MN medium. Lentiviral particles were aliquoted and stored at −80°C until further use. The lentivirus titre was determined using the Lenti-X p24 Rapid Titre kit (ClonTech) and the concentration was adjusted so that the titre of all lentiviral shRNA preparations was equal.

2.2.6.6. Transduction of primary motor neurons

To transduce primary motor neurons, lentivirus was added to the culture medium 6 h after plating. The medium was replaced with fresh motor neuron medium 16 h after transduction, and motor neurons were assayed 1 week later.

2.2.7. Imaging techniques

2.2.7.1. Immunocytochemistry and confocal imaging of fixed samples on coverslips

Cells on coverslips were fixed in 4% PFA in PBS for 15 min at room temperature. Coverslips were then washed with PBS and permeabilised and blocked for 1 h in a solution of 5% BSA and 0.1% Triton X-100 in PBS. Primary antibodies were diluted in 5% BSA in PBS and incubated overnight at 4°C. Coverslips were washed 3 times in 5% BSA, then incubated with the appropriate fluorescently conjugated secondary antibodies diluted in 5% BSA for 1 h at room temperature. Finally coverslips were washed 3 times with PBS, once with water and then mounted using Mowiol-488. Coverslips were imaged with either an invert Zeiss LSM 780 confocal microscope using either the 40X EC Plan-Neofluar oil immersion objective with a numerical aperture (NA) of 1.3 or a 63X Plan-Apochromat oil immersion objective with an NA of 1.4. Immunofluorescence staining was quantified using ImageJ.

2.2.7.2. Immunocytochemistry and confocal imaging of fixed samples in 24 well glass-bottom plates

After fixation, motor neurons were blocked and permeabilised using a solution of 10% goat serum, 2% BSA, 0.25% fish skin gelatin and 0.1% Triton X-100 in PBS for 1 h at room temperature. The motor neurons were then stained with AlexaFluor 647-conjugated donkey anti-rabbit secondary antibody diluted in 10% goat serum, 2% BSA and 0.25% fish skin gelatin in PBS for 45 min at room temperature. Finally motor neurons were washed 3 times with PBS and the plates sealed with parafilm and stored in the dark at 4°C until they were imaged.

24 well plates were imaged on an invert Zeiss LSM 510 microscope equipped with a 40X Plan-Apochromat oil immersion objective with an NA of 1.4. The Zeiss LSM 510 had an automated stage that, when used in combination with the Multi Field Acquisition (MTS) macro, allowed automated image acquisition to be performed overnight. The autofocus function of the MTS macro allowed the focal plane to be

determined using the GFP channel (i.e. focusing specifically on the motor neurons) and a tile of 36 images was acquired per well.

2.2.7.3. Live in vitro axonal transport assays

For *in vitro* assays, motor neurons were plated on poly-ornithine/laminin coated 35 mm glass bottom MatTek dishes. Assays were performed 3-5 days after embryoid body dissociation (ES cell-derived motor neurons) or 5-8 days after plating (primary motor neurons). Motor neurons were incubated with either 40 nM AlexaFluor 555 or 647-conjugated H_CT, 1 µg/ml AlexaFluor 647-conjugated α-$p75^{NTR}$ or 100 nM LysoTracker Red DND-99 (Life Technologies) for 25 min at 37°C, 5% CO_2. For samples treated with experimental compounds, the compounds were applied at the same time as the H_CT or α-$p75^{NTR}$ probe. For control samples, DMSO was added at this time. After 25 min, motor neurons were washed once with pre-warmed motor neuron medium and then imaged in 2 ml fresh pre-warmed motor neuron medium or imaging medium (156 mM NaCl, 10 mM HEPES, 10 mM D-glucose, 3 mM KCl, 2 mM $MgSO_4$, 2 mM $CaCl_2$, 1.25 mM KH_2PO_4, pH 7.35) containing the selected compound. MatTek dishes were then placed in an environmental chamber heated to 37°C and imaged using either an invert Zeiss LSM 510 or 780 confocal microscope with the 63X Plan-Apochromat oil immersion objective with a NA of 1.4. Images were acquired every 2-3 seconds at 100X zoom, using a resolution of 1024 X 1024 pixels (Movie 1).

Primary hippocampal neurons in two compartment microfluidic chambers were incubated with 0.5 nM quantum dot-wheat germ agglutinin (WGA; Life Technologies) on the axonal side for 2 h at 37°C, 5% CO_2. In drug-treated experiment, compound was added for the final 25 min of the incubation. The neurons were then washed once with pre-warmed differentiation medium and then imaged in fresh pre-warmed differentiation medium, containing compound if appropriate, using an invert microscope (Leica DMI6000 B) with a temperature-controlled stage (Warner Instrument) at a frame rate of 2 frames/second (Xie et al., 2012) (Movie 2).

2.2.7.4. In vivo imaging of axonal transport

In vivo axonal transport assays were performed in 73 d (± 3 d) old wild type (non-transgenic) and SOD1^{G93A} mice. A detailed method is described in Section 4.4.1. Briefly, mice were anesthetized using isoflurane (National Veterinary Services) and AlexaFluor 555-conjugated H_CT (13 µg) and BDNF (50 ng) were injected intramuscularly (i.m) into the exposed tibialis anterior and gastrocnemius muscles of the right hind leg and the wounds then sutured. At this time, mice were also injected intraperitoneally (i.p.) with either 100 mg/kg SB-239063 or an equivalent volume of vehicle control (1% methyl cellulose [Sigma 274429]). The skin of the hind leg was then sutured and the mice were then left to recover from the procedure and kept under standard conditions with unlimited food and water supply. Four hours later, the mice were re-anesthetized using isoflurane and the sciatic nerve of the right leg exposed. The anaesthetised mouse was placed on a heated stage in an environmental chamber (both kept at 37°C) and axonal retrograde transport was imaged in the intact sciatic nerve by time-lapse confocal microscopy. An invert Zeiss LSM 780 with 63X Plan-Apochromat oil immersion objective (NA = 1.4) was used to locate the sciatic nerve and visualise labelled axons (Movie 3). Time lapse images were then acquired at 100X zoom every 3-4 s using a resolution of 1024 X 1024 pixels (Movie 4).

2.2.8. Data analysis and quantification

2.2.8.1. Quantification of the accumulation assay screen

Confocal images were exported as TIFFs and analysed using the Cell Profiler software, developed by Anne Carpenter and Thouis John (http://www.cellprofiler.org/), which allows automated analysis of large image datasets. The software was instructed to identify cell bodies using the GFP channel (motor neurons were *Hb9-GFP* positive), according to size and intensity constraints. This "cell body" mask was then used to isolate the corresponding H_CT and α-p75^{NTR} signals. Mean staining intensity in the cell body, average number of H_CT and/or α-p75^{NTR}–labelled vesicles per cell, the size of labelled vesicles and the staining intensity in individual vesicles was measured. The resulting data were analysed using Microsoft Excel and Prism software.

2.2.8.2. Axonal transport tracking

For H_CT, α-$p75^{NTR}$ and lysotracker axonal transport experiments, time-lapse images were exported as .avi files and cargoes were manually tracked using Motion Analysis software (Kinetic Imaging). Cargoes were only tracked if they crossed the entire width of the frame. The speed of individual steps was calculated using an Excel kinetic analysis macro developed by Niran Nirmalananthan and the speed distribution was obtained using a 0.2 μm/s binning interval.

For axonal transport tracking in primary hippocampal neurons performed at the Cui laboratory (Stanford, CA), ImageJ was used to create kymographs and the average speed of individual cargoes determined as the distance moved within the observation time.

2.2.8.3. Statistical tests

Statistical analysis was performed using Graphpad Prism software. In order to determine the most appropriate statistical test to use, data were tested for normality using three tests: D'Agostino & Person omnibus normality test, Shapiro-Wilk normality test and KS normality test. If the data were found to be normally distributed (the majority of the normality tests giving a positive result), either a Student's t-test (n = 2 groups to compare) or one-way analysis of variance (ANOVA) (n > 2 groups to compare), followed by Dunnett's or Sidak's multiple comparisons test, was used. If the data were not found to be normally distributed, a Kruskal-Wallis test was used, followed by Dunn's multiple comparison test (n > 2 groups to compare). If there were too few data points to accurately test for normality, the data were assumed to be normally distributed. The test used and associated *p* values are indicated in the figure legends.

In order to determine statistical significance of axonal transport data, the average speed was calculated by taking the mean of the mean speeds for individual axons of each biological replicate and a t-test (n = 2 conditions) or ANOVA (n >2) was performed. Error bars on speed profiles represent standard error of the mean (SEM).

Chapter 3. Identifying novel enhancers of retrograde axonal transport

3.1. Introduction

The aim of the experiments performed in this Chapter was to develop and perform a screen to identify novel enhancers of retrograde axonal transport in motor neurons.

Marco Terenzio, a former PhD student in the laboratory, previously performed an siRNA screen looking for novel players in the internalisation and trafficking of neurotrophin receptors in motor neurons (Terenzio et al., 2014b, Terenzio et al., 2014a). The read-out for this screen was the intracellular accumulation of the binding fragment of tetanus toxin (H_CT) and an antibody directed against the extracellular domain of the p75 neurotrophin receptor (α-$p75^{NTR}$). The screen was performed in mouse embryonic stem cell (ES)-derived motor neurons that were engineered to express GFP under the motor neuron-specific Hb9 promoter, allowing easy identification of motor neurons after ES cell differentiation, without the need for immunofluorescence.

In this Chapter, I adapted this assay in order to screen a small molecule library of kinase inhibitors for novel pharmacological regulators of retrograde axonal transport. The accumulation assay was used as a preliminary screen to identify hit compounds, whose effects on retrograde axonal transport would then be explored in live *in vitro* axonal transport assays. In this way, relatively large numbers of compounds could be screened for their effects on retrograde axonal transport.

3.1.1. Neuronal trafficking of H_CT and α-$p75^{NTR}$

The binding, internalisation and transport of the two probes used in the screen, H_CT and α-$p75^{NTR}$, has been well characterised (Lalli and Schiavo, 2002, Lalli et al., 2003a, Deinhardt et al., 2006b). The H_CT probe used (H_CT^{441}, residues 875–1315) is a truncated form of the heavy chain of tetanus toxin (Figure 3.1), with a cysteine-rich tag fused to the amino terminus (Lalli et al., 2003a). This version of H_CT has a

long shelf life and reduced processing by tissue proteases (Restani et al., 2012). In addition, the probe is non-toxic whilst still being efficiently trafficked by neurons, and can be easily labelled with fluorophores.

H_CT has been shown to bind to nidogens and polysialogangliosides at the neuromuscular junction (Rummel et al., 2003, Bercsenyi et al., 2014) and undergo clathrin-mediated endocytosis (Deinhardt et al., 2006a). It is transported back to the soma in non-acidic endosomes and has been shown to be co-transported in signalling endosomes with $p75^{NTR}$, NGF, TrkB and BDNF (Lalli and Schiavo, 2002, Deinhardt et al., 2006b). In its full-length form, tetanus toxin is then transcytosed to inhibitory interneurons, where the light chain zinc-endopeptidase mediates synaptic silencing through cleavage of VAMP/synaptobrevin, a synaptic SNARE protein (Schiavo et al., 1992a, Schiavo et al., 1992b). The axonal transport of H_CT is therefore thought to be exclusively in the retrograde direction. As H_CT has not been localised in acidic organelles in the cell body of motor neurons (Lalli and Schiavo, 2002, Bohnert and Schiavo, 2005), it is thought that it is able to by-pass lysosomal targeting and degradation.

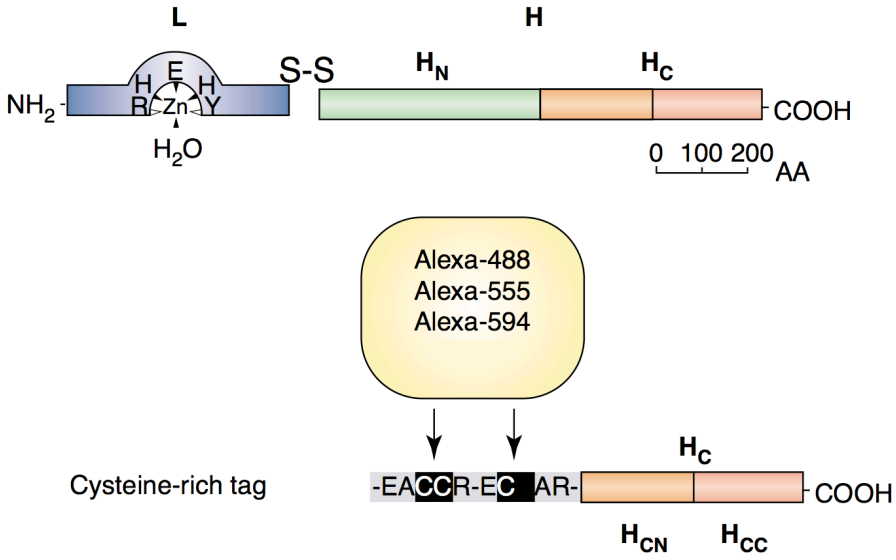

Figure 3.1. The domain structure of tetanus toxin

Tetanus toxin is composed of two chains: heavy (H) and light (L). The light chain is a zinc-endopeptidase that cleaves VAMP/synaptobrevin and causes inhibition of neurotransmitter release. The H chain is comprised of an N-terminal domain (H_N) and a C-terminal domain (H_C). The H_C domain is responsible for the toxin's neurospecific binding and mediates retrograde axonal transport. Modified from (Lalli et al., 2003a). Reprinted with permission from Elsevier.

$p75^{NTR}$ is a transmembrane receptor that binds all four members of the neurotrophin family - nerve growth factor (NGF), brain-derived neurotrophic factor (BDNF), neurotrophin-3 (NT-3) and neurotrophin-4 (NT-4). $p75^{NTR}$ is able to form heterodimers with a number of co-receptors and interacts with a variety of adapter proteins. As a result the receptor is involved in a wide range of physiological responses in the nervous system. $p75^{NTR}$ is widely expressed throughout the developing nervous system, but in most cells is switched off at adult stages. Two exceptions to this are sensory neurons and spinal cord motor neurons, which retain a low level of $p75^{NTR}$ expression (Ibanez and Simi, 2012). Like other neurotrophin receptors, $p75^{NTR}$ is activated at distal axonal sites and is subsequently internalised and retrogradely transported back to the soma where it mediates its effects. The internalisation and sorting of $p75^{NTR}$ to the retrograde transport route has been shown to be dependent on clathrin-mediated endocytosis and the activity of the small GTPases Rab5 and Rab7 (Deinhardt et al., 2006a, Deinhardt et al., 2006b, Deinhardt et al., 2007). $p75^{NTR}$ is not thought to be targeted to the lysosome for degradation, but has instead been proposed to recycle back to the plasma membrane (Deinhardt et al., 2007) and/or be released in exosomes into the extracellular medium (Escudero et al., 2014).

H_CT and α-$p75^{NTR}$ are therefore ideal probes to use to investigate the effect of pharmacological compounds on retrograde axonal transport in motor neurons.

3.1.2. Protein kinases as a therapeutic target

Protein kinases are a very popular target in current pharmaceutical development as they are involved in a huge variety of signalling cascades and have been implicated in a multitude of diseases. At present, there are over 30 compounds approved by the FDA that target protein kinases and several hundred projects involving protein kinases have been registered for clinical trials. Much of the attention of the pharmaceutical industry so far has been focused on the use of kinase-targeting drugs in the treatment of cancer and chronic inflammatory diseases.

Protein kinases have, however, also been implicated in disorders of the CNS. It has been proposed that disease-associated pathological proteins, such as Aβ and

$SOD1^{G93A}$, mediate their toxic effects through activation of specific kinase cascades (Kanaan et al., 2013). Dysregulation of kinase activity is a common feature of a number of neurodegenerative diseases, including p38 MAPK in ALS, GSK3β in Alzheimer's disease and JNK3 in Parkinson's disease, to name but a few (Chico et al., 2009). A major problem in targeting protein kinases in the CNS is designing inhibitors that are able to cross the blood brain barrier. However, this is an issue that the pharmaceutical industry has been addressing for a long time and a number of protein kinase inhibitors have now reached clinical trials for CNS disorders (Chico et al., 2009).

There is also clear evidence implicating a range of protein kinases in the regulation of axonal transport, including GSK3β, Cdk5, JNK3, Akt and p38 MAPK. Protein kinases have been shown to directly phosphorylate molecular motors and their motor adapter proteins. For example, p38 MAPK and JNK3 have been shown to phosphorylate kinesin-1 directly, reducing the efficiency with which kinesin-1 moves along axonal microtubules and therefore inhibiting anterograde axonal transport (Morfini et al., 2009, Morfini et al., 2013). Cyclin dependent kinase 5 (Cdk5), on the other hand, has been shown to positively regulate retrograde axonal transport through phosphorylation of the dynein-associated protein Ndel1 and reduction of its inhibitory effect on dynein activity (Pandey and Smith, 2011).

Given the role of protein kinases in both the regulation of axonal transport and neurodegeneration, we decided to screen a library of kinase inhibitors in search of novel enhancers of retrograde axonal transport.

3.2. Validating the accumulation assay as a screen for novel modulators of retrograde axonal transport

Based on previous work in the laboratory, our hypothesis was that the accumulation of H_CT and α-$p75^{NTR}$ in the cell body of motor neurons would act as a read-out for the efficiency of retrograde axonal transport. Robust axonal transport is only detected *in vitro* following 20-30 minutes incubation with probes such as H_CT and α-$p75^{NTR}$, therefore it was decided to assess accumulation in the cell body after two hours. Firstly, it was necessary to determine whether the somal accumulation of H_CT and α-$p75^{NTR}$ in motor neurons was a suitable assay to screen compounds for their effects on retrograde axonal transport. To this end, the assay was performed in ES-derived motor neurons in the presence of known inhibitors and enhancers of retrograde axonal transport, as well as in primary $SOD1^{G93A}$ motor neurons in which defects in retrograde axonal transport have been described (Kieran et al., 2005, Bilsland et al., 2010).

3.2.1. Determining the sensitivity of the accumulation assay to changes in retrograde axonal transport speed

In order to determine whether the accumulation assay was sensitive to decreases in axonal transport efficiency, I performed the assay in the presence of known inhibitors of retrograde axonal transport. Erythro-9-(2-hydroxy-3-nonyl)adenine (EHNA) is an established inhibitor of cytoplasmic dynein, that acts to inhibit the ATPase activity of the motor (Penningroth et al., 1982). Treatment of motor neurons with 1 mM EHNA has previously been shown to cause a significant inhibition of the retrograde axonal transport of H_CT-containing endosomes (Figure 3.2A) (Lalli et al., 2003b, Deinhardt et al., 2007, Terenzio et al., 2014b). Incubation of ES-derived motor neurons with 1 mM EHNA together with H_CT and α-$p75^{NTR}$ was found to cause a decrease in the staining intensity of both probes in the cell body (Figure 3.2B-D), indicating that the sensitivity of this assay is sufficient to detect reductions in retrograde axonal transport efficiency. However, EHNA is not a selective inhibitor of cytoplasmic dynein. It has also been reported to cause morphological and functional changes to the actin cytoskeleton (Schliwa et al., 1984), inhibit cyclic GMP-stimulated phosphodiesterase activity (Mery et al., 1995)

and potently inhibit adenosine deaminase (Woodson et al., 1998). It therefore cannot be ruled out that its effects on the somatic accumulation of H_CT and α-$p75^{NTR}$ may be a consequence of one or more of these off-target effects.

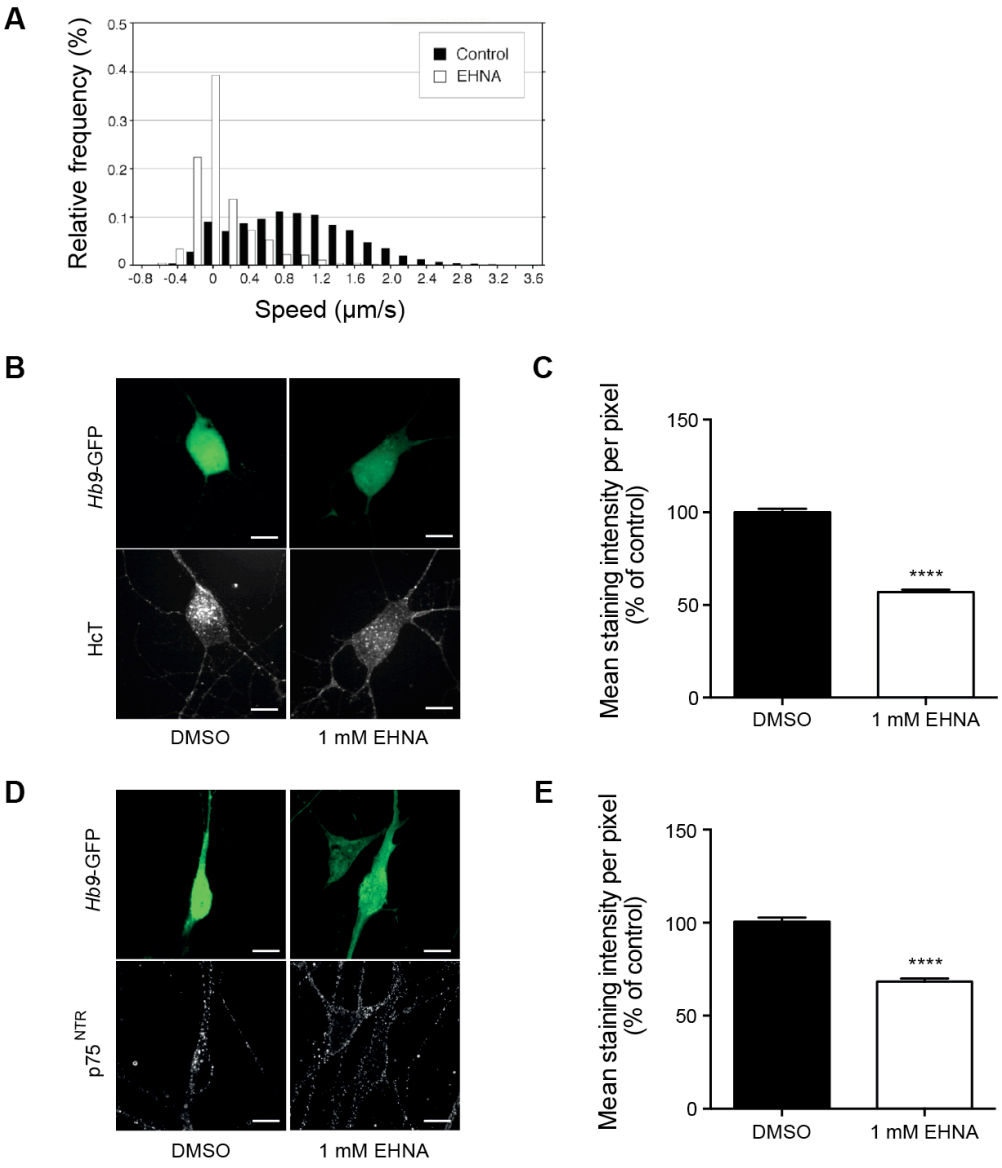

Figure 3.2. Inhibition of retrograde axonal transport by EHNA is detected by the accumulation assay

(A) Treatment of motor neurons with 1 mM EHNA has been previously shown to cause a significant inhibition of the retrograde axonal transport of H_CT (Lalli et al., 2003b). Reprinted with permission from the Company of Biologists. (B, C) Treatment of ES-derived motor neurons with 1 mM EHNA causes a significant decrease in the accumulation of H_CT in the cell body compared to the DMSO control. Results are expressed as a percentage of the DMSO control (DMSO n = 191 cell bodies, EHNA n = 161 cell bodies; 4 independent experiments). (D, E) Treatment of ES-derived motor neurons with 1 mM EHNA causes a significant decrease in the accumulation of α-$p75^{NTR}$ in the cell body compared to the DMSO control. Results are expressed as a percentage of the DMSO control (DMSO n = 223 cell bodies, EHNA n = 181 cell bodies; 4 independent experiments). **** $p < 0.0001$ (unpaired Student's *t* test). Error bars represent SEM. Scale bar, 10 μm.

To further investigate the relationship between the inhibition of cytoplasmic dynein and the somatic accumulation of H_CT and α-$p75^{NTR}$, we also investigated the effects of ciliobrevin A, a more specific inhibitor of dynein ATPase activity (Firestone et al., 2012). *In vitro* axonal transport assays revealed that treatment of ES-derived motor neurons with 100 μM ciliobrevin A caused an almost complete disruption of axonal transport (Figure 3.3A). However, when the concentration was lowered to 50 μM, a sufficient number of cargoes could be tracked to allow speed analysis to be performed. 50 μM ciliobrevin A was found to cause a significant inhibition of the retrograde axonal transport of H_CT-labelled carriers ($p = 0.045$), as shown by the shift of the speed distribution curve to the left (Figure 3.3B).

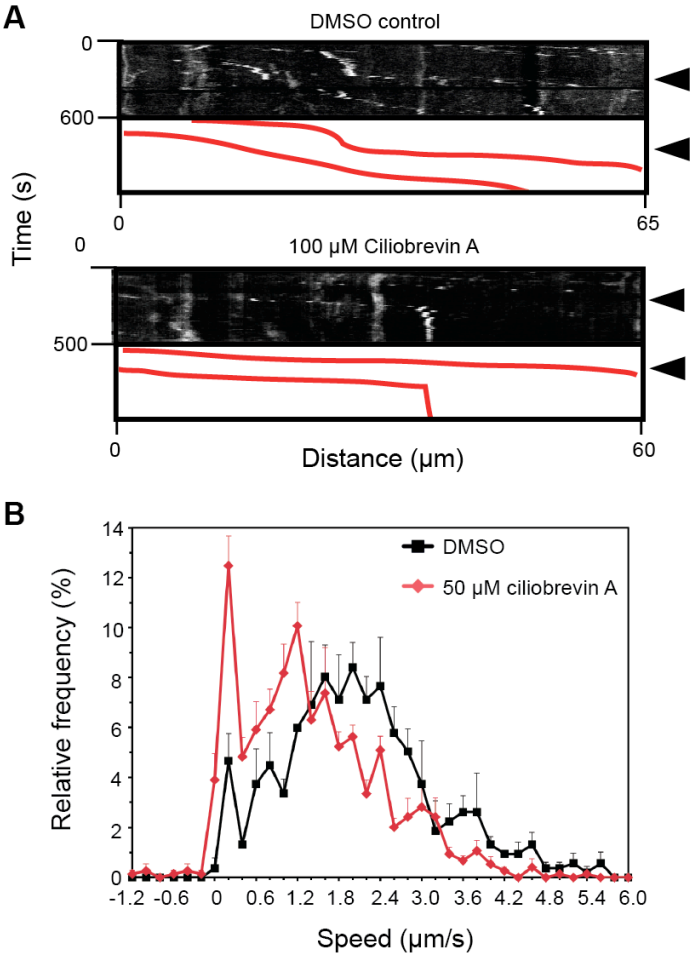

Figure 3.3. Ciliobrevin A inhibits retrograde axonal transport in motor neurons

(A) The effect of 100μM ciliobrevin A on H_CT axonal transport. MNs in mass culture were incubated with AlexaFluor 555-conjugated H_CT and treated with 100μM ciliobrevin A (or DMSO control) after the appearance of motile fluorescent carriers. Corresponding kymographs are presented and below each a scheme showing manually drawn lines tracing the movement of retrograde carriers (in red). Retrograde carriers were moving to the right. Arrowheads report when 100μM ciliobrevin A or DMSO was added. (B) Speed profiles of H_CT carriers in MNs treated with DMSO (black squares) or 50 μM ciliobrevin A (red diamonds) (DMSO: 55 carriers, 10 axons; 50 μM ciliobrevin A: 46 carriers, 8 axons; 3 independent experiments).

Importantly, the inhibition of retrograde axonal transport by ciliobrevin A was also mirrored by the reduced accumulation of H_CT and α-$p75^{NTR}$ in the soma of ES-derived motor neurons (Figure 3.4).

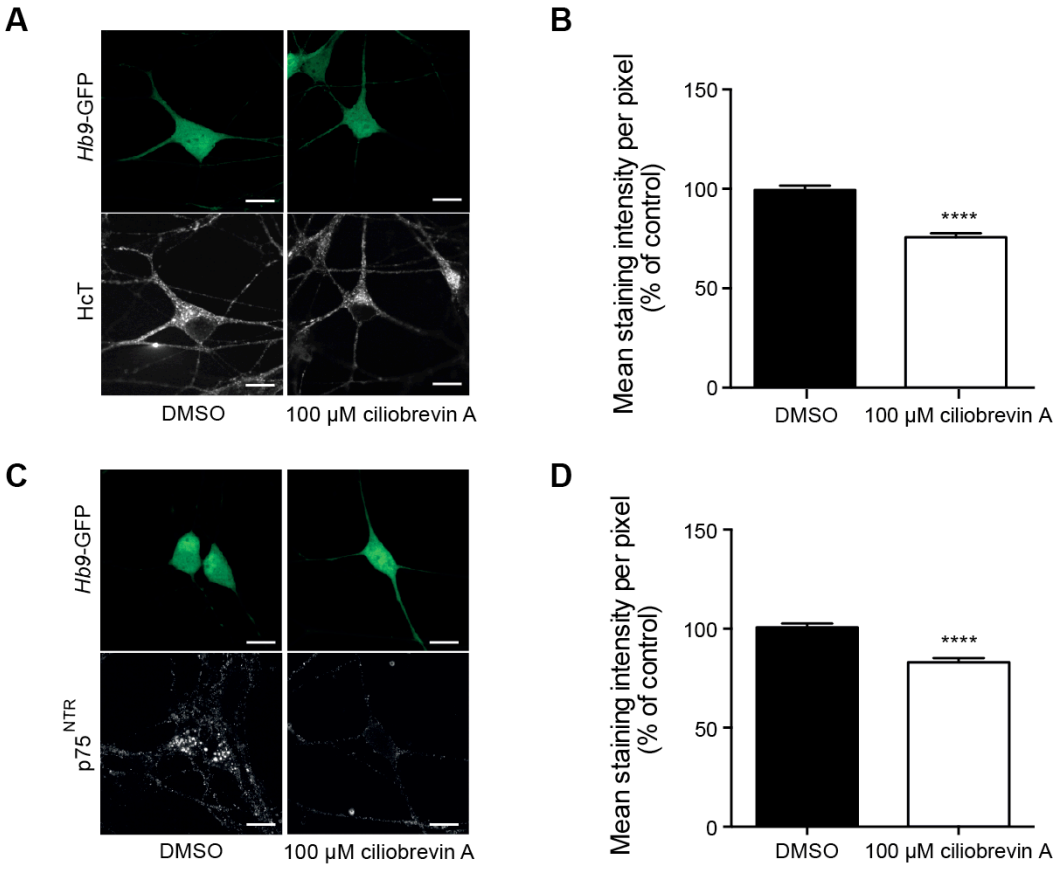

Figure 3.4. Ciliobrevin A reduces the accumulation of H_CT and α-$p75^{NTR}$ in the cell body of ES-derived motor neurons

(A, B) Treatment of ES-derived motor neurons with 100 µM ciliobrevin A causes a significant decrease in the accumulation of H_CT in the cell body compared to the DMSO control. Results are expressed as a percentage of the DMSO control (DMSO n = 212 cell bodies, Ciliobrevin A n = 229 cell bodies; 4 independent experiments). (C, D) Treatment of ES-derived motor neurons with 100 µM ciliobrevin A causes a significant decrease in the accumulation of α-$p75^{NTR}$ in the cell body compared to the DMSO control. Results are expressed as a percentage of the DMSO control (DMSO n = 253 cell bodies, Ciliobrevin A n = 250 cell bodies; 4 independent experiments). **** p< 0.0001 (unpaired Student's *t* test). Error bars represent SEM. Scale bar, 10 µm.

In contrast to inhibitors of axonal transport, very few specific enhancers of retrograde axonal transport are available. Acetyl-L-carnitine (ALCAR) has been previously reported to enhance both slow (Di Giulio et al., 1995) and fast retrograde axonal transport in diabetic rats (Kano et al., 1999). However, the effects of ALCAR had not been previously tested in mouse motor neuron cultures. I therefore tested ALCAR in our *in vitro* axonal transport assays in mouse ES-derived motor neurons. When motor neurons were incubated with 1 mM ALCAR, H_CT-labelled endosomes were transported at faster speeds ($p = 0.063$; Figure 3.5A). This subtle increase in transport efficiency could also be detected using the accumulation assay (Figure 3.5B-E).

Since EHNA, ciliobrevin A and ALCAR were applied to the motor neurons at the same time as H_CT and α-$p75^{NTR}$, it was possible that the results seen in the accumulation assay were due to an alteration in the binding of the probes, rather than the compounds' effects on retrograde axonal transport efficiency. To control for this, I assessed the effect of all three compounds on binding of the probes to ES-derived motor neurons (Figure 3.6). EHNA was found to cause a significant inhibition of the binding of both H_CT and α-$p75^{NTR}$. However, as ciliobrevin A had no inhibitory effect on binding, it appears that the accumulation assay is indeed sensitive to reductions in axonal transport efficiency. In addition the effects of ALCAR on binding did not mimic the results seen in the accumulation assay. These findings support the use of the accumulation assay to identify likely modifiers of retrograde axonal transport.

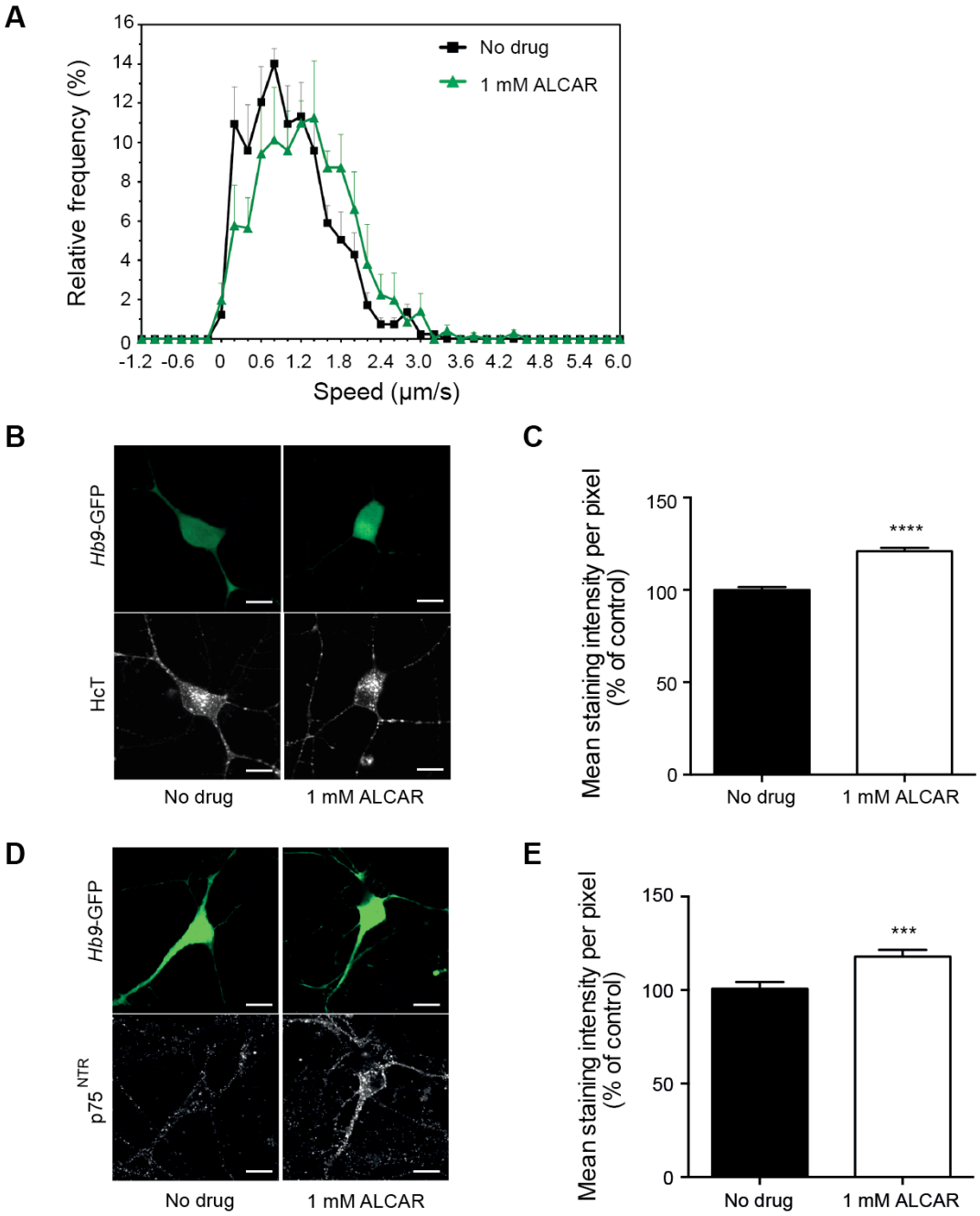

Figure 3.5. ALCAR causes a subtle enhancement of axonal transport speed in motor neurons that can be detected by the accumulation assay

(A) Speed profiles of H_CT carriers in MNs treated with control medium (black squares) or 1 mM ALCAR (green triangles) (No drug: 53 carriers, 10 axons; 1 mM ALCAR: 61 carriers, 8 axons; 3 independent experiments). (B, C) Effects of 1 mM ALCAR on accumulation of H_CT in the cell body of ES-derived MNs compared to the no drug (water treated) control. Results are expressed as a percentage of the no drug control (No drug n = 192 cell bodies, ALCAR n = 193 cell bodies; 4 independent experiments). (D, E) Effects of 1 mM ALCAR on accumulation of α-$p75^{NTR}$ in the cell body of ES-derived MNs compared to the no drug (water treated) control. Results are expressed as a percentage of the no drug control (No drug n = 125 cell bodies, ALCAR n = 153 cell bodies; 4 independent experiments). *** p< 0.001 **** p< 0.0001 (unpaired Student's *t* test). Error bars represent SEM. Scale bars, 10 µm.

Figure 3.6

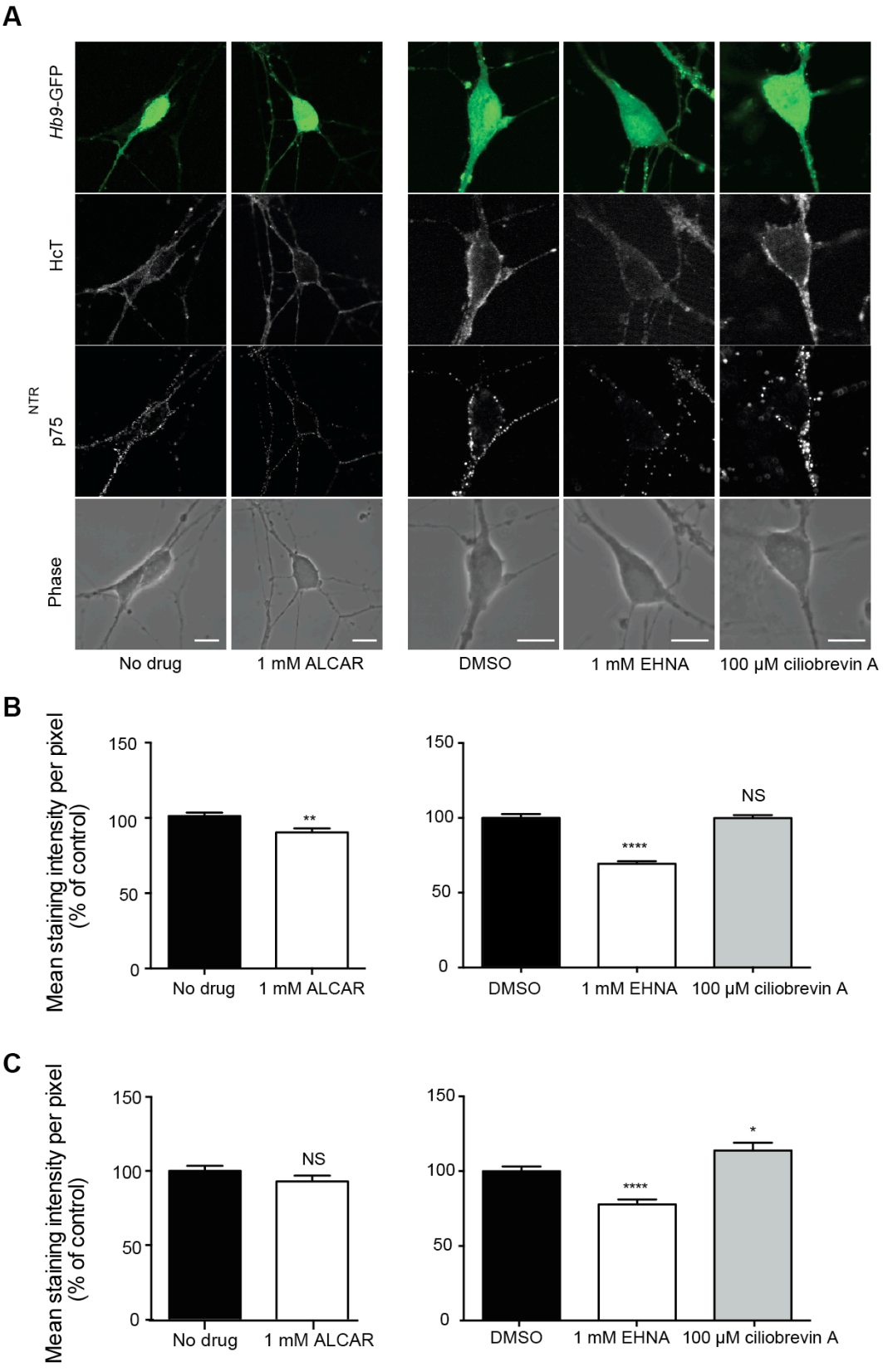
A
Hb9-GFP
HcT
p75NTR
Phase
No drug
1 mM ALCAR
DMSO
1 mM EHNA
100 µM ciliobrevin A
B
Mean staining intensity per pixel (% of control)
150
100
50
0
**
No drug
1 mM ALCAR
****
NS
DMSO
1 mM EHNA
100 µM ciliobrevin A
C
Mean staining intensity per pixel (% of control)
NS
No drug
1 mM ALCAR
****
*
DMSO
1 mM EHNA
100 µM ciliobrevin A

Figure 3.6. Testing the effect of ALCAR, EHNA and ciliobrevin A on H_CT and α-$p75^{NTR}$ binding

(A) The effect of 1 mM ALCAR, 1 mM EHNA and 100 μM ciliobrevin A on the binding of H_CT and α-$p75^{NTR}$ to ES-cell derived motor neurons. ES-derived MNs were cooled on ice and then incubated with AlexaFluor 555-conjugated H_CT and α-$p75^{NTR}$ antibody +/- drug. MNs were then washed with ice-cold Hanks, fixed on ice and stained for α-$p75^{NTR}$. The amount of H_CT and α-$p75^{NTR}$ was quantified as the mean staining intensity per pixel. Scale bars, 10 μm. (B) Quantification of H_CT binding. Results are expressed as a percentage of the control (No drug n = 134 cell bodies, ALCAR n = 127, DMSO n = 118, EHNA n = 125, ciliobrevin A n = 112; 3 independent experiments). ** $p < 0.01$ (unpaired Student's *t* test). **** $p < 0.0001$, NS = non significant (one-way ANOVA followed by Dunnett's multiple comparisons test). Error bars represent SEM. (C) Quantification of α-$p75^{NTR}$ binding. Results are expressed as a percentage of the control (No drug n = 118 cell bodies, ALCAR n = 128, DMSO n = 125, EHNA n = 140, ciliobrevin A n = 106; 3 independent experiments). NS = non significant (unpaired Student's *t* test). * $p < 0.05$ ****, $p < 0.0001$ (one-way ANOVA followed by Dunnett's multiple comparisons test). Error bars represent SEM.

A final step in validating the accumulation assay was to confirm whether the assay was sensitive enough to detect retrograde axonal transport defects in primary $SOD1^{G93A}$ motor neurons (Kieran et al., 2005). Primary wild type (non-transgenic) and $SOD1^{G93A}$ motor neuron cultures were incubated with H_CT for two hours, as previously described, and we were able to detect a significant decrease in accumulation in $SOD1^{G93A}$ motor neurons compared to the wild-type controls (Figure 3.7).

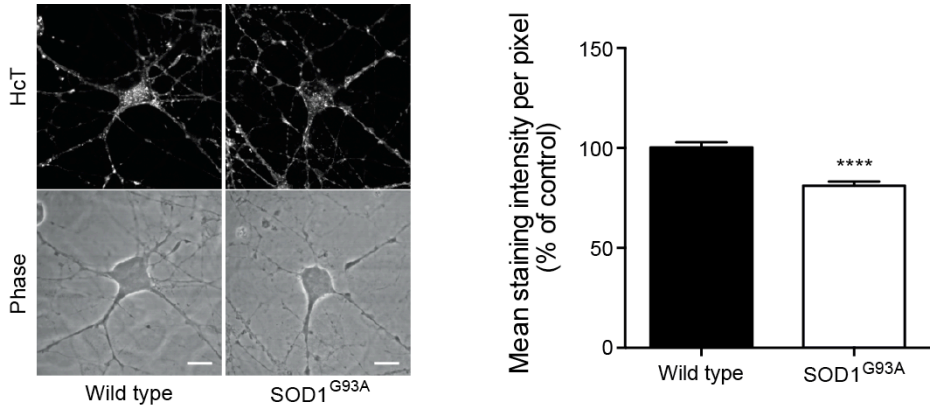

Figure 3.7. Deficits in retrograde axonal transport in $SOD1^{G93A}$ motor neurons can be detected by the accumulation assay

Defective retrograde axonal transport in $SOD1^{G93A}$ MNs is observed as a decrease in accumulation of H_CT in the cell body. Primary MNs from E13 $SOD1^{G93A}$ embryos were incubated with AlexaFluor 555-conjugated H_CT for 2 h. Cells were then acid-washed and fixed. The amount of H_CT was quantified as the mean staining intensity per pixel in the cell body. Results are expressed as a percentage of the wild type control (WT n = 161 cell bodies, $SOD1^{G93A}$ = 156 cell bodies; 3 independent experiments). **** $p < 0.0001$ (unpaired Student's *t* test). Error bars represent SEM. Scale bar, 10 μm.

3.2.2. Scaling up the accumulation assay for use as a medium through-put screen

In order to adapt the accumulation assay for screening a small library of compounds it was necessary to establish automated protocols of image acquisition and analysis.

To this aim, it was decided to perform the accumulation assay in 24-well glass bottom plates (MatTek Corporation). This would allow fixing and staining *in situ,* avoiding the use of individual coverslips, while providing a large enough surface area per well to avoid clumping of the ES-derived motor neurons as seen in 96-well plates. Glass-bottom plates also allowed the use of confocal microscopy.

The Zeiss LSM 510 inverted confocal microscope has an automated stage that, when used in combination with the Multi Field Acquisition (MTS) macro, allows automated image acquisition from a 24-well plate to be performed overnight. The autofocus function of the MTS macro allows the focal plane to be determined using the GFP channel (i.e. focussing specifically on the motor neurons) and a tile of 36 images can be acquired for each well using a 40X objective.

The confocal images were then fed into the Cell Profiler software, developed by Anne Carpenter and Thouis John (http://www.cellprofiler.org/), which allows automated analysis of large image datasets (Figure 3.8). The software can be instructed to identify cell bodies using the GFP channel and both size and intensity constraints. It can then use this “cell body” mask to isolate the corresponding H_CT and α-$p75^{NTR}$ signals and make a number of measurements, including mean staining intensity, average number of H_CT and/or α-$p75^{NTR}$–labelled vesicles per cell, the size of these vesicles and the staining intensity of individual vesicles. However, the ability of the software to distinguish individual vesicles is limited, due to the restricted resolution of the microscope images. The detection settings were optimised such that the software could sensitively detect the known changes in mean staining intensity and number of H_CT and/or α-$p75^{NTR}$-labelled vesicles after EHNA and ALCAR treatment.

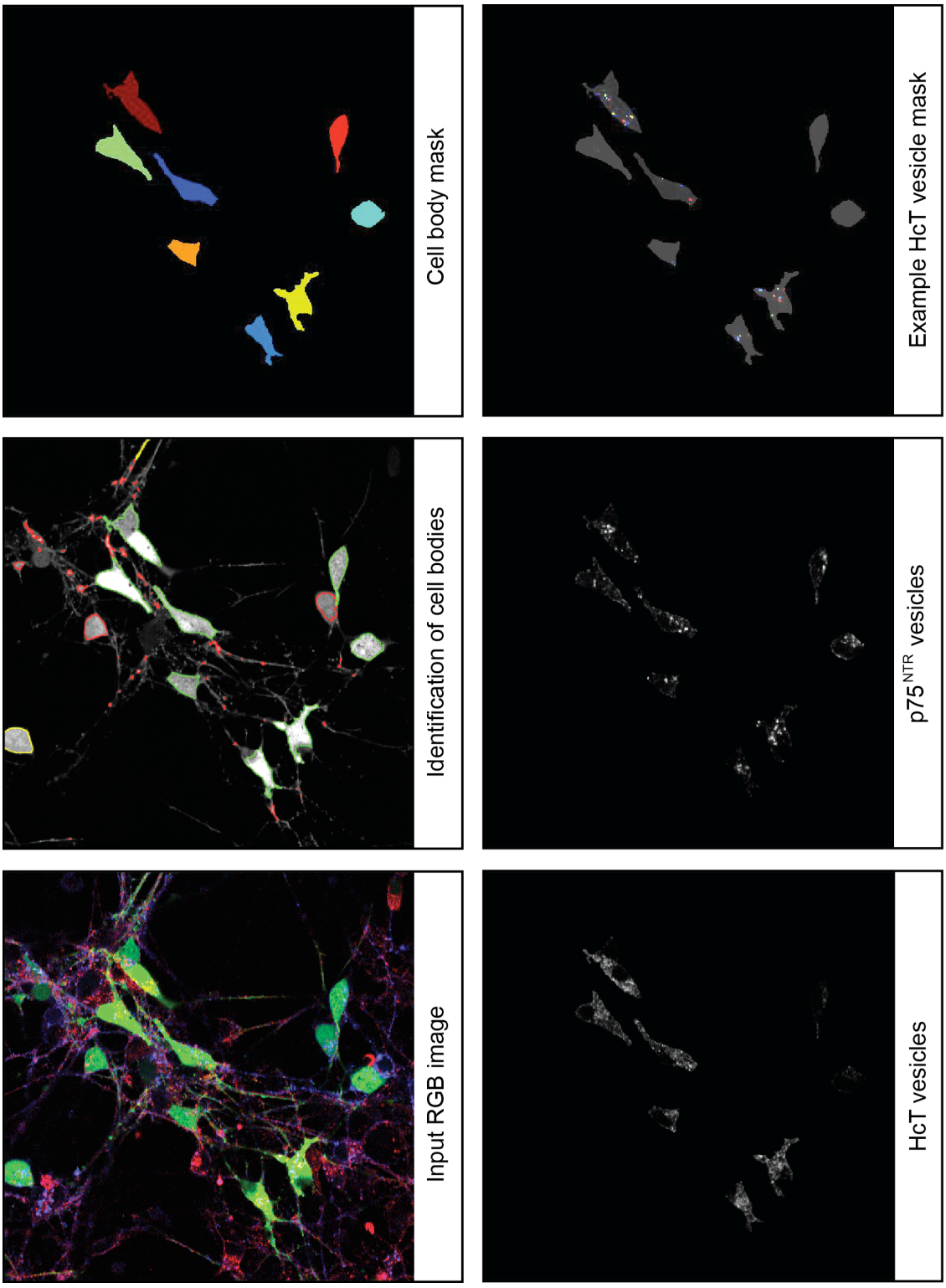

Figure 3.8. Automatic image analysis using Cell Profiler software

Images are loaded as single RGB images. The Cell Profiler software uses the GFP channel to identify motor neuron cell bodies and create a mask. Using this mask the H_CT and α-$p75^{NTR}$ receptor signals are isolated and the software can measure the mean staining intensity of each probe within each cell body. Cell Profiler can also create a mask of the vesicles and use this to count the number and staining intensity of individual vesicles. The cell body mask has been superimposed on top of the H_CT vesicle mask in this instance in order to make the identification of vesicles within cell bodies clearer.

In order to confirm that the use of automated image acquisition and analysis did not reduce the sensitivity of the assay, I compared the two approaches (manual versus automated) side-by-side. As shown in Figure 3.9, the automated approach produced very similar results and was therefore suitable to be used when screening the library of kinase inhibitors provided by GlaxoSmithKline.

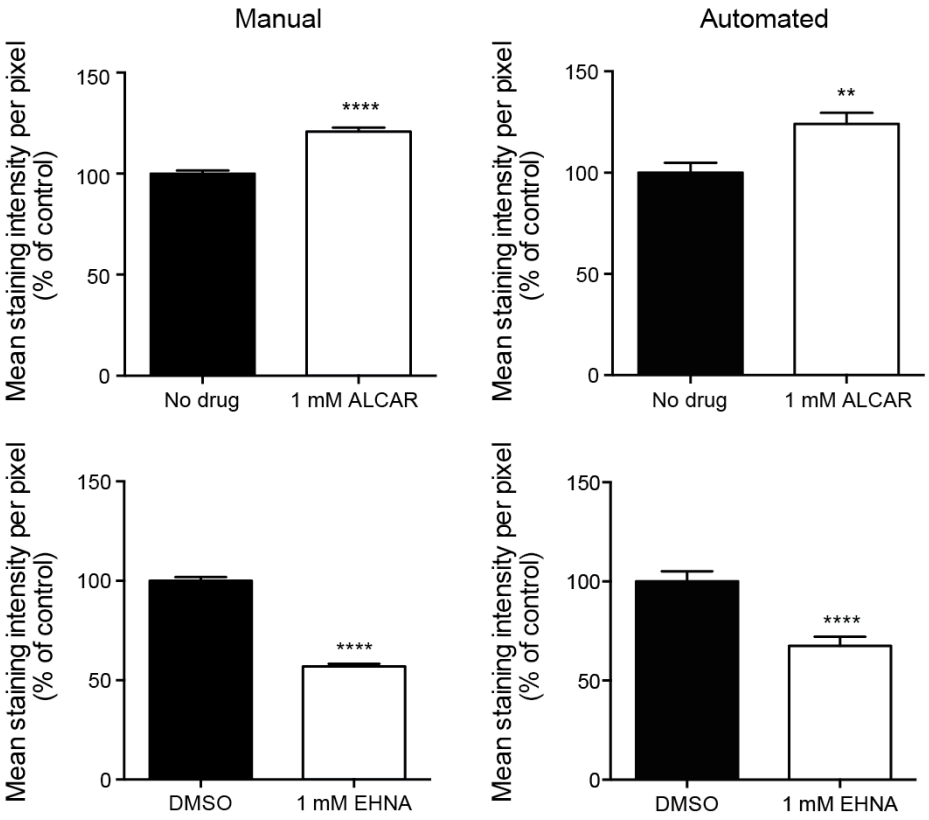

Figure 3.9. Comparison of the results obtained from manual and automated image acquisition and analysis

The results of the accumulation assay were compared when the protocol was performed manually (as described previously) or using automated image acquisition and analysis. n ≥ 25 cell bodies; *n* = 3 repeats. **** $p < 0.0001$, ** $p < 0.01$ (unpaired Student's *t* test). Error bars represent SEM.

3.3. Identification and validation of lead compounds

To identify compounds that may be enhancing retrograde axonal transport, 56 compounds (listed in Table 4) were screened at a concentration of 2 μM using the accumulation assay. These compounds were all derived from a kinase inhibitor library supplied by GlaxoSmithKline. The library was composed of previously published compounds, which targeted 24 different kinases that had been previously implicated in the regulation of axonal transport and/or that had been proposed to play a role in neurodegeneration. For the preliminary screen, accumulation was quantified using two of the Cell Profiler measurements described in Section 3.2.2 – the mean staining intensity of H_CT and α-$p75^{NTR}$ in each motor neuron cell body and the average number of H_CT or α-$p75^{NTR}$-labelled vesicles per cell body. The screen was performed blind and in triplicate for each compound.

3.3.1. Preliminary screening results

Active compounds were defined as those that increased the mean staining intensity of H_CT and/or α-$p75^{NTR}$ by at least three standard deviations above the DMSO control level, which was taken as 100% (represented as a yellow rectangle; Figure 3.10A). Four active compounds were identified on this basis – A1, A4, C3 and E4 (Figure 3.10B). In addition, four more compounds were included (C1, C2, D1 and D3), as they sat on or close to the significance boundary. Therefore, in total, eight active compounds were selected, representing a primary hit rate of 14%.

These active compounds were then confirmed, based on data collected about the average number of labelled vesicles per cell (Figure 3.10D and E). By comparison of the two data sets, six of the active compounds were confirmed as causing an increase in both the mean staining intensity *and* the number of vesicles per cell, for H_CT and/or α-$p75^{NTR}$. These were compounds A1, A4, C3, D1, D3 and E4.

Figure 3.10

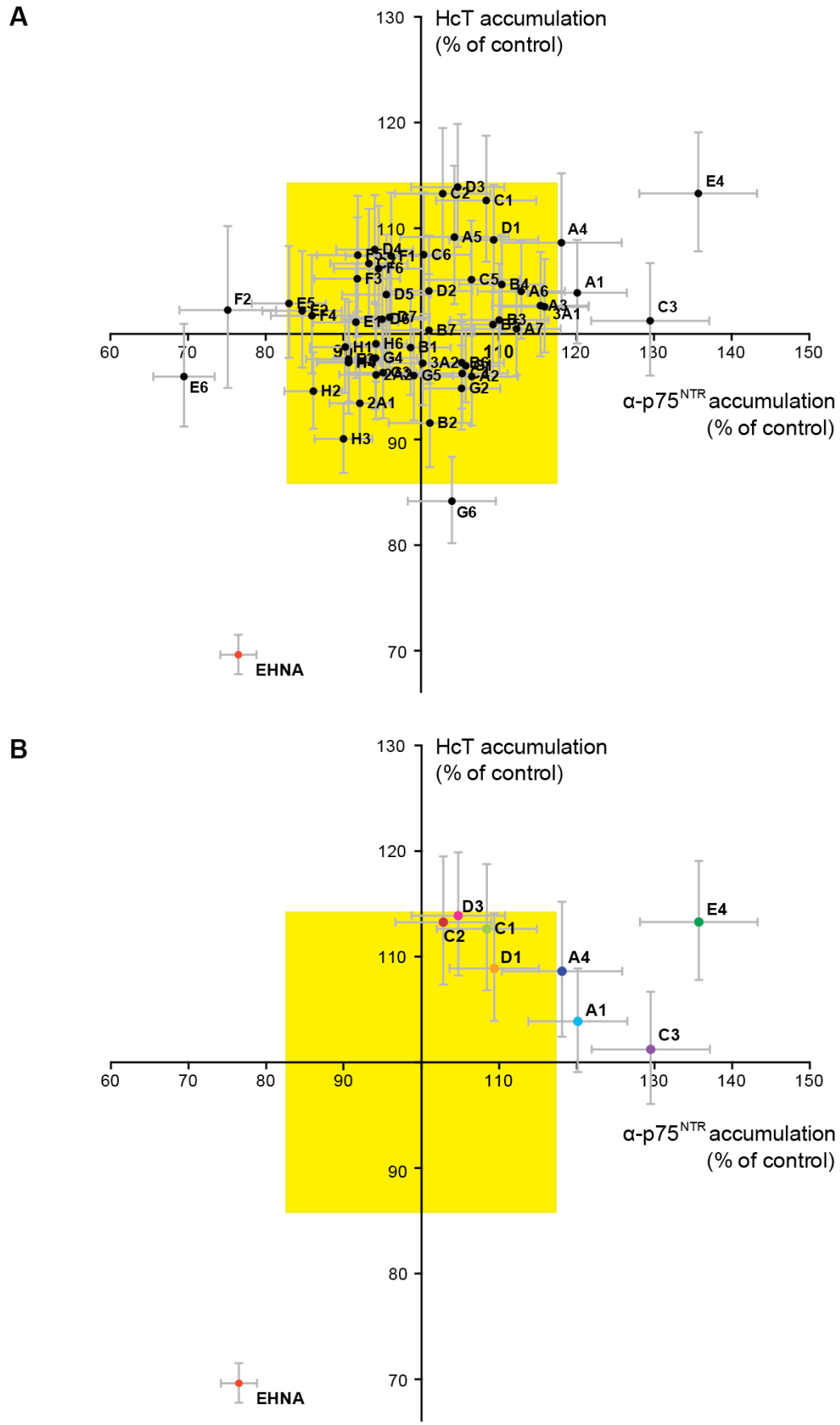
A
HcT accumulation
(% of control)
α-p75NTR accumulation
(% of control)
EHNA
B
HcT accumulation
(% of control)
α-p75NTR accumulation
(% of control)
EHNA

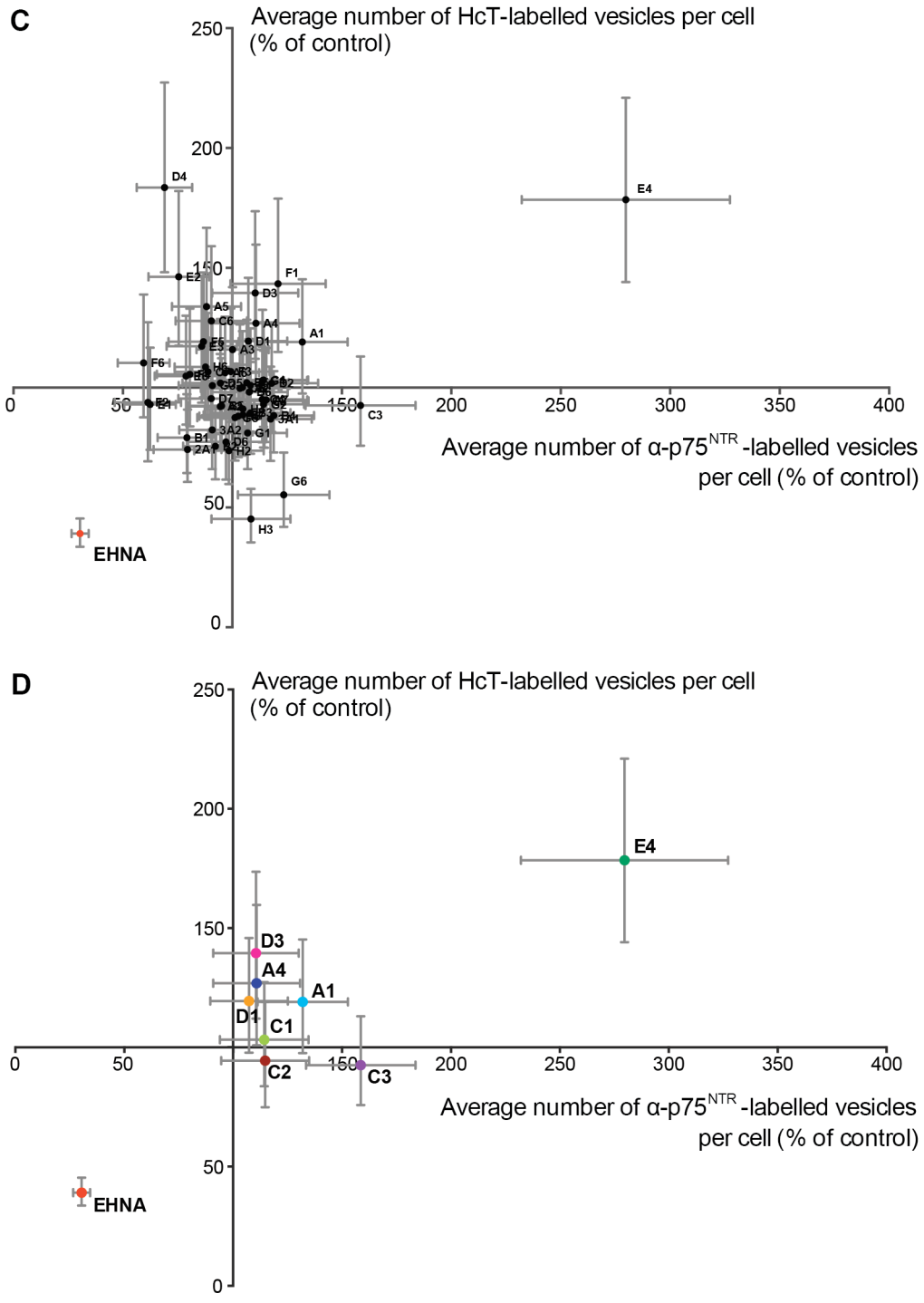

Figure 3.10. Chemical screening for the identification of enhancers of H_CT and α-p75^{NTR} accumulation in the cell body of ES-derived motor neurons

(A) Summary of preliminary screening results shown as an XY plot of the normalized *mean staining intensity* values for α-p75^{NTR} vs H_CT. Active compounds were defined as those able to increase accumulation of α-p75^{NTR} and/or H_CT by at least 3-times the standard deviation (represented by the yellow rectangle). The negative control (EHNA) is shown in red. (B) The 8 active compounds that were selected. (C) Summary of preliminary screening results shown as an XY plot of the normalized *average number of vesicles per cell body* values for α-p75^{NTR} vs H_CT. The negative control (EHNA) is shown in red. (D) *Average number of vesicles per cell body* data for the 8 active compounds identified in (B). Error bars represent SD. n ≥ 25 cell bodies per repeat; *n* = 3 repeats.

3.3.2. Identification of lead compounds

In order to validate the six active compounds, a dose-dependence study of their effect in the accumulation assay was performed. In addition to the previously tested concentration of 2 µM, the assay was also performed at five-fold lower (0.4 µM) and five-fold higher (10 µM) concentrations. All compounds were found to have a dose-dependent effect on accumulation between 0.4 µM and 2 µM. However, with the exception of C3, a concentration of 10 µM appeared to be either toxic to ES-derived motor neurons or had an inhibitory effect on the accumulation of H_CT and α-p75^{NTR} (Figure 3.11).

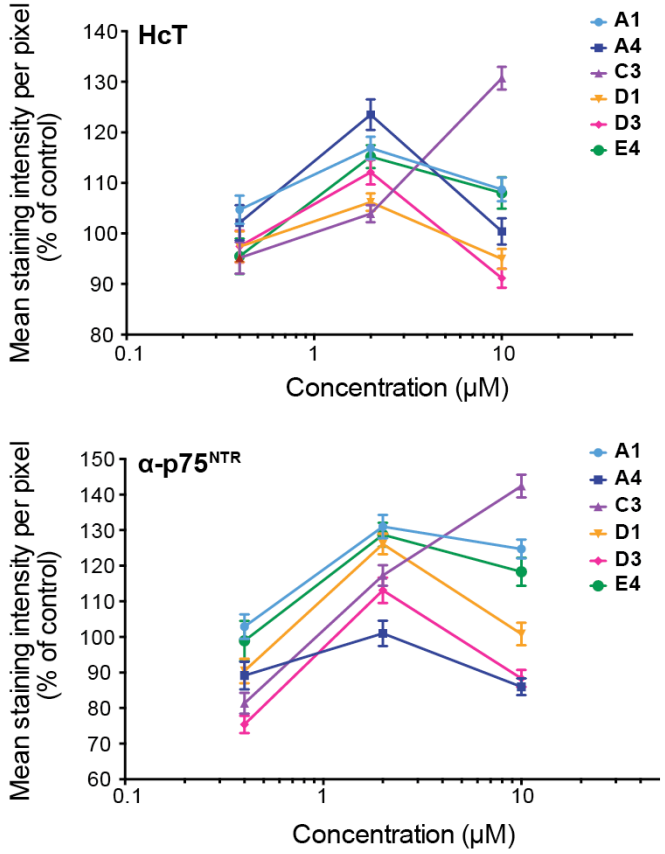

Figure 3.11. Dose-dependent effects of the active compounds

Concentration-response curves for the six active compounds. The screening assay was repeated at 0.4 µM, 2 µM and 10 µM and the amount of H_CT and α-p75^{NTR} accumulating was quantified as the mean staining intensity per pixel in the cell body. n ≥ 25 cell bodies per repeat; *n* = 3 repeats. Error bars represent SEM.

To further validate the six active compounds, the accumulation assay was repeated once more at the screening concentration of 2 µM in order to achieve three independent experimental repeats. Variability between the three repeats was found to be low, and all six compounds were confirmed as enhancers of H_CT and α-p75^{NTR} accumulation in the cell body, with compounds **A1, C3** and **E4** showing the strongest effects (Figure 3.12).

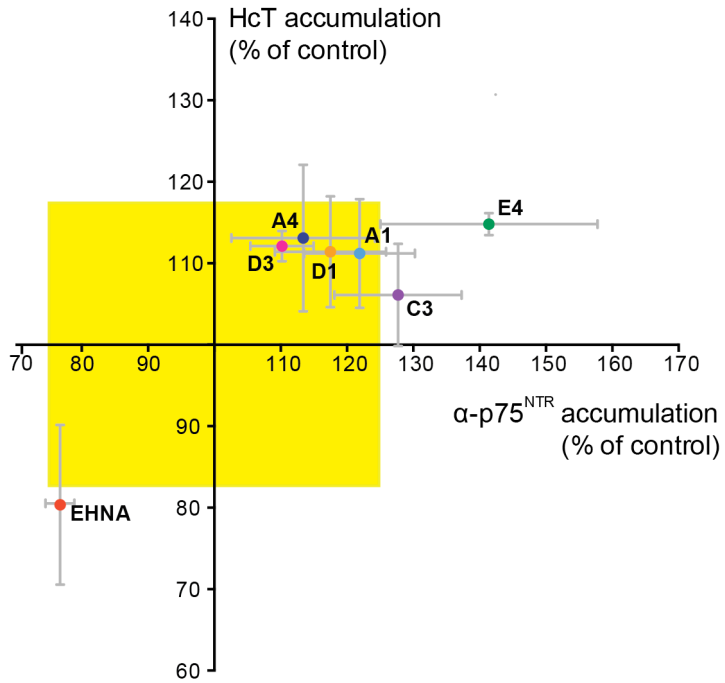

Figure 3.12. Summary of screening assay repeats for active compounds

Summary of the three runs of the screening assay at 2 µM. Results shown as an XY plot of the average *mean staining intensity* values for α-p75^{NTR} vs H_CT for the 6 active compounds at a screening concentration of 2 µM. n ≥ 75 cell bodies per experiment; *n* = 3 independent experiments. Error bars represent SD.

Based on the screening data and subsequent validation experiments, A1, C3 and E4 were chosen as the three lead compounds to be investigated further.

3.3.3. Validation of lead compounds

In order to validate the lead compounds, A1, C3 and E4 were tested for their effects on H_CT accumulation in $SOD1^{G93A}$ primary motor neurons (Figure 3.13). All three compounds were found to correct the deficits in accumulation observed in $SOD1^{G93A}$ motor neurons.

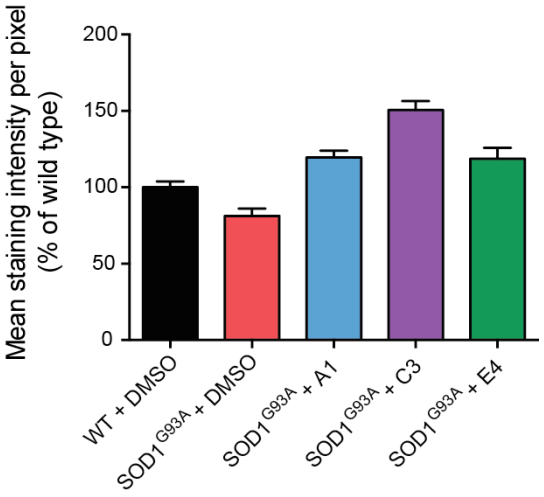

Figure 3.13. Validation of the lead compounds in $SOD1^{G93A}$ motor neurons
Effects of 2 μM A1, C3 and E4 on accumulation of H_CT in the cell body of primary motor neurons from E13 $SOD1^{G93A}$ embryos (DIV6). The amount of H_CT accumulating was quantified as the mean staining intensity per pixel in the cell body, using ImageJ. Results are expressed as a percentage of the wild type level (WT n = 33 cell bodies, $SOD1^{G93A}$ n = 38, $SOD1^{G93A}$ + A1 n = 30, $SOD1^{G93A}$ + C3 n = 33, $SOD1^{G93A}$ + E4 n = 32; 1 independent experiment). Error bars represent SEM.

Of course, one drawback of our screening assay is that the intracellular accumulation of the probes will also be affected by compounds that target pathways upstream or downstream of axonal transport, such as the binding, internalisation, recycling or degradation of H_CT and α-$p75^{NTR}$.

In order to determine whether the lead compounds were affecting the internalisation of H_CT and α-$p75^{NTR}$, the accumulation assay protocol was modified, such that accumulation in the cell body was assessed before significant axonal transport had begun. Using this modified protocol, we found that treatment of motor neurons with A1 and C3 enhanced the internalisation of α-$p75^{NTR}$ (Figure 3.14B),

but had no effect on the internalisation of H_CT (Figure 3.14A). Compound E4 had no effect on the internalisation of either probe.

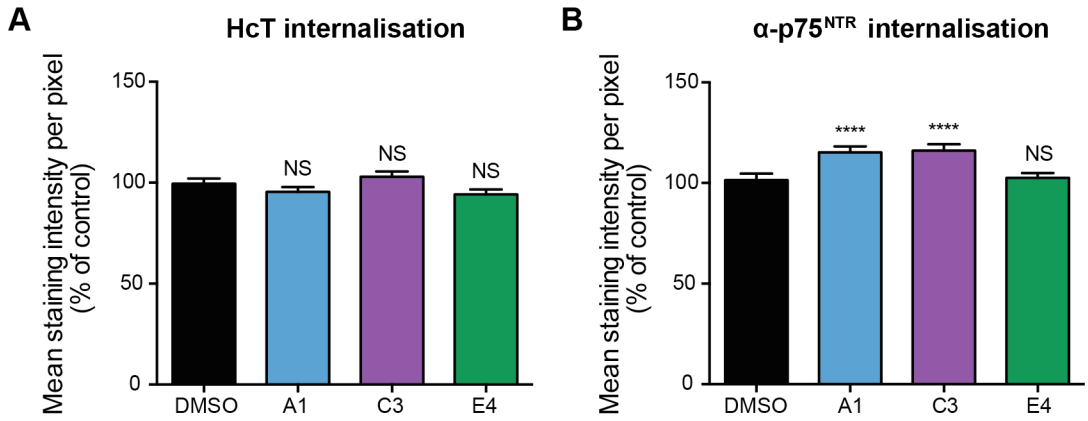

Figure 3.14. Effects of lead compounds on the internalisation of H_CT and α-p75^{NTR}
Effects of 2 μM A1, C3 and E4 on the internalisation of H_CT (A) and α-p75^{NTR} (B) in the cell body of ES-derived motor neurons. The assay was performed using the same methodology as the accumulation assay, except the incubation time with H_CT and α-p75^{NTR} was reduced to 20 minutes. The amount of H_CT and α-p75^{NTR} accumulating was quantified as the mean staining intensity per pixel in the cell body, using ImageJ (DMSO n = 241 cell bodies, A1 n = 240 cell bodies, C3 n = 238 cell bodies, E4 n = 217 cell bodies; 3 independent experiments). Results are expressed as a percentage of the DMSO control. **** p 0.0001, NS = non significant (Kruskal-Wallis test followed by Dunn's multiple comparisons test). Error bars represent SEM.

In order to confirm whether any of the lead compounds were truly enhancers of retrograde axonal transport, we next performed live *in vitro* axonal transport assays (an example of which is shown in Movie 1 on the CD provided).

3.4. *In vitro* axonal transport assays

All the compounds in our kinase inhibitor library were supplied in DMSO and therefore the first necessary step was to demonstrate that DMSO itself had no effect on retrograde axonal transport speeds in ES-derived motor neurons *in vitro* (as shown in Figure 3.15).

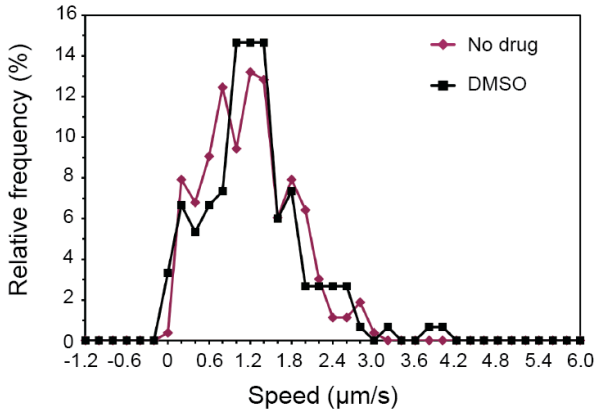

Figure 3.15. DMSO has no effect on retrograde axonal transport in motor neurons
Speed profiles of H_CT carriers in untreated and DMSO treated ES-derived motor neuron cultures (untreated: 24 carriers, 2 axons, DMSO: 20 carriers, 3 axons; *n = 1*).

Having established this, I went on to investigate the effects of each compound on the axonal transport of H_CT and α-$p75^{NTR}$ in both ES-derived and primary motor neurons.

3.4.1. Investigating the effects of compound A1 on axonal transport

After completing the preliminary screening and validation assays, compound A1 was revealed to be an inhibitor of p38 mitogen-activated protein kinase (p38 MAPK) (Boehm et al., 2001).

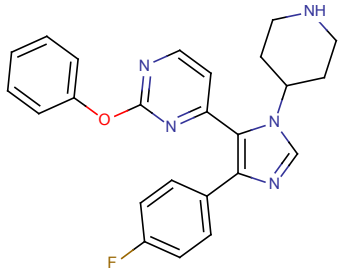

Figure 3.16. The chemical structure of the p38 MAPK inhibitor compound A1

When tested at the screening concentration of 2 µM in *in vitro* axonal transport assays, compound A1 was found to have no effect on retrograde axonal transport speeds in either ES-derived motor neurons (p = 0.514; Figure 3.17) or wild type primary motor neurons (p = 0.930; Figure 3.18A).

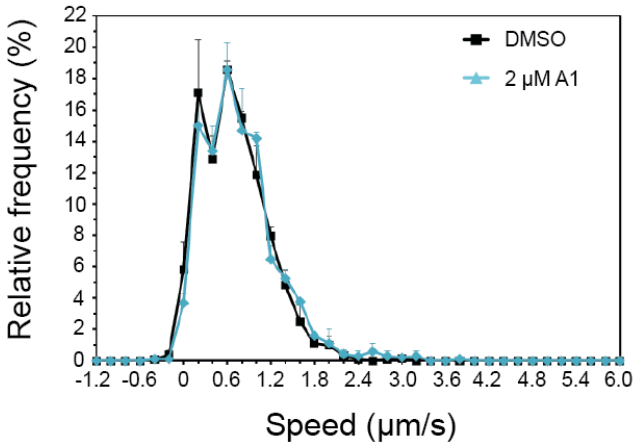

Figure 3.17. Treatment of ES-derived motor neurons with 2 µM A1 has no effect on retrograde axonal transport

Speed profiles of H_CT carriers in ES-derived motor neuron cultures treated with either DMSO or 2 µM A1 (DMSO: 56 carriers, 9 axons, A1: 54 carriers, 14 axons; *n* = 4 independent experiments).

In contrast, when tested in primary motor neurons derived from $SOD1^{G93A}$ embryos, compound A1 was able to correct defects in the retrograde axonal transport of H_CT ($SOD1^{G93A}$ versus $SOD1^{G93A}$ + 2 µM compound A1: p = 0.013; Figure 3.18B). Deconvolution of the speed distribution profiles shown in Figure 3.18A and B highlights a marked reduction in the fastest (1.41 µm/s) speed component in $SOD1^{G93A}$ motor neurons and a corresponding increase in the frequency of intermediate speed carriers (0.56 µm/s), when compared to wild type controls (Figure 3.18C). However, when treated with compound A1, $SOD1^{G93A}$ motor neurons had a speed carrier distribution indistinguishable from wild type controls (p = 0.853). Similarly for α-$p75^{NTR}$, treatment with 2 µM compound A1 was found normalise retrograde axonal transport in primary $SOD1^{G93A}$ motor neurons (WT versus $SOD1^{G93A}$ + 2 µM compound A1: p = 0.468, $SOD1^{G93A}$ versus $SOD1^{G93A}$ + 2 µM compound A1: p = 0.013; Figure 3.18D).

These results indicate that compound A1 is able to specifically rescue SOD1^{G93A}-induced deficits in retrograde axonal transport in primary motor neurons.

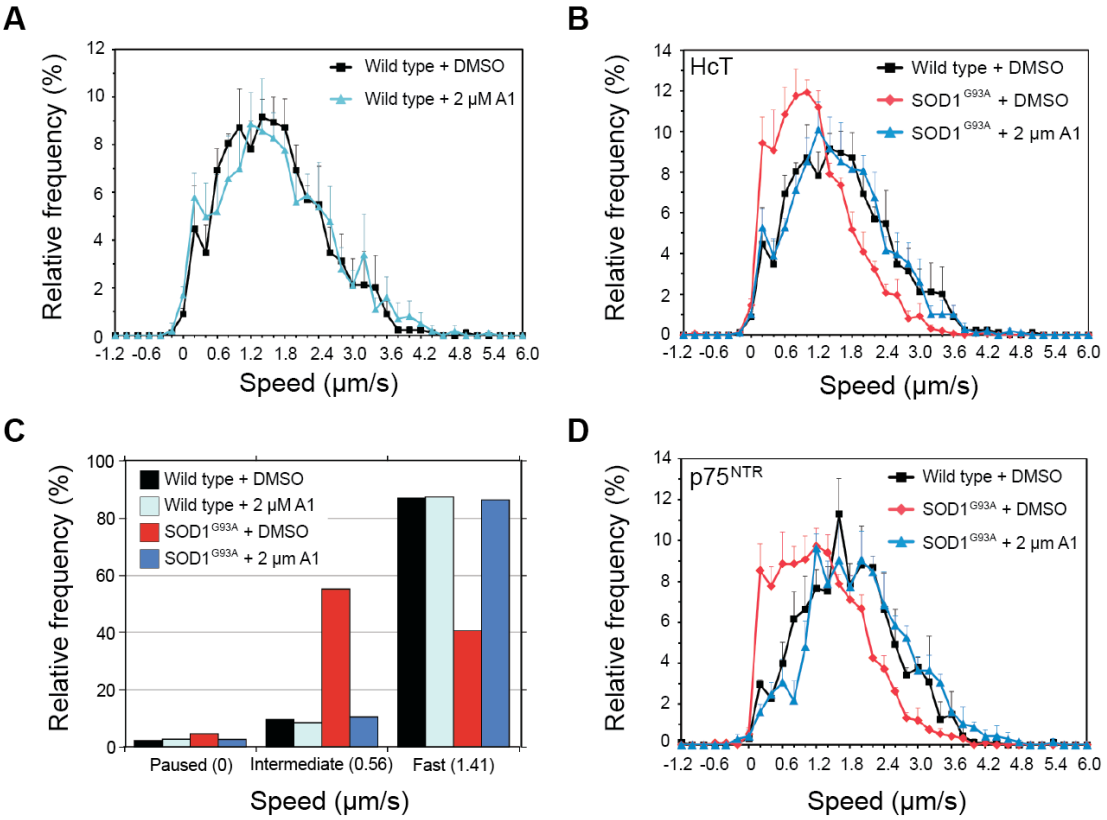

Figure 3.18. The effect of compound A1 on the axonal transport in primary motor neurons

(A) Speed profiles of H_CT carriers in wild type + DMSO (black squares) and wild type + 2 µM A1 (light blue triangles) motor neuron cultures. Comparison of the curves reveals that compound A1 has no effect on wild type axonal transport speeds (wild type: 94 carriers, 13 axons; wild type + 2 µM A1: 108 carriers, 11 axons; 4 independent experiments). (B) Speed profiles of H_CT carriers in wild type, SOD1^{G93A} and SOD1^{G93A} + 2 µM A1 motor neuron cultures. Comparison of the curves reveals SOD1^{G93A} motor neurons treated with compound A1 (blue triangles) have a similar speed distribution to wild type cultures (black squares) (wild type: 94 carriers, 13 axons; SOD1^{G93A}: 126 carriers, 14 axons; SOD1^{G93A} + 2 µM A1: 121 carriers, 16 axons; 4 independent experiments). (C) Deconvolution analysis of the *in vitro* speed profiles (as previously described in Bilsland et al., 2010) demonstrating that there are three defined speed components: 0 µm/s (slow), 0.56 µm/s (intermediate), and 1.41 µm/s (fast). Defects in axonal transport in SOD1^{G93A} motor neurons can be explained by a reduction in the number of "fast" moving carriers, and an increase in the number of "intermediate" speed carriers. Treatment of SOD1^{G93A} motor neurons with 2 µM A1 corrects the distribution of carriers back to that of wild type. (D) Compound A1 also restores retrograde axonal transport of the α-p75^{NTR} in SOD1^{G93A} motor neurons**.** Speed profiles of α-p75^{NTR} carriers in wild type, SOD1^{G93A} and SOD1^{G93A} + 2 µM A1 motor neuron cultures (wild type: 118 carriers, 6 axons; SOD1^{G93A}: 85 carriers, 6 axons; SOD1^{G93A} + 2 µM A1: 96 carriers, 8 axons; 3 independent experiments).

3.4.2. Investigating the effects of compound C3 on axonal transport

Compound C3 was revealed to be an inhibitor of the RET tyrosine kinase (Graham Robinett et al., 2007). RET is a transmembrane receptor for glial-derived neurotrophic factors (GDNFs) - GDNF, neurturin, artemin and persephin (Mulligan, 2014).

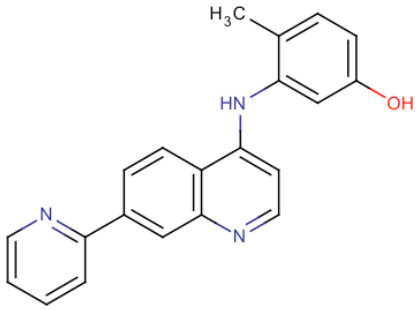

Figure 3.19. The chemical structure of the RET inhibitor compound C3

When motor neurons treated with 2 µM C3 were examined in closer detail during *in vitro* axonal transport assays, the compound was observed to be neurotoxic – causing severe blebbing of axons (Figure 3.20A). Furthermore, when the dose was lowered to a non-toxic concentration (0.5 µM), compound C3 was found to have no effect on retrograde axonal transport in ES-derived (data not shown) or wild type primary motor neurons (Figure 3.20B). As a result, compound C3 was excluded from further analysis.

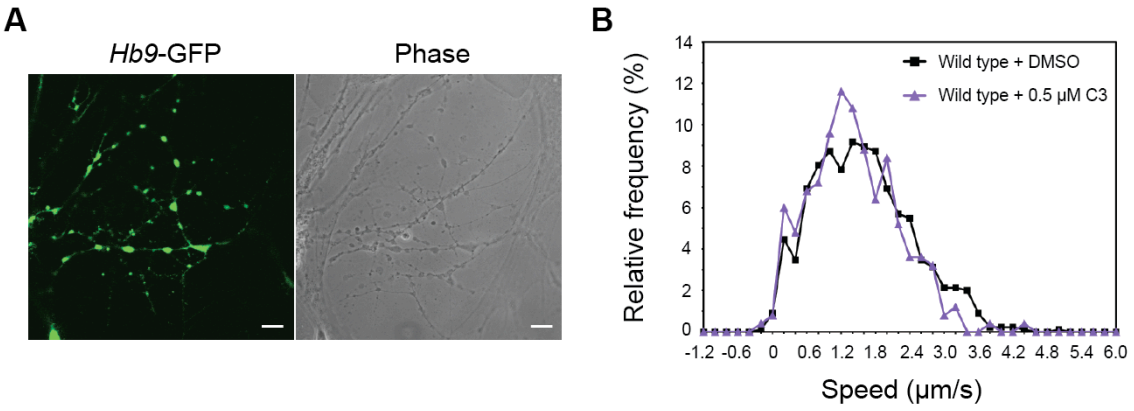

Figure 3.20. Compound C3 has no effect on retrograde axonal transport speeds
(A) Compound C3 is toxic at 2 µM, causing blebbing of axons. Scale bar, 10 µm. (B) Speed profiles of H_CT carriers in wild type motor neurons treated with either DMSO or 0.5 µM C3. *n* = 1.

3.4.3. Investigating the effects of compound E4 on axonal transport

Compound E4 was revealed to be an inhibitor of the insulin-like growth factor 1 receptor (IGF1R) (Chamberlain et al., 2009).

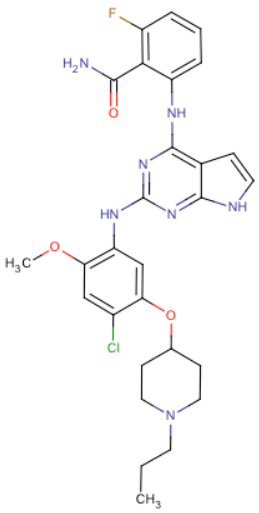

Figure 3.21. The chemical structure of the IGF1R inhibitor compound E4

Similarly to compound C3, further analysis of motor neurons treated with 2 μM E4 revealed blebbing of axons (Figure 3.22A). However, when the dose was lowered to a non-toxic concentration, compound E4 was found to accelerate the axonal transport of H_CT-labelled endosomes in ES-derived motor neurons ($p = 0.029$; Figure 3.22B).

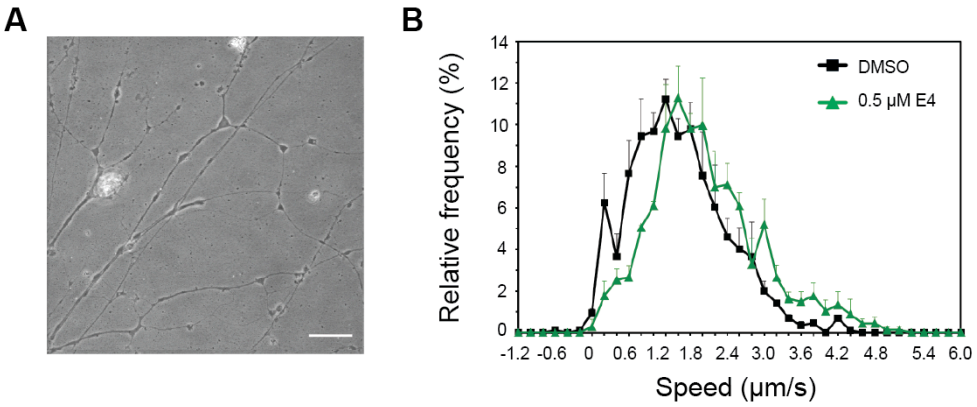

Figure 3.22. Treatment of ES-derived motor neurons with compound E4 accelerates axonal transport

(A) Compound E4 is toxic at 2 μM, causing blebbing of axons. Scale bar, 10 μm. (B) Speed profiles of H_CT carriers in wild type motor neurons treated with either DMSO or 0.5 μM E4 (DMSO: 10 axons, 84 carriers, E4: 10 axons, 89 carriers; *n* = 3 independent experiments).

Compound E4 also had a similar accelerating effect on the axonal transport of H_CT in both wild type ($p = 0.0003$; Figure 3.23A) and $SOD1^{G93A}$ ($SOD1^{G93A}$ versus $SOD1^{G93A}$ + 0.5 µM compound E4: $p = 0.108$; Figure 3.23B) primary motor neurons. Deconvolution of the wild type speed distribution profiles shown in Figure 3.23A highlights a marked reduction in the intermediate and fast (1.41 µm/s) speed components and a corresponding increase in the frequency of very fast speed carriers (2.24 µm/s), when motor neurons are treated with 0.5 µM E4 (Figure 3.23C). For $SOD1^{G93A}$ motor neurons treated with 0.5 µM E4 (Figure 3.23B), there is a large increase in the frequency of fast speed carriers and a corresponding decrease in intermediate speed carriers, compared to DMSO treated controls.

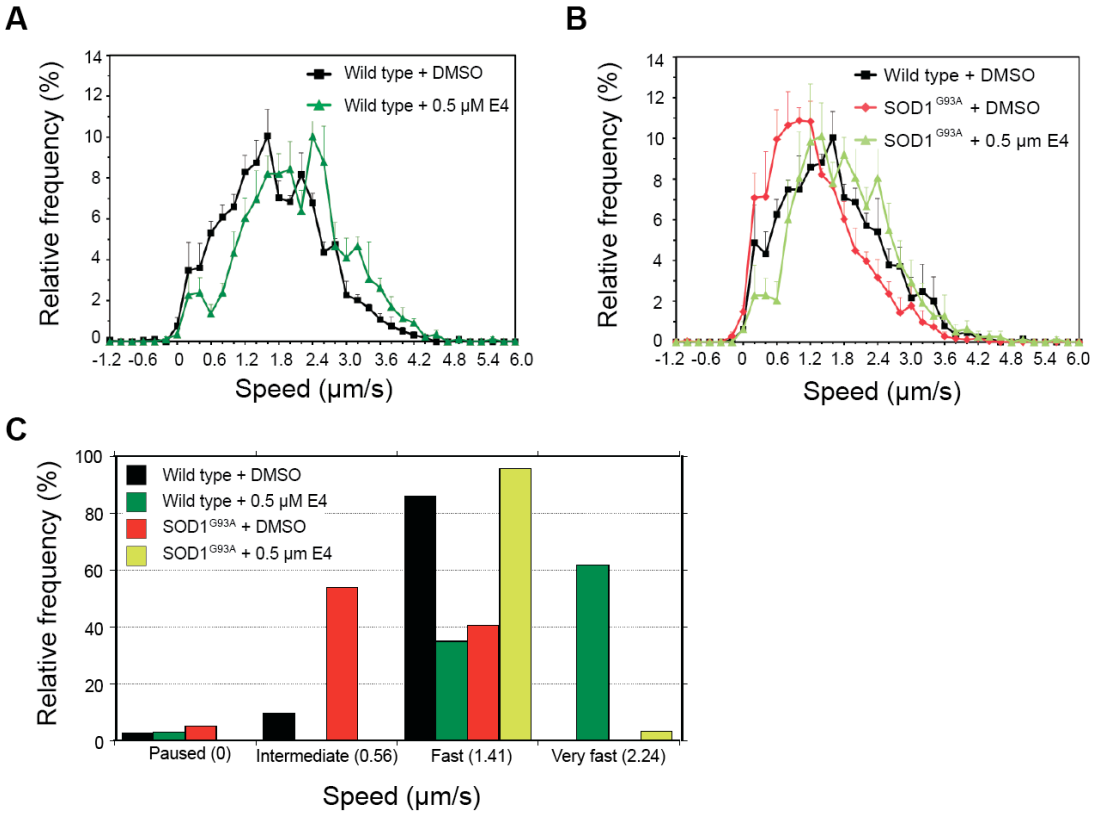

Figure 3.23. Compound E4 accelerates the axonal transport of H_CT in both wild type and $SOD1^{G93A}$ motor neurons

(A) Speed profiles of H_CT carriers in wild type + DMSO (black squares) and wild type + 0.5 µM E4 (dark green triangles) motor neuron cultures. Comparison of the curves reveals that compound E4 accelerates axonal transport in wild type motor neurons (wild type: 153 carriers, 13 axons; wild type + 0.5 µM E4: 165 carriers, 13 axons; *n* = 4 independent experiments). (B) Speed profiles of H_CT carriers in wild type + DMSO, $SOD1^{G93A}$ + DMSO and $SOD1^{G93A}$ + 0.5 µM E4 motor neuron cultures. Comparison of the curves reveals $SOD1^{G93A}$ motor neurons treated with compound E4 (light green triangles) have accelerated axonal transport compared to DMSO treated $SOD1^{G93A}$ controls (red diamonds). Wild type: 136 carriers, 12 axons; $SOD1^{G93A}$: 96 carriers, 13 axons; $SOD1^{G93A}$ + 0.5 µM E4: 136 carriers, 8 axons; *n* = 4 independent experiments. (C) Deconvolution analysis of the *in vitro* speed profiles demonstrating that there are four defined speed components: 0 µm/s (slow), 0.56 µm/s (intermediate), 1.41 µm/s (fast) and 2.24 µm/s (very fast).

Finally, compound E4 was also found to accelerate the retrograde axonal transport of α-p75^{NTR}. This was observed in both wild type (p = 0.241; Figure 3.24A) and SOD1^{G93A} (SOD1^{G93A} versus SOD1^{G93A} + 0.5 µM compound E4: p = 0.004; Figure 3.24B) motor neurons. These results suggest that compound E4 may act as a general enhancer of retrograde axonal transport in motor neurons.

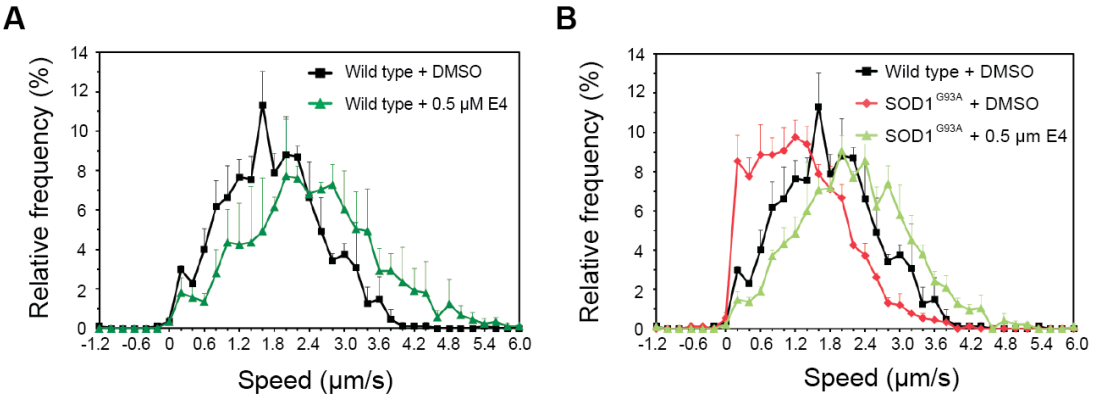

Figure 3.24. Compound E4 accelerates the axonal transport of α-p75^{NTR} in both wild type and SOD1^{G93A} motor neurons

(A) Speed profiles of α-p75^{NTR} carriers in wild type + DMSO (black squares) and wild type + 0.5 µM E4 (dark green triangles) motor neuron cultures. Comparison of the curves reveals that compound E4 accelerates axonal transport in wild type motor neurons (wild type: 118 carriers, 6 axons; wild type + 0.5 µM E4: 134 carriers, 8 axons; *n* = 3 independent experiments). (B) Speed profiles of α-p75^{NTR} carriers in wild type + DMSO, SOD1^{G93A} + DMSO and SOD1^{G93A} + 0.5 µM E4 motor neuron cultures. Comparison of the curves reveals SOD1^{G93A} motor neurons treated with compound E4 (light green triangles) also have accelerated axonal transport compared to DMSO treated SOD1^{G93A} controls (red diamonds) (wild type: 118 carriers, 6 axons; SOD1^{G93A}: 85 carriers, 6 axons; SOD1^{G93A} + 0.5 µM E4: 128 carriers, 12 axons; *n* = 3 independent experiments).

3.5. Target Validation Screening

Compound A1 (an inhibitor of p38 MAPK) and compound E4 (an inhibitor of IGF1R) were selected for further investigation. In order to confirm that their effects on retrograde axonal transport were due to inhibition of their target kinases, and not due to off-target effects, additional screening was performed. The new compound library (detailed in Table 5) was composed of structurally diverse p38 MAPK and IGF1R inhibitors. Screening was performed using the same methodology as previously described (Section 3.3).

As before, hit compounds were defined as those that increased the mean staining intensity of H_CT and α-$p75^{NTR}$ by at least three standard deviations above the DMSO control level, which was taken as 100% (yellow rectangle; Figure 3.25A). Hit compounds were further confirmed based on data about the average number of vesicles per cell (Figure 3.25B).

Four inhibitors of p38 MAPK (2-A3, 2-C3, 2-D3 and 2-H2; highlighted in blue) were found to cause a significant increase in the mean staining intensity of both probes in the cell body – mimicking the results seen for compound A1. These four compounds also caused an increase in the number of vesicles per cell body and were therefore taken forward into *in vitro* axonal transport assays (see Section 4.2.1). Only one IGF1R inhibitor, 2-C1 (highlighted in green), caused a significant increase in both H_CT and α-$p75^{NTR}$ accumulation. However two other compounds, 2-G2 and 2-B3 (also highlighted in green), caused large increases in α-$p75^{NTR}$ accumulation and were therefore also chosen to investigate further (see Section 5.2.1).

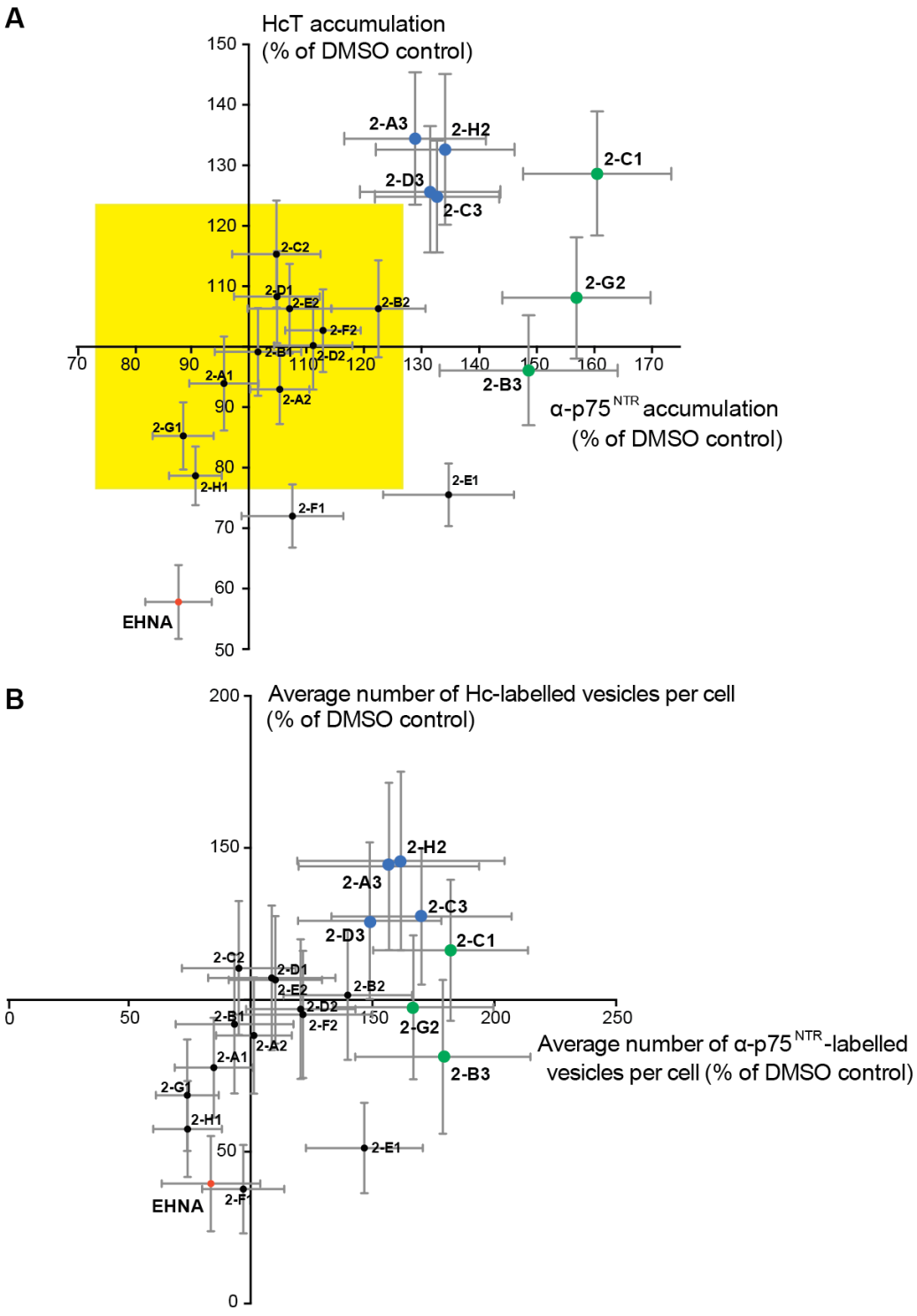

Figure 3.25. Target validation screening of additional p38 MAPK and IGF1R inhibitors

(A) Results of the target validation screening shown as an XY plot of the normalised *mean staining intensity* values for α-p75^{NTR} vs H_CT. Active compounds were defined as those able to increase accumulation by at least three-times the standard error (represented by the yellow rectangle). The negative control (EHNA) is shown in red. Lead compounds are highlighted in blue (p38 MAPK inhibitors) and green (IGF1R inhibitors). (B) Target validation screening results shown as an XY plot of the normalised *average number of vesicles per cell body* values for α-p75^{NTR} vs H_CT. The negative control (EHNA) is shown in red. Lead compounds are highlighted in blue (p38 MAPK inhibitors) and green (IGF1R inhibitors). Error bars represent SEM. n ≥ 25 cell bodies per repeat, *n* = 3 repeats.

3.6. Discussion

Deficits in axonal transport have not only been described in ALS, but also in many other neurodegenerative diseases (Millecamps and Julien, 2013), including Huntington's, Alzheimer's, Parkinson's and Charcot Marie Tooth type 2 (see Section 1.7.2). Furthermore, accelerating axonal transport using histone deacetylase 6 (HDAC6) inhibitors has been shown to be neuroprotective *in vivo* in both Parkinson's disease (Godena et al., 2014) and Charcot Marie Tooth type 2 (d'Ydewalle et al., 2011). The identification of pharmacological enhancers of axonal transport is therefore relevant to understanding the pathogenesis of many neurodegenerative diseases, including ALS.

However, we still have much to learn about the role that axonal transport defects play in neurodegeneration. In most cases, it still remains to be shown whether axonal transport defects play a key role in triggering neuronal death. In addition, it is now clear that axonal transport cannot be considered as a single process. It is necessary to try and distinguish the role of anterograde versus retrograde axonal transport defects, the presence and contribution of axonal transport defects in different neuronal types and the role of different types of cargo, for example, signalling endosomes, RNA, mitochondria, late endosomes/lysosomes and autophagosomes. The identification of pharmacological modifiers of axonal transport with cargo-, neuron- and/or direction-specific effects will enable us to investigate these questions in detail.

Modifiers of axonal transport have the potential to become novel therapeutic agents for the treatment of several neurodegenerative diseases. It is therefore of interest to screen large libraries of compounds to identify new enhancers of axonal transport. However, this is not a straightforward task. The most robust way to test a compound for its effects on axonal transport is to perform live *in vitro* or *in vivo* transport assays. Given that a typical *in vitro* assay takes around two hours to complete, and *in vivo* assays a minimum of six hours, it is not feasible to use such assays in a pharmaceutical drug discovery setting, where tens of thousands of compounds would typically be screened. For this reason, my project began with the

aim of developing a cell-based assay suitable for screening medium-size libraries of compounds for their effects on retrograde axonal transport.

3.6.1. The accumulation assay as a screen for enhancers of retrograde axonal transport efficiency

In this Chapter, I have described the development and validation of the accumulation assay, which utilises the accumulation of H_CT and α-$p75^{NTR}$ in the cell body of motor neurons as a read-out for axonal transport efficiency. These probes were chosen as their axonal transport has been previously well characterised by our laboratory (Lalli and Schiavo, 2002, Lalli et al., 2003a, Deinhardt et al., 2006b). We decided to use two probes rather than one as it allowed twice the amount of data to be collected without any increase in the time taken to perform the assay, and would help validate hit compounds. It also allowed us to potentially identify any differences in the regulation of the axonal transport and sorting of the two probes.

I was able to demonstrate that the accumulation of H_CT and α-$p75^{NTR}$ in mouse ES-derived motor neurons was sensitive to both the inhibition and acceleration of retrograde axonal transport caused by known modifiers of axonal transport. The accumulation assay was successfully adapted to allow for the screening of larger numbers of compounds, without any significant loss in sensitivity or increase in variability. The use of glass-bottom plates improved the efficiency of the assay, whilst automated microscopy allowed plates to be imaged unmonitored overnight in order to save time. In addition, automated image analysis software allowed large image datasets to be quickly and easily analysed, whilst avoiding bias.

3.6.1.1. Limitations of the accumulation assay

The use of mouse ES-derived motor neurons

The accumulation assay was performed in mouse ES-derived motor neurons that were engineered to express GFP under the motor neuron-specific promoter *Hb9* (Wichterle et al., 2002). These cells are well suited for use in screening assays, as mouse ES cells can be differentiated into motor neurons in a relatively short period of time (6 days compared to 28 days for motor neurons derived from pluripotent

human stem cells (Hu and Zhang, 2009)) and unlike primary neurons, there is almost no limitation on how many cells you can produce. In addition, a higher purity of motor neurons is achieved than with primary cultures.

However, mouse ES-derived motor neurons do have their disadvantages. From our experience culturing these cells in the laboratory, the quality and quantity of motor neurons produced can be very variable. The ES cells are very sensitive to changes in timings and media composition and therefore great care must be taken to adhere to strict protocols, keep the same suppliers and check for any changes in ingredient composition. In addition, there have been questions raised whether these mouse ES-derived motor neurons are fully developed and functional neurons, especially when assayed after just 3 DIV, as in our experiments. Indeed, it has been demonstrated that mouse ES-derived motor neurons are only able to fire repetitive trains of action potentials after 3 - 7 DIV (Miles et al., 2004, Bryson et al., 2014). In addition, when co-cultured with chick myotubules, ES-derived motor neurons do not form functional synapses until 6 DIV (Miles et al., 2004). It is therefore clear that the motor neurons we use in our assay are not fully functional. However axonal transport is observed to be robustly established at 3 DIV (see Section 3.2.1). In addition, the survival of ES-derived motor neurons *in vitro* drops significantly after 3 DIV (from 62% at 3 DIV, to 8% at 9 DIV) (Bryson et al., 2014). Therefore to ensure sample sizes were large enough for our screening purposes, we chose to assay our ES-derived motor neurons after 3 DIV.

The use of *Hb9*-GFP motor neurons is well suited for our particular screening assay as it eliminates the need for additional manipulations of the cells (immunocytochemistry), allows the microscope to autofocus on the motor neuron layer rather than underlying glial cells and allows our automated image analysis software to easily identify motor neurons. As the GFP signal is strongest in the soma and weaker in neurites, the analysis software can easily isolate cell bodies based on fluorescence intensity. It is worth noting that HB9 plays a key role in early motor neuron development and its expression peaks around E11 (Arber et al., 1999). This again suggests that the *Hb9*-GFP motor neurons assayed in our screen are not fully mature. However, since our results in ES-derived motor neurons can be reproduced both in primary motor neurons and *in vivo* (Sections 3.4 and 4.4.2),

it appears that the accumulation assay is able to produce reliable, physiologically relevant results.

Design of the assay

The most obvious limitation of the accumulation assay is the fact that it will not only detect compounds that alter axonal transport, but also those that affect other processes, such as the binding, internalisation, recycling or degradation of H_CT and α-$p75^{NTR}$. It is therefore likely to generate a number of "false positives" when used to identify modifiers of axonal transport. However, the rationale behind using the accumulation assay was that it would act as a preliminary screen, to identify compounds that were *likely* to be affecting axonal transport, and that subsequent live *in vitro* axonal transport assays would always be necessary to validate hit compounds.

Accumulation of H_CT and α-$p75^{NTR}$ was assessed in the cell body of motor neurons after two hours incubation with the probes. Robust axonal transport of the probes begins after approximately 30 minutes, and therefore the two hour time point was chosen as it would allow sufficient time for compounds to have a significant effect on axonal transport. This reasoning was validated when EHNA, ciliobrevin A and ALCAR were tested in the accumulation assay and their effects on axonal transport could be sensitively detected (Figure 3.2, Figure 3.4 and Figure 3.5). However, the assay could be improved by applying the probes as a "pulse", for example for 15 minutes, and then allowing them to accumulate for a further two hours in the presence of the compound to be tested. This would eliminate any effects of the compounds on the binding of the probes, hopefully making the assay more sensitive to changes in axonal transport.

Another limitation of the assay was that the probes were applied to motor neurons in mass culture. It is clear that a proportion of the H_CT and α-$p75^{NTR}$ accumulating in the soma will simply be a result of the probes binding and being internalised *in situ*, rather than a result of retrograde transport along the axon. One way to overcome this would be to culture motor neurons in microfluidic devices (Restani et al., 2012), which would allow the fluidic isolation of cell bodies and axon terminals. In this way, the probes could be applied selectively to the axon terminals and any

H_CT and α-$p75^{NTR}$ accumulating in the cell bodies must have been delivered by retrograde axonal transport. The only exception to this would be if motor neurons released H_CT and/or α-$p75^{NTR}$ and it was taken up by other motor neurons (rather than interneurons as is the case *in vivo).* However, the use of microfluidic devices is not yet suited for use in screening assays, as the preparation is time consuming and expensive and such devices are not available in a format suitable for automated microscopy.

The assays described in this Chapter were performed in 24 well glass bottom plates and the screening library provided by GSK contained only 56 compounds. It was therefore possible to handle the number of 24 well plates required to perform the assay in triplicate. However, such a plate format would not be suitable for screening typical pharmaceutical compound libraries. If the assay were to be used for high throughput screening, 96 well or even 384 well plates would have to be utilised. In fact, microscopy-based survival assay screens have already been successfully performed using mouse ES-derived motor neurons in 384 well plates (Yang et al., 2013). It should therefore be possible to scale up the accumulation assay in this way. However, a significant amount of work would be required to optimise the motor neuron cultures, for example to prevent clustering of the cells at the centre of the well (more likely with a reduced plating volume), and to achieve a high enough frequency of GFP-positive cells such that sufficient n numbers are reached with automated image acquisition.

Automated microscopy and analysis of results

Imaging of screening plates was performed using a confocal microscope with an automated stage and an autofocus function. This allowed plates to be imaged unattended and often overnight in order to save time. Confocal microscopy was used as it allowed sufficient resolution for individual endosomes to be visualised in the cell body. However, it was not possible to optimise the autofocus function of the microscope to ensure that every image of every well was in focus. This is most likely an inherent problem of neuronal cultures, where neuronal cell bodies are large and often at different heights due to variations in the underlying glial layer. Therefore in order to acquire in-focus, comparable images, a Z stack of four images was acquired at each location. In this way the optimal image could be

selected for analysis. However, in combination with acquiring images with a high enough resolution to see individual endosomes, this increased the imaging time significantly, with one 24 well plate taking up to 10 hours to fully image. It also added another step to the analysis process – selection of the optimal image from each Z stack – that could not be automated. Again, such a protocol would not be suitable for screening much larger libraries of compounds. To solve this problem, automated fluorescence imaging (using systems such as the Cellomics ArrayScan or Opera Phenix™) could be utilised rather than confocal microscopy. This would allow much faster image acquisition. Although it is unlikely that individual endosomes could be visualised using such a system, it is likely that robust staining intensity data could still be collected.

Image datasets were analysed using Cell Profiler – a free image analysis software that allows you to build customised analysis pipelines. In this way, a pipeline could be developed that identified cell bodies based on size constraints and the intensity of the *Hb9*-GFP signal, and then measured the intensity of the H_CT and α-$p75^{NTR}$ staining within the identified cell bodies. This part of the pipeline worked very nicely, and could sensitively and reproducibly detect changes in accumulation caused by EHNA, ciliobrevin A and ALCAR. The pipeline was also set up to identify individual vesicles within the cell bodies and determine the number of vesicles per cell body. Unfortunately, as can be seen in Figure 3.8, the software was not always able to accurately identify single endosomes. This problem was particularly obvious when there were large numbers of vesicles accumulated, as they tend to cluster and it is difficult to teach the software to recognise individual endosomes within a cluster. Increasing the resolution and magnification of the images acquired would help improve this, but it would not be conducive for screening purposes. The vesicle number data acquired from our screen did correlate with the staining intensity results (for example, E4 caused the largest increase in accumulation judged by both parameters), indicating it is a sensitive measure of H_CT and α-$p75^{NTR}$ accumulation. However, due to the limited sensitivity of this parameter, I would recommend only using this data to help validate hits from the staining intensity results, rather than as a primary source for selecting hit compounds.

3.6.2. Identification and validation of lead compounds

3.6.2.1. Preliminary screening

Limitations of the protocol

The accumulation assay was successfully used to identify three active compounds in the preliminary screen – A1, C3 and E4. When tested in *in vitro* axonal transport assays, two of these compounds were found to alter the retrograde axonal transport of H_CT and α-$p75^{NTR}$. This indicates that the accumulation assay is an effective way to screen compounds for their effects on axonal transport in motor neurons.

A limitation of our preliminary screen was the lack of a positive control in the screening plates. At the start of the Chapter, we were able to demonstrate that ALCAR causes a small acceleration of retrograde axonal transport and that this can be detected by the accumulation assay (see Section 3.2.1). It would have been a useful control in our screening plates, in order to confirm that the screening conditions, microscope settings and data analysis protocol were optimal for identifying enhancers of axonal transport and also to quantitatively compare the effects on accumulation of any active compounds with the known effect of ALCAR on accumulation and transport.

Consideration of the results

The preliminary screening identified A1 as an active compound and it was subsequently shown to correct $SOD1^{G93A}$-induced deficits in retrograde axonal transport in primary motor neurons. Interestingly, compound A1 actually had no effect on retrograde axonal transport speeds in wild type motor neurons. Considering compound A1 was identified in the accumulation assay using wild type ES-derived motor neurons, this was a somewhat surprising result. It appears that, by chance, compound A1 affects the somatic accumulation of H_CT and α-$p75^{NTR}$ through a mechanism unrelated to its effect on axonal transport in $SOD1^{G93A}$ motor neurons and this is why it was identified as a hit in the accumulation assay. When we assessed the effects of the compounds on the internalisation of the probes, compound A1 caused a small but significant increase in the internalisation of α-$p75^{NTR}$, but not H_CT (Figure 3.14). p38 MAPK has been previously implicated in

the regulation of growth factor receptor internalisation (Zwang and Yarden, 2006) and early endocytic membrane trafficking by Rab5 (Cavalli et al., 2001). However, these studies found that activated p38 MAPK enhances internalisation, rather than inhibits it, and therefore cannot explain our results.

Another point worth noting is the observed toxicity of compounds C3 and E4 when tested in live *in vitro* axonal transport assays at the screening concentration of 2 μM. This is most likely due to the fact that the compounds inhibit key neurotrophic (RET; C3) and growth factor receptors (IGF1R; E4). However it is hard to explain why this toxicity was not observed initially in the accumulation assay, as all of our screening plates were checked for overt signs of toxicity. It could be that the presence of axonal blebbing was not visible unless viewed at 63X or 100X as used for *in vitro* axonal transport assays. Alternatively it could be that the culturing conditions used for axonal transport assays (MatTek dishes versus 24-well plates) make the neurons more sensitive to the toxic effects of these compounds. These results highlight the fact that if the accumulation assay were to be used to screen more compounds, especially if it were used for larger libraries, it would be necessary to check for motor neuron toxicity in parallel.

It is also possible that some of the compounds in our screening assay were incorrectly eliminated as false negatives. This is an inherent problem with screening, as only a limited number of compounds can be taken forward for further testing. We initially identified six active compounds, based on the staining intensity and vesicle number data (see Figure 3.10 and Figure 3.11). After performing dose response analysis and additional repeats at the screening concentration, only three of these compounds were chosen for further investigation. Interestingly the three remaining compounds (A4, D1, D3) were later revealed to have the same target - vascular endothelial growth factor receptor 2 (VEGFR-2). VEGFR-2 has not been linked to the regulation of axonal transport previously. However, the receptor activates a number of downstream kinases including p38 MAPK and PKC, both of which have been shown to negatively regulate fast axonal transport (Ozsarac et al., 2003, Morfini et al., 2013) and could explain why VEGFR-2 inhibitors were identified in our screen.

3.6.2.2. Target validation screening

Additional inhibitors of p38 MAPK and IGF1R were screened using the accumulation assay to validate these kinases as the targets of A1 and E4 respectively (Figure 3.25). Four p38 MAPK inhibitors and three IGF1R inhibitors were selected as hit compounds and their effects on axonal transport are described in the following Chapters. A limitation of this screen was the bias towards inhibitors of p38 MAPK (see Table 5 in Materials and Methods). This was a reflection of GlaxoSmithKline's interests.

It should be noted that not all the p38 MAPK or IGF1R inhibitors that were screened had the same effect. In fact, the majority of compounds did not have a significant effect on the accumulation of either probe. This is not entirely surprising, as the inhibitors had only been previously tested in *in vitro* kinase assays and/or in efficacy assays in standard cell lines. It is therefore possible that these compounds have reduced permeability through the motor neuron plasma membrane, are degraded by motor neurons or the screening concentration of 2 μM is not high enough to yield significant kinase inhibition.

There are also some compounds, however, that appear to have the opposite effect on accumulation of the probes compared to our lead compounds A1 and E4. It could be that these compounds are toxic to motor neurons, or that their off-target effects alter accumulation in a way that obscures any effect on axonal transport. There also appears to be a trend in increasing effect on H_CT accumulation with the IGF1R-targeted inhibitors 2-B3, 2-G2 and 2-C1 (shown in green in Figure 3.25). It would be interesting to look into the chemical and pharmacological profiles of these compounds and try to determine what underlies this effect. This result also highlights the fact that it may be possible to identify compounds able to specifically enhance the axonal transport of just one of the probes. Colocalisation studies in our laboratory have previously shown that H_CT and α-$p75^{NTR}$ are transported in the same signalling endosomes (Lalli and Schiavo, 2002, Deinhardt et al., 2006b). However, the present results suggest there could be different mechanisms regulating their retrograde axonal transport.

3.6.3. Further applications of the accumulation assay

Deficits in axonal transport have been described in several neurodegenerative diseases (Millecamps and Julien, 2013) and therefore the identification of novel pharmacological enhancers of retrograde axonal transport could be useful for a number of CNS pathologies, in addition to ALS. The accumulation assay could be applied to different neuronal types in order to identify potential novel therapeutics and to understand the role of axonal transport defects in other neurodegenerative diseases. For example, in Huntington's disease, mutant htt has been shown to induce defects in both retrograde and anterograde axonal transport (Morfini et al., 2009, Her and Goldstein, 2008, Zala et al., 2008). Identifying novel enhancers of retrograde axonal transport in striatal and hippocampal neurons could therefore potentially allow the role of anterograde versus retrograde defects to be distinguished in Huntington's disease.

It would also be very interesting to perform the accumulation assay in both mouse ES-derived motor neurons expressing ALS-associated mutations and ALS patient iPSC-derived motor neurons. A number of different ALS patient–specific iPSCs have now been successfully differentiated into spinal cord motor neurons, including those with disease-causing mutations in SOD1 (Alami et al., 2014, Chen et al., 2014), TDP43 (Egawa et al., 2012, Devlin et al., 2015), VCP (Patani et al., 2012) and C9orf72 (Sareen et al., 2013, Devlin et al., 2015). In addition, some of these iPSC-derived motor neurons have already been utilised in screening assays (Egawa et al., 2012) and could therefore help generate more disease-relevant hits than assays performed in mouse cell lines. However, preliminary work is required to determine whether ES-derived motor neurons expressing ALS-associated mutations and ALS patient iPSC-derived motor neurons display defects in axonal transport.

Chapter 4. Inhibition of p38 MAPK rescues axonal transport defects in SOD1^{G93A} mice

4.1. Introduction

Results presented in Chapter 3 suggest that inhibition of p38 MAPK is able to restore defects in retrograde axonal transport that are observed in motor neurons derived from the SOD1^{G93A} mouse model of ALS.

p38 MAPK is a member of the mitogen-activated protein kinase family of serine/threonine kinases, which also includes extracellular signal-regulated kinases (ERKs) and c-Jun-N-terminal kinases (JNKs) (see Figure 4.1). p38 MAPK is activated in response to inflammation and stressful stimuli, for example tumour necrosis factor-α (TNFα), interleukin 1 (IL1), heat shock and UV irradiation. The kinase is involved in a wide variety of cellular processes, including phosphorylation of cytoskeletal proteins, biosynthesis of cytokines and nitric oxide, protein degradation and endocytosis (Cuadrado and Nebreda, 2010).

There are four p38 MAPK isoforms: α (MAPK14), β (MAPK11), γ (MAPK12) and δ (MAPK13), all of which are widely expressed in mammalian tissues. However, p38 MAPKα and β are considered to be the major isoforms expressed in the central nervous system (Morfini et al., 2013). There is some overlapping substrate specificity between the four isoforms and a degree of functional redundancy has been hypothesised (Cuenda and Rousseau, 2007).

4.1.1. The p38 MAPK signalling cascade

All isoforms are activated by phosphorylation at Thr180 and Tyr182 in the activation loop. Phosphorylation induces a conformational change that removes steric blocking of the active site and stabilizes the activation loop in an open conformation, allowing substrate binding (Cuenda and Rousseau, 2007). For all four isoforms, this phosphorylation is mediated by the upstream kinase (MAPKK) MKK6. In addition, p38 MAPK α, γ and δ are also phosphorylated by MKK3 and p38 MAPK α and δ can also be phosphorylated by MKK4, an activator of JNK

(Cuadrado and Nebreda, 2010). All of these MKKs are in turn activated by upstream kinases (MAPKKKs), such as ASK1 (Bendotti et al., 2005) (illustrated in Figure 4.1).

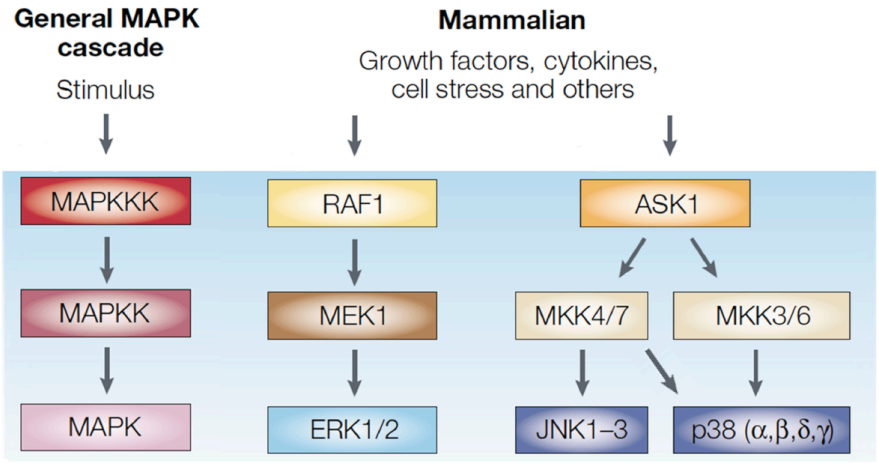

Figure 4.1. The mitogen-activated protein kinase (MAPK) signalling cascade
MAPK cascades are comprised of a MAPK kinase kinase (MAPKKK) which, when activated by phosphorylation, phosphorylates a MAPK kinase (MAPKK). This MAPKK goes on to phosphorylate and activate its target MAPK. In mammals, there are three families of MAPKs: the extracellular signal-regulated kinases 1 and 2 (ERK1/2), the c-Jun amino-terminal kinases (JNKs) and the p38 MAPKs. Modified from (Pierce et al., 2002). Reprinted with permission from the Nature Publishing Group.

p38 MAPK signalling is terminated by the activity of a number of phosphatases. These enzymes dephosphorylate Thr180 and Tyr182 in the activation loop and return p38 MAPK to its resting conformation. This termination of signalling can be mediated by generic serine/threonine phosphatases, such as protein phosphatase 2A and 2C, and/or generic tyrosine phosphatases, such as striatal enriched tyrosine phosphatase (STEP). Dephosphorylation can also be mediated by a family of dual-specificity phosphatases that are able to dephosphorylate both phospho-tyrosine and phospho-threonine residues (Cuadrado and Nebreda, 2010).

4.1.2. Downstream targets

p38 MAPK is implicated in the regulation of a wide variety of cellular processes. Therefore it is not surprising that it has been shown to phosphorylate a plethora of downstream targets. As well as activating downstream kinases such as

MAPAPK2/3, MNK1/2 and MSK1/2 (Cuadrado and Nebreda, 2010), p38 MAPK also phosphorylates a variety of non-kinase cytoplasmic and nuclear proteins directly (see Figure 4.2). It is of particular interest to note that p38 MAPK has been shown to phosphorylate proteins involved in endocytic trafficking, including Rho-GDI (Cavalli et al., 2001) and the Rab5 effector EEA1 (Mace et al., 2005). p38 MAPK has also been demonstrated to phosphorylate the microtubule-associated protein tau (Reynolds et al., 2000).

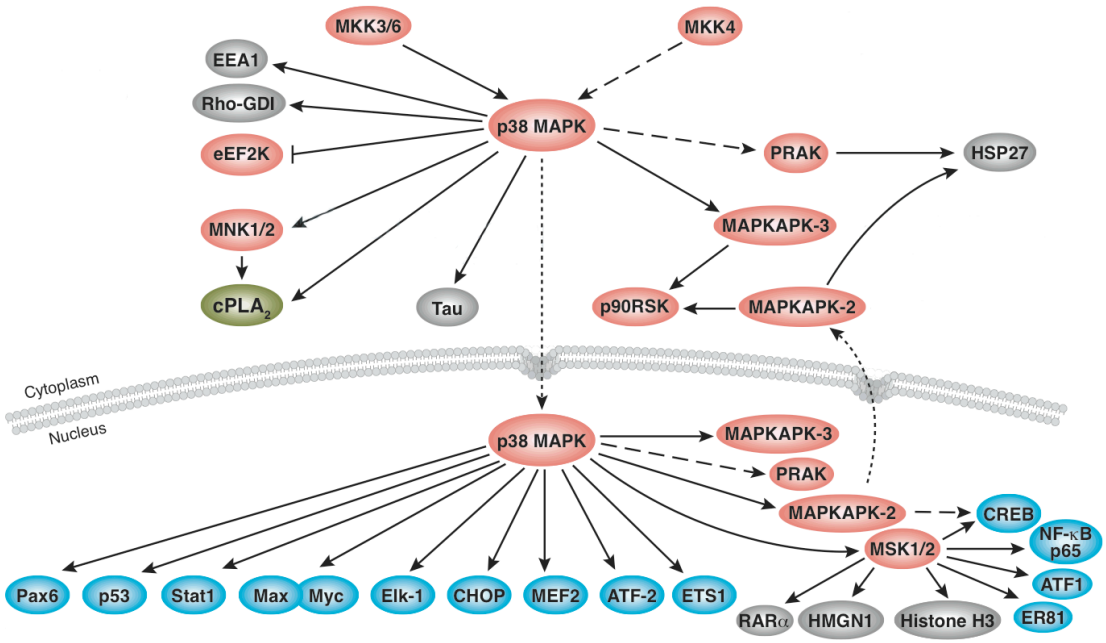

Figure 4.2. Downstream targets of p38 mitogen-activated protein kinase
p38 MAPK has been shown to phosphorylate a wide range of downstream targets, including both cytoplasmic and nuclear proteins. Illustration reproduced with permission from Cell Signaling Technology, Inc. (www.cellsignal.com).

The aim of this Chapter was to determine the role of p38 MAPK in inducing retrograde axonal transport deficits in the SOD1^{G93A} mouse model of ALS.

4.2. *In vitro* validation of p38 MAPK as the target kinase

The results of the preliminary screening assay and *in vitro* axonal transport experiments described in 0 suggest that inhibitors of p38 MAPK are able to rescue deficits in retrograde axonal transport *in vitro* in $SOD1^{G93A}$ motor neurons.

In this Chapter, p38 MAPK is validated as the target kinase responsible for the observed effects on axonal transport and its activity in $SOD1^{G93A}$ motor neurons is investigated both *in vitro* and *in vivo*. In addition, the effects of p38 MAPK inhibition on retrograde axonal transport *in vivo* are investigated.

4.2.1. Confirming the hits of the validation screen

In order to confirm that the effects of compound A1 were due to inhibition of p38 MAPK and not due to off-target effects, additional inhibitors were screened in ES-derived motor neurons using the accumulation assay (described in Section 3.5). Four active compounds were identified (2-A3, 2-C3, 2-D3, 2-H2) and tested in live *in vitro* axonal transport assays in primary $SOD1^{G93A}$ motor neurons. All four compounds were found to mimic the effect of compound A1, restoring retrograde axonal transport in $SOD1^{G93A}$ motor neurons (Figure 4.3; $SOD1^{G93A}$ versus $SOD1^{G93A}$ + 2 μM compound 2-A3: $p = 0.010$, $SOD1^{G93A}$ versus $SOD1^{G93A}$ + 2 μM compound 2-C3: $p = 0.047$, $SOD1^{G93A}$ versus $SOD1^{G93A}$ + 2 μM compound 2-D3: $p = 0.053$, $SOD1^{G93A}$ versus $SOD1^{G93A}$ + 2 μM compound 2-H2: $p = 0.020$).

To further validate p38 MAPK as the target, we next investigated the effect of activating p38 MAPK on retrograde axonal transport in wild type motor neurons. Live *in vitro* axonal transport assays were performed in the presence of 0.5 μg/ml anisomycin, an established activator of p38 MAPK (Figure 4.4A). Activation of p38 MAPK in primary wild type motor neurons was found to significantly inhibit the retrograde axonal transport of H_CT-labelled carriers ($p = 0.0003$; Figure 4.4B).

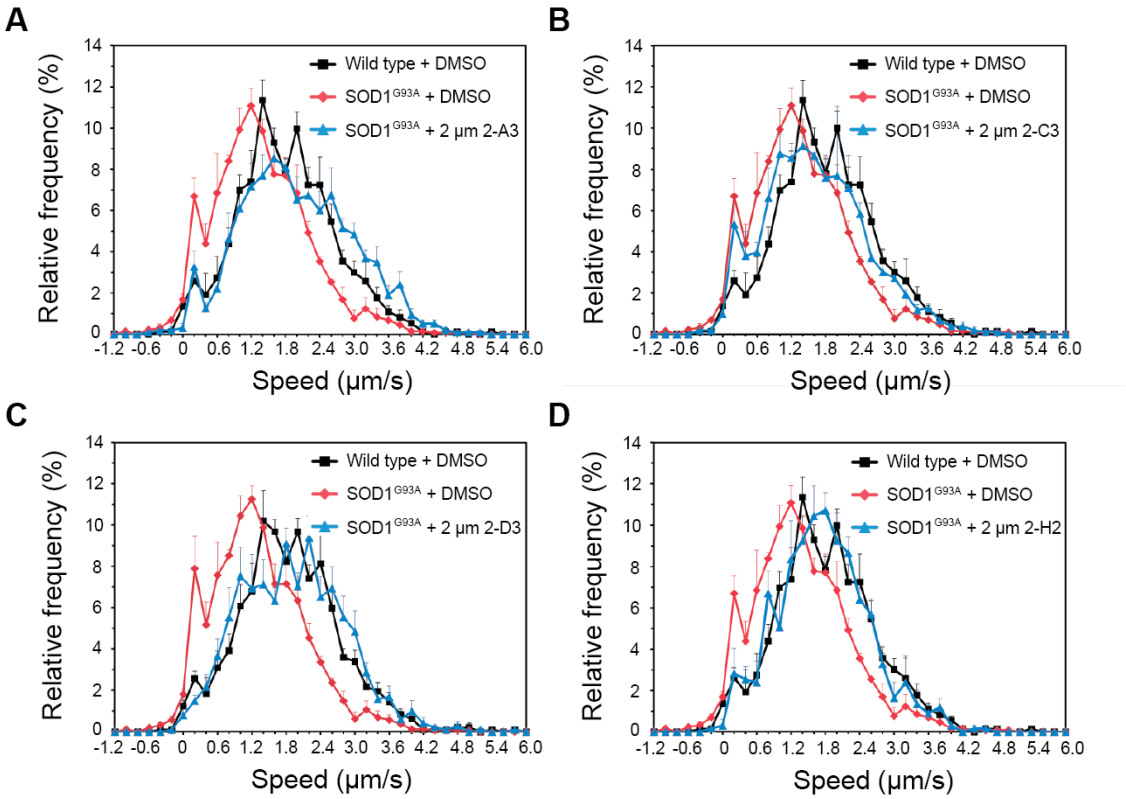

Figure 4.3. Structurally diverse inhibitors of p38 MAPK also correct retrograde axonal transport defects in SOD1^{G93A} motor neurons

Speed profiles of H_CT carriers in wild type + DMSO (black squares), SOD1^{G93A} + DMSO (red diamonds) and SOD1^{G93A} motor neurons treated with 2 µM of each of the hit p38 MAPK compounds (blue triangles): 2-A3 (A), 2-C3 (B), 2-D3 (C), 2-H2 (D). Wild type: 74 carriers, 8 axons; SOD1^{G93A}: 119 carriers, 7 axons; SOD1^{G93A} + 2 µM 2-A3: 120 carriers, 7 axons; SOD1^{G93A} + 2 µM 2-C3: 117 carriers, 8 axons; SOD1^{G93A} + 2 µM 2-D3: 166 carriers, 9 axons; SOD1^{G93A} + 2 µM 2-H2: 94 carriers, 7 axons. 3 independent experiments.

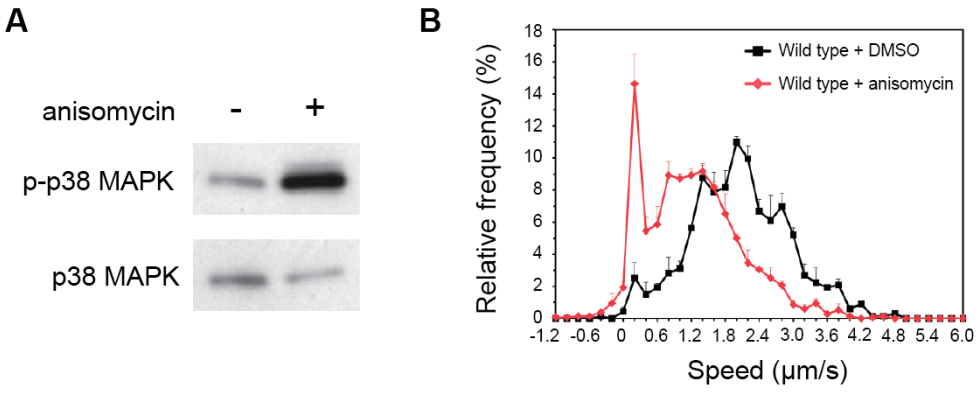

Figure 4.4. Activation of p38 MAPK inhibits retrograde axonal transport of H_CT

(A) Treatment of wild type motor neuron cultures with 0.5 µg/ml anisomycin for 30 min causes a substantial activation of p38 MAPK. (B) Speed profiles of H_CT carriers in primary wild type motor neuron cultures treated with either DMSO (black squares) or 0.5 µg/ml anisomycin (red diamonds). Anisomycin causes a shift to slower transport speeds (DMSO treated: 77 carriers, 8 axons; 76 Anisomycin treated: carriers, 8 axons; 3 independent experiments).

4.2.2. Determining the effects of p38 MAPK inhibition on the retrograde axonal transport of late endosomes/lysosomes and autophagosomes

Up until this point, the effect of p38 MAPK inhibition had only been studied using H_CT and α-75^{NTR} (cargoes of signalling endosomes). It was therefore interesting to investigate whether p38 MAPK was responsible for defects in the axonal transport of other cargoes. To this end, we performed *in vitro* axonal transport assays in primary motor neurons using Lysotracker™. Lysotracker™ is a fluorescent dye that labels all acidic organelles (late endosomes/lysosomes and autophagosomes) and therefore allows both retrograde and anterograde axonal transport to be analysed. The direction of transport was determined in these experiments by co-incubation with H_CT. The results with Lysotracker™ indicate that there is a defect in the retrograde axonal transport of acidic organelles in $SOD1^{G93A}$ motor neurons (Figure 4.5A; p = 0.145). As in our experiments investigating the axonal transport of signalling endosomes, we found that treatment of $SOD1^{G93A}$ motor neurons with 2 µM A1 was able to correct deficits in Lysotracker™ retrograde transport (Figure 4.5B; $SOD1^{G93A}$ versus $SOD1^{G93A}$ + 2 µM compound A1: p = 0.026).

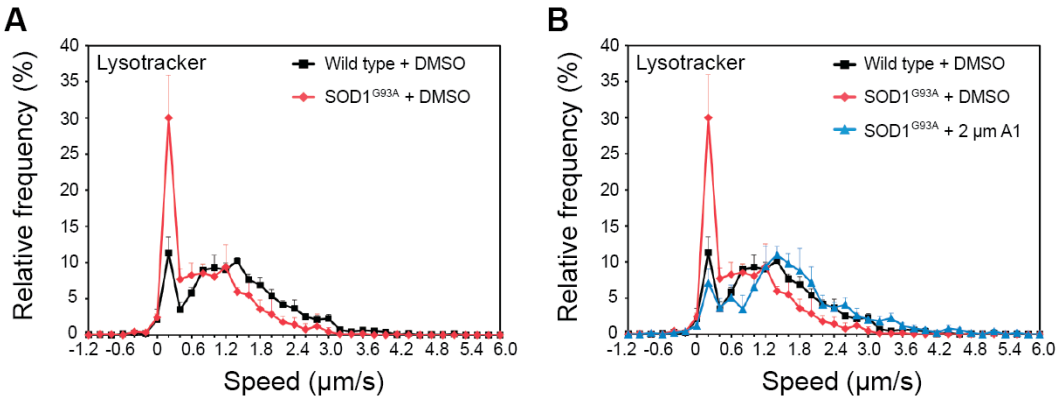

Figure 4.5. Compound A1 rescues defects in the retrograde axonal transport of Lysotracker™ in $SOD1^{G93A}$ motor neurons

(A) Retrograde speed profiles of Lysotracker™-labelled carriers in wild type (black squares) and $SOD1^{G93A}$ (red diamonds) motor neuron cultures. (B) Retrograde speed profiles of Lysotracker™-labelled carriers in wild type + DMSO (black squares), $SOD1^{G93A}$ + DMSO (red diamonds) and $SOD1^{G93A}$ + 2 µM A1 (blue triangles) motor neuron cultures (wild type: 85 carriers, 12 axons; $SOD1^{G93A}$: 30 carriers, 15 axons; $SOD1^{G93A}$ + 2 µM A1: 39 carriers, 13 axons; 5 independent experiments).

The anterograde axonal transport of mitochondria and RNA has also been previously shown to be defective in ALS (Alami et al., 2014, Bilsland et al., 2010)

and p38 MAPK has been suggested to be responsible for mutant SOD1-induced defects in anterograde axonal transport in squid axoplasm (Morfini et al., 2013).

However, in our *in vitro* axonal transport assays using Lysotracker™, we could not detect any deficit in anterograde axonal transport (Figure 4.6; p = 0.698). This suggests that axonal transport defects in ALS are both cargo and direction-specific.

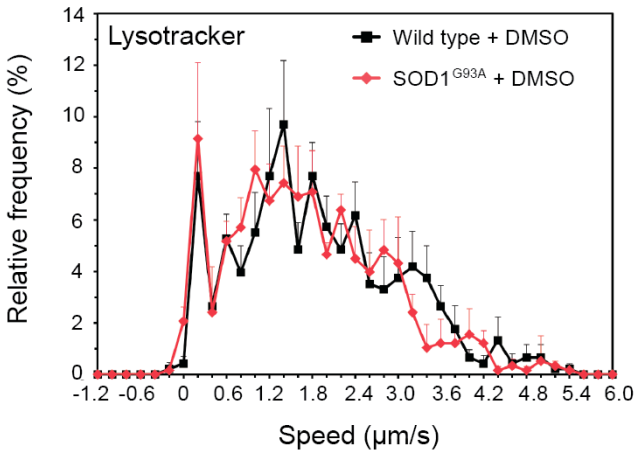

Figure 4.6. The anterograde axonal transport of Lysotracker™ is not defective in SOD1^{G93A} motor neurons

Speed profiles of Lysotracker™-labelled carriers moving in the anterograde direction in wild type (black squares) and SOD1^{G93A} (red diamonds) motor neuron cultures (wild type + DMSO: 44 carriers, 14 axons; SOD1^{G93A} + DMSO: 45 carriers, 15 axons; 5 independent experiments).

4.2.2.1. p38 MAPK is activated in motor neurons isolated from SOD1^{G93A} mice

The ability of inhibitors of p38 MAPK to rescue defects in retrograde axonal transport in SOD1^{G93A} motor neurons, whilst having no effect on transport speeds in wild type motor neurons, suggests that the kinase is specifically activated in SOD1^{G93A} motor neurons.

Indeed, p38 MAPK has been previously shown to be activated in motor neurons of adult SOD1^{G93A} mice (Tortarolo et al., 2003, Dewil et al., 2007, Morfini et al., 2013). However, given the effect of compound A1 in our *in vitro* axonal transport assays, it was important to assess the levels of phosphorylated p38 MAPK in primary

SOD1^{G93A} motor neurons. Immunofluorescence analysis revealed increased levels of phospho-p38 MAPK in motor neurons overexpressing human SOD1^{G93A} (Figure 4.7A), whilst overexpression of the wild type form of the human SOD1 protein (SOD1^{WT}) had no effect (Figure 4.7B).

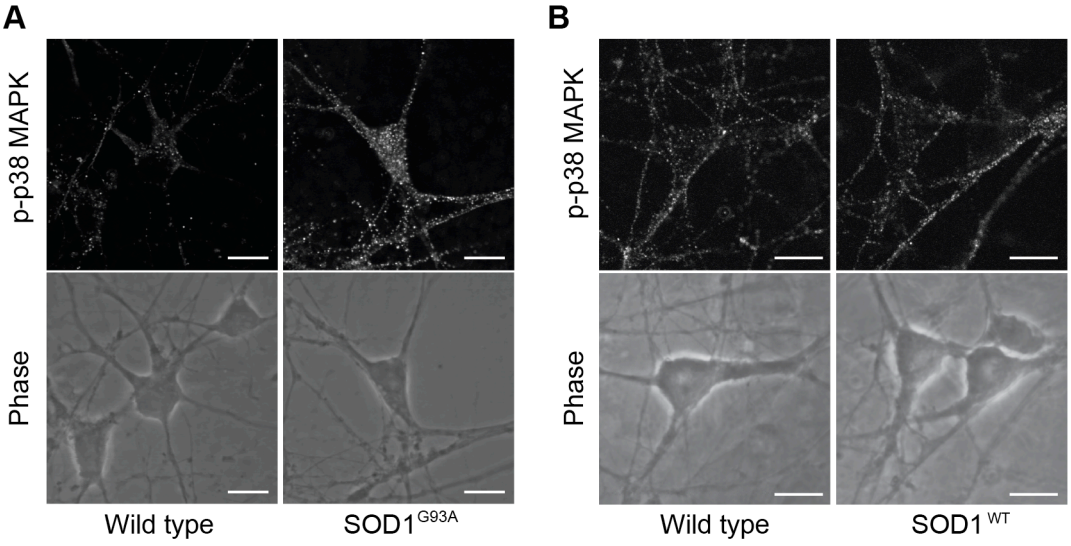

Figure 4.7. p38 MAPK activation can be seen by immunofluorescence in primary SOD1^{G93A} motor neurons

(A) Immunofluorescence staining using an antibody directed against phosphorylated p38 MAPK reveals an increase in phopsho-p38 MAPK levels in SOD1^{G93A} motor neurons compared to wild type controls. (B) As a control, motor neurons overexpressing wild type SOD1 were compared with wild type motor neurons. p38 MAPK is not activated in these motor neurons. Scale bars, 10 μm.

Western blot analysis of lysates made from primary motor neuron cultures confirmed that there was a small but significant increase in phospho-p38 MAPK levels in SOD1^{G93A} motor neurons compared to wild type controls and also confirmed that 2 μM compound A1 caused a significant inhibition of p38 MAPK activity in SOD1^{G93A} motor neurons (Figure 4.8A). In addition, we confirmed that overexpression of wild type human SOD1 (SOD1^{WT}) was not responsible for the increased levels of phospho-p38 MAPK in these cultures (Figure 4.8B).

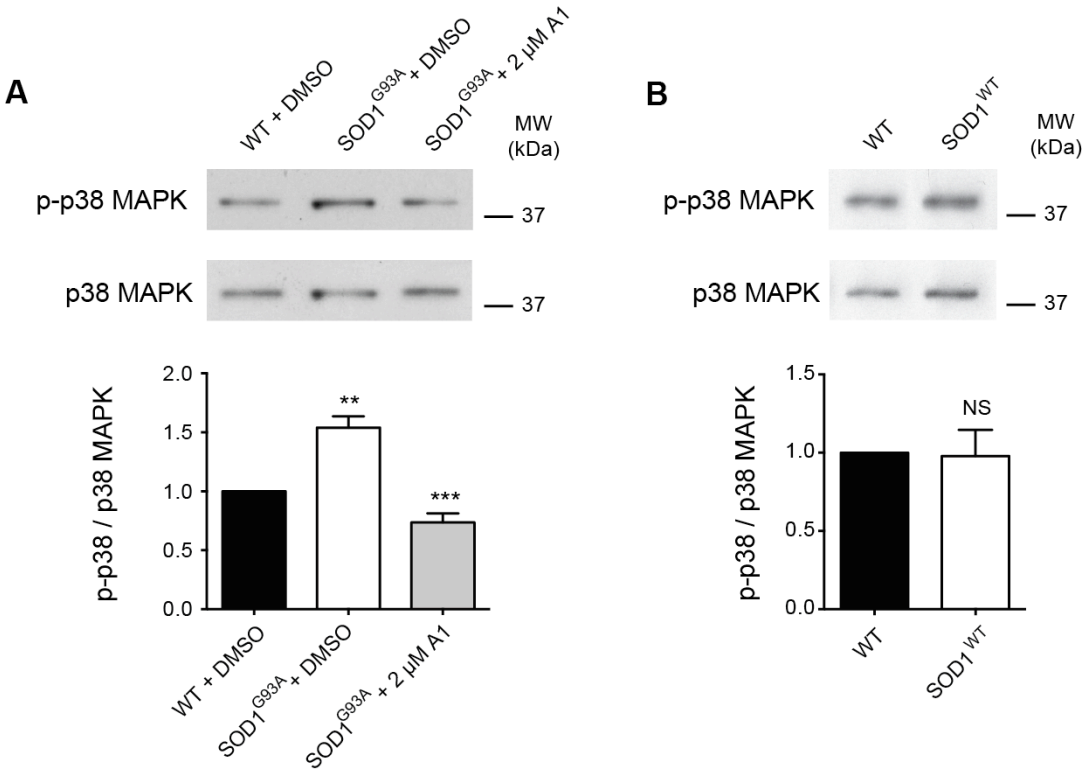

Figure 4.8. p38 MAPK is activated in primary SOD1^{G93A} motor neurons

(A) *Top* Western blot showing activation of p38 MAPK in SOD1^{G93A} motor neuron cultures compared to wild type controls. Compound A1 normalises phospho-p38 MAPK in SOD1^{G93A} cultures to wild type levels. *Bottom* Western blot quantification reveals a 1.5 fold increase in phospho-p38 MAPK levels in SOD1^{G93A} motor neuron cultures compared to wild type cells, and confirms the normalisation of p38 MAPK activity by compound A1 (n = 3 independent experiments). ** p< 0.01, *** p < 0.001 (One-way ANOVA followed by Sidak's multiple comparison test). (B) *Top* Western blot showing p38 MAPK activity in motor neurons overexpressing the SOD1^{WT} protein. *Bottom* Western blot quantification detected no significant difference in phospho-p38 MAPK levels between wild type cultures and motor neurons overexpressing SOD1^{WT} (n = 3 independent experiments). Non-significant using unpaired Student's *t* test. Error bars represent SEM.

Western blot analysis was also performed on lysates of spinal cords collected from adult SOD1^{G93A} and SOD1^{WT} mice. Pre-symptomatic (36 d), early symptomatic (73 d), symptomatic (96 d) and late symptomatic (115 d) SOD1^{G93A} mice were chosen so that phospho-p38 MAPK levels could be directly correlated with the *in vivo* axonal transport defects previously described by our laboratory (Bilsland et al., 2010). Phospho-p38 MAPK levels were found to be increased in the spinal cord of pre-symptomatic SOD1^{G93A} mice, whilst SOD1^{WT} controls showed no increase compared to wild type mice (Figure 4.9). Phospho-p38 MAPK levels were observed

to be highest in early symptomatic SOD1^{G93A} mice - the age at which *in vivo* axonal transport defects are most severe (Bilsland et al., 2010).

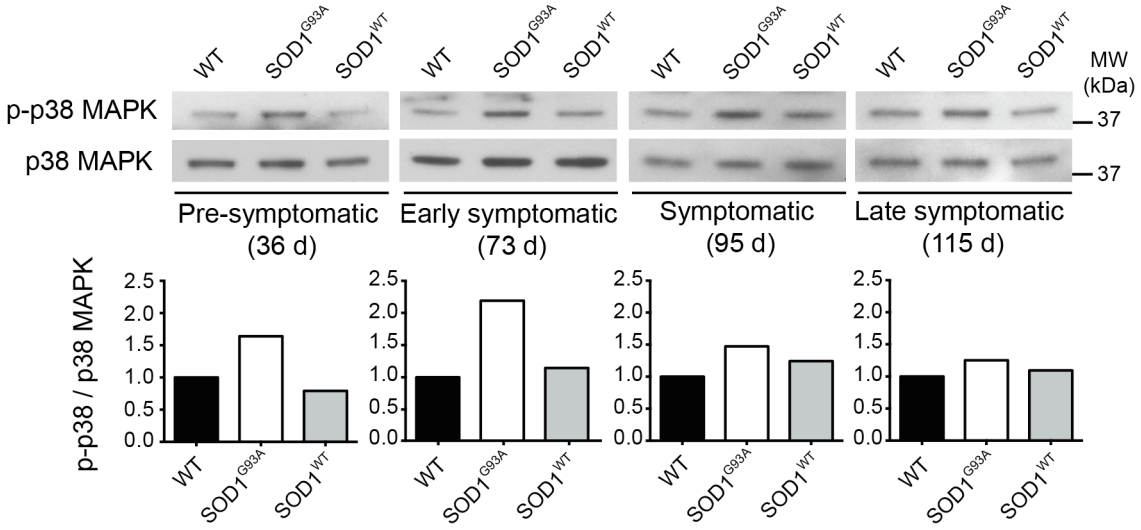

Figure 4.9. p38 MAPK is activated in an age-dependent manner in the spinal cord of adult SOD1^{G93A} mice

Western blot showing levels of phospho-p38 MAPK in spinal cord lysates from wild type, SOD1^{G93A} and SOD1^{WT} overexpressing mice. Phospho-p38 MAPK levels are increased in pre-symptomatic (36 d) and early symptomatic (73 d) SOD1^{G93A} mice. Spinal cords from SOD1^{WT} overexpressing mice show no change in phospho-p38 MAPK levels compared to wild type controls (n = 1 animal per condition).

Finally, the intracellular localisation of phospho-p38 MAPK was investigated *in vitro* in primary SOD1^{G93A} motor neurons. The punctate staining of phospho-p38 MAPK (as seen in Figure 4.7) suggested that the kinase might be located on endosomes. However phospho-p38 MAPK was not found to colocalise with either H_CT or Rab7 (Figure 4.10A and B). This was in agreement with previous data from our laboratory characterising the composition of H_CT-labelled endosomes using mass spectrometry (Solène Debaiseux, UCL Institute of Neurology). Furthermore, there was no colocalisation with AlexaFluor 488-conjugated wheat germ agglutinin (WGA; Figure 4.10C), which binds to sialic acid and *N*-acetylglucosaminyl residues and therefore labels all membranous compartments. To date, the intracellular location of activated p38 MAPK remains unclear.

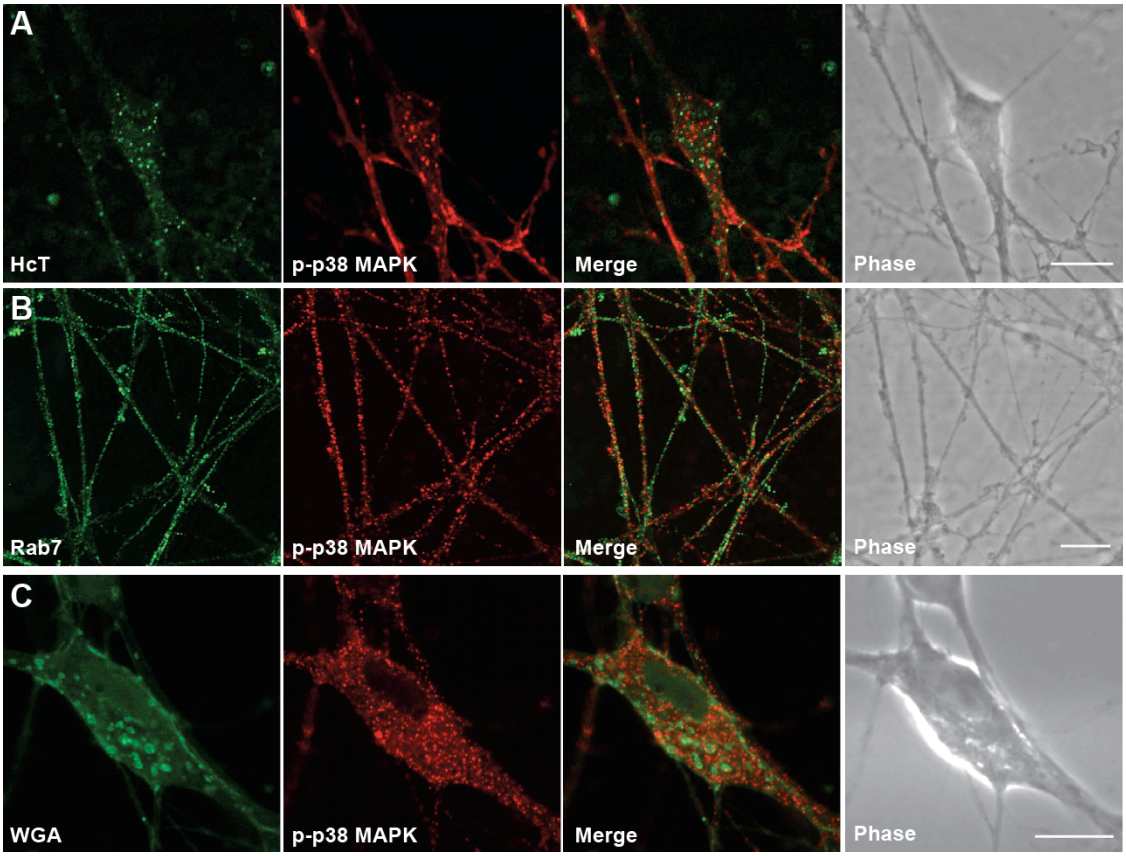

Figure 4.10. Activated p38 MAPK does not colocalise with endocytic markers
Primary SOD1^{G93A} motor neurons were fixed and co-stained for phospho-p38 MAPK and H_CT (A), Rab7 (B) or WGA (C). No colocalisation was found with any of the markers tested. Scale bars, 10 µm.

4.3. Identification of the p38 MAPK isoform responsible for axonal transport deficits in SOD1^{G93A} motor neurons

As there are four isoforms of p38 MAPK (α, β, γ and δ), it was important to distinguish which isoform(s) is responsible for the axonal transport defects observed in SOD1^{G93A} motor neurons.

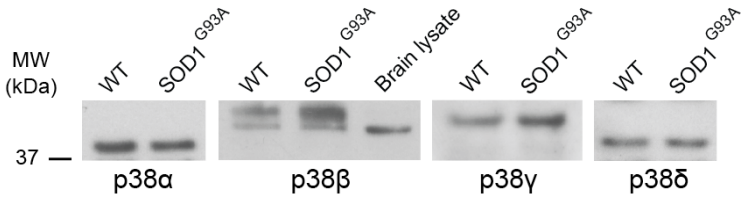

Figure 4.11. All four p38 MAPK isoforms are expressed in primary motor neurons
Lysates of primary wild type and SOD1^{G93A} motor neurons were subjected to western blotting using isoform-specific antibodies. Mouse brain lysate was loaded as an antibody control for p38 MAPKβ.

All four isoforms were found to be expressed in primary motor neuron cultures (Figure 4.11), therefore both genetic knockdown and pharmacological inhibition approaches were utilised in order to determine which isoform was affecting retrograde axonal transport.

4.3.1. Knockdown of p38 MAPK isoforms in N2A cells and primary motor neurons

p38 MAPKα (also known as MAPK14) is strongly expressed in both embryonic and adult motor neurons and has been previously shown to inhibit anterograde axonal transport in isolated squid axoplasm (Morfini et al., 2013). To investigate whether p38 MAPKα is responsible for the defects in retrograde axonal transport observed in mouse primary SOD1^{G93A} motor neurons, we ordered four shRNAs targeted against different sequences within the MAPK14 mRNA. The shRNA constructs contained an eGFP reporter gene, to allow easy identification of transfected/transduced cells. The shRNA constructs were first tested in N2A cells, in order to determine which caused the most efficient knockdown of p38 MAPKα.

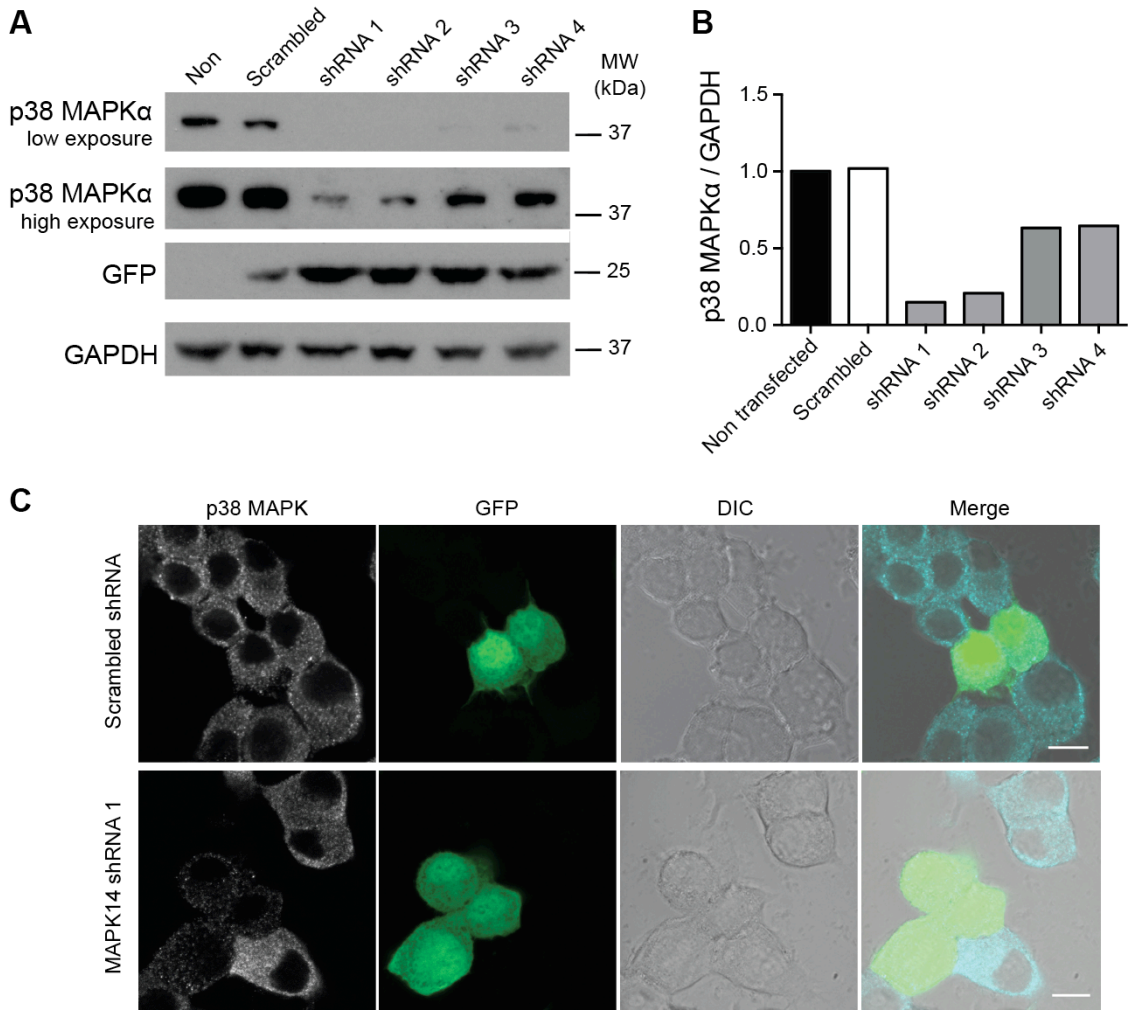

Figure 4.12. Testing MAPK14 shRNA constructs in N2A cells

(A) N2A cells were transfected with four different shRNA constructs against MAPK14 (p38 MAPKα), as well as a scrambled control. GFP indicates expression of the construct. (B) Quantification of the western blot in (A) showing knockdown of p38 MAPKα in N2A cells with different shRNA constructs. n = 1. (C) N2A cells transfected with either scrambled shRNA (*top)* or MAPK14 shRNA construct 1 (*bottom)* were stained with an antibody against p38 MAPK. GFP indicates transfected cells. Scale bars, 10 μm.

N2A cells were transfected with the shRNA constructs using Lipofectamine™ and lysates were prepared. Western blot analysis revealed that shRNA 1 caused the strongest knockdown of p38 MAPKα (Figure 4.12A and B), and this was confirmed by immunofluorescence (Figure 4.12C).

The MAPK14 shRNA 1 construct was therefore used to produce lentiviral particles, along with the scrambled construct as a control, so that we could knockdown p38 MAPKα in our primary motor neuron cultures.

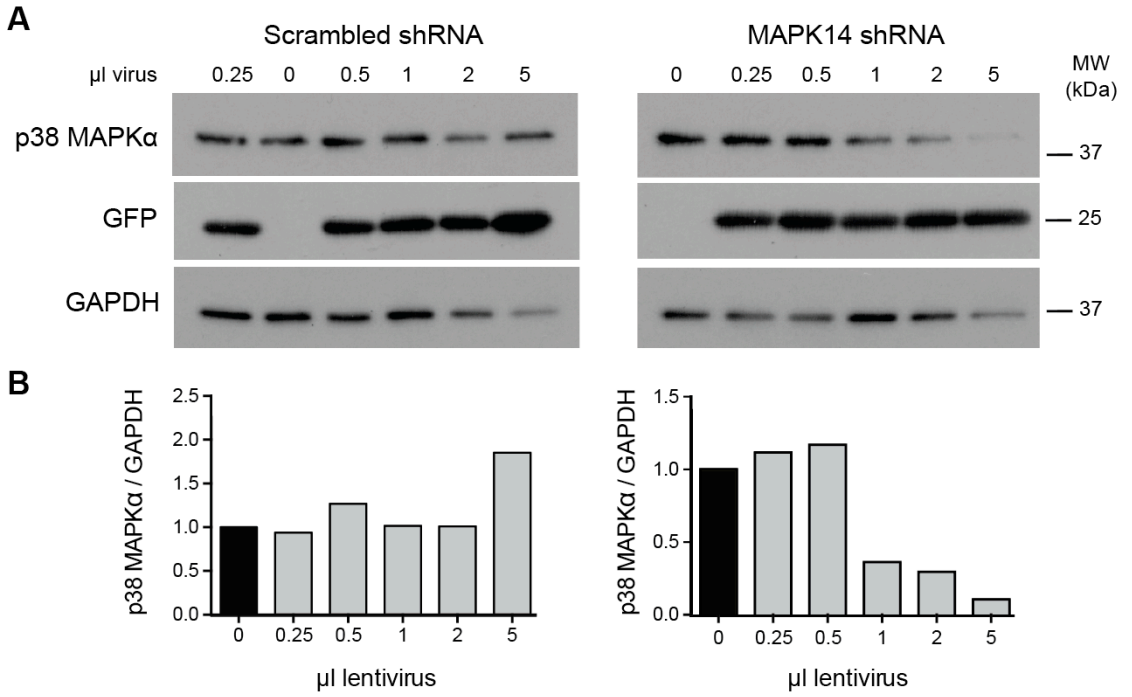

Figure 4.13. Knocking down p38 MAPKα in primary motor neuron cultures
(A) Lysates were made from motor neurons transduced with increasing amounts of lentivirus expressing either scrambled or MAPK14 shRNA. Western blotting with an antibody specific for p38 MAPKα reveals a dose-dependent knockdown with the MAPK14 shRNA but not when scrambled shRNA is used. GFP indicates expression of the shRNA construct. (B) Quantification of the blots shown in (A). Levels of p38 MAPKα are normalised to the loading control GAPDH. n = 1.

Lentiviral transduction of primary motor neurons with increasing amounts of MAPK14 shRNA was found to cause a dose-dependent reduction in p38 MAPKα protein levels, whilst scrambled shRNA had no effect (Figure 4.13). These results were also confirmed by immunofluorescence in primary motor neuron cultures (Figure 4.14).

Our lentiviral shRNA vectors could therefore be used to determine the effect of knocking down p38 MAPKα on retrograde axonal transport in primary motor neurons.

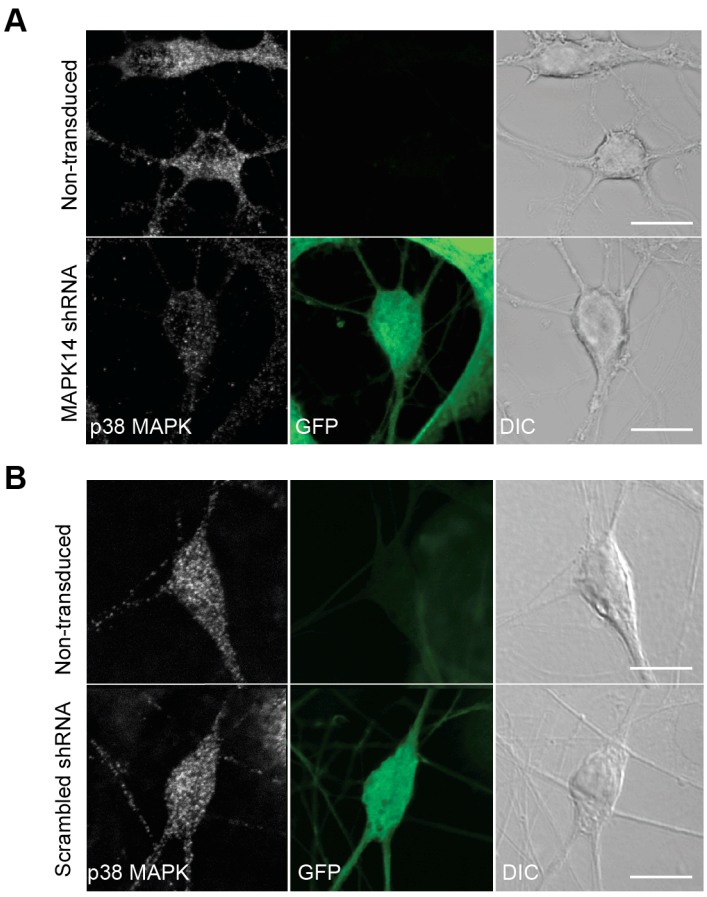

Figure 4.14. Immunofluorescence reveals knockdown of p38 MAPKα in motor neurons
(A) Comparison of non-transduced primary motor neurons with those transduced with MAPK14 shRNA. Motor neurons were stained with an antibody against pan p38 MAPK. GFP marks transduced motor neurons. Representative images were acquired from motor neurons on the same coverslip. (B) Comparison of non-transduced primary motor neurons with those transduced with a scrambled shRNA construct. Motor neurons were stained with an antibody against pan p38 MAPK. GFP expression indicates transduced motor neurons. Representative images were acquired from motor neurons on the same coverslip. Scale bars, 10 μm.

Firstly, an important control experiment was to determine whether transfection of primary motor neurons with the scrambled shRNA control had any effect on axonal transport speeds. This experiment was performed in both wild type and $SOD1^{G93A}$ motor neurons using the H_CT probe and 1 μl of the scrambled shRNA lentiviral vector. Scrambled shRNA was found to have no effect on retrograde axonal transport in either genotype (Figure 4.15; wild type untreated versus wild type + scram shRNA: $p = 0.624$, $SOD1^{G93A}$ versus $SOD1^{G93A}$ + scram shRNA: $p = 0.449$).

We therefore investigated the effect of knocking down p38 MAPKα in both wild type and $SOD1^{G93A}$ primary motor neurons (Figure 4.16).

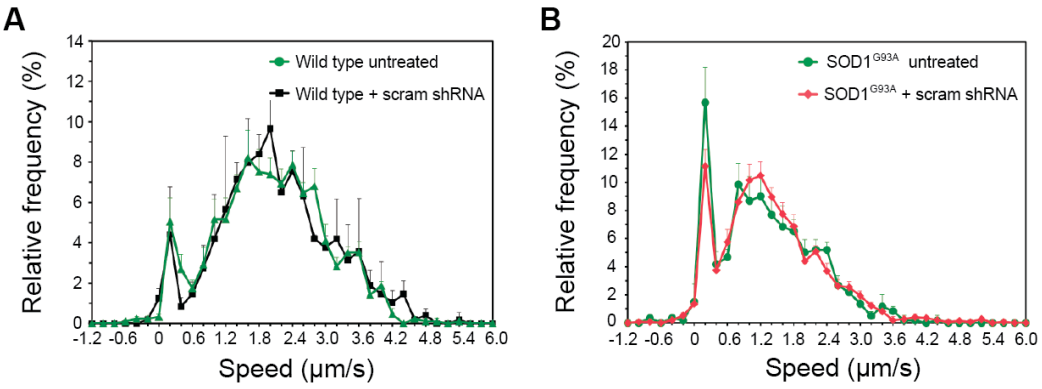

Figure 4.15. Transduction with scrambled shRNA has no effect on retrograde axonal transport in primary motor neurons

(A) Speed profiles of H_CT carriers in untreated wild type motor neurons (green circles) and wild type motor neurons transduced with 1 µl scrambled shRNA lentivirus (black squares). Comparison of the curves reveals that scrambled shRNA constructs have no effect on retrograde axonal transport speeds (wild type untreated: 62 carriers, 5 axons; wild type + scrambled shRNA: 89 carriers, 17 axons; 3 independent experiments). (B) Speed profiles of H_CT carriers in untreated SOD1^{G93A} motor neurons (green circles) and SOD1^{G93A} motor neurons transduced with 1 µl scrambled shRNA lentivirus (red diamonds). Comparison of the curves reveals that the scrambled shRNA construct (green triangles) has no effect on axonal transport speeds (SOD1^{G93A} untreated: 45 carriers, 7 axons; SOD1^{G93A} + scrambled shRNA: 104 carriers, 24 axons; 4 independent experiments).

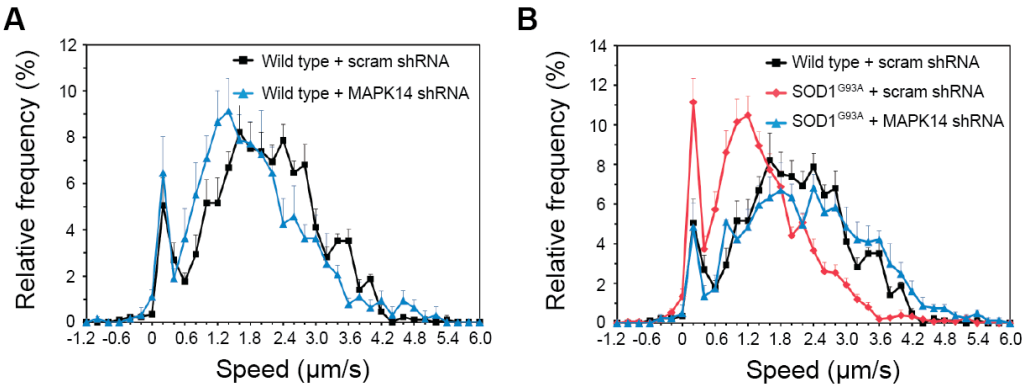

Figure 4.16. The effect of knocking down p38 MAPKα on retrograde axonal transport in primary wild type and SOD1^{G93A} motor neurons

(A) Speed profiles of H_CT-labelled signalling endosomes in wild type motor neurons transduced with 1 µl scrambled shRNA lentivirus (black squares) or 1 µl MAPK14 shRNA lentivirus (blue triangles). Comparison of the curves reveals that knocking down MAPK14 in wild type motor neurons has no enhancing effect on axonal transport (wild type + scrambled shRNA: 89 carriers, 17 axons; wild type + MAPK14 shRNA: 62 carriers, 14 axons; 4 independent experiments). (B) Speed profiles of H_CT-labelled signalling endosomes in wild type motor neurons transduced with 1 µl scrambled shRNA lentivirus (black squares), SOD1^{G93A} motor neurons transduced with 1 µl scrambled shRNA lentivirus (red diamonds) and SOD1^{G93A} motor neurons transduced with 1 µl MAPK14 shRNA lentivirus (blue triangles). Comparison of the curves reveals that knocking down MAPK14 in SOD1^{G93A} motor neurons (blue triangles) accelerates axonal transport to wild type speeds (black squares) (wild type + scrambled shRNA: 89 carriers, 17 axons; SOD1^{G93A} + scrambled shRNA: 104 carriers, 24 axons; SOD1^{G93A} + MAPK14 shRNA: 99 carriers, 20 axons; 4 independent experiments).

In wild type motor neurons, p38 MAPKα knockdown caused a small, but non-significant, slowing of retrograde axonal transport speeds (p = 0.257; Figure 4.16A). On the other hand, knocking down p38 MAPKα in SOD1^{G93A} motor neurons was able to effectively restore axonal transport speeds to physiological wild type levels (WT + scram shRNA versus SOD1^{G93A} + MAPK14 shRNA: p = 0.194, SOD1^{G93A} + scram shRNA versus SOD1^{G93A} + MAPK14 shRNA: p = 0.0003; Figure 4.16B). This result mimics those seen previously using pharmacological inhibitors of p38 MAPK (Figure 3.18) and suggests that p38 MAPKα is responsible for SOD1^{G93A}-induced defects in retrograde axonal transport.

In order to demonstrate that the results of our knockdown experiments were specific to p38 MAPKα, we also ordered an shRNA clone set targeted against p38 MAPKδ (MAPK13). Again the four shRNA constructs were tested in N2A cells, in order to determine which produced the most efficient knockdown. Western blot analysis revealed that MAPK13 shRNA 3 could reduce p38 MAPKδ levels by ~60% (Figure 4.17) and this construct was therefore chosen to produce lentiviral particles.

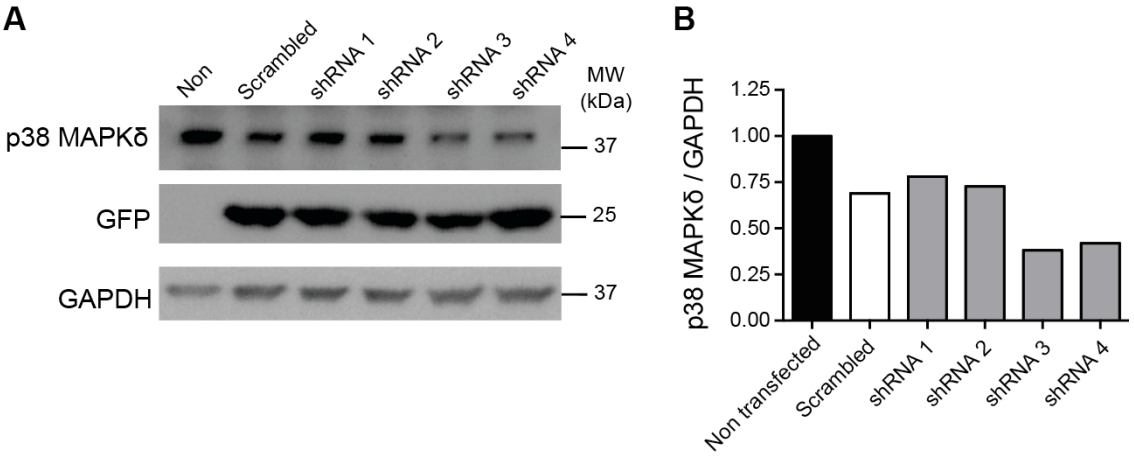

Figure 4.17. Testing MAPK13 shRNA constructs in N2A cells

(A) N2A cells were transfected with four different shRNA constructs against MAPK13 (p38 MAPKδ), as well as a scrambled control. GFP indicates expression of the construct. (B) Quantification of the western blot in (A) showing knockdown of p38 MAPKδ in N2A cells with different shRNA constructs. n = 1.

Lentiviral transduction of primary motor neurons with MAPK13 shRNA caused a dose-dependent reduction in the levels of p38 MAPKδ (Figure 4.18). However, knockdown of p38 MAPKδ in SOD1^{G93A} motor neurons had no effect on retrograde

axonal transport speeds (p = 0.097; Figure 4.19), indicating that p38 MAPKα alone is responsible for the deficits seen in ALS motor neurons.

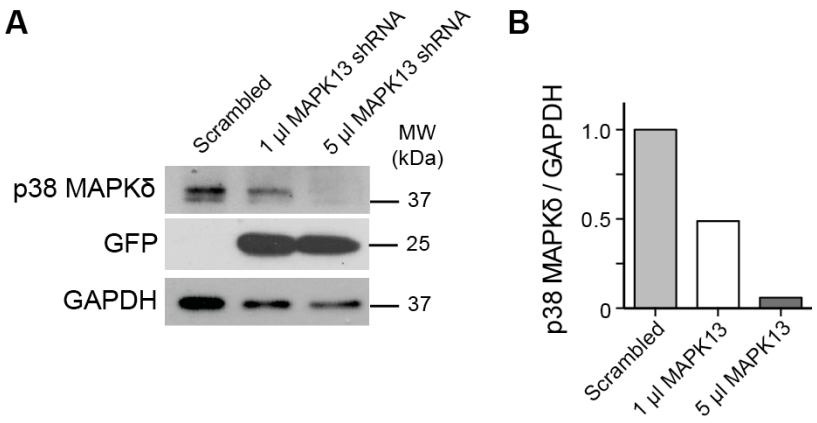

Figure 4.18. Lentiviral-mediated knockdown of p38 MAPKδ in primary motor neurons
(A) Western blot showing lentivirus-mediated knockdown of p38 MAPKδ. GFP indicates expression of the shRNA construct. GAPDH acts as a loading control. B) Quantification of the western blot in (A). p38 MAPKδ levels were quantified relative to the GAPDH loading control. n = 1.

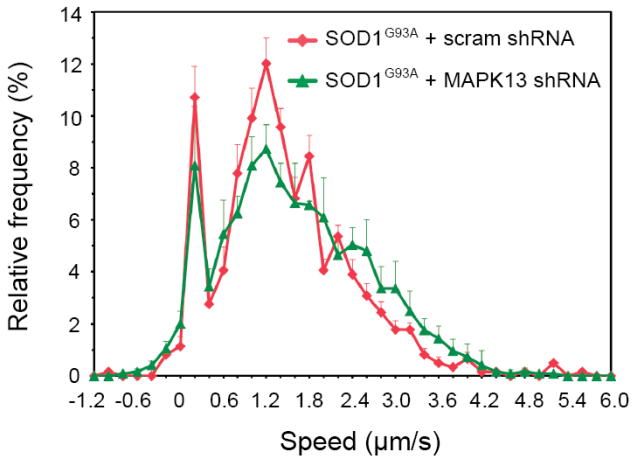

Figure 4.19. Knockdown of p38 MAPKδ has no effect on retrograde axonal transport speeds in SOD1^{G93A} motor neurons
Speed profiles of H_CT carriers in SOD1^{G93A} motor neurons transduced with scrambled shRNA (red diamonds) and SOD1^{G93A} motor neurons transduced with MAPK13 shRNA (green triangles). Comparison of the curves reveals that knockdown of p38 MAPK delta has no effect on axonal transport speeds (SOD1^{G93A} + scrambled shRNA: 46 carriers, 10 axons; SOD1^{G93A} + MAPK13 shRNA: 101 carriers, 12 axons; 3 independent experiments).

4.3.2. Pharmacological inhibition of p38 MAPK alpha corrects defects in axonal transport

In order to confirm the results of our p38 MAPKα knockdown experiments, we acquired two isoform-specific p38 MAPK inhibitors from GlaxoSmithKline. SB-203580 is an established inhibitor of p38 MAPKα and β that has been demonstrated to prevent SOD1^{G93A}-induced motor neuron death *in vitro* (Dewil et al., 2007). When tested at 2 µM in our *in vitro* axonal transport assays, we found that SB-203580 was able to correct SOD1^{G93A}-induced deficits in retrograde axonal transport (WT + DMSO versus SOD1^{G93A} + 2 µM SB-203580: p = 0.149, SOD1^{G93A} + DMSO versus SOD1^{G93A} + 2 µM SB-203580: p = 0.008; Figure 4.20A). However, SB-203580 is also known to inhibit JNK 2/3 (Coffey et al., 2002). In order to demonstrate that inhibition of JNK 2/3 is not involved in the restoration of axonal transport, we also tested SB-239063, a second-generation p38 MAPKα and β inhibitor with greatly reduced activity towards JNK 2/3. As with SB-203580, SB-239063 could rescue retrograde axonal transport in SOD1^{G93A} motor neurons (WT + DMSO versus SOD1^{G93A} + 2 µM SB-239063: p = 0.273, SOD1^{G93A} + DMSO versus SOD1^{G93A} + 2 µM SB-239063: p = 0.017; Figure 4.20).

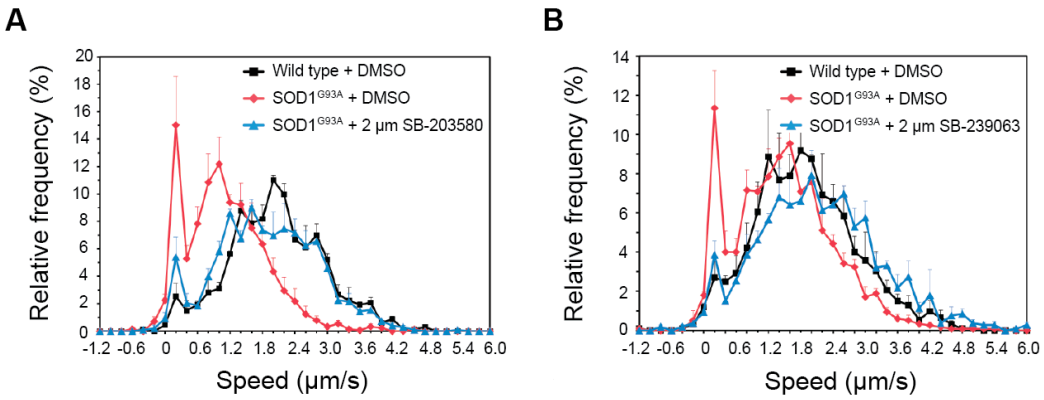

Figure 4.20. Pharmacological inhibition of p38 MAPKα corrects defects in retrograde axonal transport in SOD1^{G93A} motor neurons *in vitro*

(A) Speed profiles of H_CT carriers in wild type motor neurons treated with DMSO (black squares), SOD1^{G93A} motor neurons treated with DMSO (red diamonds) and SOD1^{G93A} motor neurons treated with 2 µM SB-203580 (blue triangles). Comparison of the speed profiles reveals SOD1^{G93A} motor neurons treated with 2 µM SB-203580 have a similar speed distribution to wild type cultures (black squares) (wild type: 50 carriers, 8 axons; SOD1^{G93A}: 56 carriers, 7 axons; SOD1^{G93A} + 2 µM SB-203580: 75 carriers, 10 axons; 3 independent experiments). (B) Speed distribution profiles of H_CT carriers in wild type motor neurons treated with DMSO (black squares), SOD1^{G93A} motor neurons treated with DMSO (red diamonds) and SOD1^{G93A} motor neurons treated with 2 µM SB-239063 (blue triangles). Comparison of the speed profiles reveals SOD1^{G93A} motor neurons treated with 2 µM SB-239063 have a similar speed distribution curve to wild type cultures (wild type: 84 carriers, 8 axons; SOD1^{G93A}: 56 carriers, 5 axons; SOD1^{G93A} + 2 µM SB-239063: 85 carriers, 9 axons; 3 independent experiments).

SB-239063 has been demonstrated to be suitable for *in vivo* use (see Figure 4.26). We therefore performed a limited dose response with this compound *in vitro* in order to gain a better understanding of the concentration required to correct $SOD1^{G93A}$-induced transport deficits. This, in combination with pharmacokinetic analysis, described in Figure 4.26, would allow us to pick a suitable dose to be tested in axonal transport assays *in vivo*.

In vitro axonal transport assays were therefore performed in $SOD1^{G93A}$ motor neurons with either a ten-fold lower (0.2 µM) or ten-fold higher (20 µM) concentration of SB-239063 to that previously tested. 0.2 µM SB-239063 was able to effectively restore axonal transport in $SOD1^{G93A}$ motor neurons to wild type levels (WT + DMSO versus $SOD1^{G93A}$ + 0.2 µM SB-239063: $p = 0.996$, $SOD1^{G93A}$ + DMSO versus $SOD1^{G93A}$ + 0.2 µM SB-239063: $p = 0.003$; Figure 4.21A). In addition, 20 µM did not appear to be toxic, causing no axon blebbing or obvious decrease in motor neuron survival, and was also able to rescue deficits in transport (WT + DMSO versus $SOD1^{G93A}$ + 20 µM SB-239063: $p = 0.610$, $SOD1^{G93A}$ + DMSO versus $SOD1^{G93A}$ + 20 µM SB-239063: $p = 0.021$; Figure 4.21B).

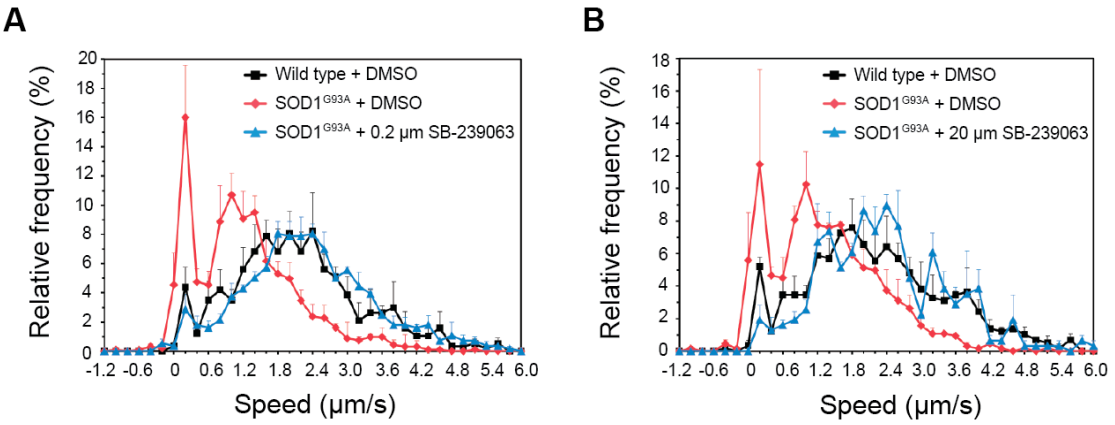

Figure 4.21. *In vitro* axonal transport dose-response tests with SB-239063

(A) Speed profiles of H_CT carriers in wild type motor neurons treated with DMSO (black squares), $SOD1^{G93A}$ motor neurons treated with DMSO (red diamonds) and $SOD1^{G93A}$ motor neurons treated with 0.2 µM SB-239063 (blue triangles). Comparison of the curves reveals $SOD1^{G93A}$ motor neurons treated with 0.2 µM SB-239063 have a similar speed distribution to wild type cultures (wild type: 59 carriers, 12 axons; $SOD1^{G93A}$: 47 carriers, 12 axons; $SOD1^{G93A}$ + 0.2 µM SB-239063: 57 carriers, 10 axons; 4 independent experiments). (B) Speed distribution profiles of H_CT carriers in wild type motor neurons treated with DMSO (black squares), $SOD1^{G93A}$ motor neurons treated with DMSO (red diamonds) and $SOD1^{G93A}$ motor neurons treated with 20 µM SB-239063 (blue triangles). Comparison of the speed profiles reveals $SOD1^{G93A}$ motor neurons treated with 20 µM SB-239063 have a similar speed distribution curve to wild type cultures (wild type: 55 carriers, 8 axons; $SOD1^{G93A}$: 37 carriers, 11 axons; $SOD1^{G93A}$ + 20 µM SB-239063: 36 carriers, 7 axons; 3 independent experiments).

4.4. Testing the effect of p38 MAPK alpha inhibition on axonal transport *in vivo* in the SOD1^{G93A} mouse

Having established the effect of p38 MAPKα inhibition on retrograde axonal transport in primary SOD1^{G93A} motor neurons *in vitro*, it was important to confirm our findings at a more disease-relevant stage. Since the most severe *in vivo* axonal transport defects were observed in SOD1^{G93A} mice at an early symptomatic stage, we decided to test whether SB-239063 could rescue retrograde axonal transport defects at this stage of the disease.

4.4.1. Establishing the *in vivo* axonal transport protocol

A method for imaging axonal transport in the exposed sciatic nerve of live anaesthetised mice had been previously established in our laboratory by Lynsey Bilsland (Bilsland et al., 2010) but was no longer in current use when I arrived in the laboratory. Therefore, in collaboration with Bernadett Kalmar (UCL Institute of Neurology), we set about re-establishing and optimising the protocol, so that it could be used to test the effect of our kinase inhibitors *in vivo.*

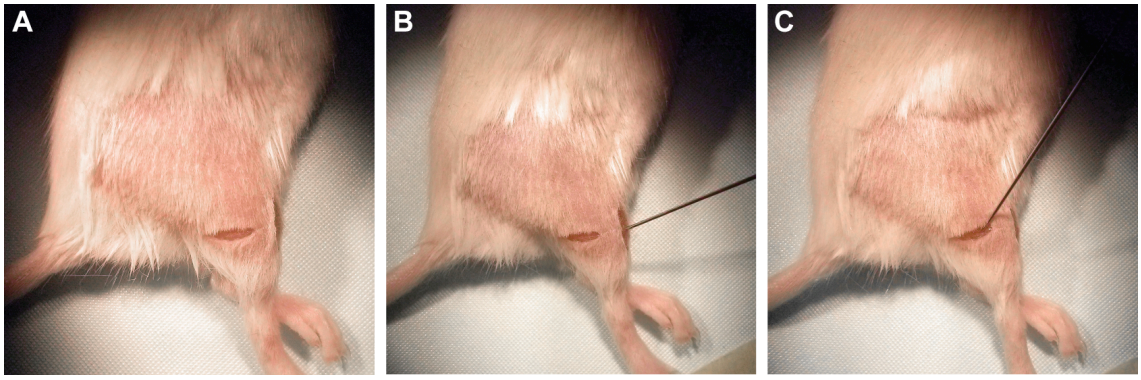

Figure 4.22. Intramuscular injection of fluorescently labelled H_CT into the tibialis anterior and gastrocnemius muscles

(A) Incisions are made through the skin above the tibialis anterior and gastrocnemius muscles in one hind leg to expose the muscles. (B) Position of the needle required for injection of the probe into the exposed tibialis anterior muscle. (C) Position of the needle required for injection of the fluorescently labelled probe into the exposed gastrocnemius muscle.

In the first step of the protocol, AlexaFluor 555-conjugated H_CT and BDNF are injected into the tibialis anterior and gastrocnemius muscles of one hind leg (Figure 4.22). BDNF acts to increase the internalisation of the probe by the nerve (Roux et al., 2006). In order to determine the optimal incubation time before imaging the sciatic nerve, we collected nerves at 2, 4, 6 and 24 hours after i.m. injection of H_CT, as well as a nerve from a non-injected animal as a control. Sectioning and imaging of the nerves revealed that after 4 hours there were a significant number of H_CT-labelled axons (Figure 4.23). At 6 hours, although there was an increase in the number of labelled axons, the background increased significantly. 4 hours post-injection was therefore chosen as the optimal time for imaging. We also noted that labelling in the nerve persisted for at least 24 hours (Figure 4.23).

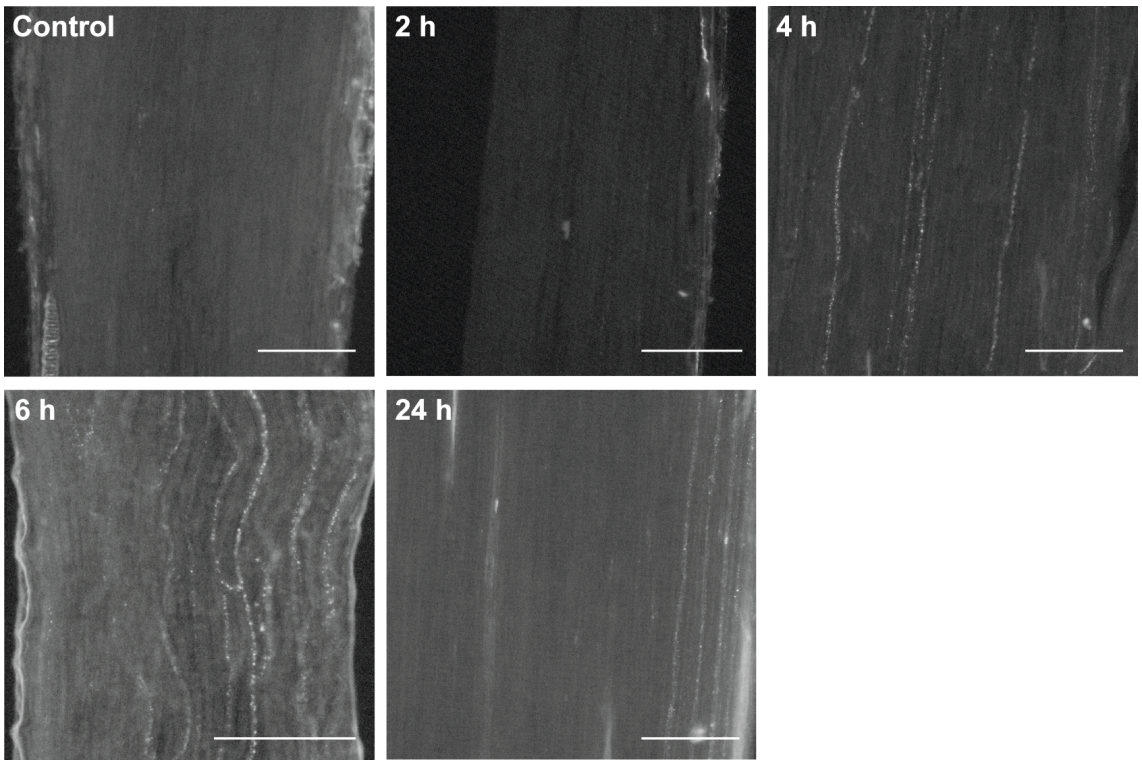

Figure 4.23. Time-dependent accumulation of fluorescently labelled H_CT in the sciatic nerve

AlexaFluor 555-labelled H_CT was injected i.m. into the tibialis anterior and gastrocnemius muscles of anaesthetised mice. Sciatic nerves were then collected at 2, 4, 6 and 24 h, fixed and sectioned. H_CT-labelled endosomes can be seen to appear at 4 h and persist in the sciatic nerve until 24 h. Scale bars, 100 μm.

In order to image the sciatic nerve using a confocal microscope, surgery must be performed to remove surrounding tissue and expose the underlying nerve (Figure

4.24). This is a relatively simple surgery, taking a maximum of 10-15 minutes, but requires careful attention to ensure the sciatic nerve is not damaged nor contaminated with blood or hair that would impede imaging.

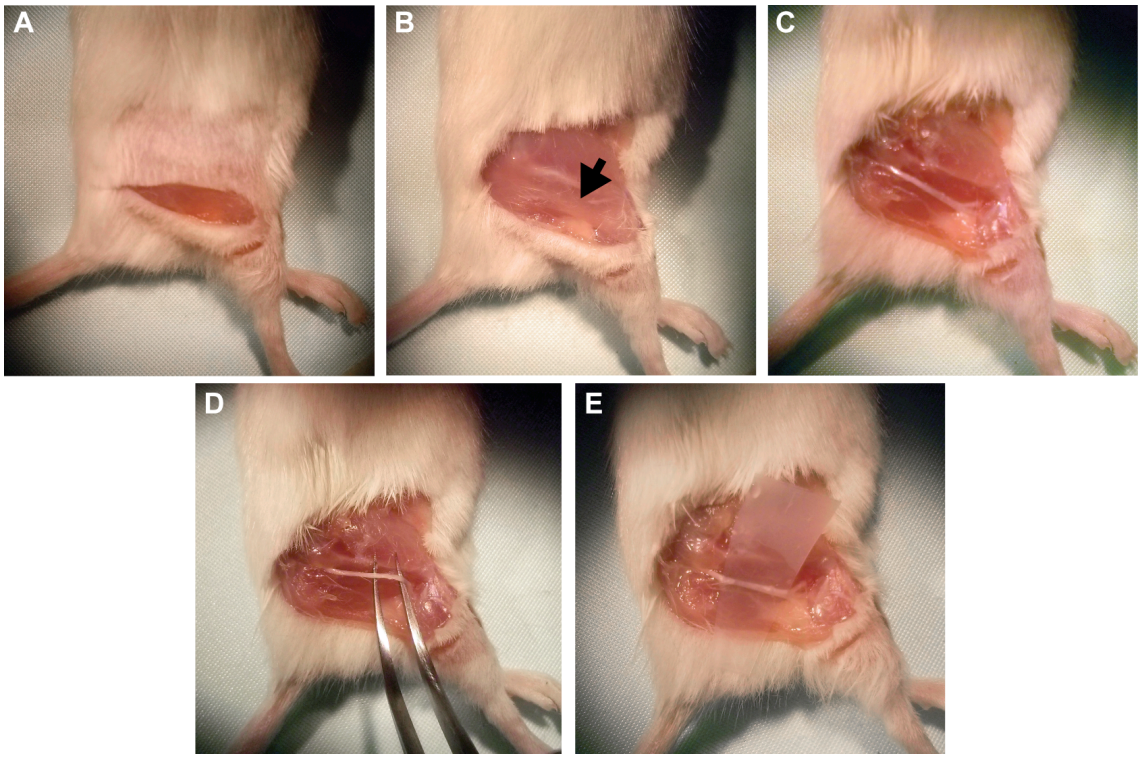

Figure 4.24. Surgical exposure of the sciatic nerve for *in vivo* imaging

(A) An incision is made through the skin between the knee and hip joints to expose the underlying muscle and nerves. (B) The skin around the operating field is removed and the sciatic nerve is visible underneath the muscle, beneath the femur (black arrow). (C) The muscle is carefully removed to reveal the underlying sciatic nerve. (D) The sciatic nerve is separated from the surrounding tissue using a pair of curved forceps. (E) A small piece of plastic is inserted beneath the sciatic nerve to separate it from underlying tissues, facilitating imaging of the nerve.

Once the nerve is exposed, we developed a technique of placing a small piece of plastic underneath the nerve (Figure 4.24E). This facilitates locating the nerve underneath the microscope as the nerve is separated from the underlying tissue.

For confocal imaging, the anaesthetised mouse is placed on a custom-made stage with a small imaging window (Figure 4.25A). The imaging window is covered with a glass coverslip and the sciatic nerve is placed carefully on top of the coverslip, directly above the 63X objective (Figure 4.25B).

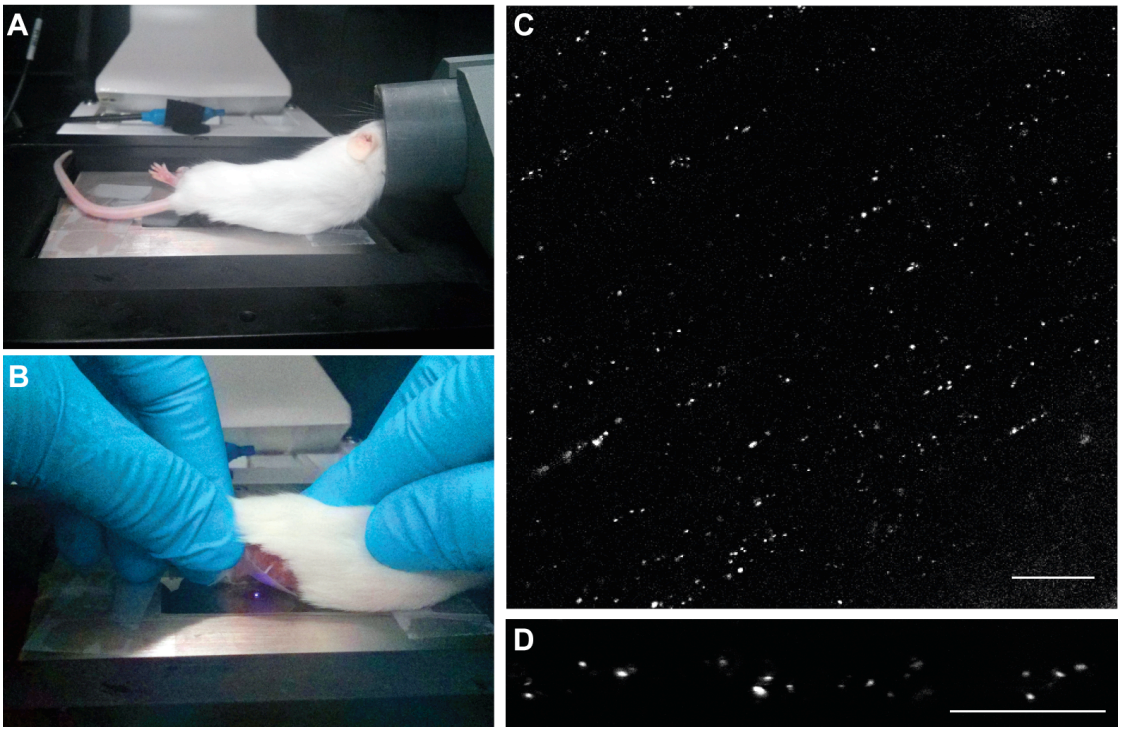

Figure 4.25. *In vivo* imaging of the exposed sciatic nerve using confocal microscopy
(A) The exposed sciatic nerve is carefully positioned on the glass coverslip, directly above the microscope objective. (B) Correct positioning of the anaesthetised mouse on the microscope stage. (C) Initial imaging of the sciatic nerve using the 63X objective shows clearly labelled endosomes within axons. A representative collection of axons is chosen to be monitored. Scale bar, 10 µm. (D) Imaging of a collection of axons using the 100X objective allows sufficient time and spatial resolution for individual endosomes to be tracked. Scale bar, 10 µm.

Using this protocol, we were able to acquire high-resolution images of individual endosomes within the sciatic nerve (63X, Figure 4.25C, Movie 3). Zooming in at 100X allows time-lapse movies to be acquired (Figure 4.25D, Movie 4) and the speed of axonal transport of individual endosomes to be analysed.

4.4.2. Testing the effect of SB-239063 on axonal transport *in vivo*

In order to determine the optimal dose to test in our *in vivo* axonal transport assays, GlaxoSmithKline performed pharmacokinetic analysis with SB-239063. The concentration of SB-239063 was determined in the brain, spinal cord and muscle after i.p. injection at either 30 mg/kg or 100 mg/kg. The 100 mg/kg dose allowed for

circulating concentrations similar to those tested in our *in vitro* axonal transport assays and was therefore chosen as the first dose to be tested *in vivo.*

A

Dose (mg/kg)	Time (h)	Brain (µM) ^	Spinal Cord (µM) ^	Muscle (µM) ^^
30	1	0.464	0.405	1.182
30	1	0.555	0.546	1.274
100	1	1.784	1.82	3.241
100	1	1.337	1.379	3.476

B

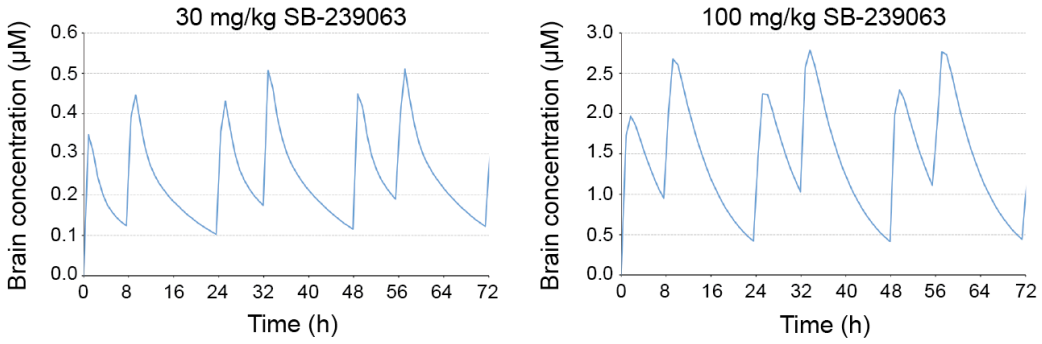

Figure 4.26. Pharmacokinetics of SB-239063

(A) Mice were administered SB-239063 i.p. at either 30 mg/kg or 100 mg/kg. The free concentration in the brain, spinal cord and muscle was determined after 1 h. ^ based on fraction unbound in mouse brain. ^^ based on fraction unbound in mouse blood. (B) Predicted brain free concentration profiles with twice-daily i.p. dosing at 0 and 8 hours for 30 mg/kg and 100 mg/kg. This work was performed by the GlaxoSmithKline DMPK team in Singapore.

Early symptomatic mice were injected with 100 mg/kg SB-239063 i.p. at the same time as the H_CT probe was injected i.m. into the tibialis anterior and gastrocnemius muscles. The sciatic nerve was then imaged four hours later (Figure 4.27A). Treatment of $SOD1^{G93A}$ mice with SB-239063 was observed to accelerate retrograde axonal transport compared to untreated $SOD1^{G93A}$ controls, restoring transport to physiological wild type levels (WT versus $SOD1^{G93A}$ + 100 mg/kg SB-239063: $p = 0.744$, $SOD1^{G93A}$ versus $SOD1^{G93A}$ + 100 mg/kg SB-239063: $p = 0.004$; Figure 4.27B). Deconvolution of the speed distribution profiles shown in Figure 4.27B highlights a marked reduction in the fastest (2.39 µm/s) speed component in $SOD1^{G93A}$ mice and a corresponding increase in the frequency of intermediate speed carriers (1.24 µm/s), when compared to wild type controls

(Figure 4.27C). However, when treated with SB-239063, SOD1^{G93A} mice had a speed carrier distribution very similar to wild type.

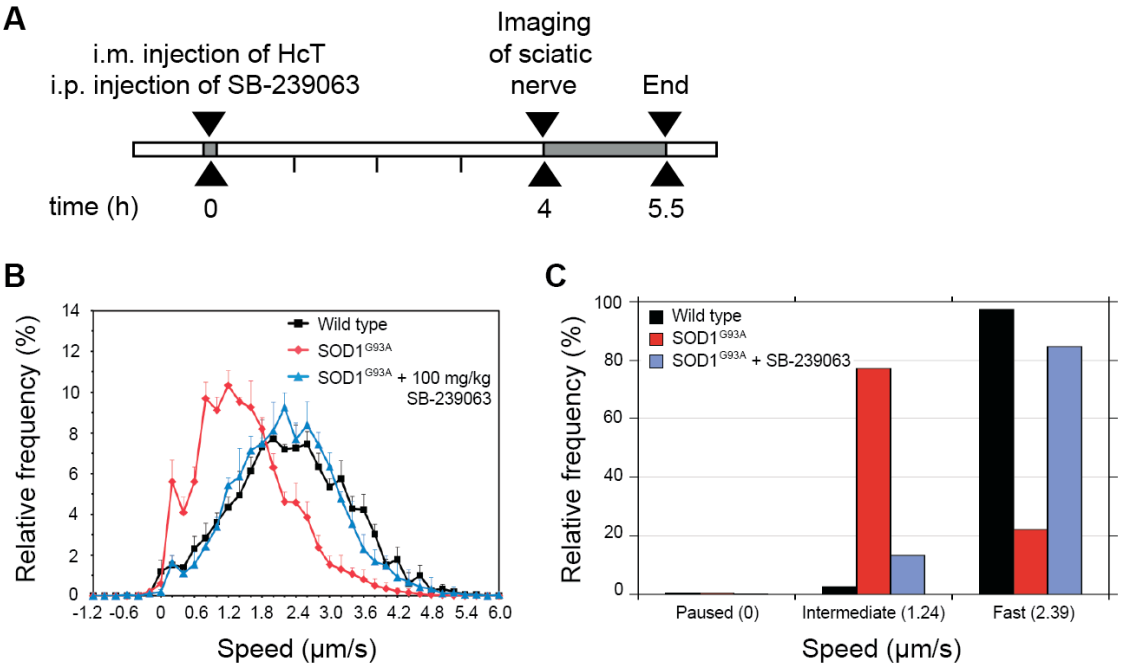

Figure 4.27. SB-239063 corrects retrograde axonal transport defects *in vivo* in the SOD1^{G93A} mouse

(A) Mice were anaesthetised and AlexaFluor 555-conjugated H_CT was injected i.m. into the tibialis anterior and gastrocnemius muscles. At the same time, 100 mg/kg SB-239063 or vehicle control was injected i.p. Mice were allowed to recover for 4 h, then re-anaesthetised and axonal transport imaged in the exposed sciatic nerve. (B) Retrograde axonal transport in single axons of the sciatic nerve was assessed in 73 d wild type (black squares), SOD1^{G93A} (red diamonds) and SOD1^{G93A} mice treated with 100 mg/kg SB-239063 (blue triangles). SOD1^{G93A} mice displayed a significant impairment in retrograde transport, whilst SOD1^{G93A} mice treated with 100 mg/kg SB-239063 showed transport speeds similar to those of wild type mice. Wild type: 161 carriers, n (animals) = 4; SOD1^{G93A}: 185 carriers, n = 5; SOD1^{G93A} + 100 mg/kg SB-239063: 238 carriers, n = 4. (C) Deconvolution analysis of the *in vivo* speed profiles demonstrating there are three defined speed components: 0.0 (paused), 1.24 (intermediate), and 2.39 (fast). Defects in axonal transport in the sciatic nerve of early symptomatic SOD1^{G93A} mice can be explained by a reduction in the number of "fast" moving carriers and an increase in the number of "intermediate" speed carriers. Treatment of SOD1^{G93A} mice with 100 mg/kg SB-239063 corrects the distribution of carriers back to that of wild type.

Our *in vivo* axonal transport results highlight SB-239063 as a tool to test whether deficits in retrograde axonal transport play a role in disease progression in the SOD1^{G93A} mouse. However, 100 mg/kg is a very high dose to test in a chronic dosing study, especially when you consider the amount of drug that would ultimately be required to treat a human patient. We therefore tested different concentrations of SB-239063 to identify a lower effective dose and found that at

10-mg/kg the compound was still able to correct deficits in axonal transport *in vivo* (Figure 4.28A). In addition, we identified 0.3 mg/kg as a non-effective dose (Figure 4.28B) that could be used as a control in chronic dosing studies to allow us to better understand the relationship between the effects of p38 MAPK inhibition on axonal transport and its effects on disease progression.

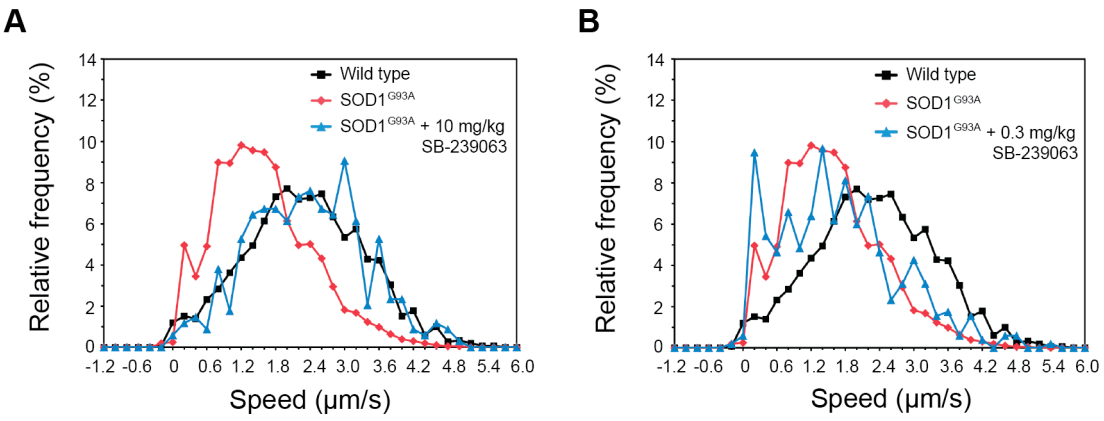

Figure 4.28. Dose-dependent effects of SB-239063 on axonal transport *in vivo*

(A) Retrograde transport in single axons of the sciatic nerve was assessed in 73 d wild type (black squares), $SOD1^{G93A}$ (red diamonds) and $SOD1^{G93A}$ mice treated with 10 mg/kg SB-239063 (blue triangles). $SOD1^{G93A}$ mice treated with 10 mg/kg SB-239063 showed transport speeds similar to those of wild type mice (wild type: 161 carriers, n (animals) = 4; $SOD1^{G93A}$: 185 carriers, n = 5; $SOD1^{G93A}$ + 10 mg/kg SB-239063: 35 carriers, n = 1). (B) Retrograde transport in single axons of the sciatic nerve was assessed in 73 d wild type (black squares), $SOD1^{G93A}$ (red diamonds) and $SOD1^{G93A}$ mice treated with 0.3 mg/kg SB-239063 (blue triangles). $SOD1^{G93A}$ mice treated with 0.3 mg/kg SB-239063 showed transport speeds similar to those of $SOD1^{G93A}$ mice (wild type: 161 carriers, n (animals) = 4; $SOD1^{G93A}$: 185 carriers, n = 5; $SOD1^{G93A}$ + 10 mg/kg SB-239063: 42 carriers, n = 1).

4.5. Discussion

Previous work from our laboratory has demonstrated that retrograde axonal transport is defective both *in vitro* and *in vivo* in SOD1^{G93A} motor neurons. In this Chapter, I was able to demonstrate that structurally diverse inhibitors of p38 MAPK are able to correct deficits in retrograde axonal transport *in vitro* in SOD1^{G93A} motor neurons. In addition, we found that activation of p38 MAPK in wild type motor neurons inhibits retrograde axonal transport. Together these data support the conclusion that p38 MAPK is a negative regulator of retrograde axonal transport.

p38 MAPK has been previously implicated in ALS pathogenesis. Our results support these past studies which demonstrate that p38 MAPK is activated in a disease-dependent manner in SOD1^{G93A} mice (Dewil et al., 2007, Tortarolo et al., 2003, Veglianese et al., 2006) and that this pathological activation is responsible for axonal transport defects induced by SOD1^{G93A} (Morfini et al., 2013).

Using both pharmacological and genetic approaches, we were able to show that p38 MAPKα is responsible for the retrograde axonal transport defects observed *in vitro* in SOD1^{G93A} motor neurons. One of the p38 MAPKα/β specific inhibitors tested, SB-239063, was suitable for use *in vivo* and we were therefore able to demonstrate that inhibition of p38 MAPKα could also correct retrograde axonal transport defects in early symptomatic SOD1^{G93A} mice. These findings therefore provide the basis for a longer-term study to determine the role of p38 MAPKα-induced axonal transport defects in ALS disease progression.

4.5.1. Anterograde versus retrograde axonal transport defects

The work in this Chapter has focused primarily on correcting deficits in retrograde axonal transport. However, it is important to recognise that defects in anterograde axonal transport have also been reported in ALS (Bilsland et al., 2010, Morfini et al., 2013, Alami et al., 2014). There is still much to be understood about the specific roles of both anterograde and retrograde axonal transport in neurodegeneration.

The analysis of anterograde axonal transport in motor neurons is more challenging than for retrograde axonal transport, due to difficulties in finding a suitable cargo to label and track. Anterograde axonal transport is typically followed in hippocampal, striatal and cortical neurons by expressing fluorescently tagged anterograde cargoes, for example BDNF-mCherry and APP-yellow fluorescent protein (YFP) (Her and Goldstein, 2008). However, this approach relies on transfection of neurons using reagents such as Lipofectamine™ or Nucleofection™. The efficiency of these transfection techniques in motor neurons is typically too low to be used for axonal transport studies. There is also the additional problem that these transfection procedures can induce morphological changes and cell death (Deinhardt and Schiavo, 2005), which could affect the efficiency of axonal transport.

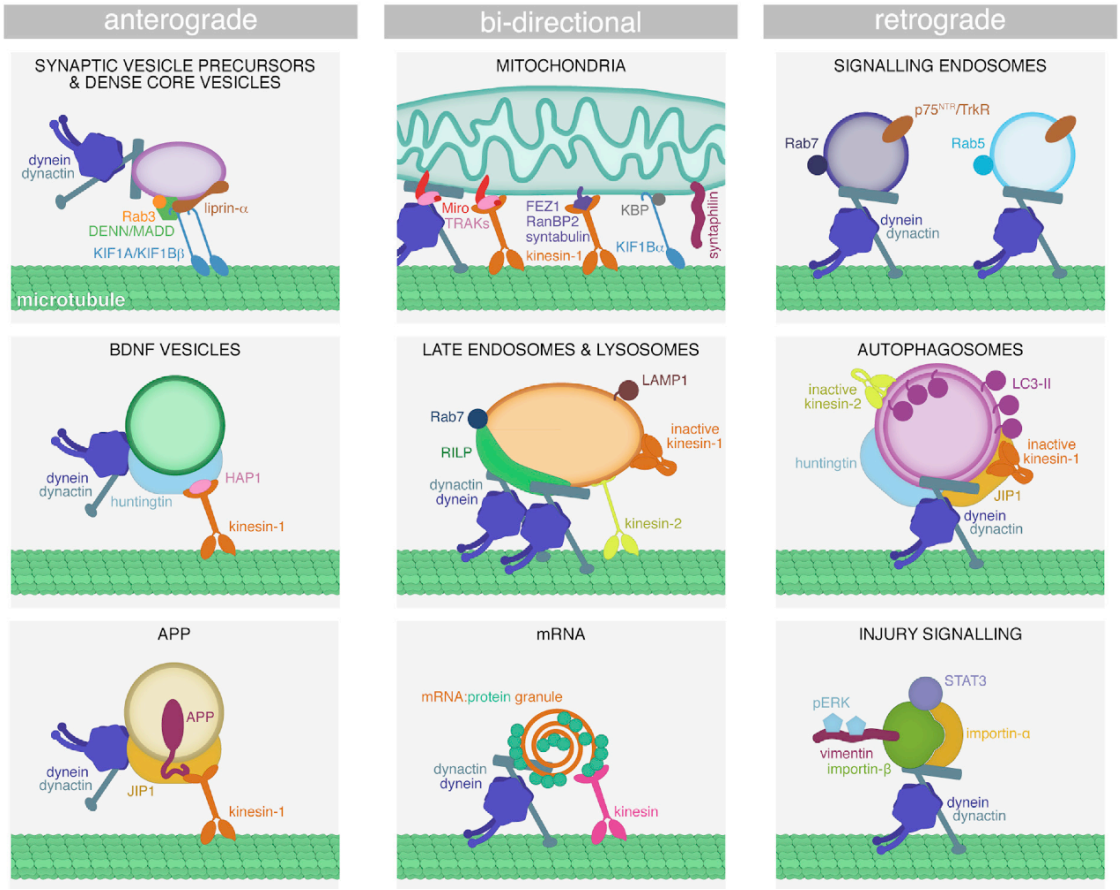

Figure 4.29. Cargoes transported by fast axonal transport

Schematic illustrating cargoes that are transported by anterograde (left), bidirectional (middle) and retrograde (right) fast axonal transport. Reprinted with permission from Elsevier (Maday et al., 2014).

We therefore considered analysing the anterograde axonal transport of cargoes that are transported bidirectionally (see Figure 4.29), as there are a number of probes available that allow easy labelling of these cargoes. Since the anterograde axonal transport of both mitochondria and mRNA has been reported to be defective in ALS (Bilsland et al., 2010, Alami et al., 2014), these cargoes were considered first.

Live imaging protocols for mitochondrial axonal transport are well established both *in vitro* and *in vivo* (Bilsland et al., 2010, Misgeld et al., 2007, De Vos and Sheetz, 2007), due to the well-documented relationship between mitochondrial defects and neurodegenerative disease (Johri and Beal, 2012). However, it has been shown that reversing mitochondrial trafficking deficits does not prevent neuronal death and disease progression in the $SOD1^{G93A}$ mouse (Zhu and Sheng, 2011). In addition, the axonal transport of mitochondria is differentially regulated from that of other fast axonal transport cargoes (Zala et al., 2013) and has very different transport characteristics (De Vos and Sheetz, 2007). Mitochondria were therefore not a suitable cargo to use to determine whether our compounds affected anterograde and retrograde axonal transport in the same way in $SOD1^{G93A}$ motor neurons.

Next we attempted to image anterograde axonal transport using the SYTO RNA Select™ dye to label mRNA. Although the labelling was very good, few motile cargoes were seen and as a result it was not possible to achieve high enough *n* numbers to reliably analyse anterograde axonal transport.

Finally we tested Lysotracker™, which labels acidic organelles, such as late endosomes/lysosomes and autophagosomes. With Lysotracker™ there was a much larger number of brightly labelled, motile carriers, moving in both directions. It was therefore deemed the best probe to use to study anterograde axonal transport in our $SOD1^{G93A}$ motor neurons.

Surprisingly, in our *in vitro* axonal transport assays using Lysotracker™ we were only able to detect defects in retrograde axonal transport. The anterograde axonal transport of Lysotracker™ in $SOD1^{G93A}$ motor neurons was identical to wild type. This suggests that anterograde and retrograde axonal transport may be

differentially regulated and may not always be in equilibrium. At first glance, our results also appear to disagree with previous work by Morfini et al., demonstrating that ALS-associated SOD1 mutants (including $SOD1^{G93A}$) induce defects in anterograde axonal transport (Morfini et al., 2013). However, it is important to note that Morfini et al. analysed the axonal transport of all types of vesicles (using differential interference contrast (DIC) microscopy) whilst our analysis of anterograde axonal transport focused on Lysotracker™-labelled organelles only.

In ALS model systems, retrograde axonal transport defects have now been described for acidic organelles (late endosomes/lysosomes and autophagosomes), signalling endosomes (H_CT and α-$p75^{NTR}$) (Kieran et al., 2005, Bilsland et al., 2010), mitochondria (Bilsland et al., 2010) and APP-labelled vesicles (De Vos et al., 2007). These results support the hypothesis that defective retrograde axonal transport plays a significant role in motor neuron degeneration in ALS. However, as shown by work investigating the role of mitochondrial axonal transport in ALS (Zhu and Sheng, 2011), it is possible that defects in the axonal transport of different cargoes are mediated by different mechanisms and may also play different roles in disease progression. It is therefore important that we investigate the axonal transport of these cargoes individually in order to fully understand their contribution to neurodegeneration in ALS.

4.5.2. p38 MAPKα is responsible for defects in axonal transport in $SOD1^{G93A}$ motor neurons

In this Chapter, we were able to demonstrate using genetic knockdown that p38 MAPKα is the isoform responsible for retrograde axonal transport defects in $SOD1^{G93A}$ motor neurons. One shortcoming of our approach is that our lentiviral vectors transduced both glial cells and motor neurons; therefore we do not know whether p38 MAPKα is acting via a cell autonomous or non-autonomous mechanism. This question could be addressed in the future by building lentiviral vectors with neuron-specific promoters (Hioki et al., 2007).

Previous experiments in isolated squid axoplasm have reported that addition of recombinant p38 MAPKα induces defects in anterograde axonal transport only,

with no effect on retrograde transport (Morfini et al., 2013). These contrasting results are difficult to explain, but could represent differences in the biological systems used (squid axoplasm versus mouse primary motor neurons). It could be that squid axoplasm is not an accurate model of the mammalian axonal transport system. Unfortunately, as we were unable to detect defects in the anterograde axonal transport of Lysotracker™ in mouse SOD1^{G93A} motor neurons, we were not able to test whether our p38 MAPK inhibitors could also correct defects in anterograde axonal transport.

In order to help understand the role of p38 MAPKα-mediated axonal transport defects in ALS disease progression, we identified a pharmacological inhibitor of the kinase that is able to restore retrograde axonal transport to wild type levels in early symptomatic SOD1^{G93A} mice. It would also be interesting to address this question *in vivo* using a genetic approach. Knocking out p38 MAPKα results in embryonic lethality (E11.5-12.5) mainly due to placental insufficiency (Mudgett, 1998). However, MAPK14 *lox/lox* mice are available (Nishida et al., 2004) and therefore it should be possible to generate motor neuron-specific p38 MAPKα knockout mice. If these mice are viable, they could be crossed with SOD1^{G93A} mice to determine the effects of motor neuron-specific p38 MAPKα knockout on both axonal transport and disease progression. However, it is likely that knocking out p38 MAPKα during development will have deleterious effects. To avoid potential problems with knocking out p38 MAPKα, gene therapy could be used to knockdown p38 MAPKα in adult mice instead. For example, pre- or early symptomatic SOD1^{G93A} mice could be treated with adeno-associated viral (AAV) vectors encoding shRNA against p38 MAPKα. Preferential targeting of motor neurons with AAV vectors has been previously described in adult mice using intrathecal delivery and the *cmv* promoter (Dirren et al., 2015).

In contrast to our results using pharmacological inhibitors, lentivirus-mediated knockdown of p38 MAPKα in wild type motor neurons was found to have a small inhibitory effect on retrograde axonal transport (Figure 4.16). This suggests that, at basal levels, activated p38 MAPKα may play a role in axonal transport regulation and/or maintaining normal neuronal function and indicates that too great a degree of p38 MAPKα inhibition *in vivo* may be deleterious.

4.5.3. p38 MAPK is a negative regulator of axonal transport

In this Chapter, we have demonstrated that p38 MAPK is responsible for defects in the retrograde axonal transport of signalling endosomes and acidic organelles in $SOD1^{G93A}$ motor neurons. The question that remains to be answered is *how* p38 MAPK exerts its effects on axonal transport. Both direct (phosphorylation of motors and/or their adaptor proteins) and indirect mechanisms have been proposed.

4.5.3.1. Phosphorylation of motors and motor adaptor proteins

Work performed using isolated squid axoplasm has demonstrated that p38 MAPKα inhibits anterograde axonal transport through direct phosphorylation of kinesin-1 (Morfini et al., 2013). The authors demonstrated that p38 MAPKα-mediated phosphorylation of kinesin heavy chain KIF5c reduced the efficiency with which the motor moved along axonal microtubules in cultured hippocampal neurons.

p38 MAPK-mediated inhibition of retrograde axonal transport could potentially be explained by a similar model, in which one or more subunits of cytoplasmic dynein are directly phosphorylated. Dynein has been previously shown to be regulated by phosphorylation (Dillman and Pfister, 1994, Mitchell et al., 2012, Kumar et al., 2000, Runnegar et al., 1999). Although p38 MAPK has not yet been demonstrated to phosphorylate neuronal dynein, another member of the MAP kinase family, ERK1/2, has. In hippocampal and cortical neurons, the dynein intermediate chain IC-1 was reported to be phosphorylated by ERK1/2 in response to neurotrophin stimulation (Mitchell et al., 2012). Inhibition of ERK1/2 was found to reduce the association of dynein with TrkB-containing endosomes and cause a reduction in the number of motile endosomes in the retrograde direction in hippocampal neurons.

There are also reports that dynein motor activity can be negatively regulated by phosphorylation. Phosphorylation of residues in the light, intermediate and heavy chains of cytoplasmic dynein have all been reported to reduce the ATPase activity of the motor and binding of the motor to microtubules (Kumar et al., 2000, Runnegar et al., 1999). Although the kinase(s) responsible were not identified, this mechanism of regulation would explain the inhibitory effect of p38 MAPK on

retrograde axonal transport in ALS. However, it remains to be seen if p38 MAPK does indeed phosphorylate any of the dynein subunits and if so, what effect this has on the motor's activity.

The activity of dynein adaptor proteins can also be regulated by phosphorylation. For example, phosphorylation of Ndel1 by Cdk5 stimulates the retrograde axonal transport of acidic organelles (Pandey and Smith, 2011), whilst phosphorylation of huntingtin (htt) at serine 421 by Akt has been shown to cause the preferential recruitment of kinesin-1 to BDNF-containing vesicles and an acceleration of their anterograde axonal transport (Colin et al., 2008). The authors of this latter study speculate that htt phosphorylation may act as a switch between anterograde and retrograde axonal transport. p38 MAPK has been shown to increase the expression of serum- and glucocorticoid-induced kinase (SGK), which, like Akt, also phosphorylates htt at Ser421 (Rangone et al., 2004). Inhibition of p38 MAPK could therefore indirectly lead to reduced SGK-mediated htt phosphorylation and preferential retrograde axonal transport. However, a mechanism based on translation would not explain the acute effects we have observed in our *in vitro* axonal transport assays.

It is clear that future work must focus on determining whether p38 MAPK phosphorylates components of the axonal transport machinery. Mass spectrometry analysis of changes in the phosphorylation state of proteins (Mann et al., 2002) between wild type and $SOD1^{G93A}$ samples could help elucidate the effector protein(s) responsible for p38 MAPK's effect on axonal transport. Differential phosphorylation analysis including $SOD1^{G93A}$ samples treated with one of our p38 MAPK inhibitors that are active in axonal transport assays could help decipher which phosphorylated proteins may be involved in p38 MAPK-mediated inhibition of retrograde axonal transport.

4.5.3.2. Indirect mechanisms of p38 MAPK-mediated axonal transport inhibition

One mechanism by which p38 MAPK could indirectly inhibit axonal transport is through the phosphorylation of neurofilaments. Neurofilaments are a type of

intermediate filament, found specifically in neurons and are thought to provide structural support for axons, regulate axon diameter and act as a scaffold for the docking of various axoplasmic components (Yuan et al., 2012). They are composed of three major subunits: light (NF-L), medium (NF-M) and heavy (NF-H). Neurofilament subunits are synthesised in the cell body of neurons and transported via slow axonal transport to the axon where they are incorporated into the existing neurofilament network.

Under normal conditions, phosphorylation of the subunits regulates both their transport along the axon and their assembly into neurofilaments (Yuan et al., 2012, Miller et al., 2002). However, aberrant hyperphosphorylation is thought to slow their transport and induce bundling, leading to large accumulations of neurofilaments in the cell body and proximal axons (Miller et al., 2002). Interestingly, slowing of neurofilament axonal transport (through ^{35}S labelling of NF-L) is considered an early pathological feature in mutant SOD1 mice (Williamson and Cleveland, 1999, Zhang et al., 1997). In addition, accumulations of phosphorylated neurofilaments have been reported in motor neurons of patients with both familial and sporadic ALS as well as in the $SOD1^{G93A}$ mouse model at a presymptomatic stage (Bendotti et al., 2004, Ackerley et al., 2004, Tortarolo et al., 2003).

p38 MAPKα is known to phosphorylate the tail domains of NF-M and H (Ackerley et al., 2004). Phosphorylation of these domains has been demonstrated to regulate the axonal transport of neurofilaments by regulating their attachment to motor proteins (Miller et al., 2002). Aberrant activity of p38 MAPK could therefore cause the release of neurofilaments from their motors, resulting in the accumulation of phosphorylated neurofilaments. The role of p38 MAPK in hyper-phosphorylating neurofilaments in ALS is also supported by the fact that the kinase colocalises with phosphorylated neurofilaments in the cell bodies and proximal axons of motor neurons in spinal cord sections from $SOD1^{G93A}$ mice (Tortarolo et al., 2003).

The mechanism by which hyperphosphorylated neurofilaments could disrupt axonal transport is not fully understood. It is possible that phosphorylation-induced slowing of neurofilament axonal transport leads to the formation of accumulations that cause a general blockade of transport along the axon. Alternatively, the loss of

structural support to the axon that is normally provided by neurofilaments could reduce axonal transport efficiency. Such hypotheses would explain why p38 MAPK has been reported to induce both retro- and anterograde axonal transport defects in ALS. It is also interesting to note that deletion of the tail domains of NF-M and NF-L, which are phosphorylated by p38 MAPK, delays disease onset, increases lifespan and increases the number of surviving motor neurons in $SOD1^{G93A}$ mice (Lobsiger et al., 2005). In addition, riluzole, the only drug approved for the treatment of ALS, has been shown to prevent glutamate-induced slowing of neurofilament transport in primary rat cortical neurons (Stevenson et al., 2009). The authors found that this correlated with reduced phosphorylation of the NF-M/NF-H tail domains and a reduction in the level of activated p38 MAPK.

An alternative explanation for the inhibitory effect of p38 MAPK on axonal transport focuses on the fact that p38 MAPK phosphorylates the microtubule-associated protein tau. Tau binds and stabilises microtubules and its activity is regulated by phosphorylation. p38 MAPK has been shown to directly phosphorylate tau at several sites, including Thr231, Ser235 and Ser356 (Reynolds et al., 2000). Phosphorylation at these three sites has been demonstrated to reduce the association of tau with microtubules (Cho and Johnson, 2004). If aberrantly activated, p38 MAPK could destabilise microtubules and thereby cause a disruption in axonal transport. Indeed, hyperphosphorylated tau has been reported in the $SOD1^{G37R}$ mouse model of ALS before disease onset (Farah et al., 2003).

Davunetide (NAP), an eight amino acid peptide that is derived from activity-dependent neuroprotective peptide (ANDP) has been demonstrated to reduce tau hyperphosphorylation by two-fold in $SOD1^{G93A}$ mice (Jouroukhin et al., 2013). Interestingly, the authors were also able to demonstrate that treatment of $SOD1^{G93A}$ mice with davunetide could rescue defects in anterograde axonal transport in olfactory neurons (Jouroukhin et al., 2013). These results support the idea that hyperphosphorylated tau could be responsible for axonal transport defects in ALS. However, no significant difference was observed in neurodegeneration between $SOD1^{G93A}$ mice with normal tau levels and those with reduced tau levels (Taes et al., 2010). In addition, there is no association of polymorphisms in the gene encoding tau (*MAPT*) with human ALS (Taes et al., 2010).

An alternative explanation relates to the fact that phosphorylation of tau at Thr231 and Ser235 has also been reported to reduce α-tubulin acetylation (Cho and Johnson, 2004). The degree of acetylation of microtubules has been demonstrated to affect the binding of motor proteins and therefore axonal transport. Increasing α-tubulin acetylation using histone deacetylase 6 (HDAC6) inhibitors has been shown to accelerate the microtubule-based transport of BDNF in mouse striatal cells (Dompierre et al., 2007). This increase in trafficking was found to be due to an increase in the recruitment of both dynein and kinesin motor complexes to the microtubules. Phosphorylation of tau by p38 MAPK could therefore cause a reduction in the association of motors with the microtubules and inhibit axonal transport as a result. Deletion of the HDAC6 gene in SOD1^{G93A} mice has been shown to extend survival and maintain motor axon integrity, correlating with an increase in α-tubulin acetylation in the spinal cord and sciatic nerve (Taes et al., 2013). However there are no reports of reduced α-tubulin acetylation in ALS motor neurons to date, suggesting that this may not be the mechanism underlying the defects in axonal transport.

A shortcoming of these proposed indirect mechanisms of p38 MAPK-mediated inhibition of axonal transport is the fact that they would be expected to inhibit all types of transport. However, we were not able to detect defects in anterograde axonal transport in our experiments with Lysotracker™.

4.5.4. p38 MAPK is aberrantly activated in SOD1^{G93A} mice

In this Chapter, I was able to demonstrate that p38 MAPK is activated in SOD1^{G93A} motor neurons both *in vitro* and *in vivo.* In adult mouse spinal cords, we found that the aberrant activation of p38 MAPK correlated with the appearance and worsening of *in vivo* retrograde axonal transport defects (Bilsland et al., 2010). Our results agree with data that has been previously published on p38 MAPK activation in ALS. A limitation of our analysis was the use of western blotting and whole spinal cord lysates to assess phospho-p38 MAPK levels. However, Dewil et al. have previously shown using immunofluorescence that p38 MAPK is activated in the motor neurons and microglia of the SOD1^{G93A} spinal cord, but not in astrocytes (Dewil et al., 2007). Abnormally activated p38 MAPK is also found in motor neurons of sporadic ALS

patients (Bendotti et al., 2004). To date, the pathological activation of p38 MAPK has only been demonstrated in mutant SOD1-mediated ALS. In the future, it will be interesting to examine whether p38 MAPK is activated in other forms of fALS and whether this also correlates with the presence of axonal transport defects.

It still remains to be determined what causes the pathological activation of p38 MAPK in mutant SOD1-mediated ALS. Analysis of $SOD1^{G93A}$ spinal cords reveals that the upstream kinases MKK3/6, MKK4 and ASK1 are all activated presymptomatically, indicating that the whole p38 MAPK cascade is activated (Veglianese et al., 2006). This is supported by the observation that pharmacological inhibition of ASK1 can rescue defects in anterograde axonal transport induced by $SOD1^{G93A}$ in squid axoplasm assays (Song et al., 2013).

p38 MAPK could be activated due to a gain-in-function of $SOD1^{G93A}$ that we have not yet been able to understand. Alternatively, a number of pathways that activate p38 MAPK have already been implicated in ALS pathogenesis, including inflammatory signalling, excitotoxicity and oxidative stress, and could contribute in part or in full to the pathological activation of the kinase.

4.5.4.1. Inflammatory signalling

TNFα is a well-established activator of the p38 MAPK signalling cascade and is produced by astrocytes, microglia and neurons. TNFα was detected as one of the earliest inflammatory stimuli to be induced in $SOD1^{G93A}$ mice (11 weeks) (Yoshihara et al., 2002). This could be explained by the observation that there are an increased number of activated microglia in the ventral horn of presymptomatic $SOD1^{G93A}$ mice (Tortarolo et al., 2003). TNFα receptors (TNFR1 and R2) are also reported to be overexpressed in these mice (Veglianese et al., 2006). Pathological TNFα signalling could therefore be responsible for the early and persistent activation of p38 MAPK in ALS. TNFα knockout in $SOD1^{G93A}$ mice has been reported to have no effect on lifespan or motor neuron loss (Gowing et al., 2006). However, treatment of $SOD1^{G93A}$ mice with thalidomide, which reduces TNFα levels by causing degradation of its mRNA, was found to improve motor performance, reduce motor neuron death and increase lifespan (Damiano et al., 2006). This

discrepancy could be explained by the fact that thalidomide was also observed to reduce levels of interleukin-1α and β (IL-1α and β) and IL-12p40. It is therefore possible that reduction of a number of inflammatory mediators is required to effect disease progression in $SOD1^{G93A}$ mice. This is supported by the observation that knocking out IL-1β, another established activator of p38 MAPK (Sung et al., 2005) that is upregulated in the spinal cord of symptomatic $SOD1^{G93A}$ and $SOD1^{G37R}$ mice (Nguyen et al., 2001, Hensley et al., 2002), has no effect on disease progression in $SOD1^{G37R}$ mice (Nguyen et al., 2001).

4.5.4.2. Excitotoxicity

Glutamate-induced excitotoxicity is a well-established mechanism of motor neuron death in ALS. It has been proposed that the excitotoxic effect of glutamate is mediated in part by p38 MAPK. *In vivo* it has been demonstrated that intracortical injection of quinolinic acid (a glutamate analogue) leads to a transient increase in p38 MAPK activation in surrounding neurons and astrocytes prior to induction of neuronal death (Ferrer et al., 2001). The early appearance of cortical hyperexcitability in ALS patients suggests that dysregulated glutamate signalling could be responsible for the presymptomatic p38 MAPK-induced defects in retrograde axonal transport in ALS. In addition, the FDA-approved drug riluzole has been shown to cause a dose-dependent decrease in glutamate-induced activation of p38 MAPK (Stevenson et al., 2009). Riluzole could therefore mediate some of its beneficial effects by inhibiting aberrantly activated p38 MAPK.

4.5.4.3. Oxidative stress

There are a number of reports of increased oxidative stress in both sporadic and familial ALS patients and also mouse models of the disease (see Section 1.5.1). Although it is clear that reactive oxygen species (ROS) activate the p38 MAPK cascade, the mechanism(s) responsible are still not fully understood. One suggestion is that ROS alter the activity of key signalling proteins by modifying critical amino acids and/or inducing a change in the protein's structure (Son et al., 2011). Interestingly, streptozotocin-treated mice, which develop experimental diabetes, were found to have significantly higher levels of ROS and this was found

to correlate with slower axonal transport rates in the olfactory system (Sharma et al., 2010). Streptozotocin-treated mice were also shown to have increased p38 MAPK activation and tau phosphorylation. This supports the idea that oxidative stress, p38 MAPK activation and axonal transport defects could be linked in ALS. Oxidative stress is reported to be present before the onset of disease and could therefore explain the presymptomatic activation of p38 MAPK in ALS mutant mice (Pollari et al., 2014).

4.5.5. p38 MAPK as a potential therapeutic target

In this Chapter we were able to demonstrate that the p38 MAPKα/β-specific inhibitor SB-239063 could correct retrograde axonal transport defects in the SOD1^{G93A} mouse *in vivo.* The next step of the project will therefore be to perform a longitudinal study to test whether SB-239063 can affect disease progression in these mice.

One past study has tested the effect of p38 MAPK inhibition on motor neuron survival and lifespan in the SOD1^{G93A} mouse. Presymptomatic mice were treated daily until the end stage of the disease with semapimod, an inhibitor of c-Raf, which activates p38 MAPK and JNK through MEK phosphorylation. Although semapimod was able to significantly improve motor neuron survival both *in vitro* and *in vivo*, there were no significant changes in disease onset or survival in treated SOD1^{G93A} mice (Dewil et al., 2007). However, treatment of SOD1^{G93A} mice with semapimod daily decreased levels of phospho-p38 MAPK in the spinal cord by only 30%. It is possible that significant effects on survival would be seen with higher doses of the drug. However the toxicity of semapimod at higher concentrations prevented the authors from trying this. Alternatively, it is possible that inhibition of p38 MAPK is sufficient to prevent motor neuron death but is unable to fully restore the function of the entire motor unit in order to affect survival and disease onset significantly. Alternatively, the lack of effect on disease onset and survival could be because semapimod is not a specific inhibitor of p38 MAPK. Deleterious effects resulting from inhibition of JNK and MEK could have disguised the beneficial effects of p38 MAPK inhibition. It is therefore necessary to test more potent and selective p38

MAPK inhibitors to truly understand whether axonal transport defects play an important role in ALS disease pathogenesis.

p38 MAPK is activated at very low levels in wild type cells and therefore poses an attractive therapeutic target, as its inhibition should have few off-target effects in cells unaffected by the disease. Many compounds have been developed that are able to selectively target p38 MAPK, due to the role of the kinase in inflammatory diseases and cancer (Yong et al., 2009). However, to date, few have been tested for their effects in neurodegenerative diseases; most likely because many of these compounds do not efficiently cross the blood brain barrier (BBB). Finding isoform-specific, BBB-permeable p38 MAPK inhibitors that do not cause adverse side effects is certainly a major challenge in the field.

Pyridinyl-imidazole compounds, such as SB-203580 and SB-239063 used in this study, were the first p38 MAPK inhibitors to be identified that bind competitively at the ATP-binding pocket and exploit this to achieve isoform specificity (Tong et al., 1997). These compounds are able to selectively inhibit p38 MAPKα and β because a substitution of threonine106 for a methionine in the ATP binding pocket of the γ and δ isoforms blocks the binding of the compounds (Cuadrado and Nebreda, 2010). However, to date, pyridinyl-imidazole compounds have not been designed to selectively inhibit p38 MAPKα.

There have been reports of p38 MAPKα-specific inhibitors. Vertex reported the development of a BBB permeable, orally available p38 MAPKα-specific inhibitor, VX-745. However, when undergoing clinical trials, the compound was found to cause adverse neurological effects (Kumar et al., 2003). This could be unrelated to the p38 MAPK activity and rather an off-target effect of this particular compound. Another example is MW01-2-069A-SRM, a CNS-penetrant, orally available, small molecule inhibitor of p38 MAPKα. MW01-2-069A-SRM has been shown to prevent excessive proinflammatory cytokine production in the hippocampus and reduce synaptic dysfunction and hippocampus-dependent behavioural deficits in a mouse model of Alzheimer's disease, without causing any adverse effects (Munoz et al., 2007). The compound is also reported to have good oral bioavailability and brain

penetrance in rodents (Borders et al., 2008). However no clinical trial results using this compound have been reported to date.

If we can identify the downstream target(s) of p38 MAPK that are responsible for its effects on axonal transport, an alternative therapeutic approach would be to inhibit these targets rather than the kinase itself. However, development of inhibitors that target the downstream kinases of p38 MAPK have not been very successful to date. Pfizer reported the development of PF-3644022, an orally available ATP-competitive MK2 inhibitor. However, the clinical development of this compound was stopped due to poor serum availability and hepatotoxicity (Arthur and Ley, 2013).

Chapter 5. Inhibitors of the IGF1 receptor accelerate retrograde axonal transport

5.1. Introduction

Results presented in Chapter 3 suggest that inhibition of the insulin-like growth factor 1 receptor (IGF1R) accelerates retrograde axonal transport *in vitro* in both wild type and SOD1^{G93A} primary motor neurons.

The IGF signalling system is comprised of two peptide ligands – IGF1 and IGF2 - and two receptors – IGF1R and IGF2R (illustrated in Figure 5.1). IGF1R is a type II receptor tyrosine kinase and is involved in a variety of cellular processes, including cellular proliferation, growth, migration and apoptosis (Brahmkhatri et al., 2015). IGF2R, on the other hand, has no intracellular kinase domain and has in fact been shown to have an antagonistic role on IGF signalling – internalising IGF2 and targeting it for lysosomal degradation, thereby preventing it from binding to and activating IGF1R (Kornfeld, 1992).

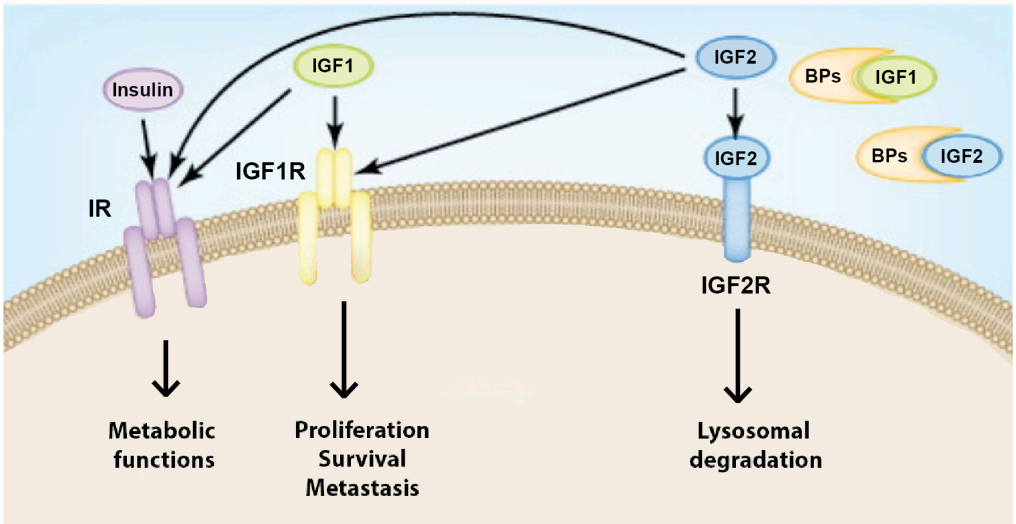

Figure 5.1. Insulin-like growth factors and their receptors
The IGF signalling system is comprised of two ligands – IGF1 and IGF2, two membrane-spanning receptors – IGF1R and IGF2R, and six high-affinity IGF-binding proteins – IGFBP1-6. IGF1R is a type 2 tyrosine kinase receptor that plays important roles in cellular proliferation, migration and apoptosis. IGF2R, on the other hand, is a type 1 integral membrane glycoprotein that targets IGF2 for lysosomal degradation. The insulin receptor (IR) is also able to bind IGF1 and 2, and plays a key role in the regulation of glucose homeostasis. Figure modified from (Alberini and Chen, 2012). Reprinted with permission from Elsevier.

IGF2R is also known as the mannose-6-phosphate (M6P) receptor and has been shown to bind M6P-containing ligands both at the cell surface (e.g. transforming growth factor-1β, TGF-1β) and in the trans-Golgi network (e.g. lysosomal acid hydrolases). In addition to its role in regulating IGF signalling, IGF2R is known to play important roles in growth regulation and lysosomal biogenesis. For example, the receptor has been shown to facilitate activation of the growth suppressor TGF-1β (Dennis and Rifkin, 1991), mediate the internalisation of granzyme B, which is crucial for the induction of target cell apoptosis by cytotoxic T cells (Motyka et al., 2000), and regulate the targeting of acid hydrolases to the lysosome (Ludwig et al., 1994).

IGF1R is not only expressed in insulin-responsive tissues (liver, adipose tissue and skeletal muscle) but also in many other tissues, including the brain and spinal cord (Kouroupi et al., 2010). The receptor is a heterotetramer, consisting of two extracellular ligand-binding chains (IGF1Rα) and two membrane-spanning chains (IGF1Rβ), held together by disulphide bonds. The four IGF1R chains are encoded by a single gene. The IGF1Rβ subunits contain the tyrosine kinase domain. Ligand binding to the IGF1Rα subunits results in IGF1Rβ transphosphorylation of activation loop tyrosines (Tyr1161/Tyr1165/Tyr1166) and full kinase activation (Singh et al., 2014).

There is 62% amino acid homology between IGF1 and IGF2 and 40% homology between the IGFs and pro-insulin (Li et al., 2009). IGF1 is the main ligand for IGF1R (K_D = 1 nM), whilst IGF2 binds with a lower affinity (K_D = 15-20 nM). Insulin can also bind to IGF1R, but with 100-fold lower affinity than IGF1 (K_D = 100 nM). IGF1 is produced by various tissues in response to growth hormone, which is synthesised by the liver. In contrast, the regulation of IGF2 production is thought to be much more complex and is not controlled by growth hormone (Tognon and Sorensen, 2012). The majority of circulating IGF1 and 2 is found bound to IGF binding proteins, which have been proposed to act as “reservoirs”, increasing the half-life of the IGFs and extending signalling duration (Singh et al., 2014).

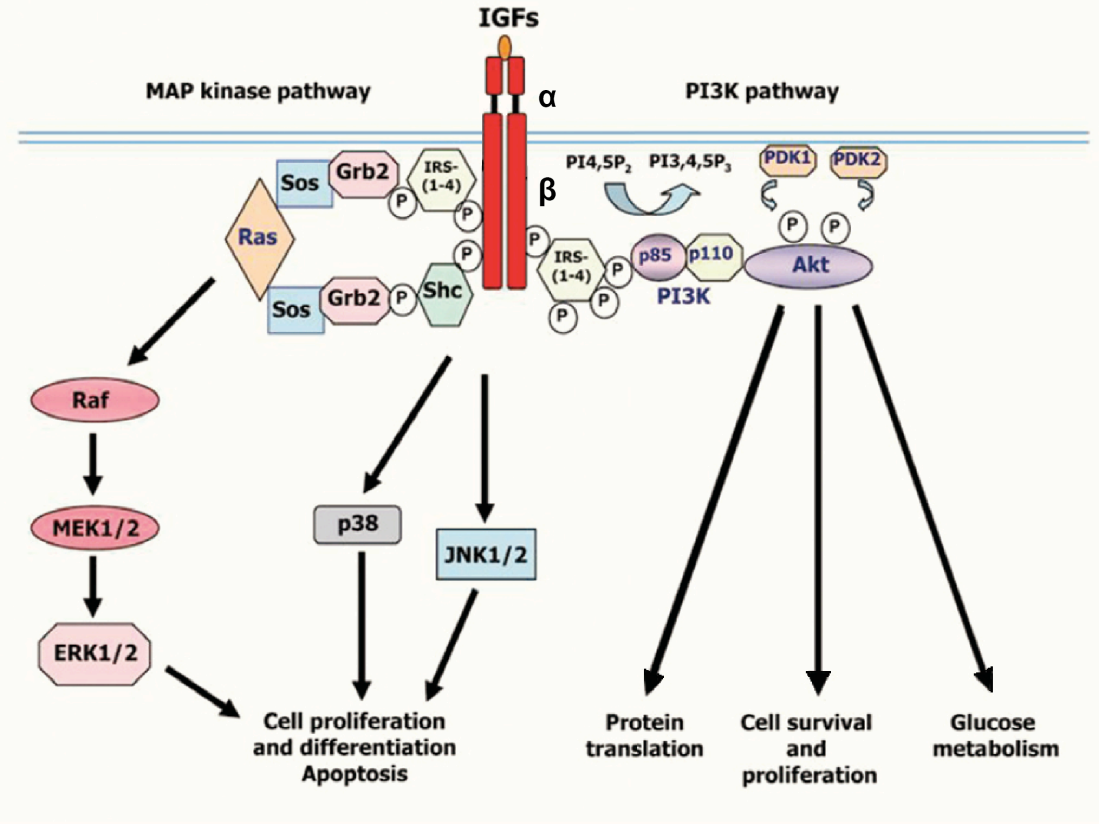

Figure 5.2. Signalling cascades activated by IGF1R stimulation
IGF1R activates several downstream kinase cascades, including those involving ERK1/2, p38 MAPK, JNK1/2 and Akt. As a result, it regulates a wide variety of cellular processes (Hematulin, 2010).

IGF1R signalling stimulates a cascade of complex cellular responses. After ligand binding and phosphorylation of the activation loop tyrosines, a number of other tyrosine residues in the juxtamembrane region, kinase domain, and carboxy-terminus of the IGF1Rβ subunits are autophosphorylated. These phospho-tyrosines act as docking sites for a variety of adaptor proteins, including the SH2 domain-containing insulin receptor substrates (IRS1-4) and src homology 2 containing (Shc) transforming protein (Singh et al., 2014). Ligand binding results in the activation of many signalling pathways, including a number of downstream kinase cascades, including ERK1/2, p38 MAPK, Akt and JNK (illustrated in Figure 5.2).

The aim of the experiments performed in this Chapter was to investigate the role of IGF1R signalling in the regulation of axonal transport.

5.2. *In vitro* validation of IGF1R as the target kinase

The results of the preliminary screening assay and subsequent *in vitro* axonal transport assays suggested that inhibition of IGF1R accelerates retrograde axonal transport in motor neurons. In order to validate IGF1R as the target kinase, additional inhibitors were screened using the accumulation assay (Figure 3.25). From this target validation screen, three compounds were selected to investigate further: compounds 2-C1, 2-G2 and 2-B3.

5.2.1. Investigating the hits of the target validation screen

Compound 2-C1 was found to cause a significant increase in the somal accumulation of both H_CT and α-p75^{NTR} in ES-derived motor neurons. *In vitro* axonal transport assays were performed in wild type and SOD1^{G93A} primary motor neurons, as our active inhibitor from the preliminary screen, compound E4, could accelerate retrograde axonal transport in motor neurons from both genotypes. All the IGF1R inhibitors were tested at 0.5 μM due to the previously observed toxicity of compound E4 at 2 μM in *in vitro* axonal transport assays.

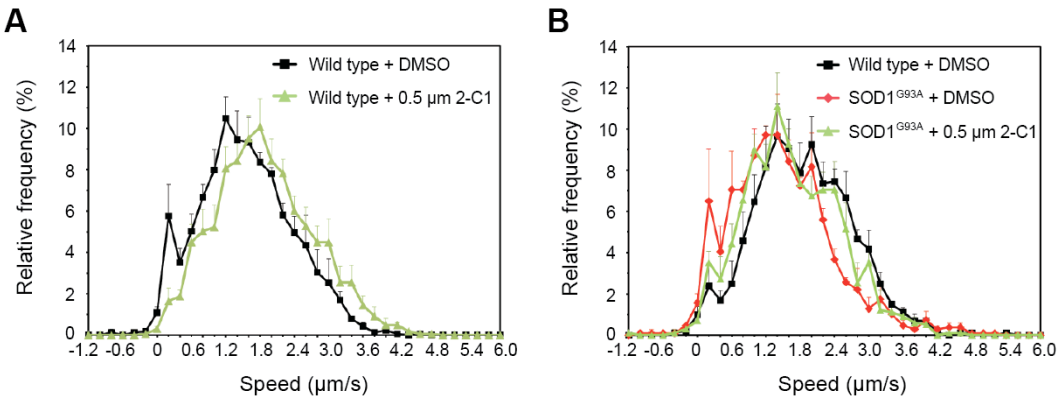

Figure 5.3. The effects of 2-C1 on the retrograde axonal transport of H_CT-labelled vesicles in primary motor neurons

(A) Speed profiles of H_CT carriers in wild type motor neurons (black squares) treated with 0.5 μM 2-C1 (green triangles). Wild type: 182 carriers, 14 axons; wild type + 2-C1: 233 carriers, 16 axons; 5 independent experiments. (B) Speed profiles of H_CT carriers in wild type motor neurons (black squares), SOD1^{G93A} motor neurons (red diamonds) and SOD1^{G93A} motor neurons treated with 0.5 μM 2-C1 (green triangles). Wild type: 74 carriers, 10 axons; SOD1^{G93A}: 119 carriers, 8 axons; SOD1^{G93A} + 0.5 μM 2-C1: 110 carriers, 8 axons; 3 independent experiments.

Compound 2-C1 was found to cause a small increase in the retrograde axonal transport of H_CT-labelled vesicles in wild type and $SOD1^{G93A}$ motor neurons (Figure 5.3; WT + DMSO versus WT + 0.5 µM 2-C1: $p = 0.130$, $SOD1^{G93A}$ + DMSO versus $SOD1^{G93A}$ + 0.5 µM 2-C1: $p = 0.428$), but did not fully restore axonal transport speeds in $SOD1^{G93A}$ motor neurons to wild type levels.

Compound 2-G2, on the other hand, had a more promising effect on the retrograde axonal transport of H_CT. Incubation of wild type motor neurons with 0.5 µM 2-G2 caused a shift to faster axonal transport speeds ($p = 0.016$; Figure 5.4A) and in $SOD1^{G93A}$ motor neurons, 2-G2 could fully restore H_CT axonal transport to wild type levels (Figure 5.4B; $SOD1^{G93A}$ + DMSO versus $SOD1^{G93A}$ + 0.5 µM 2-G2: $p = 0.046$).

However, compound 2-G2 did not have the same effects on the retrograde axonal transport of $\alpha\text{-}p75^{NTR}$. Compound 2-G2 was found to have very little effect on $\alpha\text{-}p75^{NTR}$ axonal transport speeds in either wild type ($p = 0.301$) or $SOD1^{G93A}$ motor neurons ($p = 0.227$) (Figure 5.4C and D).

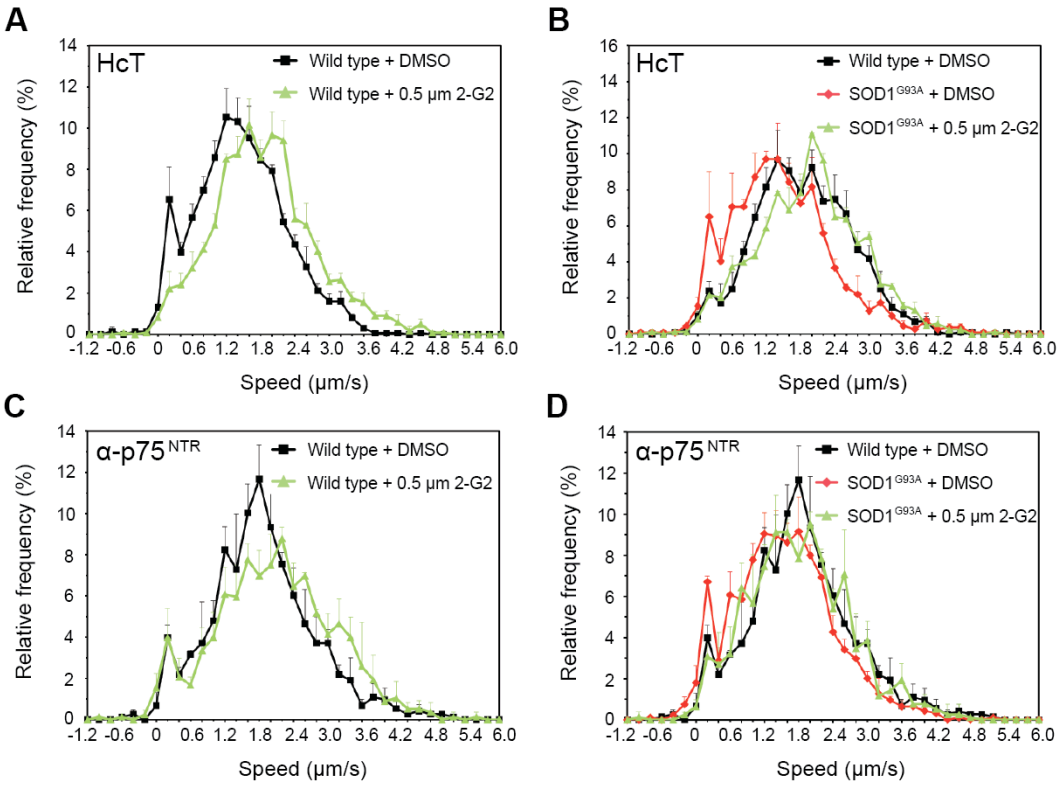

Figure 5.4. The effects of 2-G2 on retrograde axonal transport in primary motor neurons
(A) Speed profiles of H_CT carriers in wild type motor neurons (black squares) compared to wild type motor neurons treated with 0.5 µM 2-G2 (green triangles). Wild type: 141 carriers, 11 axons; wild type + 2-G2: 164 carriers, 9 axons; 4 independent experiments. (B) Speed profiles of H_CT carriers in wild type motor neurons (black squares), $SOD1^{G93A}$ motor neurons (red diamonds) and $SOD1^{G93A}$ motor neurons treated with 0.5 µM 2-G2 (green triangles). Wild type: 74 carriers, 10 axons; $SOD1^{G93A}$: 119 carriers, 8 axons; $SOD1^{G93A}$ + 0.5 µM 2-G2: 127 carriers, 7 axons; 3 independent experiments. (C) Speed profiles of α-$p75^{NTR}$ carriers in wild type motor neurons (black squares) compared to wild type motor neurons treated with 0.5 µM 2-G2 (green triangles). Wild type: 100 carriers, 6 axons; wild type + 2-G2: 95 carriers, 6 axons; 3 independent experiments. (D) Speed profiles of α-$p75^{NTR}$ carriers in wild type (black squares), $SOD1^{G93A}$ (red diamonds) and $SOD1^{G93A}$ motor neurons treated with 0.5 µM 2-G2 (green triangles). Wild type: 83 carriers, 7 axons; $SOD1^{G93A}$: 77 carriers, 7 axons; $SOD1^{G93A}$ + 0.5 µM 2-G2: 81 carriers, 7 axons; 3 independent experiments.

The final compound selected from the target validation screen was 2-B3. In the accumulation assay, 2-B3 had no effect on H_CT accumulation, but caused a significant increase in the accumulation of α-$p75^{NTR}$ (Figure 3.25).

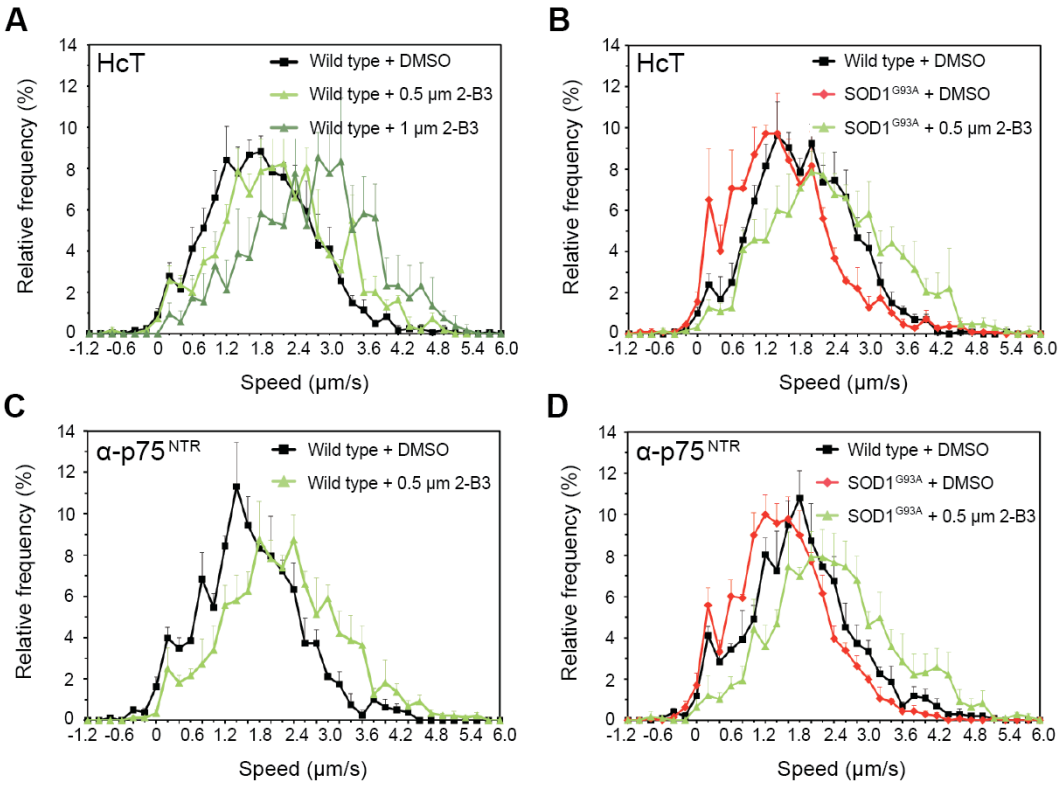

Figure 5.5. The effects of 2-B3 on retrograde axonal transport in primary motor neurons

(A) Speed profiles of H_CT carriers in wild type motor neurons (black squares) treated with 0.5 µM 2-B3 (light green triangles) and 1 µM 2-B3 (dark green triangles). Wild type: 157 carriers, 8 axons; wild type + 0.5 µM 2-B3: 86 carriers, 13 axons; wild type + 1 µM 2-B3: 85 carriers, 6 axons; 3 independent experiments. (B) Speed profiles of H_CT carriers in wild type motor neurons (black squares), $SOD1^{G93A}$ motor neurons (red diamonds) and $SOD1^{G93A}$ motor neurons treated with 0.5 µM 2-B3 (green triangles). Wild type: 74 carriers, 10 axons; $SOD1^{G93A}$: 119 carriers, 9 axons; $SOD1^{G93A}$ + 0.5 µM 2-B3: 98 carriers, 8 axons; 3 independent experiments. (C) Speed profiles of $\alpha\text{-p75}^{NTR}$ carriers in wild type motor neurons (black squares) treated with 0.5 µM 2-B3 (green triangles). Wild type: 75 carriers, 7 axons; wild type + 2-B3: 110 carriers, 6 axons; 3 independent experiments. (D) Speed profiles of $\alpha\text{-p75}^{NTR}$ carriers in wild type motor neurons (black squares), $SOD1^{G93A}$ motor neurons (red diamonds) and $SOD1^{G93A}$ motor neurons treated with 0.5 µM 2-B3 (green triangles). Wild type: 113 carriers, 8 axons; $SOD1^{G93A}$: 126 carriers, 9 axons; $SOD1^{G93A}$ + 0.5 µM 2-B3: 149 carriers, 8 axons; 3 independent experiments.

However, when tested in our *in vitro* axonal transport assays, compound 2-B3 was able to accelerate axonal transport of H_CT in both wild type and $SOD1^{G93A}$ motor neurons (WT + DMSO versus WT + 0.5 µM 2-B3: $p = 0.104$, $SOD1^{G93A}$ + DMSO versus $SOD1^{G93A}$ + 0.5 µM 2-B3: $p = 0.037$; Figure 5.5A and B). In addition, the enhancing effect of 2-B3 on H_CT axonal transport in wild type neurons was found to be dose-dependent (0.5 µM versus 1 µM: $p = 0.236$; Figure 5.5A). Compound 2-B3 was also found to accelerate the axonal transport of $\alpha\text{-p75}^{NTR}$ in both wild type and

$SOD1^{G93A}$ motor neurons (WT + DMSO versus WT + 0.5 µM 2-B3: p = 0.046, $SOD1^{G93A}$ + DMSO versus $SOD1^{G93A}$ + 0.5 µM 2-B3: p = 0.027; Figure 5.5C and D).

5.2.2. Investigating the effect of stimulating the IGF1R cascade on retrograde axonal transport in motor neurons

To further confirm that IGF1R is a negative regulator of retrograde axonal transport, wild type motor neurons were stimulated with the receptor's main ligand, IGF1. Treatment of wild type primary motor neurons with 50 ng/ml IGF1 was found to cause a strong stimulation of IGF1R phosphorylation (Figure 5.6A) and significant inhibition of the *in vitro* retrograde axonal transport of H_CT-labelled vesicles compared to untreated wild type controls (p = 0.003; Figure 5.6B).

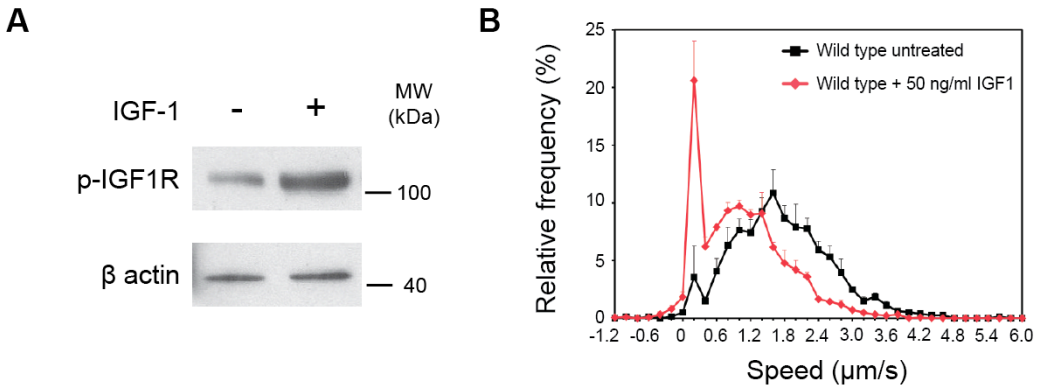

Figure 5.6. Stimulation of IGF1R inhibits retrograde axonal transport in primary wild type motor neurons

(A) Treatment of wild type motor neuron cultures with 50 ng/ml IGF-1 for 30 min causes a substantial activation of IGF1R. β actin is used as a loading control. (B) Speed profiles of H_CT carriers in motor neuron cultures treated with either DMSO (black squares) or 50 ng/ml IGF-1 (red diamonds). IGF-1 causes a shift to slower transport speeds (Untreated: 82 carriers, 11 axons; IGF-1 treated: 83 carriers, 9 axons; 3 independent experiments).

5.2.3. Investigating the effects of compounds E4 and 2-B3 on the IGF1R signalling cascade

As IGF1R stimulates a complex cascade of downstream pathways (illustrated in Figure 5.2), we investigated the effects of our active inhibitors (E4 and 2-B3) on the downstream signalling of the receptor (Figure 5.7).

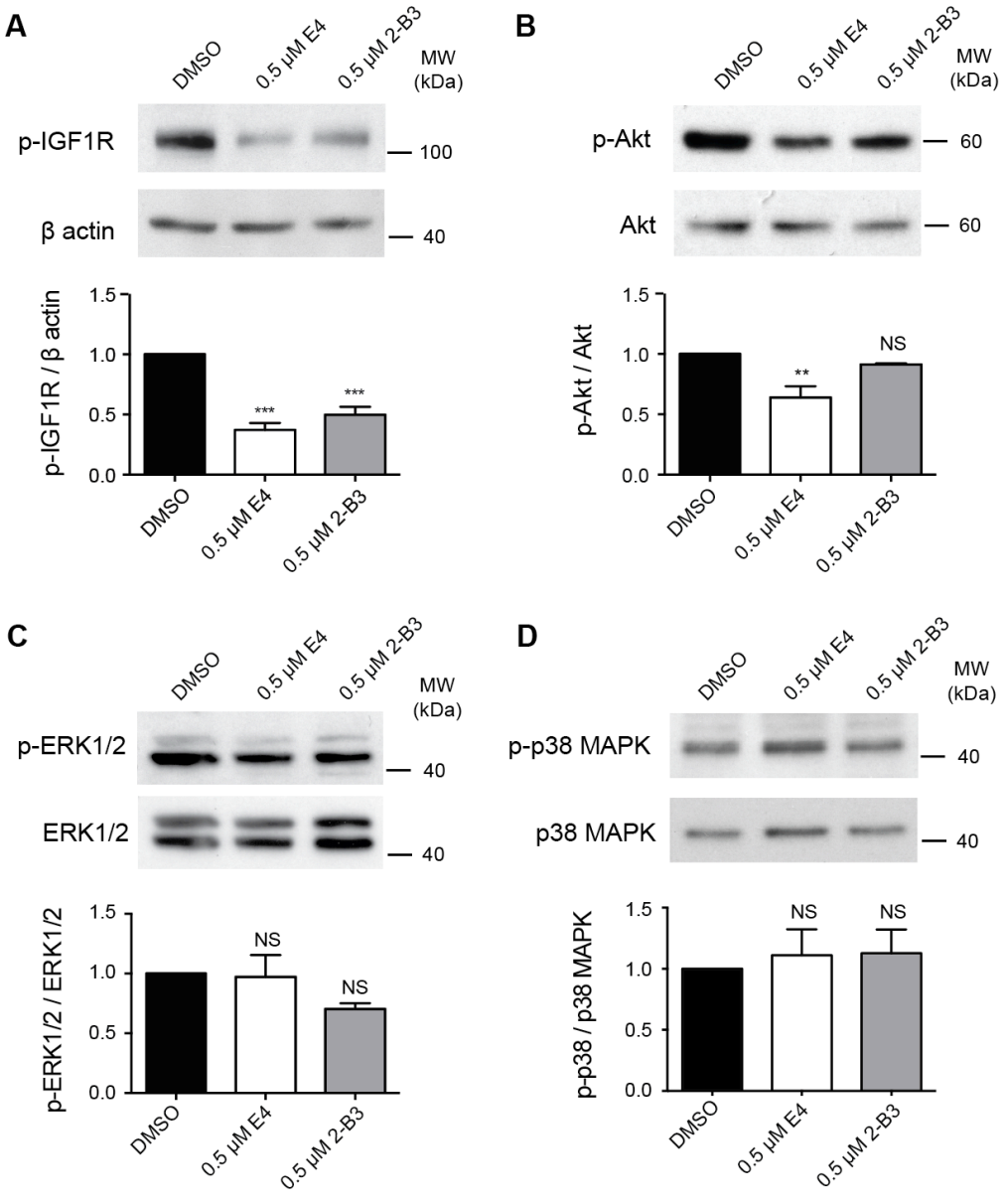

Figure 5.7. The effects of compounds E4 and 2-B3 on the activity of components of the IGF1R signalling cascade

Western blots showing the effect of 0.5 μM E4 and 2-B3 on activation of IGF1R (A), Akt (B), ERK1/2 (C) and p38 MAPK (D) in wild type motor neuron cultures compared to DMSO treated controls (IGF1R: n = 3, Akt: n = 4, ERK1/2: n = 3, p38 MAPK: n = 2). ** p< 0.01, *** p < 0.001, NS = non significant (One-way ANOVA followed by Dunnett's multiple comparison test).

Compound 2-B3 was tested alongside compound E4, as they had very similar effects on the axonal transport of H_CT and α-$p75^{NTR}$ (Figure 3.23, Figure 3.24 and Figure 5.5). Firstly, we confirmed by western blot that E4 and 2-B3 were indeed acting to inhibit IGF1R activity (Figure 5.7A). Having established that both compounds caused a significant inhibition of IGF1R phosphorylation, we went on to investigate the effects of the inhibitors on three downstream kinases: Akt, ERK1/2 and p38 MAPK (as shown in the IGF1R signalling schematic in Figure 5.2). Both E4 and 2-B3 were observed to inhibit Akt activity, although the effect of 2-B3 was not statistically significant (Figure 5.7B). Neither compound was found to have a significant effect on either ERK1/2 or p38 MAPK activation (Figure 5.7C and D).

Finally, IGF1R activity was investigated in primary $SOD1^{G93A}$ motor neurons, as the aim of the project was to identify compounds that would ultimately be used to accelerate axonal transport in ALS. No significant difference in IGF1R activity was observed between wild type and $SOD1^{G93A}$ motor neurons (Figure 5.8A), nor did expression of the $SOD1^{WT}$ protein have any effect (Figure 5.8B). This was not surprising given the ability of E4 and 2-B3 to accelerate axonal transport in both wild type and $SOD1^{G93A}$ motor neurons.

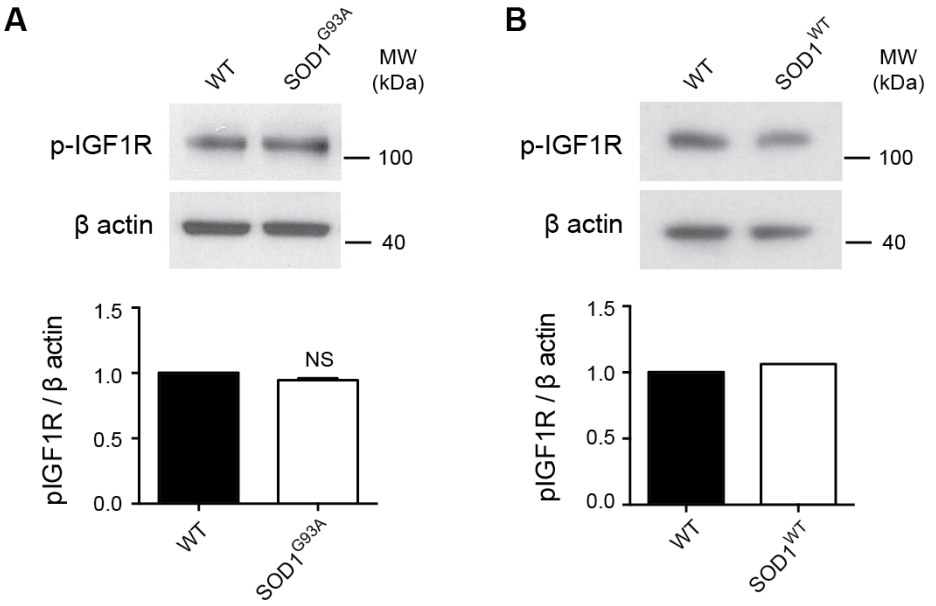

Figure 5.8. IGF1R activity is not altered in $SOD1^{G93A}$ motor neurons

Western blots showing IGF1R activity in motor neurons overexpressing $SOD1^{G93A}$ (A) and $SOD1^{WT}$ protein (B). Western blot quantification detected no significant difference in IGF1R activity between wild type cultures and motor neurons overexpressing either $SOD1^{G93A}$ or $SOD1^{WT}$ ($SOD1^{G93A}$ n = 3, $SOD1^{WT}$ n = 1). Non-significant using unpaired Student's *t* test.

5.2.4. Knockdown of IGF1R in N2A cells and primary motor neurons

In order to determine whether IGF1R was the target kinase of our active compounds, we ordered four shRNAs targeted against different sequences within the IGF1R mRNA. The shRNA constructs contained an eGFP reporter gene, to allow easy identification of transfected/transduced cells. The shRNA constructs were first tested in N2A cells, in order to determine which caused the most efficient knockdown of IGF1R.

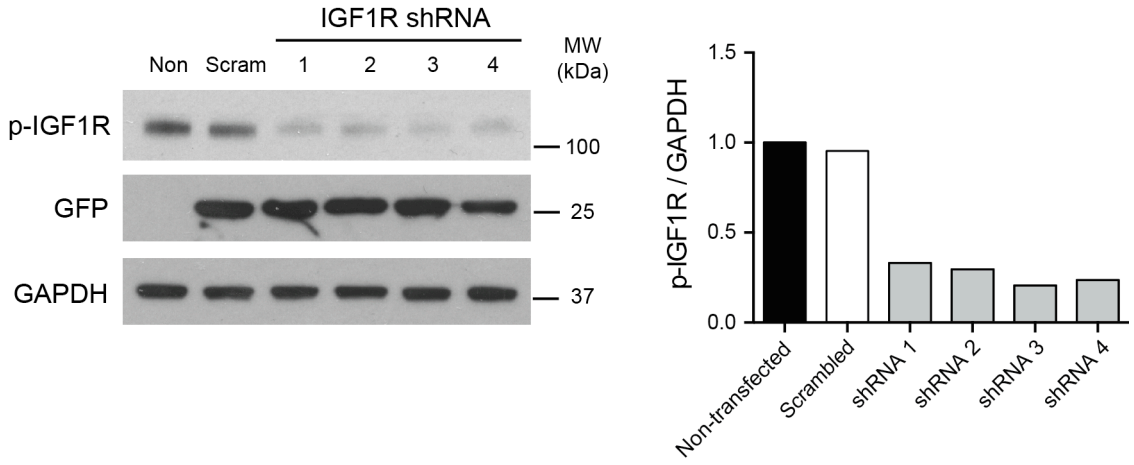

Figure 5.9. Testing IGF1R shRNA constructs in N2A cells
N2A cells were transfected with four different shRNA constructs against IGF1R, as well as a scrambled control. GFP indicates expression of the construct. Quantification of the western blot shows different levels of knockdown of IGF1R with different shRNA constructs. n = 1.

Western blot analysis revealed that shRNA 3 caused the greatest reduction in IGF1R protein levels (Figure 5.9). The phospho-IGF1R antibody was used as we could not identify a suitable IGF1R antibody that worked in western blot. shRNA construct 3 was used to produce lentiviral particles, along with the scrambled construct as a control, to enable us to knockdown IGF1R in wild type and $SOD1^{G93A}$ primary motor neuron cultures.

Transduction of primary motor neurons with IGF1R shRNA lentiviral particles was performed with the help of a rotation student in the laboratory, Alexander Fellows. Transduction of primary motor neurons with increasing amounts of IGF1R shRNA

was found to cause a dose-dependent reduction in IGF1R protein levels, whilst scrambled shRNA had no effect (Figure 5.10).

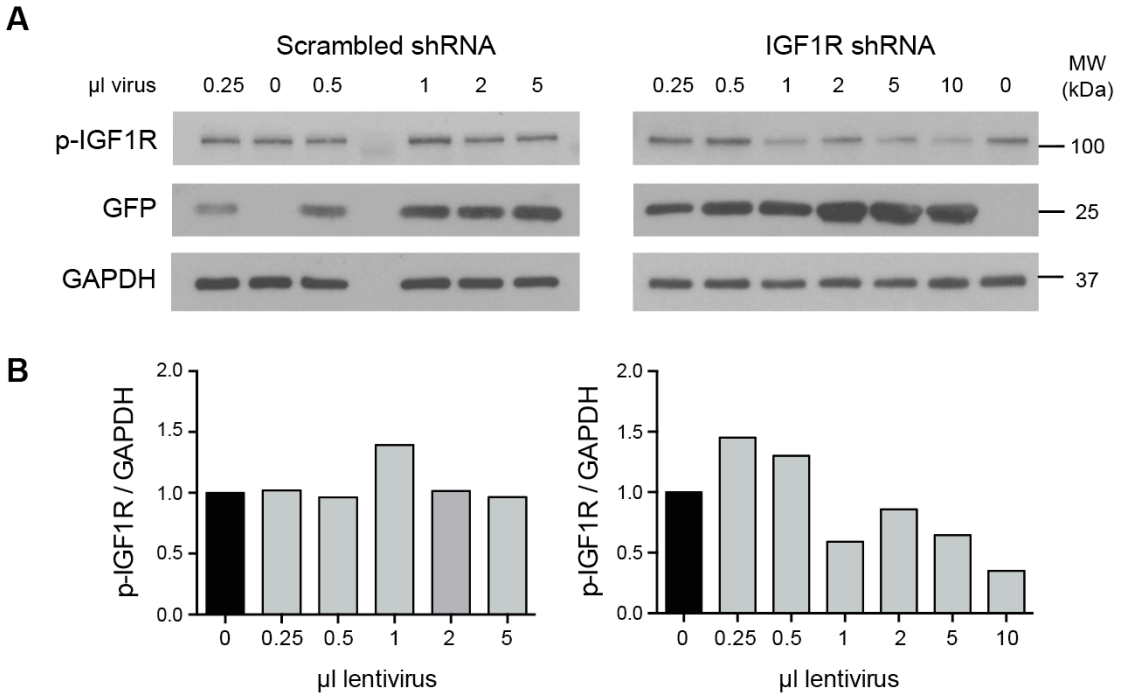

Figure 5.10. Knocking down IGF1R in primary motor neuron cultures

(A) Lysates were made from motor neurons transduced with increasing amounts of lentivirus expressing either scrambled or IGF1R shRNA. Western blotting with an antibody specific for phospho-IGF1R reveals a dose-dependent knockdown with the IGF1R shRNA but not when scrambled shRNA is used. GFP indicates expression of the shRNA construct. (B) Quantification of the blots shown in (A). Levels of IGF1R are normalised to the loading control GAPDH. n = 1.

Our lentiviral IGF1R shRNA particles could therefore be used to determine whether knocking down IGF1R in primary motor neurons had the same effect on retrograde axonal transport as our active IGF1R inhibitors (compounds E4 and 2-B3).

Treatment with 1 µl IGF1R shRNA lentivirus, however, was found to have no effect on the axonal transport of H_CT in either wild type or $SOD1^{G93A}$ motor neuron cultures (WT + scram shRNA versus WT + IGF1R shRNA: p = 0.873, $SOD1^{G93A}$ + scram shRNA versus $SOD1^{G93A}$ + IGF1R shRNA: p = 0.231; Figure 5.11). In addition, higher concentrations of lentivirus were found to cause severe blebbing of axons and therefore could not be used for *in vitro* axonal transport assays. As a

result, we were unable to determine whether knockdown of IGF1R recapitulates the results observed with our active compounds.

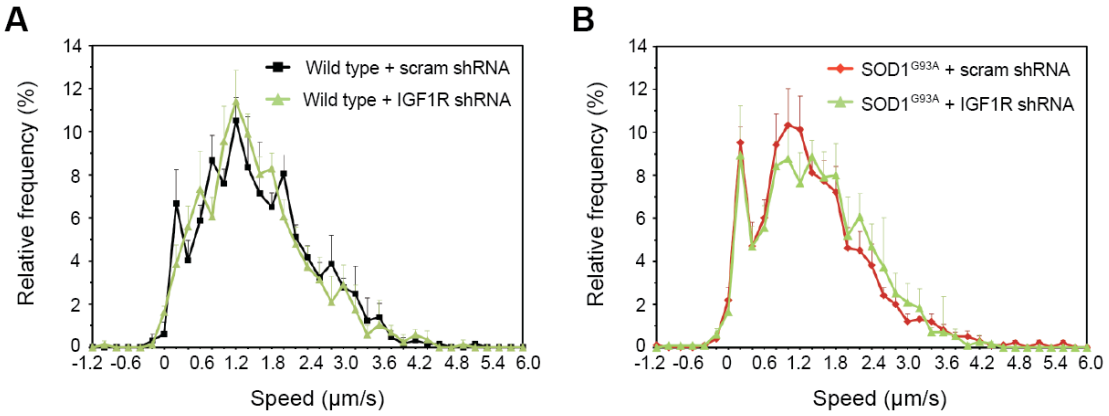

Figure 5.11. Retrograde axonal transport in primary motor neuron cultures treated with IGF1R shRNA

(A) Speed profiles of H_CT-labelled signalling endosomes in wild type motor neurons transduced with 1 µl scrambled shRNA lentivirus (black squares) or 1 µl IGF1R shRNA lentivirus (green triangles). Comparison of the curves reveals that knocking down IGF1R in wild type motor neuron cultures has no effect on retrograde axonal transport (wild type + scrambled shRNA: 70 carriers, 16 axons; wild type + IGF1R shRNA: 93 carriers, 21 axons; 4 independent experiments). (B) Speed profiles of H_CT-labelled signalling endosomes in $SOD1^{G93A}$ motor neurons transduced with 1 µl scrambled shRNA lentivirus (red diamonds) and $SOD1^{G93A}$ motor neurons transduced with 1 µl IGF1R shRNA lentivirus (green triangles). Comparison of the curves reveals that knocking down IGF1R in $SOD1^{G93A}$ motor neurons has little effect on retrograde axonal transport ($SOD1^{G93A}$ + scrambled shRNA: 84 carriers, 18 axons; $SOD1^{G93A}$ + IGF1R shRNA: 107 carriers, 25 axons; 5 independent experiments).

5.3. Are IGF1R inhibitors general enhancers of axonal transport?

As compound E4 was able to enhance the retrograde axonal transport of H_CT and α-$p75^{NTR}$ in both wild type and $SOD1^{G93A}$ motor neurons, we wanted to investigate whether the compound was a general enhancer of axonal transport. We therefore tested the effect of compound E4 on the axonal transport of different cargoes (Lysotracker™ and WGA), on anterograde axonal transport and also in different neuronal types (sensory and hippocampal).

Firstly, we investigated whether compound E4 affected the retrograde axonal transport of cargoes other than H_CT and α-$p75^{NTR}$. We therefore used

Lysotracker™ to label acidic organelles (late endosomes/lysosomes and autophagosomes). Motor neurons were co-incubated with Lysotracker™ and H_CT so that the direction of axonal transport could be determined. Treatment of motor neurons with 0.5 µM E4 caused a small acceleration of the retrograde axonal transport of acidic organelles in wild type motor neurons (p = 0.312; Figure 5.12A). In $SOD1^{G93A}$ motor neurons, the ability of compound E4 to accelerate axonal transport was more pronounced and could restore retrograde axonal transport speeds to wild type levels ($SOD1^{G93A}$ + DMSO versus $SOD1^{G93A}$ + 0.5 µM E4: p = 0.147; Figure 5.12B).

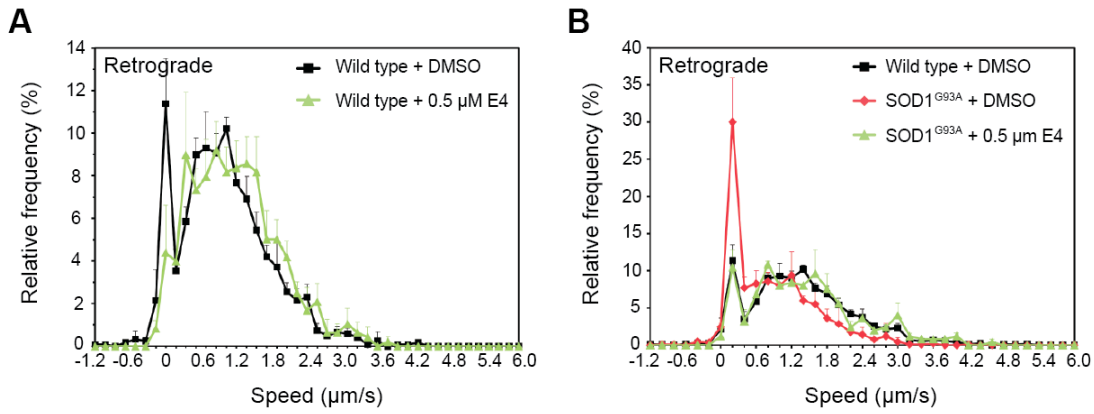

Figure 5.12. The effect of compound E4 on retrograde axonal transport of Lysotracker™ in wild type and $SOD1^{G93A}$ motor neurons

(A) Retrograde speed profiles of Lysotracker™-labelled carriers in wild type motor neuron cultures treated with DMSO (black squares) or 0.5 µM E4 (green triangles) (DMSO: 85 carriers, 12 axons; E4: 42 carriers, 13 axons; 3 independent experiments). (B) Retrograde speed profiles of Lysotracker™-labelled carriers in wild type (black squares), $SOD1^{G93A}$ (red diamonds) and $SOD1^{G93A}$ + 0.5 µM E4 (green triangles) motor neuron cultures (wild type: 85 carriers, 12 axons; $SOD1^{G93A}$: 30 carriers, 15 axons; $SOD1^{G93A}$ + 0.5 µM E4: 16 carriers, 6 axons; 3 independent experiments).

In vitro axonal transport experiments with Lysotracker™ also allowed us to analyse the effect of compound E4 on anterograde axonal transport. In contrast to its effects on retrograde axonal transport, treatment with 0.5 µM E4 had no effect on anterograde axonal transport speeds (Figure 5.13). This result was seen in assays performed in both wild type (p = 0.934; Figure 5.13A) and $SOD1^{G93A}$ motor neurons (p = 0.847; Figure 5.13B).

Our analysis of axonal transport had so far focused on motor neurons, due to our interest in correcting axonal transport defects in ALS. However, to determine whether compound E4 was a general enhancer of retrograde axonal transport, it was important to test its effects in other neuronal types.

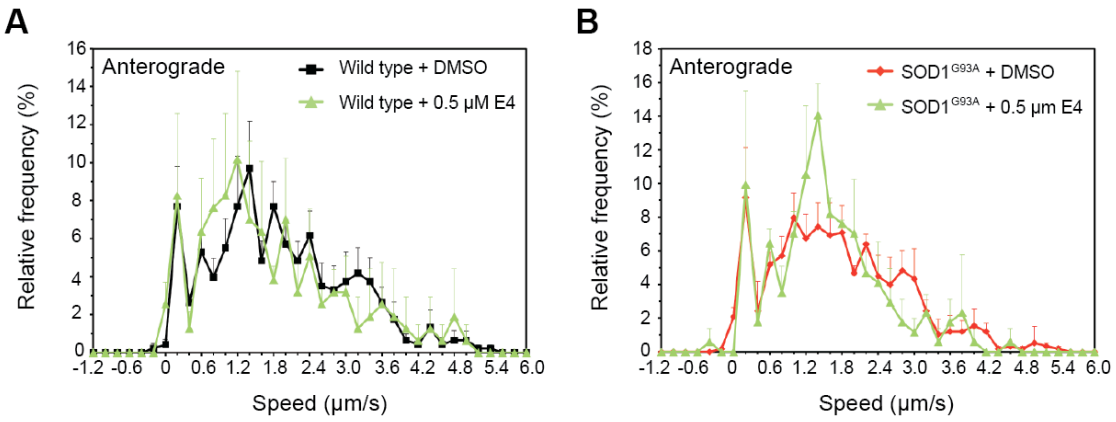

Figure 5.13. The effect of compound E4 on anterograde axonal transport of Lysotracker™ in primary wild type and SOD1^{G93A} motor neurons

(A) Anterograde speed profiles of Lysotracker™-labelled carriers in wild type motor neuron cultures treated with DMSO (black squares) or 0.5 µM E4 (green triangles) (DMSO: 44 carriers, 12 axons; E4: 14 carriers, 6 axons; 3 independent experiments). (B) Anterograde speed profiles of Lysotracker™-labelled carriers in wild type (black squares), SOD1^{G93A} (red diamonds) and SOD1^{G93A} + 0.5 µM E4 (green triangles) motor neuron cultures (wild type: 44 carriers, 12 axons; SOD1^{G93A}: 45 carriers, 15 axons; SOD1^{G93A} + 0.5 µM E4: 12 carriers, 5 axons; 3 independent experiments).

Firstly, we analysed the effect of compound E4 on the retrograde axonal transport of H_CT-labelled vesicles in wild type adult DRG cultures. Treatment with 0.5 µM E4 was found to have no effect on axonal transport speeds ($p = 0.777$; Figure 5.14). Next, we tested the effect of compound E4 on retrograde axonal transport in wild type hippocampal neurons. These experiments were performed during a visit to the laboratory of Bianxiao Cui (Stanford University, USA). Hippocampal neurons were plated in microfluidic chambers, allowing fluidic isolation of the axon terminals from the cell body. In this way, quantum dot-labelled WGA (QD-WGA) could be applied selectively to the axon compartment and its retrograde axonal transport imaged using fluorescence microscopy (as illustrated in Movie 2). WGA binds to sialic acid and N-acetylglucosaminyl residues and therefore labels all membranous compartments. Kymographs were generated from time-lapse images in order to analyse the speed of retrograde axonal transport (Figure 5.15A). Incubation with

0.5 µM E4 was found to cause a small shift to faster axonal transport speeds (p = 0.062; Figure 5.15B).

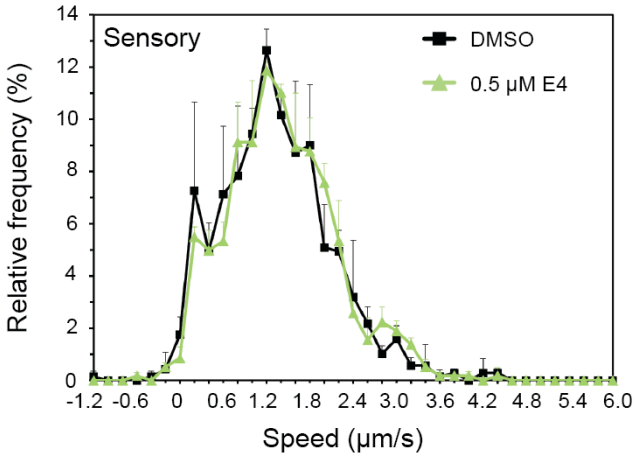

Figure 5.14. IGF1R inhibitor compound E4 has no effect on retrograde axonal transport in wild type sensory neurons

Speed profiles of H_CT carriers in wild type DRG cultures treated with either DMSO (black squares) or 0.5 µM E4 (green triangles). E4 has no effect on axonal transport speeds (DMSO: 39 carriers, 6 axons; E4 treated: 35 carriers, 12 axons; 3 independent experiments).

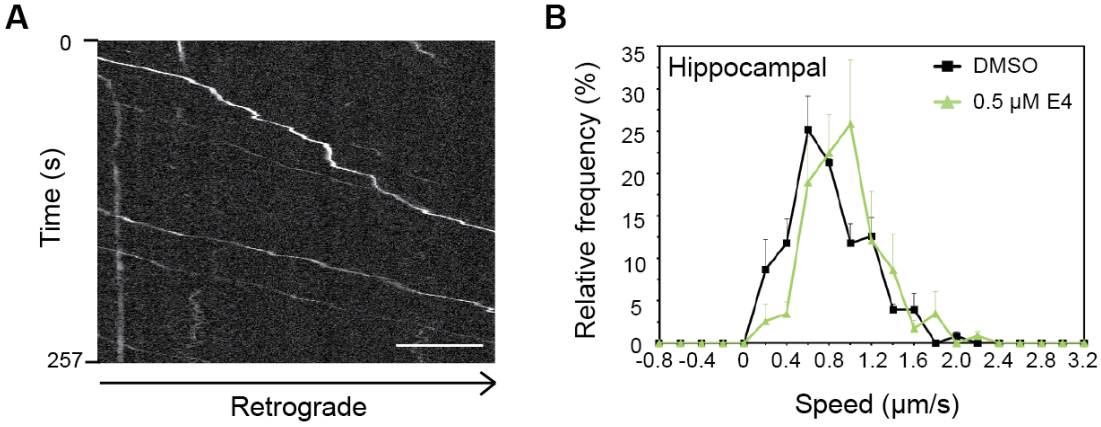

Figure 5.15. IGF1R inhibitor compound E4 accelerates retrograde axonal transport in hippocampal neurons

The effect of 0.5 µM E4 on the retrograde axonal transport of QD-WGA was analysed in hippocampal neurons. (A) Kymographs were generated from time-lapse series in order to calculate the speed of individual cargoes. Scale bar, 15 µm. (B) Speed profiles of WGA-labelled carriers in hippocampal cultures treated with either DMSO (black squares) or 0.5 µM E4 (green triangles). DMSO: 127 carriers; PPP treated: 116 carriers; 3 independent experiments.

5.4. Determining the effect of IGF1R inhibitors on retrograde axonal transport *in vivo*

Finally, we wanted to investigate the effect of IGF1R inhibitors on retrograde axonal transport in motor neurons *in vivo.* Unfortunately, neither of the inhibitors tested previously (E4 and 2-B3) were suitable to be used *in vivo.* We therefore had to identify a BBB permeable, *in vivo* tolerable IGF1R inhibitor that could be tested in our *in vivo* axonal transport assays.

5.4.1. Picropodophyllotoxin accelerates retrograde axonal transport *in vitro*

Picropodophyllotoxin (PPP) (shown in Figure 5.16) is a non-ATP competitive antagonist of IGF1R. It inhibits IGF1R auto-phosphorylation (IC_{50} ~ 1 nM), but does not inhibit the insulin receptor or other related growth factor receptors, such as epidermal growth factor receptor (Girnita et al., 2004). PPP has been previously demonstrated to be suitable for *in vivo* use and has been shown to cross the BBB (Yin et al., 2010).

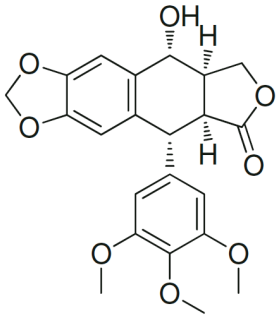

Figure 5.16. The chemical structure of the IGF1R inhibitor picropodophyllotoxin (PPP)

Firstly, we confirmed that treatment with 0.5 μM PPP was able to inhibit IGF1R activity in primary motor neuron cultures. Western blot analysis revealed that incubation of wild type motor neurons with PPP caused a substantial reduction in the levels of phosphorylated IGF1R, similar to that seen with compounds E4 and 2-B3 (Figure 5.17).

Next, we investigated whether PPP could also accelerate retrograde axonal transport *in vitro.* As with compounds E4 and 2-B3, incubation of wild type primary motor neurons with 0.5 µM PPP was found to accelerate the axonal transport of H_CT-labelled vesicles (p = 0.083; Figure 5.18).

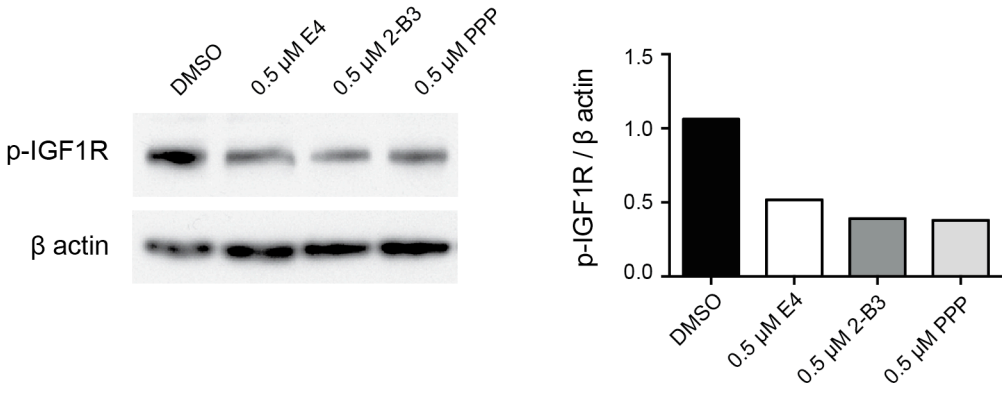

Figure 5.17. Picropodophyllotoxin (PPP) inhibits IGF1R activity in primary motor neurons
Western blot showing the effect of IGF1R inhibitors E4, 2-B3 and PPP on IGF1R activity in primary wild type motor neurons. Incubation of motor neurons with 0.5 µM PPP inhibits the IGF1R to a similar extent as E4 and 2-B3. n = 1.

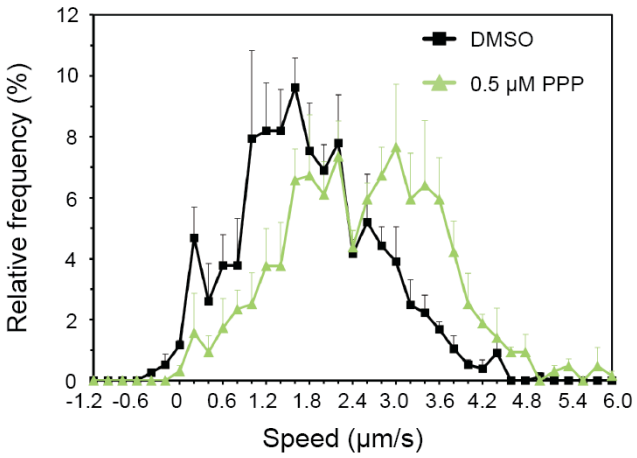

Figure 5.18. Treatment of primary motor neurons with 0.5 µM picropodophyllotoxin (PPP) accelerates retrograde axonal transport
Speed profiles of H_CT carriers in motor neuron cultures treated with either DMSO (black squares) or 0.5 µM PPP (green triangles). PPP causes a shift to faster transport speeds (DMSO: 84 carriers, 9 axons; PPP treated: 76 carriers, 10 axons; 3 independent experiments).

5.4.2. Investigating the effect of picropodophyllotoxin on retrograde axonal transport *in vivo*

As PPP has been previously tested *in vivo* and shown to cross the BBB (Yin et al., 2010), we could investigate the effect of PPP in our *in vivo* axonal transport assay (described in Section 4.4.1). We decided to test the effect of PPP in early symptomatic SOD1^{G93A} mice, as the ultimate aim of the project was to determine the role of retrograde axonal transport defects in ALS pathogenesis. In previous studies, PPP was shown to inhibit IGF1R signalling when administered i.p. at 20 mg/kg in rats, with no side effects reported. However, when this dose was tested in early symptomatic SOD1^{G93A} mice, it caused severe adverse effects. Lowering the dose to 10 or 5 mg/kg reduced these adverse effects, allowing axonal transport to be assessed *in vivo* in treated mice. As described in Section 4.4.2, the compound was administered i.p. at the same time as the H_CT fragment was injected i.m., and retrograde axonal transport was imaged in the sciatic nerve four hours later. Preliminary data collected from two mice treated with 5 mg/kg PPP and one mouse treated with 10 mg/kg PPP indicates that PPP is able to accelerate retrograde axonal transport in early symptomatic SOD1^{G93A} mice, restoring axonal transport to almost wild type speeds (WT versus SOD1^{G93A} + PPP: p = 0.859, SOD1^{G93A} versus SOD1^{G93A} + PPP: p = 0.0579; Figure 5.19). This work was performed with help from James Sleigh (Institute of Neurology, UCL).

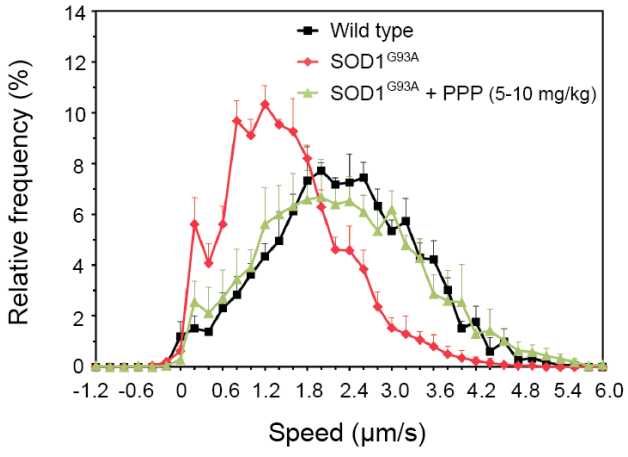

Figure 5.19. PPP accelerates retrograde axonal transport *in vivo* in the SOD1^{G93A} mouse
Retrograde axonal transport in single axons of the sciatic nerve was assessed in 73 d wild type (black squares), SOD1^{G93A} (red diamonds) and SOD1^{G93A} mice treated with PPP (green triangles). 5 mg/kg PPP (2 mice) and 10 mg/kg PPP (1 mouse) were found to have the same effect on retrograde axonal transport, therefore the data from all 3 treated mice were pooled. Wild type: 161 carriers, n (animals) = 4; SOD1^{G93A}: 185 carriers, n = 5; SOD1^{G93A} + PPP (5-10 mg/kg): 201 carriers, n = 3.

5.5. Discussion

The aim of this Chapter was to investigate the effects of compound E4 on axonal transport in more detail and to determine whether inhibition of IGF1R was responsible for the acceleration of retrograde axonal transport caused by this compound.

In this Chapter, I was able to demonstrate that compound E4 accelerates the *in vitro* retrograde axonal transport of H_CT, α-$p75^{NTR}$ and Lysotracker™ in primary motor neurons and WGA in hippocampal neurons. However, compound E4 had no effect on the retrograde axonal transport of H_CT in sensory neurons, nor any effect on the anterograde axonal transport of Lysotracker™ in motor neurons. These results suggest that the regulatory mechanisms governing axonal transport are highly specific for different neuronal types, transport directions and cargoes, and that these mechanisms can be exploited pharmacologically. This is particularly relevant for diseases such as ALS, where defects in retrograde axonal transport are found in motor neurons, and not sensory neurons for example, and it would therefore be advantageous to modify axonal transport only in affected neuronal types. This conclusion also indicates that more work must be done to investigate the effects of compound E4 and our other active inhibitors (compound 2-B3 and PPP) on axonal transport in different neuronal types. This will allow us to determine whether these compounds could be utilised in other neurodegenerative diseases in which axonal transport defects have been implicated as a pathogenic mechanism.

In order to establish whether IGF1R was the target kinase of compound E4, additional structurally diverse IGF1R inhibitors were screened using the accumulation assay (described in Chapter 3) and hit compounds were tested in *in vitro* axonal transport assays in primary motor neurons in this Chapter. The effects of the hit compounds on retrograde axonal transport were varied. Compound 2-C1 had little effect on retrograde axonal transport speeds, while compound 2-G2 caused an enhancement of H_CT axonal transport only, with no effect on α-$p75^{NTR}$ transport. Compound 2-B3, on the other hand, mimicked the effects of compound E4, accelerating the retrograde axonal transport of both probes. There are a number of possible explanations for the variable effects of the IGF1R inhibitors

tested. It could be that the compounds have differential effects on the kinase cascades downstream of IGF1R, such that different compounds cause preferential inhibition of different signalling cascades. Although pathway-selective antagonism of IGF1R has not been previously reported, I did observe that compounds E4 and 2-B3 appeared to preferentially inhibit Akt over other kinases that are downstream of IGF1R. Additional signalling experiments, testing the effects of both axonal transport active and inactive compounds, would help elucidate whether there is a correlation between axonal transport activity and downstream kinase inhibition that would explain the results reported in this Chapter. Another possible explanation is that our active compounds, E4 and 2-B3, may not only inhibit IGF1R, but could also share additional target(s) that are critical for their effect on axonal transport. Given that picropodophyllotoxin (PPP), a published IGF1R inhibitor, also has the same effect as E4 and 2-B3, it is likely that inhibition of IGF1R does play a role in the enhancement of axonal transport, but it may not fully explain the results seen. This is supported by the fact that knocking down IGF1R had no effect on retrograde axonal transport in primary motor neuron cultures. The involvement of additional targets would also explain why some of our IGF1R inhibitors did not affect retrograde axonal transport in the same way as E4, 2-B3 and PPP. A detailed analysis of the structures of our active compounds plus a comparison of their known targets other than IGF1R could help elucidate whether these compounds share additional target(s) that may underlie their enhancing effects on retrograde axonal transport. It is also possible that compounds 2-C1 and 2-G2 have reduced plasma membrane permeability or lower efficacy than compounds E4 and 2-B3, and this may underlie their reduced effects on axonal transport.

Although compound 2-G2 did not mimic the effects of compound E4 in *in vitro* axonal transport assays and was therefore not investigated further, it could in fact be an interesting compound to study in the future. Our experiments demonstrated that compound 2-G2 was able to accelerate H_CT axonal transport but had little effect on α-$p75^{NTR}$. These results support the idea that the intracellular sorting and trafficking of these two cargoes may be differentially regulated and further study of compound 2-G2 and its mechanism of action could help elucidate the signalling machinery involved.

Moving on to consider the IGF1R knockdown experiments performed in this Chapter, it is possible that a technical problem may have been responsible for the lack of effect of our lentiviral shRNA vectors on retrograde axonal transport. It is possible that the knockdown of IGF1R we observed in our primary motor neuron cultures by western blot was mostly a result of reduced IGF1R protein levels in glial cells, and not in the motor neurons themselves. If the acceleration of axonal transport caused by our active compounds is a result of IGF1R inhibition in motor neurons (i.e. our IGF1R inhibitors act cell autonomously), then this would explain the lack of effect of our IGF1R shRNA in axonal transport assays. Unfortunately we were unable to find an IGF1R antibody that worked in immunofluorescence, so we could not determine whether IGF1R was knocked down in motor neurons. In addition to identifying a better antibody, this problem could also be addressed by designing lentiviral vectors with neuron-specific promoters. Alternatively, our IGF1R shRNA lentivirus preparation may have been contaminated in some way, which obscured any effect of IGF1R knockdown on axonal transport. Finally, the discrepancy between the results could be due to the fact that pharmacological inhibition of IGF1R was always performed acutely (25 min for *in vitro* axonal transport assays), whilst the IGF1R shRNA was applied on the day of plating (DIV0) and transport assays were performed on DIV7. It is therefore possible that motor neurons are able to adapt to long-term reductions in IGF1R signalling. Further work is clearly required to optimise the knockdown experiments and confirm whether IGF1R is in fact the target responsible for the acceleration of retrograde axonal transport caused by our active compounds.

5.5.1. Possible links between IGF1R and retrograde axonal transport

To date, there have been few connections made between IGF1R signalling and the regulation of axonal transport. In this Chapter, we investigated the effect of our axonal transport-active IGF1R inhibitors (compounds E4 and 2-B3) on the downstream targets of IGF1R (Figure 5.2 and Figure 5.7). We found that compounds E4 and 2-B3 had little effect on the downstream kinases ERK1/2 and p38 MAPK, suggesting that the compounds do not accelerate axonal transport through inhibition of these kinases. ERK1/2 has in fact been shown to phosphorylate the intermediate chains of cytoplasmic dynein leading to enhanced

binding of dynein to the signalling endosome in cortical neurons (Mitchell et al., 2012). Therefore inhibition of ERK1/2 would be expected to inhibit retrograde axonal transport, not accelerate it. We have also demonstrated in Chapter 3 that inhibition of p38 MAPK has no effect on axonal transport in wild type motor neurons, therefore we would not expect IGF1R to be acting through this kinase. Furthermore, JNK, another kinase downstream of IGF1R that was not investigated in this Chapter, has been previously shown to have no effect on anterograde or retrograde axonal transport velocities in rodent hippocampal and DRG neurons (Stagi et al., 2006, Fu and Holzbaur, 2013). Of course, the regulatory mechanisms governing axonal transport may be neuron-specific, so it will be necessary to test the effects of inhibiting ERK1/2 and JNK in motor neurons to truly determine whether or not they play a role in the acceleration of axonal transport caused by our active compounds.

Compounds E4 and 2-B3 both caused a detectable reduction in Akt phosphorylation. As discussed earlier, htt has been proposed to act as a molecular switch between anterograde and retrograde axonal transport, and this “switch” activity is directly regulated by Akt (Colin et al., 2008). The authors demonstrated that if Akt-mediated phosphorylation of htt is prevented, the retrograde axonal transport of BDNF is accelerated in cortical neurons. Conversely, transfection of neurons with a phospho-mimic form of htt led to accelerated anterograde axonal transport. Stimulation of cortical neurons with 50 ng/ml IGF1 was shown to induce phosphorylation of htt and lead to an acceleration of anterograde axonal transport. However, in contrast to our results in motor neurons (where IGF1 was observed to inhibit H_CT axonal transport), stimulation of cortical neurons with IGF1 had no effect on retrograde axonal transport speeds. The authors proposed that when htt is dephosphorylated, kinesin-1 is detached from the microtubules and vesicles. Activation of IGF1R leads to phosphorylation of htt and increased association of kinesin with microtubules and vesicles. Based on the “tug of war” theory of axonal transport, which proposes that the direction of cargo movement is determined by which pool of molecular motors successfully ‘outcompetes’ its counterpart for binding to the microtubule network (Welte, 2004, Gross, 2004), inhibition of IGF1R signalling should lead to enhanced binding of dynein to microtubules and therefore increased retrograde axonal transport. It would be interesting to test inhibitors of

Akt in our *in vitro* axonal transport assays in motor neurons to see if they mimic the effects of our active IGF1R inhibitors.

It is worth noting that insulin has been described to positively regulate axonal transport through activation of Akt (Takach et al., 2015). The authors of this study proposed that, in response to insulin stimulation, Akt inhibits GSK3β, which has been shown to be a negative regulator of both anterograde and retrograde axonal transport (Weaver et al., 2013, Chen et al., 2007a, Morfini et al., 2002). These results indicate that the insulin and IGF1R signalling pathways may have distinct roles in the regulation of axonal transport.

An alternate hypothesis to explain the ability of our IGF1R inhibitors to accelerate retrograde axonal transport comes from work performed in *C. elegans. C. elegans* have a single insulin/IGF receptor, DAF-2. RNAi-mediated knockdown of DAF-2 results in long-lived, stress-resistant worms (Kenyon, 2005). Ewald et al. demonstrated that reduced insulin/IGF signalling leads to increased expression of collagens and other extracellular matrix (ECM) genes (Ewald et al., 2015). The authors proposed that ECM remodelling plays a key role in increasing longevity in DAF-2 knockdown worms. The ECM has been shown to sequester growth factors, storing them in the vicinity of cells and protecting them from degradation (Schultz and Wysocki, 2009). ECM remodelling in response to reduced IGF signalling in neurons could therefore lead to the local release of growth factors and stimulation of retrograde axonal transport. Such a mechanism could explain how our IGF1R inhibitors accelerate retrograde axonal transport. It would be interesting to investigate whether our active inhibitors stimulate ECM remodelling. Given it has been recently shown that the ECM component nidogen is internalised together with H_CT in motor neurons (Bercsenyi et al., 2014), we could test whether our IGF1R inhibitors enhance the neuronal uptake of such ECM components.

5.5.2. IGF1R and ALS

It is important to acknowledge that stimulation of IGF1R signalling has been proposed to be beneficial in ALS. Firstly, experiments in $SOD1^{G93A}$ mice indicated that increased IGF1 was neuroprotective and could improve survival (Kaspar et al.,

2003). The group demonstrated that adeno-associated virus (AAV)-mediated delivery of IGF1 could protect motor neurons and extend survival, when the virus was injected into the quadriceps muscle of symptomatic $SOD1^{G93A}$ mice. Delivery of AAV-IGF1 vectors to the deep cerebellar nuclei (DCN) has also been shown to have the same effects (Dodge et al., 2008). In fact, the delivery of a number of growth factors has been shown to be beneficial in ALS mouse models, including GDNF (Acsadi et al., 2002), VEGF (Azzouz et al., 2004) and CNTF (Sendtner et al., 1992, Mitsumoto et al., 1994). It is therefore possible that the beneficial effects of increasing growth factor levels are not due to the fact that they are targeting a disease-specific pathology, but rather that growth factors act to boost motor neuron health and survival under disease conditions, due to their role in maintaining neuronal function and protecting against toxic insults.

However, clinical trials with growth factors have been disappointing. Three clinical trials have been published testing the effect of subcutaneously administered IGF1 in ALS patients. These trials reported few (Lai et al., 1997) or no beneficial effects (Borasio et al., 1998, Sorenson et al., 2008). In addition, the administration of growth hormone (which stimulates IGF1 production) has been tested in ALS patients and did not produce any benefit compared to patients that received placebo (Saccà et al., 2012). A similar lack of beneficial effects has also been seen for CNTF (ALS CNTF Treatment Study Group, 1996) and BDNF (The BDNF Study Group, 1999). These results may reflect the limitations of using proteins as therapeutics, such as their limited bioavailability, poor CNS penetration and short half-lives. Alternatively, they may be the result of poor trial design, inadequate dosing and/or poor translation of results from animal models.

5.5.3. Inhibiting IGF1R as a potential therapeutic strategy

Although more work is required to determine the mechanism of action of our active compounds, a key result in this Chapter was the demonstration that the IGF1R inhibitor PPP accelerates retrograde axonal transport in the mouse sciatic nerve *in vivo.* If retrograde axonal transport is shown to play a key role in motor neuron degeneration, PPP or similar compounds may have potential as therapeutic approaches for ALS.

Our *in vitro* assays indicate that, at the concentration required to accelerate retrograde axonal transport (0.5 μm), our active IGF1R inhibitors are not toxic to primary motor neurons. However, we did observe substantial toxicity of compound E4 at 2 μM, suggesting that careful dosing is required if the beneficial effects of IGF1R inhibitors are to be seen. In addition, when we tested the BBB-permeable IGF1R inhibitor PPP *in vivo*, it was found to cause a number of adverse effects in $SOD1^{G93A}$ mice. Adverse effects of PPP have not been previously reported in rodents with either i.p. or oral dosing (Yin et al., 2010, Economou et al., 2008). It is possible that our results may reflect a problem with the particular formulation of the compound we used or an interaction with the $SOD1^{G93A}$ pathology. Testing our batch of PPP in wild type mice will help determine where the problem lies. PPP has in fact reached clinical trials for the treatment of a number of different types of cancer (https://www.clinicaltrials.gov/ct2/results?term=axl1717) but was associated with an increased risk of neutropenic episodes, some of which developed into serious events and were fatal (Bergqvist et al., 2013).

Reduced IGF1R signalling has been previously shown to have beneficial effects on longevity (Cohen, 2011). Mice with reduced IGF1R signalling ($IGF1R^{+/-}$) have been shown to live 26% longer than control mice (Holzenberger et al., 2003). Furthermore, in humans, mutations in IGF1R that lead to reduced activity of the receptor have been associated with extreme longevity (Suh et al., 2008). Full knockout of IGF1R, however, causes neonatal lethality and dwarfism in mice (Liu et al., 1993). It has been proposed that the increased longevity of $IGF1R^{+/-}$ mice is a result of their improved resistance to oxidative stress (Holzenberger et al., 2003) and increased protection from proteotoxicity (El-Ami et al., 2014).

The effects of reduced IGF1R signalling have also been investigated in relation to neurodegeneration. Crossing $IGF1R^{+/-}$ mice with an Alzheimer's disease (AD) mouse model (APP_{Swe}/Presenillin1ΔE9) led to an improvement in behavioural deficits in these mice. This was associated with reduced neuronal loss and reduced inflammatory signalling (fewer activated astrocytes) (Cohen et al., 2009). Furthermore, hippocampus-specific knockout of IGF1R ($hIGF1R^{-/-}$) in another model of Alzheimer's disease, Tg2576, has been shown to rescue these mice from the premature death associated with this model (Freude et al., 2009). However the

authors did not look at the effect of hIGF1R$^{-/-}$ on neuronal survival or behavioural deficits in these mice. Both groups proposed that reduced IGF1R signalling protected AD mice from Aβ toxicity, either by causing the formation of dense Aβ aggregates of lower toxicity (Cohen et al., 2009) or by reducing APP processing and therefore Aβ production (Freude et al., 2009).

Unfortunately, the survival data for hIGF1R$^{-/-}$ mice was only collected until 60 weeks of age, at which point survival of hIGF1R$^{-/-}$ mice was the same as controls. It would have been interesting to see whether the hIGF1R$^{-/-}$ mice live longer than controls, as is seen for IGF1R$^{+/-}$ mice (Holzenberger et al., 2003), as this would allow us to begin to understand how IGF1R signalling in different neuronal types may contribute to the regulation of lifespan.

In all of the above studies, IGF1R signalling was reduced presymptomatically and therefore the results may not be clinically relevant when considering developing a new therapeutic approach for neurodegenerative diseases. There is, however, evidence to suggest that reducing IGF1R signalling after symptom onset may still be beneficial. *C.elegans* expressing Aβ in their body wall muscles develop progressive paralysis due to the formation of toxic Aβ aggregates. Cohen et al. demonstrated that RNAi-mediated knockdown of DAF-2 could protect *C.elegans* from Aβ-mediated toxicity, even when RNAi treatment was initiated later in life (Cohen et al., 2010).

These studies suggest that reduced IGF1R signalling is neuroprotective and could be beneficial in neurodegenerative diseases associated with proteotoxicity. This neuroprotective effect has been explained by the fact that IGF1R signalling inhibition leads to enhanced resistance to oxidative stress (Holzenberger et al., 2003), enhanced DNA repair (Cohen et al., 2009) and protection from proteotoxicity (Cohen et al., 2009, Cohen et al., 2006). IGF1 signalling has also been described to inhibit regeneration of aging adult motor neurons in *C.elegans* (Byrne et al., 2014). It therefore appears that reduced IGF1R signalling could have a number of beneficial effects that are relevant to ALS and other neurodegenerative diseases.

Furthermore, reduced activity of downstream components of the IGF1R cascade has been previously shown to improve the survival of primary motor neurons transduced with mutant SOD1 *in vitro.* In mammals, activation of the IGF1R/PI3K/Akt cascade leads to phosphorylation of the transcription factor FOXO3a. FOXO3a controls the expression of genes that help the cell to cope with stress and promote longevity. Phosphorylation of FOXO3a leads to its translocation out of the nucleus (Birkenkamp and Coffer, 2003). Expression of HSV-TM-FOXO3a, which cannot be phosphorylated and therefore remains constitutively in the nucleus, was shown to restore the survival of primary motor neurons transduced with HSV-SOD1^{G85R} to wild type levels (Mojsilovic-Petrovic et al., 2009). In addition, the group were able to demonstrate that an inhibitor of FOXO3a nuclear export, Psammaplysene A, could also restore the survival of these motor neurons. This highlights an additional mechanism by which IGF1R inhibition could be beneficial in ALS. It will be interesting to test whether our axonal transport-active IGF1R inhibitors affect the phosphorylation state and cellular localisation of FOXO3a, and whether they are able to improve the survival of SOD1^{G93A} motor neurons both *in vitro* and *in vivo*.

Due to the interest in inhibiting IGF1R signalling for the treatment of cancer, a number of different targeting strategies have already been developed. These include antibodies against both IGF1 and IGF1R, IGF1R kinase inhibitors and also inhibitors of downstream kinases (Pollak, 2008). A number of IGF1R monoclonal antibodies and kinase inhibitors are currently in clinical development for various types of cancer. A disadvantage of the pharmacological inhibitors currently being investigated is the lack of specificity for IGF1R over the insulin receptor. Inhibition of the insulin receptor increases the risk of adverse events, particularly the risk of hyperglycaemia. PPP is the only BBB permeable IGF1R inhibitor in clinical development at the moment, so there is clearly a need to develop additional selective inhibitors suitable for use in CNS disorders. Of course, the usefulness of IGF1R inhibitors in ALS still needs to be determined. However, if we are to investigate the effect of IGF1R inhibition on disease progression in the SOD1^{G93A} mouse, we will need to identify an IGF1R targeting strategy that is able to cross the BBB and does not cause the adverse effects we have observed with PPP.

Chapter 6. Conclusions and future perspectives

The aim of the work presented in this Thesis was to develop and perform a screen to identify enhancers of retrograde axonal transport in motor neurons and validate the effects of hit compounds on axonal transport both *in vitro* and *in vivo*.

I was able to demonstrate that the accumulation of H_CT and α-$p75^{NTR}$ in the cell body of mouse ES-derived motor neurons is sensitive to changes in retrograde axonal transport efficiency and could therefore be used as a read-out in screening assays to identify novel pharmacological enhancers of retrograde axonal transport. This accumulation assay was successfully used to identify two novel enhancers of retrograde axonal transport (compounds A1 and E4) from a small library of kinase inhibitors.

Compound A1 was found to correct $SOD1^{G93A}$-induced deficits in retrograde axonal transport in primary motor neurons, whilst having no effect on axonal transport speeds in wild type motor neurons. Compound A1 was revealed to be an inhibitor of p38 MAPK. Additional, structurally diverse, inhibitors of p38 MAPK were also found to correct deficits in retrograde axonal transport in $SOD1^{G93A}$ motor neurons, indicating that p38 MAPK was the kinase responsible for transport defects. In agreement with this, p38 MAPK was found to be activated in both embryonic $SOD1^{G93A}$ motor neurons and in the spinal cord of adult $SOD1^{G93A}$ mice. Levels of phospho-p38 MAPK were found to be highest at an early symptomatic stage – the age at which *in vivo* axonal transport defects are most severe. Lentiviral-mediated knockdown experiments in primary motor neurons revealed that p38 MAPKα was responsible for $SOD1^{G93A}$-induced deficits in retrograde axonal transport. This was also confirmed using a pharmacological approach. SB-239063, a p38 MAPKα/β specific inhibitor, was shown to correct defects in retrograde axonal transport *in vitro* in $SOD1^{G93A}$ motor neurons. Furthermore, we were able to demonstrate that SB-239063 could correct defects in retrograde axonal transport in early symptomatic $SOD1^{G93A}$ mice. Plans are now in action to determine the effect of SB-239063 on disease progression in the $SOD1^{G93A}$ mouse model.

In contrast to compound A1, compound E4 was found to accelerate retrograde axonal transport *in vitro* in both wild type and $SOD1^{G93A}$ motor neurons. The compound was revealed to be an inhibitor of IGF1R. Compound E4 was observed to have both direction- and neuron-specific effects on axonal transport. The compound was shown to accelerate the retrograde axonal transport of signalling endosomes and acidic organelles (late endosomes/lysosomes and autophagosomes) in motor and hippocampal neurons. However, it had no effect on the anterograde axonal transport of acidic organelles in motor neurons, nor any effect on the retrograde axonal transport of signalling endosomes in sensory neurons. We were able to identify additional IGF1R inhibitors that mimicked the effects of compound E4 (2-B3 and PPP). However, lentiviral-mediated knockdown of IGF1R had no effect on retrograde axonal transport speeds in motor neurons *in vitro*. It is therefore still unclear whether IGF1R is the kinase responsible for the effects of our active compounds. PPP, one of our IGF1R inhibitors that enhanced retrograde axonal transport *in vitro,* was suitable to be tested *in vivo* and was found to accelerate the axonal transport of H_CT in the sciatic nerve of early symptomatic $SOD1^{G93A}$ mice. Future work must focus on determining the target(s) and mechanism of action of the axonal transport-active IGF1R inhibitors and identifying a compound suitable to be used in efficacy studies in mice.

6.1. Future work

The accumulation assay has proved successful in identifying novel modulators of retrograde axonal transport from a small library of compounds. The next step will therefore be to extend our pilot studies and screen larger compound libraries, looking for both enhancers and inhibitors of retrograde axonal transport. Since our pilot studies were carried out in wild type ES-derived motor neurons only, it will be interesting to perform the assay in both mouse ES-derived motor neurons expressing ALS-associated mutations and ALS patient iPSC-derived motor neurons (as described in Section 3.6.3), in order to generate more disease-relevant hits. However, preliminary work is required to determine whether ALS-associated ES- and iPSC-derived motor neurons display defects in retrograde axonal transport. In addition, the accumulation assay could also be used in other neuronal types,

such as cortical, sensory or hippocampal neurons, in order to identify modifiers of retrograde axonal transport relevant to other neurodegenerative diseases.

One of the key results of this work was the discovery that the p38 MAPKα/β inhibitor SB-239063 is able to correct retrograde axonal transport defects *in vivo* in the $SOD1^{G93A}$ mouse, without causing overt adverse effects. This compound therefore has the potential to determine conclusively whether axonal transport defects play a key role in ALS pathogenesis. Plans are already in motion to perform a full efficacy study, testing the effect of SB-239063 on motor function, lifespan, muscle physiology and motor neuron survival when administered from an early symptomatic age. It would also be interesting to test this compound in other mouse models of ALS that display retrograde axonal transport defects, in order to determine whether pathological p38 MAPK activation and subsequent transport inhibition are unique to $SOD1^{G93A}$-mediated ALS or a common pathological hallmark of the disease. In addition, given that ALS is thought to result from the interaction of multiple different pathological mechanisms, we could administer SB-239063 in combination with other disease-modifying agents, such as riluzole or dexpramipexole, to determine whether multi-target therapy has a synergistic effect on ALS disease progression.

Given that approximately 15% of ALS patients display clinical symptoms of frontotemporal dementia (FTD), it will also be interesting to investigate the role of axonal transport defects and p38 MAPK in FTD. Axonal transport deficits have been reported in experimental models of FTD with parkinsonism-17 (FTDP-17). Mice expressing FTDP-17 associated P301L mutant tau were found to have significant impairments in axonal transport in olfactory neurons before cognitive dysfunction was first observed (Majid et al., 2014). In addition, knocking down components of the dynein/dynactin complex was found to exacerbate tau pathology and locomotor deficits in a *Drosophila* model overexpressing FTDP-17 associated R406W tau, indicating that retrograde axonal transport defects contribute to the pathology (Butzlaff et al., 2015). Given that hexanucleotide repeat expansions in C9orf72 are the major cause of both fALS and FTD and that C9orf72 has been implicated in the regulation of membrane trafficking (Farg et al., 2014), it will be interesting to see whether animal and cell culture models expressing expanded

C9orf72 display defects in axonal transport. Testing SB-239063 in FTD models will allow us to investigate whether p38 MAPK-induced axonal transport defects are a common pathogenic mechanism of ALS and FTD.

Our p38 MAPK and IGF1R inhibitors could also potentially be used to determine the role of axonal transport defects in the pathogenesis of other neurodegenerative diseases, such as Huntington's disease (Her and Goldstein, 2008) and Alzheimer's disease (Smith et al., 2007). p38 MAPK has in fact already been implicated in the axonal transport defects found in Alzheimer's disease (AD). Treatment with oligomeric Aβ has been shown to induce defects in mitochondrial axonal transport in cultured hippocampal neurons through activation of p38 MAPKα/β (Guo et al., 2013). In addition, an isoform-selective inhibitor of p38 MAPKα has recently been demonstrated to attenuate declines in cognitive performance in two mouse models of AD (Roy et al., 2015), indicating that p38 MAPK-induced defects in axonal transport may play a key role in AD pathogenesis. Furthermore, it will also be interesting to explore whether our active IGF1R inhibitors (E4, 2-B3 and PPP) have the potential to correct axonal transport deficits in other neurodegenerative diseases. Compound E4 has already been shown to accelerate retrograde axonal transport in motor and hippocampal neurons, but not sensory neurons. It will be interesting to see if our active IGF1R inhibitors accelerate axonal transport in additional neuronal types, for example striatal neurons, in order to determine the full spectrum of neurodegenerative diseases in which they may be useful.

6.2. Concluding remarks

It is clear that ALS is a complex disease, likely resulting from the interaction of multiple different pathological mechanisms. The role of axonal transport defects in neurodegeneration is a subject of much controversy in the field. The pharmacological enhancers of retrograde axonal transport identified in this thesis will allow us to determine conclusively whether defects in axonal transport play a key role in ALS pathogenesis. However, even if restoring axonal transport does prove beneficial, the future of ALS therapy likely lies in a multi-target approach. Future work must focus on dissecting out the key pathological mechanisms

responsible for motor neuron degeneration in ALS and determining which combination of therapeutic approaches has the largest impact on disease progression.

Reference List

ACKERLEY, S., GRIERSON, A. J., BANNER, S., PERKINTON, M. S., BROWNLEES, J., BYERS, H. L., WARD, M., THORNHILL, P., HUSSAIN, K., WABY, J. S., ANDERTON, B. H., COOPER, J. D., DINGWALL, C., LEIGH, P. N., SHAW, C. E. & MILLER, C. C. 2004. p38alpha stress-activated protein kinase phosphorylates neurofilaments and is associated with neurofilament pathology in amyotrophic lateral sclerosis. *Mol Cell Neurosci,* 26**,** 354-64.

ACSADI, G., ANGUELOV, R. A., YANG, H., TOTH, G., THOMAS, R., JANI, A., WANG, Y., IANAKOVA, E., MOHAMMAD, S., LEWIS, R. A. & SHY, M. E. 2002. Increased survival and function of SOD1 mice after glial cell-derived neurotrophic factor gene therapy. *Hum Gene Ther,* 13**,** 1047-59.

AL-CHALABI, A., ANDERSEN, P. M., NILSSON, P., CHIOZA, B., ANDERSSON, J. L., RUSS, C., SHAW, C. E., POWELL, J. F. & LEIGH, P. N. 1999. Deletions of the heavy neurofilament subunit tail in amyotrophic lateral sclerosis. *Hum Mol Genet,* 8**,** 157-64.

ALAMI, N. H., SMITH, R. B., CARRASCO, M. A., WILLIAMS, L. A., WINBORN, C. S., HAN, S. S., KISKINIS, E., WINBORN, B., FREIBAUM, B. D., KANAGARAJ, A., CLARE, A. J., BADDERS, N. M., BILICAN, B., CHAUM, E., CHANDRAN, S., SHAW, C. E., EGGAN, K. C., MANIATIS, T. & TAYLOR, J. P. 2014. Axonal transport of TDP-43 mRNA granules is impaired by ALS-causing mutations. *Neuron,* 81**,** 536-43.

ALAVIAN, K. N., DWORETZKY, S. I., BONANNI, L., ZHANG, P., SACCHETTI, S., MARIGGIO, M. A., ONOFRJ, M., THOMAS, A., LI, H., MANGOLD, J. E., SIGNORE, A. P., DEMARCO, U., DEMADY, D. R., NABILI, P., LAZROVE, E., SMITH, P. J., GRIBKOFF, V. K. & JONAS, E. A. 2012. Effects of dexpramipexole on brain mitochondrial conductances and cellular bioenergetic efficiency. *Brain Res,* 1446**,** 1-11.

ALBERINI, C. M. & CHEN, D. Y. 2012. Memory enhancement: consolidation, reconsolidation and insulin-like growth factor 2. *Trends Neurosci,* 35**,** 274-83.

ANDERSEN, P. M., SIMS, K. B., XIN, W. W., KIELY, R., O'NEILL, G., RAVITS, J., PIORO, E., HARATI, Y., BROWER, R. D., LEVINE, J. S., HEINICKE, H. U., SELTZER, W., BOSS, M. & BROWN, R. H., JR. 2003. Sixteen novel mutations in the Cu/Zn superoxide dismutase gene in amyotrophic lateral sclerosis: a decade of discoveries, defects and disputes. *Amyotroph Lateral Scler Other Motor Neuron Disord,* 4**,** 62-73.

ARBER, S., HAN, B., MENDELSOHN, M., SMITH, M., JESSELL, T. M. & SOCKANATHAN, S. 1999. Requirement for the homeobox gene Hb9 in the consolidation of motor neuron identity. *Neuron,* 23**,** 659-74.

ARCE, V., GARCES, A., DE BOVIS, B., FILIPPI, P., HENDERSON, C., PETTMANN, B. & DELAPEYRIERE, O. 1999. Cardiotrophin-1 requires LIFRbeta to promote survival of mouse motoneurons purified by a novel technique. *J Neurosci Res,* 55**,** 119-26.

ARNOLD, E. S., LING, S. C., HUELGA, S. C., LAGIER-TOURENNE, C., POLYMENIDOU, M., DITSWORTH, D., KORDASIEWICZ, H. B., MCALONIS-DOWNES, M., PLATOSHYN, O., PARONE, P. A., DA CRUZ, S., CLUTARIO, K. M., SWING, D., TESSAROLLO, L., MARSALA, M., SHAW, C. E., YEO, G. W. & CLEVELAND, D. W. 2013. ALS-linked TDP-43 mutations produce aberrant RNA splicing and adult-onset motor neuron disease without aggregation or loss of nuclear TDP-43. *Proc Natl Acad Sci U S A,* 110**,** E736-45.

ARRIZA, J. L., FAIRMAN, W. A., WADICHE, J. I., MURDOCH, G. H., KAVANAUGH, M. P. & AMARA, S. G. 1994. Functional comparisons of three glutamate transporter subtypes cloned from human motor cortex. *J Neurosci,* 14**,** 5559-69.

ARTHUR, J. S. & LEY, S. C. 2013. Mitogen-activated protein kinases in innate immunity. *Nat Rev Immunol,* 13**,** 679-92.

AZZOUZ, M., RALPH, G. S., STORKEBAUM, E., WALMSLEY, L. E., MITROPHANOUS, K. A., KINGSMAN, S. M., CARMELIET, P. & MAZARAKIS, N. D. 2004. VEGF delivery with retrogradely transported lentivector prolongs survival in a mouse ALS model. *Nature,* 429**,** 413-7.

BEGHI, E., PUPILLO, E., BONITO, V., BUZZI, P., CAPONNETTO, C., CHIO, A., CORBO, M., GIANNINI, F., INGHILLERI, M., BELLA, V. L., LOGROSCINO, G., LORUSSO, L.,

LUNETTA, C., MAZZINI, L., MESSINA, P., MORA, G., PERINI, M., QUADRELLI, M. L., SILANI, V., SIMONE, I. L. & TREMOLIZZO, L. 2013. Randomized double-blind placebo-controlled trial of acetyl-L-carnitine for ALS. *Amyotroph Lateral Scler Frontotemporal Degener,* 14**,** 397-405.

BENDOTTI, C., ATZORI, C., PIVA, R., TORTAROLO, M., STRONG, M. J., DEBIASI, S. & MIGHELI, A. 2004. Activated p38MAPK is a novel component of the intracellular inclusions found in human amyotrophic lateral sclerosis and mutant SOD1 transgenic mice. *J Neuropathol Exp Neurol,* 63**,** 113-9.

BENDOTTI, C., BAO CUTRONA, M., CHERONI, C., GRIGNASCHI, G., LO COCO, D., PEVIANI, M., TORTAROLO, M., VEGLIANESE, P. & ZENNARO, E. 2005. Inter- and intracellular signaling in amyotrophic lateral sclerosis: role of p38 mitogen-activated protein kinase. *Neurodegener Dis,* 2**,** 128-34.

BERCSENYI, K., SCHMIEG, N., BRYSON, J. B., WALLACE, M., CACCIN, P., GOLDING, M., ZANOTTI, G., GREENSMITH, L., NISCHT, R. & SCHIAVO, G. 2014. Tetanus toxin entry. Nidogens are therapeutic targets for the prevention of tetanus. *Science,* 346**,** 1118-23.

BEREZUK, M. A. & SCHROER, T. A. 2007. Dynactin enhances the processivity of kinesin-2. *Traffic,* 8**,** 124-9.

BERGQVIST, M., BONDARENKO, I., THURESSON, M., KLOCKARE, M. & HARMENBERG, J. 2013. Randomized, Controlled, Multicenter, Multinational Phase II Study of Docetaxel (DCT) or AXL1717 Treatment in Patients with Squamous Cell Carcinoma (SCC) or Adenocarcinoma (AC) of Non-Small Cell Lung Cancer (NSCLC). *2014 ASCO Annual Meeting,* Poster abstract.

BILSLAND, L. G., SAHAI, E., KELLY, G., GOLDING, M., GREENSMITH, L. & SCHIAVO, G. 2010. Deficits in axonal transport precede ALS symptoms in vivo. *Proceedings of the National Academy of Sciences of the United States of America,* 107**,** 20523-8.

BIRKENKAMP, K. U. & COFFER, P. J. 2003. Regulation of cell survival and proliferation by the FOXO (Forkhead box, class O) subfamily of Forkhead transcription factors. *Biochem Soc Trans,* 31**,** 292-7.

BOEHM, J. C., BOWER, M. J., GALLAGHER, T. F., KASSIS, S., JOHNSON, S. R. & ADAMS, J. L. 2001. Phenoxypyrimidine inhibitors of p38alpha kinase: synthesis and statistical evaluation of the p38 inhibitory potencies of a series of 1-(piperidin-4-yl)-4-(4-fluorophenyl)-5-(2-phenoxypyrimidin-4-yl) imidazoles. *Bioorg Med Chem Lett,* 11**,** 1123-6.

BOHNERT, S. & SCHIAVO, G. 2005. Tetanus toxin is transported in a novel neuronal compartment characterized by a specialized pH regulation. *J Biol Chem,* 280**,** 42336-44.

BOILLEE, S., YAMANAKA, K., LOBSIGER, C. S., COPELAND, N. G., JENKINS, N. A., KASSIOTIS, G., KOLLIAS, G. & CLEVELAND, D. W. 2006. Onset and progression in inherited ALS determined by motor neurons and microglia. *Science,* 312**,** 1389-92.

BORASIO, G. D., ROBBERECHT, W., LEIGH, P. N., EMILE, J., GUILOFF, R. J., JERUSALEM, F., SILANI, V., VOS, P. E., WOKKE, J. H. & DOBBINS, T. 1998. A placebo-controlled trial of insulin-like growth factor-I in amyotrophic lateral sclerosis. European ALS/IGF-I Study Group. *Neurology,* 51**,** 583-6.

BORDERS, A. S., DE ALMEIDA, L., VAN ELDIK, L. J. & WATTERSON, D. M. 2008. The p38alpha mitogen-activated protein kinase as a central nervous system drug discovery target. *BMC Neurosci,* 9 Suppl 2**,** S12.

BRAHMKHATRI, V. P., PRASANNA, C. & ATREYA, H. S. 2015. Insulin-Like Growth Factor System in Cancer: Novel Targeted Therapies. *Biomed Res Int,* 2015**,** 538019.

BROWN, C. L., MAIER, K. C., STAUBER, T., GINKEL, L. M., WORDEMAN, L., VERNOS, I. & SCHROER, T. A. 2005. Kinesin-2 is a motor for late endosomes and lysosomes. *Traffic,* 6**,** 1114-24.

BRYSON, J. B., MACHADO, C. B., CROSSLEY, M., STEVENSON, D., BROS-FACER, V., BURRONE, J., GREENSMITH, L. & LIEBERAM, I. 2014. Optical control of muscle function by transplantation of stem cell-derived motor neurons in mice. *Science,* 344**,** 94-7.

BUTZLAFF, M., HANNAN, S. B., KARSTEN, P., LENZ, S., NG, J., VOSSFELDT, H., PRUSSING, K., PFLANZ, R., SCHULZ, J. B., RASSE, T. & VOIGT, A. 2015. Impaired

retrograde transport by the Dynein/Dynactin complex contributes to Tau-induced toxicity. *Hum Mol Genet*.

BYRNE, A. B., WALRADT, T., GARDNER, K. E., HUBBERT, A., REINKE, V. & HAMMARLUND, M. 2014. Insulin/IGF1 signaling inhibits age-dependent axon regeneration. *Neuron,* 81**,** 561-73.

CAVALLI, V., VILBOIS, F., CORTI, M., MARCOTE, M. J., TAMURA, K., KARIN, M., ARKINSTALL, S. & GRUENBERG, J. 2001. The stress-induced MAP kinase p38 regulates endocytic trafficking via the GDI:Rab5 complex. *Mol Cell,* 7**,** 421-32.

CHAMBERLAIN, S. D., REDMAN, A. M., WILSON, J. W., DEANDA, F., SHOTWELL, J. B., GERDING, R., LEI, H., YANG, B., STEVENS, K. L., HASSELL, A. M., SHEWCHUK, L. M., LEESNITZER, M. A., SMITH, J. L., SABBATINI, P., ATKINS, C., GROY, A., ROWAND, J. L., KUMAR, R., MOOK, R. A., JR., MOORTHY, G. & PATNAIK, S. 2009. Optimization of 4,6-bis-anilino-1H-pyrrolo[2,3-d]pyrimidine IGF-1R tyrosine kinase inhibitors towards JNK selectivity. *Bioorg Med Chem Lett,* 19**,** 360-4.

CHANG, Y., KONG, Q., SHAN, X., TIAN, G., ILIEVA, H., CLEVELAND, D. W., ROTHSTEIN, J. D., BORCHELT, D. R., WONG, P. C. & LIN, C. L. 2008. Messenger RNA oxidation occurs early in disease pathogenesis and promotes motor neuron degeneration in ALS. *PLoS One,* 3**,** e2849.

CHEN, H., QIAN, K., DU, Z., CAO, J., PETERSEN, A., LIU, H., BLACKBOURN, L. W. T., HUANG, C. L., ERRIGO, A., YIN, Y., LU, J., AYALA, M. & ZHANG, S. C. 2014. Modeling ALS with iPSCs reveals that mutant SOD1 misregulates neurofilament balance in motor neurons. *Cell Stem Cell,* 14**,** 796-809.

CHEN, S., OWENS, G. C., CROSSIN, K. L. & EDELMAN, D. B. 2007a. Serotonin stimulates mitochondrial transport in hippocampal neurons. *Mol Cell Neurosci,* 36**,** 472-83.

CHEN, X. J., LEVEDAKOU, E. N., MILLEN, K. J., WOLLMANN, R. L., SOLIVEN, B. & POPKO, B. 2007b. Proprioceptive sensory neuropathy in mice with a mutation in the cytoplasmic Dynein heavy chain 1 gene. *J Neurosci,* 27**,** 14515-24.

CHEN, Y. Z., BENNETT, C. L., HUYNH, H. M., BLAIR, I. P., PULS, I., IROBI, J., DIERICK, I., ABEL, A., KENNERSON, M. L., RABIN, B. A., NICHOLSON, G. A., AUER-GRUMBACH, M., WAGNER, K., DE JONGHE, P., GRIFFIN, J. W., FISCHBECK, K. H., TIMMERMAN, V., CORNBLATH, D. R. & CHANCE, P. F. 2004. DNA/RNA helicase gene mutations in a form of juvenile amyotrophic lateral sclerosis (ALS4). *Am J Hum Genet,* 74**,** 1128-35.

CHEW, J., GENDRON, T. F., PRUDENCIO, M., SASAGURI, H., ZHANG, Y. J., CASTANEDES-CASEY, M., LEE, C. W., JANSEN-WEST, K., KURTI, A., MURRAY, M. E., BIENIEK, K. F., BAUER, P. O., WHITELAW, E. C., ROUSSEAU, L., STANKOWSKI, J. N., STETLER, C., DAUGHRITY, L. M., PERKERSON, E. A., DESARO, P., JOHNSTON, A., OVERSTREET, K., EDBAUER, D., RADEMAKERS, R., BOYLAN, K. B., DICKSON, D. W., FRYER, J. D. & PETRUCELLI, L. 2015. C9ORF72 repeat expansions in mice cause TDP-43 pathology, neuronal loss, and behavioral deficits. *Science*.

CHICO, L. K., VAN ELDIK, L. J. & WATTERSON, D. M. 2009. Targeting protein kinases in central nervous system disorders. *Nat Rev Drug Discov,* 8**,** 892-909.

CHIO, A., CALVO, A., MAZZINI, L., CANTELLO, R., MORA, G., MOGLIA, C., CORRADO, L., D'ALFONSO, S., MAJOUNIE, E., RENTON, A., PISANO, F., OSSOLA, I., BRUNETTI, M., TRAYNOR, B. J. & RESTAGNO, G. 2012. Extensive genetics of ALS: a population-based study in Italy. *Neurology,* 79**,** 1983-9.

CHIO, A., TRAYNOR, B. J., LOMBARDO, F., FIMOGNARI, M., CALVO, A., GHIGLIONE, P., MUTANI, R. & RESTAGNO, G. 2008. Prevalence of SOD1 mutations in the Italian ALS population. *Neurology,* 70**,** 533-7.

CHO, J. H. & JOHNSON, G. V. 2004. Primed phosphorylation of tau at Thr231 by glycogen synthase kinase 3beta (GSK3beta) plays a critical role in regulating tau's ability to bind and stabilize microtubules. *J Neurochem,* 88**,** 349-58.

CHOW, C. Y., LANDERS, J. E., BERGREN, S. K., SAPP, P. C., GRANT, A. E., JONES, J. M., EVERETT, L., LENK, G. M., MCKENNA-YASEK, D. M., WEISMAN, L. S., FIGLEWICZ, D., BROWN, R. H. & MEISLER, M. H. 2009. Deleterious variants of FIG4, a phosphoinositide phosphatase, in patients with ALS. *Am J Hum Genet,* 84**,** 85-8.

CHOWDARY, P. D., CHE, D. L. & CUI, B. 2012. Neurotrophin signaling via long-distance axonal transport. *Annu Rev Phys Chem,* 63**,** 571-94.

CLEMENT, A. M., NGUYEN, M. D., ROBERTS, E. A., GARCIA, M. L., BOILLEE, S., RULE, M., MCMAHON, A. P., DOUCETTE, W., SIWEK, D., FERRANTE, R. J., BROWN, R. H., JR., JULIEN, J. P., GOLDSTEIN, L. S. & CLEVELAND, D. W. 2003. Wild-type nonneuronal cells extend survival of SOD1 mutant motor neurons in ALS mice. *Science,* 302**,** 113-7.

COFFEY, E. T., SMICIENE, G., HONGISTO, V., CAO, J., BRECHT, S., HERDEGEN, T. & COURTNEY, M. J. 2002. c-Jun N-terminal protein kinase (JNK) 2/3 is specifically activated by stress, mediating c-Jun activation, in the presence of constitutive JNK1 activity in cerebellar neurons. *J Neurosci,* 22**,** 4335-45.

COHEN, E. 2011. Countering neurodegeneration by reducing the activity of the insulin/IGF signaling pathway: current knowledge and future prospects. *Exp Gerontol,* 46**,** 124-8.

COHEN, E., BIESCHKE, J., PERCIAVALLE, R. M., KELLY, J. W. & DILLIN, A. 2006. Opposing activities protect against age-onset proteotoxicity. *Science,* 313**,** 1604-10.

COHEN, E., DU, D., JOYCE, D., KAPERNICK, E. A., VOLOVIK, Y., KELLY, J. W. & DILLIN, A. 2010. Temporal requirements of insulin/IGF-1 signaling for proteotoxicity protection. *Aging Cell,* 9**,** 126-34.

COHEN, E., PAULSSON, J. F., BLINDER, P., BURSTYN-COHEN, T., DU, D., ESTEPA, G., ADAME, A., PHAM, H. M., HOLZENBERGER, M., KELLY, J. W., MASLIAH, E. & DILLIN, A. 2009. Reduced IGF-1 signaling delays age-associated proteotoxicity in mice. *Cell,* 139**,** 1157-69.

COLIN, E., ZALA, D., LIOT, G., RANGONE, H., BORRELL-PAGES, M., LI, X. J., SAUDOU, F. & HUMBERT, S. 2008. Huntingtin phosphorylation acts as a molecular switch for anterograde/retrograde transport in neurons. *Embo j,* 27**,** 2124-34.

COOPER-KNOCK, J., BURY, J. J., HEATH, P. R., WYLES, M., HIGGINBOTTOM, A., GELSTHORPE, C., HIGHLEY, J. R., HAUTBERGUE, G., RATTRAY, M., KIRBY, J. & SHAW, P. J. 2015. C9ORF72 GGGGCC Expanded Repeats Produce Splicing Dysregulation which Correlates with Disease Severity in Amyotrophic Lateral Sclerosis. *PLoS One,* 10**,** e0127376.

COOPER-KNOCK, J., WALSH, M. J., HIGGINBOTTOM, A., ROBIN HIGHLEY, J., DICKMAN, M. J., EDBAUER, D., INCE, P. G., WHARTON, S. B., WILSON, S. A., KIRBY, J., HAUTBERGUE, G. M. & SHAW, P. J. 2014. Sequestration of multiple RNA recognition motif-containing proteins by C9orf72 repeat expansions. *Brain,* 137**,** 2040-51.

CUADRADO, A. & NEBREDA, A. R. 2010. Mechanisms and functions of p38 MAPK signalling. *Biochem J,* 429**,** 403-17.

CUDKOWICZ, M. E., VAN DEN BERG, L. H., SHEFNER, J. M., MITSUMOTO, H., MORA, J. S., LUDOLPH, A., HARDIMAN, O., BOZIK, M. E., INGERSOLL, E. W., ARCHIBALD, D., MEYERS, A. L., DONG, Y., FARWELL, W. R. & KERR, D. A. 2013. Dexpramipexole versus placebo for patients with amyotrophic lateral sclerosis (EMPOWER): a randomised, double-blind, phase 3 trial. *Lancet Neurol,* 12**,** 1059-67.

CUENDA, A. & ROUSSEAU, S. 2007. p38 MAP-kinases pathway regulation, function and role in human diseases. *Biochim Biophys Acta,* 1773**,** 1358-75.

D'YDEWALLE, C., KRISHNAN, J., CHIHEB, D. M., VAN DAMME, P., IROBI, J., KOZIKOWSKI, A. P., VANDEN BERGHE, P., TIMMERMAN, V., ROBBERECHT, W. & VAN DEN BOSCH, L. 2011. HDAC6 inhibitors reverse axonal loss in a mouse model of mutant HSPB1-induced Charcot-Marie-Tooth disease. *Nat Med,* 17**,** 968-74.

DAMIANO, M., STARKOV, A. A., PETRI, S., KIPIANI, K., KIAEI, M., MATTIAZZI, M., FLINT BEAL, M. & MANFREDI, G. 2006. Neural mitochondrial Ca2+ capacity impairment precedes the onset of motor symptoms in G93A Cu/Zn-superoxide dismutase mutant mice. *J Neurochem,* 96**,** 1349-61.

DE VOS, K. J., CHAPMAN, A. L., TENNANT, M. E., MANSER, C., TUDOR, E. L., LAU, K.-F., BROWNLEES, J., ACKERLEY, S., SHAW, P. J., MCLOUGHLIN, D. M., SHAW, C. E., LEIGH, P. N., MILLER, C. C. J. & GRIERSON, A. J. 2007. Familial amyotrophic lateral sclerosis-linked SOD1 mutants perturb fast axonal transport to reduce axonal mitochondria content. *Human Molecular Genetics,* 16**,** 2720-8.

DE VOS, K. J. & SHEETZ, M. P. 2007. Visualization and quantification of mitochondrial dynamics in living animal cells. *Methods Cell Biol,* 80**,** 627-82.

DEINHARDT, K., BERNINGHAUSEN, O., WILLISON, H. J., HOPKINS, C. R. & SCHIAVO, G. 2006a. Tetanus toxin is internalized by a sequential clathrin-dependent mechanism initiated within lipid microdomains and independent of epsin1. *J Cell Biol,* 174**,** 459-71.

DEINHARDT, K., REVERSI, A., BERNINGHAUSEN, O., HOPKINS, C. R. & SCHIAVO, G. 2007. Neurotrophins Redirect p75NTR from a clathrin-independent to a clathrin-dependent endocytic pathway coupled to axonal transport. *Traffic (Copenhagen, Denmark),* 8**,** 1736-49.

DEINHARDT, K., SALINAS, S., VERASTEGUI, C., WATSON, R., WORTH, D., HANRAHAN, S., BUCCI, C. & SCHIAVO, G. 2006b. Rab5 and Rab7 control endocytic sorting along the axonal retrograde transport pathway. *Neuron,* 52**,** 293-305.

DEINHARDT, K. & SCHIAVO, G. 2005. Endocytosis and retrograde axonal traffic in motor neurons. *Biochem Soc Symp***,** 139-50.

DEJESUS-HERNANDEZ, M., MACKENZIE, I. R., BOEVE, B. F., BOXER, A. L., BAKER, M., RUTHERFORD, N. J., NICHOLSON, A. M., FINCH, N. A., FLYNN, H., ADAMSON, J., KOURI, N., WOJTAS, A., SENGDY, P., HSIUNG, G. Y., KARYDAS, A., SEELEY, W. W., JOSEPHS, K. A., COPPOLA, G., GESCHWIND, D. H., WSZOLEK, Z. K., FELDMAN, H., KNOPMAN, D. S., PETERSEN, R. C., MILLER, B. L., DICKSON, D. W., BOYLAN, K. B., GRAFF-RADFORD, N. R. & RADEMAKERS, R. 2011. Expanded GGGGCC hexanucleotide repeat in noncoding region of C9ORF72 causes chromosome 9p-linked FTD and ALS. *Neuron,* 72**,** 245-56.

DENG, H. X., CHEN, W., HONG, S. T., BOYCOTT, K. M., GORRIE, G. H., SIDDIQUE, N., YANG, Y., FECTO, F., SHI, Y., ZHAI, H., JIANG, H., HIRANO, M., RAMPERSAUD, E., JANSEN, G. H., DONKERVOORT, S., BIGIO, E. H., BROOKS, B. R., AJROUD, K., SUFIT, R. L., HAINES, J. L., MUGNAINI, E., PERICAK-VANCE, M. A. & SIDDIQUE, T. 2011. Mutations in UBQLN2 cause dominant X-linked juvenile and adult-onset ALS and ALS/dementia. *Nature,* 477**,** 211-5.

DENNIS, P. A. & RIFKIN, D. B. 1991. Cellular activation of latent transforming growth factor beta requires binding to the cation-independent mannose 6-phosphate/insulin-like growth factor type II receptor. *Proc Natl Acad Sci U S A,* 88**,** 580-4.

DEVLIN, A. C., BURR, K., BOROOAH, S., FOSTER, J. D., CLEARY, E. M., GETI, I., VALLIER, L., SHAW, C. E., CHANDRAN, S. & MILES, G. B. 2015. Human iPSC-derived motoneurons harbouring TARDBP or C9ORF72 ALS mutations are dysfunctional despite maintaining viability. *Nat Commun,* 6**,** 5999.

DEWIL, M., DELA CRUZ, V. F., VAN DEN BOSCH, L. & ROBBERECHT, W. 2007. Inhibition of p38 mitogen activated protein kinase activation and mutant SOD1(G93A)-induced motor neuron death. *Neurobiol Dis,* 26**,** 332-41.

DI GIORGIO, F. P., CARRASCO, M. A., SIAO, M. C., MANIATIS, T. & EGGAN, K. 2007. Non–cell autonomous effect of glia on motor neurons in an embryonic stem cell–based ALS model. *Nature Neuroscience,* 10**,** 608-614.

DI GIULIO, A. M., LESMA, E. & GORIO, A. 1995. Diabetic neuropathy in the rat: 1. Alcar augments the reduced levels and axoplasmic transport of substance P. *J Neurosci Res,* 40**,** 414-9.

DILLMAN, J. F., 3RD & PFISTER, K. K. 1994. Differential phosphorylation in vivo of cytoplasmic dynein associated with anterogradely moving organelles. *J Cell Biol,* 127**,** 1671-81.

DIRREN, E., AEBISCHER, J., ROCHAT, C., TOWNE, C., SCHNEIDER, B. L. & AEBISCHER, P. 2015. SOD1 silencing in motoneurons or glia rescues neuromuscular function in ALS mice. *Ann Clin Transl Neurol,* 2**,** 167-84.

DOBLE, A. 1996. The pharmacology and mechanism of action of riluzole. *Neurology,* 47**,** S233-41.

DOBROWOLNY, G., AUCELLO, M., RIZZUTO, E., BECCAFICO, S., MAMMUCARI, C., BONCOMPAGNI, S., BELIA, S., WANNENES, F., NICOLETTI, C., DEL PRETE, Z., ROSENTHAL, N., MOLINARO, M., PROTASI, F., FANO, G., SANDRI, M. & MUSARO, A. 2008. Skeletal muscle is a primary target of SOD1G93A-mediated toxicity. *Cell Metab,* 8**,** 425-36.

DODDING, M. P. & WAY, M. 2011. Coupling viruses to dynein and kinesin-1. *Embo j,* 30**,** 3527-39.

DODGE, J. C., HAIDET, A. M., YANG, W., PASSINI, M. A., HESTER, M., CLARKE, J., ROSKELLEY, E. M., TRELEAVEN, C. M., RIZO, L., MARTIN, H., KIM, S. H., KASPAR,

R., TAKSIR, T. V., GRIFFITHS, D. A., CHENG, S. H., SHIHABUDDIN, L. S. & KASPAR, B. K. 2008. Delivery of AAV-IGF-1 to the CNS extends survival in ALS mice through modification of aberrant glial cell activity. *Mol Ther,* 16**,** 1056-64.

DOMPIERRE, J. P., GODIN, J. D., CHARRIN, B. C., CORDELIERES, F. P., KING, S. J., HUMBERT, S. & SAUDOU, F. 2007. Histone deacetylase 6 inhibition compensates for the transport deficit in Huntington's disease by increasing tubulin acetylation. *J Neurosci,* 27**,** 3571-83.

DUAN, W., LI, X., SHI, J., GUO, Y., LI, Z. & LI, C. 2010. Mutant TAR DNA-binding protein-43 induces oxidative injury in motor neuron-like cell. *Neuroscience,* 169**,** 1621-9.

ECONOMOU, M. A., ANDERSSON, S., VASILCANU, D., ALL-ERICSSON, C., MENU, E., GIRNITA, A., GIRNITA, L., AXELSON, M., SEREGARD, S. & LARSSON, O. 2008. Oral picropodophyllin (PPP) is well tolerated in vivo and inhibits IGF-1R expression and growth of uveal melanoma. *Invest Ophthalmol Vis Sci,* 49**,** 2337-42.

EGAWA, N., KITAOKA, S., TSUKITA, K., NAITOH, M., TAKAHASHI, K., YAMAMOTO, T., ADACHI, F., KONDO, T., OKITA, K., ASAKA, I., AOI, T., WATANABE, A., YAMADA, Y., MORIZANE, A., TAKAHASHI, J., AYAKI, T., ITO, H., YOSHIKAWA, K., YAMAWAKI, S., SUZUKI, S., WATANABE, D., HIOKI, H., KANEKO, T., MAKIOKA, K., OKAMOTO, K., TAKUMA, H., TAMAOKA, A., HASEGAWA, K., NONAKA, T., HASEGAWA, M., KAWATA, A., YOSHIDA, M., NAKAHATA, T., TAKAHASHI, R., MARCHETTO, M. C., GAGE, F. H., YAMANAKA, S. & INOUE, H. 2012. Drug screening for ALS using patient-specific induced pluripotent stem cells. *Sci Transl Med,* 4**,** 145ra104.

EL-AMI, T., MOLL, L., CARVALHAL MARQUES, F., VOLOVIK, Y., REUVENI, H. & COHEN, E. 2014. A novel inhibitor of the insulin/IGF signaling pathway protects from age-onset, neurodegeneration-linked proteotoxicity. *Aging Cell,* 13**,** 165-74.

ELDEN, A. C., KIM, H. J., HART, M. P., CHEN-PLOTKIN, A. S., JOHNSON, B. S., FANG, X., ARMAKOLA, M., GESER, F., GREENE, R., LU, M. M., PADMANABHAN, A., CLAY-FALCONE, D., MCCLUSKEY, L., ELMAN, L., JUHR, D., GRUBER, P. J., RUB, U., AUBURGER, G., TROJANOWSKI, J. Q., LEE, V. M., VAN DEERLIN, V. M., BONINI, N. M. & GITLER, A. D. 2010. Ataxin-2 intermediate-length polyglutamine expansions are associated with increased risk for ALS. *Nature,* 466**,** 1069-75.

ESCUDERO, C. A., LAZO, O. M., GALLEGUILLOS, C., PARRAGUEZ, J. I., LOPEZ-VERRILLI, M. A., CABEZA, C., LEON, L., SAEED, U., RETAMAL, C., GONZALEZ, A., MARZOLO, M. P., CARTER, B. D., COURT, F. A. & BRONFMAN, F. C. 2014. The p75 neurotrophin receptor evades the endolysosomal route in neuronal cells, favouring multivesicular bodies specialised for exosomal release. *J Cell Sci,* 127**,** 1966-79.

EWALD, C. Y., LANDIS, J. N., PORTER ABATE, J., MURPHY, C. T. & BLACKWELL, T. K. 2015. Dauer-independent insulin/IGF-1-signalling implicates collagen remodelling in longevity. *Nature,* 519**,** 97-101.

FARAH, C. A., NGUYEN, M. D., JULIEN, J. P. & LECLERC, N. 2003. Altered levels and distribution of microtubule-associated proteins before disease onset in a mouse model of amyotrophic lateral sclerosis. *J Neurochem,* 84**,** 77-86.

FARG, M. A., SUNDARAMOORTHY, V., SULTANA, J. M., YANG, S., ATKINSON, R. A., LEVINA, V., HALLORAN, M. A., GLEESON, P. A., BLAIR, I. P., SOO, K. Y., KING, A. E. & ATKIN, J. D. 2014. C9ORF72, implicated in amytrophic lateral sclerosis and frontotemporal dementia, regulates endosomal trafficking. *Hum Mol Genet,* 23**,** 3579-95.

FECTO, F., YAN, J., VEMULA, S. P., LIU, E., YANG, Y., CHEN, W., ZHENG, J. G., SHI, Y., SIDDIQUE, N., ARRAT, H., DONKERVOORT, S., AJROUD-DRISS, S., SUFIT, R. L., HELLER, S. L., DENG, H. X. & SIDDIQUE, T. 2011. SQSTM1 mutations in familial and sporadic amyotrophic lateral sclerosis. *Arch Neurol,* 68**,** 1440-6.

FERRER, I., BLANCO, R. & CARMONA, M. 2001. Differential expression of active, phosphorylation-dependent MAP kinases, MAPK/ERK, SAPK/JNK and p38, and specific transcription factor substrates following quinolinic acid excitotoxicity in the rat. *Brain Res Mol Brain Res,* 94**,** 48-58.

FERRI, A., COZZOLINO, M., CROSIO, C., NENCINI, M., CASCIATI, A., GRALLA, E. B., ROTILIO, G., VALENTINE, J. S. & CARRI, M. T. 2006. Familial ALS-superoxide dismutases associate with mitochondria and shift their redox potentials. *Proc Natl Acad Sci U S A,* 103**,** 13860-5.

FIRESTONE, A. J., WEINGER, J. S., MALDONADO, M., BARLAN, K., LANGSTON, L. D., O'DONNELL, M., GELFAND, V. I., KAPOOR, T. M. & CHEN, J. K. 2012. Small-molecule inhibitors of the AAA+ ATPase motor cytoplasmic dynein. *Nature,* 484**,** 125-9.

FISCHER, L. R., IGOUDJIL, A., MAGRANE, J., LI, Y., HANSEN, J. M., MANFREDI, G. & GLASS, J. D. 2011. SOD1 targeted to the mitochondrial intermembrane space prevents motor neuropathy in the Sod1 knockout mouse. *Brain,* 134**,** 196-209.

FITZMAURICE, P. S., SHAW, I. C., KLEINER, H. E., MILLER, R. T., MONKS, T. J., LAU, S. S., MITCHELL, J. D. & LYNCH, P. G. 1996. Evidence for DNA damage in amyotrophic lateral sclerosis. *Muscle Nerve,* 19**,** 797-8.

FORLONI, G., ANGERETTI, N. & SMIROLDO, S. 1994. Neuroprotective activity of acetyl-L-carnitine: studies in vitro. *J Neurosci Res,* 37**,** 92-6.

FREISCHMIDT, A., WIELAND, T., RICHTER, B., RUF, W., SCHAEFFER, V., MULLER, K., MARROQUIN, N., NORDIN, F., HUBERS, A., WEYDT, P., PINTO, S., PRESS, R., MILLECAMPS, S., MOLKO, N., BERNARD, E., DESNUELLE, C., SORIANI, M. H., DORST, J., GRAF, E., NORDSTROM, U., FEILER, M. S., PUTZ, S., BOECKERS, T. M., MEYER, T., WINKLER, A. S., WINKELMAN, J., DE CARVALHO, M., THAL, D. R., OTTO, M., BRANNSTROM, T., VOLK, A. E., KURSULA, P., DANZER, K. M., LICHTNER, P., DIKIC, I., MEITINGER, T., LUDOLPH, A. C., STROM, T. M., ANDERSEN, P. M. & WEISHAUPT, J. H. 2015. Haploinsufficiency of TBK1 causes familial ALS and fronto-temporal dementia. *Nat Neurosci,* 18**,** 631-6.

FREUDE, S., HETTICH, M. M., SCHUMANN, C., STOHR, O., KOCH, L., KOHLER, C., UDELHOVEN, M., LEESER, U., MULLER, M., KUBOTA, N., KADOWAKI, T., KRONE, W., SCHRODER, H., BRUNING, J. C. & SCHUBERT, M. 2009. Neuronal IGF-1 resistance reduces Abeta accumulation and protects against premature death in a model of Alzheimer's disease. *Faseb j,* 23**,** 3315-24.

FU, M. M. & HOLZBAUR, E. L. 2013. JIP1 regulates the directionality of APP axonal transport by coordinating kinesin and dynein motors. *J Cell Biol,* 202**,** 495-508.

FUMAGALLI, E., FUNICELLO, M., RAUEN, T., GOBBI, M. & MENNINI, T. 2008. Riluzole enhances the activity of glutamate transporters GLAST, GLT1 and EAAC1. *Eur J Pharmacol,* 578**,** 171-6.

GAL, J., CHEN, J., BARNETT, K. R., YANG, L., BRUMLEY, E. & ZHU, H. 2013. HDAC6 regulates mutant SOD1 aggregation through two SMIR motifs and tubulin acetylation. *J Biol Chem,* 288**,** 15035-45.

GAUTHIER, L. R., CHARRIN, B. C., BORRELL-PAGES, M., DOMPIERRE, J. P., RANGONE, H., CORDELIERES, F. P., DE MEY, J., MACDONALD, M. E., LESSMANN, V., HUMBERT, S. & SAUDOU, F. 2004. Huntingtin controls neurotrophic support and survival of neurons by enhancing BDNF vesicular transport along microtubules. *Cell,* 118**,** 127-38.

GIORDANA, M. T., PICCININI, M., GRIFONI, S., DE MARCO, G., VERCELLINO, M., MAGISTRELLO, M., PELLERINO, A., BUCCINNA, B., LUPINO, E. & RINAUDO, M. T. 2010. TDP-43 redistribution is an early event in sporadic amyotrophic lateral sclerosis. *Brain Pathol,* 20**,** 351-60.

GIRNITA, A., GIRNITA, L., DEL PRETE, F., BARTOLAZZI, A., LARSSON, O. & AXELSON, M. 2004. Cyclolignans as inhibitors of the insulin-like growth factor-1 receptor and malignant cell growth. *Cancer Res,* 64**,** 236-42.

GITCHO, M. A., BALOH, R. H., CHAKRAVERTY, S., MAYO, K., NORTON, J. B., LEVITCH, D., HATANPAA, K. J., WHITE, C. L., 3RD, BIGIO, E. H., CASELLI, R., BAKER, M., AL-LOZI, M. T., MORRIS, J. C., PESTRONK, A., RADEMAKERS, R., GOATE, A. M. & CAIRNS, N. J. 2008. TDP-43 A315T mutation in familial motor neuron disease. *Ann Neurol,* 63**,** 535-8.

GODENA, V. K., BROOKES-HOCKING, N., MOLLER, A., SHAW, G., OSWALD, M., SANCHO, R. M., MILLER, C. C., WHITWORTH, A. J. & DE VOS, K. J. 2014. Increasing microtubule acetylation rescues axonal transport and locomotor deficits caused by LRRK2 Roc-COR domain mutations. *Nat Commun,* 5**,** 5245.

GONG, Y. H., PARSADANIAN, A. S., ANDREEVA, A., SNIDER, W. D. & ELLIOTT, J. L. 2000. Restricted expression of G86R Cu/Zn superoxide dismutase in astrocytes results in astrocytosis but does not cause motoneuron degeneration. *J Neurosci,* 20**,** 660-5.

GOWING, G., DEQUEN, F., SOUCY, G. & JULIEN, J. P. 2006. Absence of tumor necrosis factor-alpha does not affect motor neuron disease caused by superoxide dismutase 1 mutations. *J Neurosci,* 26**,** 11397-402.

GRAF, M., ECKER, D., HOROWSKI, R., KRAMER, B., RIEDERER, P., GERLACH, M., HAGER, C., LUDOLPH, A. C., BECKER, G., OSTERHAGE, J., JOST, W. H., SCHRANK, B., STEIN, C., KOSTOPULOS, P., LUBIK, S., WEKWERTH, K., DENGLER, R., TROEGER, M., WUERZ, A., HOGE, A., SCHRADER, C., SCHIMKE, N., KRAMPFL, K., PETRI, S., ZIERZ, S., EGER, K., NEUDECKER, S., TRAUFELLER, K., SIEVERT, M., NEUNDORFER, B. & HECHT, M. 2005. High dose vitamin E therapy in amyotrophic lateral sclerosis as add-on therapy to riluzole: results of a placebo-controlled double-blind study. *J Neural Transm,* 112**,** 649-60.

GRAFFMO, K. S., FORSBERG, K., BERGH, J., BIRVE, A., ZETTERSTROM, P., ANDERSEN, P. M., MARKLUND, S. L. & BRANNSTROM, T. 2013. Expression of wild-type human superoxide dismutase-1 in mice causes amyotrophic lateral sclerosis. *Hum Mol Genet,* 22**,** 51-60.

GRAHAM ROBINETT, R., FREEMERMAN, A. J., SKINNER, M. A., SHEWCHUK, L. & LACKEY, K. 2007. The discovery of substituted 4-(3-hydroxyanilino)-quinolines as potent RET kinase inhibitors. *Bioorg Med Chem Lett,* 17**,** 5886-93.

GREENWAY, M. J., ANDERSEN, P. M., RUSS, C., ENNIS, S., CASHMAN, S., DONAGHY, C., PATTERSON, V., SWINGLER, R., KIERAN, D., PREHN, J., MORRISON, K. E., GREEN, A., ACHARYA, K. R., BROWN, R. H., JR. & HARDIMAN, O. 2006. ANG mutations segregate with familial and 'sporadic' amyotrophic lateral sclerosis. *Nat Genet,* 38**,** 411-3.

GROSS, S. P. 2004. Hither and yon: a review of bi-directional microtubule-based transport. *Phys Biol,* 1**,** R1-11.

GUNAWARDENA, S., HER, L. S., BRUSCH, R. G., LAYMON, R. A., NIESMAN, I. R., GORDESKY-GOLD, B., SINTASATH, L., BONINI, N. M. & GOLDSTEIN, L. S. 2003. Disruption of axonal transport by loss of huntingtin or expression of pathogenic polyQ proteins in Drosophila. *Neuron,* 40**,** 25-40.

GUO, L., DU, H., YAN, S., WU, X., MCKHANN, G. M., CHEN, J. X. & YAN, S. S. 2013. Cyclophilin D deficiency rescues axonal mitochondrial transport in Alzheimer's neurons. *PLoS One,* 8**,** e54914.

GURNEY, M. E., PU, H., CHIU, A. Y., DAL CANTO, M. C., POLCHOW, C. Y., ALEXANDER, D. D., CALIENDO, J., HENTATI, A., KWON, Y. W. & DENG, H. X. 1994. Motor neuron degeneration in mice that express a human Cu,Zn superoxide dismutase mutation. *Science (New York, N.Y.),* 264**,** 1772-5.

HADANO, S., HAND, C. K., OSUGA, H., YANAGISAWA, Y., OTOMO, A., DEVON, R. S., MIYAMOTO, N., SHOWGUCHI-MIYATA, J., OKADA, Y., SINGARAJA, R., FIGLEWICZ, D. A., KWIATKOWSKI, T., HOSLER, B. A., SAGIE, T., SKAUG, J., NASIR, J., BROWN, R. H., JR., SCHERER, S. W., ROULEAU, G. A., HAYDEN, M. R. & IKEDA, J. E. 2001. A gene encoding a putative GTPase regulator is mutated in familial amyotrophic lateral sclerosis 2. *Nat Genet,* 29**,** 166-73.

HAFEZPARAST, M., KLOCKE, R., RUHRBERG, C., MARQUARDT, A., AHMAD-ANNUAR, A., BOWEN, S., LALLI, G., WITHERDEN, A. S., HUMMERICH, H., NICHOLSON, S., MORGAN, P. J., OOZAGEER, R., PRIESTLEY, J. V., AVERILL, S., KING, V. R., BALL, S., PETERS, J., TODA, T., YAMAMOTO, A., HIRAOKA, Y., AUGUSTIN, M., KORTHAUS, D., WATTLER, S., WABNITZ, P., DICKNEITE, C., LAMPEL, S., BOEHME, F., PERAUS, G., POPP, A., RUDELIUS, M., SCHLEGEL, J., FUCHS, H., HRABE DE ANGELIS, M., SCHIAVO, G., SHIMA, D. T., RUSS, A. P., STUMM, G., MARTIN, J. E. & FISHER, E. M. C. 2003. Mutations in dynein link motor neuron degeneration to defects in retrograde transport. *Science (New York, N.Y.),* 300**,** 808-12.

HAIDET-PHILLIPS, A. M., HESTER, M. E., MIRANDA, C. J., MEYER, K., BRAUN, L., FRAKES, A., SONG, S., LIKHITE, S., MURTHA, M. J., FOUST, K. D., RAO, M., EAGLE, A., KAMMESHEIDT, A., CHRISTENSEN, A., MENDELL, J. R., BURGHES, A. H. & KASPAR, B. K. 2011. Astrocytes from familial and sporadic ALS patients are toxic to motor neurons. *Nat Biotechnol,* 29**,** 824-8.

HEMATULIN, A. 2010. Insulin-like Growth Factor 1 Signalling and Its Role in Cell Survival and Radiation Sensitivity. *Siriraj Medical Jounral,* 62**,** 263 - 268.

HENSLEY, K., FLOYD, R. A., GORDON, B., MOU, S., PYE, Q. N., STEWART, C., WEST, M. & WILLIAMSON, K. 2002. Temporal patterns of cytokine and apoptosis-related gene expression in spinal cords of the G93A-SOD1 mouse model of amyotrophic lateral sclerosis. *J Neurochem,* 82**,** 365-74.

HER, L. S. & GOLDSTEIN, L. S. 2008. Enhanced sensitivity of striatal neurons to axonal transport defects induced by mutant huntingtin. *J Neurosci,* 28**,** 13662-72.

HIGGINS, C. M., JUNG, C., DING, H. & XU, Z. 2002. Mutant Cu, Zn superoxide dismutase that causes motoneuron degeneration is present in mitochondria in the CNS. *J Neurosci,* 22**,** Rc215.

HIGHLEY, J. R., KIRBY, J., HEATH, P. R., JANSWEIJER, J. A., MILO, M., INCE, P. G. & SHAW, P. J. 2010. TARDBP mutations, amyotrophic lateral sclerosis and alternative splicing in human fibroblasts. *BRAIN PATHOLOGY,* 20**,** 32.

HIOKI, H., KAMEDA, H., NAKAMURA, H., OKUNOMIYA, T., OHIRA, K., NAKAMURA, K., KURODA, M., FURUTA, T. & KANEKO, T. 2007. Efficient gene transduction of neurons by lentivirus with enhanced neuron-specific promoters. *Gene Ther,* 14**,** 872-82.

HOLZENBERGER, M., DUPONT, J., DUCOS, B., LENEUVE, P., GELOEN, A., EVEN, P. C., CERVERA, P. & LE BOUC, Y. 2003. IGF-1 receptor regulates lifespan and resistance to oxidative stress in mice. *Nature,* 421**,** 182-7.

HU, B. Y. & ZHANG, S. C. 2009. Differentiation of spinal motor neurons from pluripotent human stem cells. *Nat Protoc,* 4**,** 1295-304.

IBANEZ, C. F. & SIMI, A. 2012. p75 neurotrophin receptor signaling in nervous system injury and degeneration: paradox and opportunity. *Trends Neurosci,* 35**,** 431-40.

INCE, P. G., TOMKINS, J., SLADE, J. Y., THATCHER, N. M. & SHAW, P. J. 1998. Amyotrophic lateral sclerosis associated with genetic abnormalities in the gene encoding Cu/Zn superoxide dismutase: molecular pathology of five new cases, and comparison with previous reports and 73 sporadic cases of ALS. *J Neuropathol Exp Neurol,* 57**,** 895-904.

JALAL, F. Y., BOHLKE, M. & MAHER, T. J. 2010. Acetyl-L-carnitine reduces the infarct size and striatal glutamate outflow following focal cerebral ischemia in rats. *Ann N Y Acad Sci,* 1199**,** 95-104.

JOHNSON, J. O., GLYNN, S. M., GIBBS, J. R., NALLS, M. A., SABATELLI, M., RESTAGNO, G., DRORY, V. E., CHIO, A., ROGAEVA, E. & TRAYNOR, B. J. 2014a. Mutations in the CHCHD10 gene are a common cause of familial amyotrophic lateral sclerosis. *Brain,* 137**,** e311.

JOHNSON, J. O., MANDRIOLI, J., BENATAR, M., ABRAMZON, Y., VAN DEERLIN, V. M., TROJANOWSKI, J. Q., GIBBS, J. R., BRUNETTI, M., GRONKA, S., WUU, J., DING, J., MCCLUSKEY, L., MARTINEZ-LAGE, M., FALCONE, D., HERNANDEZ, D. G., AREPALLI, S., CHONG, S., SCHYMICK, J. C., ROTHSTEIN, J., LANDI, F., WANG, Y. D., CALVO, A., MORA, G., SABATELLI, M., MONSURRO, M. R., BATTISTINI, S., SALVI, F., SPATARO, R., SOLA, P., BORGHERO, G., GALASSI, G., SCHOLZ, S. W., TAYLOR, J. P., RESTAGNO, G., CHIO, A. & TRAYNOR, B. J. 2010. Exome sequencing reveals VCP mutations as a cause of familial ALS. *Neuron,* 68**,** 857-64.

JOHNSON, J. O., PIORO, E. P., BOEHRINGER, A., CHIA, R., FEIT, H., RENTON, A. E., PLINER, H. A., ABRAMZON, Y., MARANGI, G., WINBORN, B. J., GIBBS, J. R., NALLS, M. A., MORGAN, S., SHOAI, M., HARDY, J., PITTMAN, A., ORRELL, R. W., MALASPINA, A., SIDLE, K. C., FRATTA, P., HARMS, M. B., BALOH, R. H., PESTRONK, A., WEIHL, C. C., ROGAEVA, E., ZINMAN, L., DRORY, V. E., BORGHERO, G., MORA, G., CALVO, A., ROTHSTEIN, J. D., DREPPER, C., SENDTNER, M., SINGLETON, A. B., TAYLOR, J. P., COOKSON, M. R., RESTAGNO, G., SABATELLI, M., BOWSER, R., CHIO, A. & TRAYNOR, B. J. 2014b. Mutations in the Matrin 3 gene cause familial amyotrophic lateral sclerosis. *Nat Neurosci,* 17**,** 664-6.

JOHRI, A. & BEAL, M. F. 2012. Mitochondrial dysfunction in neurodegenerative diseases. *J Pharmacol Exp Ther,* 342**,** 619-30.

JOUROUKHIN, Y., OSTRITSKY, R., ASSAF, Y., PELLED, G., GILADI, E. & GOZES, I. 2013. NAP (davunetide) modifies disease progression in a mouse model of severe neurodegeneration: protection against impairments in axonal transport. *Neurobiol Dis,* 56**,** 79-94.

JOYCE, P. I., MCGOLDRICK, P., SACCON, R. A., WEBER, W., FRATTA, P., WEST, S. J., ZHU, N., CARTER, S., PHATAK, V., STEWART, M., SIMON, M., KUMAR, S., HEISE, I.,

BROS-FACER, V., DICK, J., CORROCHANO, S., STANFORD, M. J., LUONG, T. V., NOLAN, P. M., MEYER, T., BRANDNER, S., BENNETT, D. L., OZDINLER, P. H., GREENSMITH, L., FISHER, E. M. & ACEVEDO-AROZENA, A. 2015. A novel SOD1-ALS mutation separates central and peripheral effects of mutant SOD1 toxicity. *Hum Mol Genet,* 24**,** 1883-97.

KABASHI, E., VALDMANIS, P. N., DION, P., SPIEGELMAN, D., MCCONKEY, B. J., VANDE VELDE, C., BOUCHARD, J. P., LACOMBLEZ, L., POCHIGAEVA, K., SALACHAS, F., PRADAT, P. F., CAMU, W., MEININGER, V., DUPRE, N. & ROULEAU, G. A. 2008. TARDBP mutations in individuals with sporadic and familial amyotrophic lateral sclerosis. *Nat Genet,* 40**,** 572-4.

KALMAR, B., NOVOSELOV, S., GRAY, A., CHEETHAM, M. E., MARGULIS, B. & GREENSMITH, L. 2008. Late stage treatment with arimoclomol delays disease progression and prevents protein aggregation in the SOD1 mouse model of ALS. *Journal of Neurochemistry,* 107**,** 339-50.

KANAAN, N. M., PIGINO, G. F., BRADY, S. T., LAZAROV, O., BINDER, L. I. & MORFINI, G. A. 2013. Axonal degeneration in Alzheimer's disease: when signaling abnormalities meet the axonal transport system. *Exp Neurol,* 246**,** 44-53.

KANO, M., KAWAKAMI, T., HORI, H., HASHIMOTO, Y., TAO, Y., ISHIKAWA, Y. & TAKENAKA, T. 1999. Effects of ALCAR on the fast axoplasmic transport in cultured sensory neurons of streptozotocin-induced diabetic rats. *Neurosci Res,* 33**,** 207-13.

KARLSSON, P., DROCE, A., MOSER, J. M., CUHLMANN, S., PADILLA, C. O., HEIMANN, P., BARTSCH, J. W., FUCHTBAUER, A., FUCHTBAUER, E. M. & SCHMITT-JOHN, T. 2013. Loss of vps54 function leads to vesicle traffic impairment, protein mis-sorting and embryonic lethality. *Int J Mol Sci,* 14**,** 10908-25.

KASPAR, B. K., LLADO, J., SHERKAT, N., ROTHSTEIN, J. D. & GAGE, F. H. 2003. Retrograde viral delivery of IGF-1 prolongs survival in a mouse ALS model. *Science,* 301**,** 839-42.

KEMP, M. Q., POORT, J. L., BAQRI, R. M., LIEBERMAN, A. P., BREEDLOVE, S. M., MILLER, K. E. & JORDAN, C. L. 2011. Impaired motoneuronal retrograde transport in two models of SBMA implicates two sites of androgen action. *Human Molecular Genetics***,** 1-16.

KENYON, C. 2005. The plasticity of aging: insights from long-lived mutants. *Cell,* 120**,** 449-60.

KIERAN, D., HAFEZPARAST, M., BOHNERT, S., DICK, J. R., MARTIN, J., SCHIAVO, G., FISHER, E. M. & GREENSMITH, L. 2005. A mutation in dynein rescues axonal transport defects and extends the life span of ALS mice. *J Cell Biol,* 169**,** 561-7.

KIM, H. J., KIM, N. C., WANG, Y. D., SCARBOROUGH, E. A., MOORE, J., DIAZ, Z., MACLEA, K. S., FREIBAUM, B., LI, S., MOLLIEX, A., KANAGARAJ, A. P., CARTER, R., BOYLAN, K. B., WOJTAS, A. M., RADEMAKERS, R., PINKUS, J. L., GREENBERG, S. A., TROJANOWSKI, J. Q., TRAYNOR, B. J., SMITH, B. N., TOPP, S., GKAZI, A. S., MILLER, J., SHAW, C. E., KOTTLORS, M., KIRSCHNER, J., PESTRONK, A., LI, Y. R., FORD, A. F., GITLER, A. D., BENATAR, M., KING, O. D., KIMONIS, V. E., ROSS, E. D., WEIHL, C. C., SHORTER, J. & TAYLOR, J. P. 2013. Mutations in prion-like domains in hnRNPA2B1 and hnRNPA1 cause multisystem proteinopathy and ALS. *Nature,* 495**,** 467-73.

KIRIS, E., NUSS, J. E., BURNETT, J. C., KOTA, K. P., KOH, D. C., WANNER, L. M., TORRES-MELENDEZ, E., GUSSIO, R., TESSAROLLO, L. & BAVARI, S. 2011. Embryonic stem cell-derived motoneurons provide a highly sensitive cell culture model for botulinum neurotoxin studies, with implications for high-throughput drug discovery. *Stem Cell Research,* 6**,** 195-205.

KON, T., OYAMA, T., SHIMO-KON, R., IMAMULA, K., SHIMA, T., SUTOH, K. & KURISU, G. 2012. The 2.8 A crystal structure of the dynein motor domain. *Nature,* 484**,** 345-50.

KONG, J. & XU, Z. 1998. Massive mitochondrial degeneration in motor neurons triggers the onset of amyotrophic lateral sclerosis in mice expressing a mutant SOD1. *J Neurosci,* 18**,** 3241-50.

KOPPERS, M., BLOKHUIS, A. M., WESTENENG, H. J., TERPSTRA, M. L., ZUNDEL, C. A., VIEIRA DE SA, R., SCHELLEVIS, R. D., WAITE, A. J., BLAKE, D. J., VELDINK, J. H., VAN DEN BERG, L. H. & JEROEN PASTERKAMP, R. 2015. C9orf72 ablation in mice does not cause motor neuron degeneration or motor deficits. *Ann Neurol*.

KORNFELD, S. 1992. Structure and function of the mannose 6-phosphate/insulinlike growth factor II receptors. *Annu Rev Biochem,* 61**,** 307-30.

KOUROUPI, G., LAVDAS, A. A., GAITANOU, M., THOMAIDOU, D., STYLIANOPOULOU, F. & MATSAS, R. 2010. Lentivirus-mediated expression of insulin-like growth factor-I promotes neural stem/precursor cell proliferation and enhances their potential to generate neurons. *J Neurochem,* 115**,** 460-74.

KULL, F. J., SABLIN, E. P., LAU, R., FLETTERICK, R. J. & VALE, R. D. 1996. Crystal structure of the kinesin motor domain reveals a structural similarity to myosin. *Nature,* 380**,** 550-5.

KUMAR, S., BOEHM, J. & LEE, J. C. 2003. p38 MAP kinases: key signalling molecules as therapeutic targets for inflammatory diseases. *Nat Rev Drug Discov,* 2**,** 717-26.

KUMAR, S., LEE, I. H. & PLAMANN, M. 2000. Cytoplasmic dynein ATPase activity is regulated by dynactin-dependent phosphorylation. *J Biol Chem,* 275**,** 31798-804.

KWIATKOWSKI, T. J., JR., BOSCO, D. A., LECLERC, A. L., TAMRAZIAN, E., VANDERBURG, C. R., RUSS, C., DAVIS, A., GILCHRIST, J., KASARSKIS, E. J., MUNSAT, T., VALDMANIS, P., ROULEAU, G. A., HOSLER, B. A., CORTELLI, P., DE JONG, P. J., YOSHINAGA, Y., HAINES, J. L., PERICAK-VANCE, M. A., YAN, J., TICOZZI, N., SIDDIQUE, T., MCKENNA-YASEK, D., SAPP, P. C., HORVITZ, H. R., LANDERS, J. E. & BROWN, R. H., JR. 2009. Mutations in the FUS/TLS gene on chromosome 16 cause familial amyotrophic lateral sclerosis. *Science,* 323**,** 1205-8.

LAGIER-TOURENNE, C., POLYMENIDOU, M. & CLEVELAND, D. W. 2010. TDP-43 and FUS/TLS: emerging roles in RNA processing and neurodegeneration. *Hum Mol Genet,* 19**,** R46-64.

LAI, E. C., FELICE, K. J., FESTOFF, B. W., GAWEL, M. J., GELINAS, D. F., KRATZ, R., MURPHY, M. F., NATTER, H. M., NORRIS, F. H. & RUDNICKI, S. A. 1997. Effect of recombinant human insulin-like growth factor-I on progression of ALS. A placebo-controlled study. The North America ALS/IGF-I Study Group. *Neurology,* 49**,** 1621-30.

LALLI, G., BOHNERT, S., DEINHARDT, K., VERASTEGUI, C. & SCHIAVO, G. 2003a. The journey of tetanus and botulinum neurotoxins in neurons. *Trends in Microbiology,* 11**,** 431-437.

LALLI, G., GSCHMEISSNER, S. & SCHIAVO, G. 2003b. Myosin Va and microtubule-based motors are required for fast axonal retrograde transport of tetanus toxin in motor neurons. *Journal of Cell Science,* 116**,** 4639-50.

LALLI, G. & SCHIAVO, G. 2002. Analysis of retrograde transport in motor neurons reveals common endocytic carriers for tetanus toxin and neurotrophin receptor p75NTR. *J Cell Biol,* 156**,** 233-9.

LENGLET, T., LACOMBLEZ, L., ABITBOL, J. L., LUDOLPH, A., MORA, J. S., ROBBERECHT, W., SHAW, P. J., PRUSS, R. M., CUVIER, V. & MEININGER, V. 2014. A phase II-III trial of olesoxime in subjects with amyotrophic lateral sclerosis. *Eur J Neurol,* 21**,** 529-36.

LEVINE, T. P., DANIELS, R. D., GATTA, A. T., WONG, L. H. & HAYES, M. J. 2013. The product of C9orf72, a gene strongly implicated in neurodegeneration, is structurally related to DENN Rab-GEFs. *Bioinformatics*.

LI, R., POURPAK, A. & MORRIS, S. W. 2009. Inhibition of the insulin-like growth factor-1 receptor (IGF1R) tyrosine kinase as a novel cancer therapy approach. *J Med Chem,* 52**,** 4981-5004.

LI, S. H., GUTEKUNST, C. A., HERSCH, S. M. & LI, X. J. 1998. Interaction of huntingtin-associated protein with dynactin P150Glued. *J Neurosci,* 18**,** 1261-9.

LIU, J. P., BAKER, J., PERKINS, A. S., ROBERTSON, E. J. & EFSTRATIADIS, A. 1993. Mice carrying null mutations of the genes encoding insulin-like growth factor I (Igf-1) and type 1 IGF receptor (Igf1r). *Cell,* 75**,** 59-72.

LIU, R., YANG, G., NONAKA, T., ARAI, T., JIA, W. & CYNADER, M. S. 2013. Reducing TDP-43 aggregation does not prevent its cytotoxicity. *Acta Neuropathol Commun,* 1**,** 49.

LOBSIGER, C. S., GARCIA, M. L., WARD, C. M. & CLEVELAND, D. W. 2005. Altered axonal architecture by removal of the heavily phosphorylated neurofilament tail domains strongly slows superoxide dismutase 1 mutant-mediated ALS. *Proc Natl Acad Sci U S A,* 102**,** 10351-6.

LUDWIG, T., MUNIER-LEHMANN, H., BAUER, U., HOLLINSHEAD, M., OVITT, C., LOBEL, P. & HOFLACK, B. 1994. Differential sorting of lysosomal enzymes in mannose 6-phosphate receptor-deficient fibroblasts. *Embo j,* 13**,** 3430-7.

MACE, G., MIACZYNSKA, M., ZERIAL, M. & NEBREDA, A. R. 2005. Phosphorylation of EEA1 by p38 MAP kinase regulates mu opioid receptor endocytosis. *Embo j,* 24**,** 3235-46.

MACKENZIE, I. R., BIGIO, E. H., INCE, P. G., GESER, F., NEUMANN, M., CAIRNS, N. J., KWONG, L. K., FORMAN, M. S., RAVITS, J., STEWART, H., EISEN, A., MCCLUSKY, L., KRETZSCHMAR, H. A., MONORANU, C. M., HIGHLEY, J. R., KIRBY, J., SIDDIQUE, T., SHAW, P. J., LEE, V. M. & TROJANOWSKI, J. Q. 2007. Pathological TDP-43 distinguishes sporadic amyotrophic lateral sclerosis from amyotrophic lateral sclerosis with SOD1 mutations. *Ann Neurol,* 61**,** 427-34.

MADAY, S., TWELVETREES, A. E., MOUGHAMIAN, A. J. & HOLZBAUR, E. L. 2014. Axonal transport: cargo-specific mechanisms of motility and regulation. *Neuron,* 84**,** 292-309.

MAJID, T., ALI, Y. O., VENKITARAMANI, D. V., JANG, M. K., LU, H. C. & PAUTLER, R. G. 2014. In vivo axonal transport deficits in a mouse model of fronto-temporal dementia. *Neuroimage Clin,* 4**,** 711-7.

MALIK, B., NIRMALANANTHAN, N., BILSLAND, L. G., LA SPADA, A. R., HANNA, M. G., SCHIAVO, G., GALLO, J.-M. & GREENSMITH, L. 2011. Absence of disturbed axonal transport in spinal and bulbar muscular atrophy. *Human Molecular Genetics,* 20**,** 1776-86.

MALIN, S. A., DAVIS, B. M. & MOLLIVER, D. C. 2007. Production of dissociated sensory neuron cultures and considerations for their use in studying neuronal function and plasticity. *Nat Protoc,* 2**,** 152-60.

MANCUSO, R., OLIVAN, S., MANCERA, P., PASTEN-ZAMORANO, A., MANZANO, R., CASAS, C., OSTA, R. & NAVARRO, X. 2012. Effect of genetic background on onset and disease progression in the SOD1-G93A model of amyotrophic lateral sclerosis. *Amyotroph Lateral Scler,* 13**,** 302-10.

MANN, M., ONG, S. E., GRONBORG, M., STEEN, H., JENSEN, O. N. & PANDEY, A. 2002. Analysis of protein phosphorylation using mass spectrometry: deciphering the phosphoproteome. *Trends Biotechnol,* 20**,** 261-8.

MARINKOVIC, P., REUTER, M. S., BRILL, M. S., GODINHO, L., KERSCHENSTEINER, M. & MISGELD, T. 2012. Axonal transport deficits and degeneration can evolve independently in mouse models of amyotrophic lateral sclerosis. *Proc Natl Acad Sci U S A,* 109**,** 4296-301.

MARUYAMA, H., MORINO, H., ITO, H., IZUMI, Y., KATO, H., WATANABE, Y., KINOSHITA, Y., KAMADA, M., NODERA, H., SUZUKI, H., KOMURE, O., MATSUURA, S., KOBATAKE, K., MORIMOTO, N., ABE, K., SUZUKI, N., AOKI, M., KAWATA, A., HIRAI, T., KATO, T., OGASAWARA, K., HIRANO, A., TAKUMI, T., KUSAKA, H., HAGIWARA, K., KAJI, R. & KAWAKAMI, H. 2010. Mutations of optineurin in amyotrophic lateral sclerosis. *Nature,* 465**,** 223-6.

MCGOLDRICK, P., JOYCE, P. I., FISHER, E. M. & GREENSMITH, L. 2013. Rodent models of amyotrophic lateral sclerosis. *Biochim Biophys Acta,* 1832**,** 1421-36.

MELKONIAN, K. A., MAIER, K. C., GODFREY, J. E., RODGERS, M. & SCHROER, T. A. 2007. Mechanism of dynamitin-mediated disruption of dynactin. *J Biol Chem,* 282**,** 19355-64.

MERY, P. F., PAVOINE, C., PECKER, F. & FISCHMEISTER, R. 1995. Erythro-9-(2-hydroxy-3-nonyl)adenine inhibits cyclic GMP-stimulated phosphodiesterase in isolated cardiac myocytes. *Mol Pharmacol,* 48**,** 121-30.

MEYER, K., FERRAIUOLO, L., MIRANDA, C. J., LIKHITE, S., MCELROY, S., RENUSCH, S., DITSWORTH, D., LAGIER-TOURENNE, C., SMITH, R. A., RAVITS, J., BURGHES, A. H., SHAW, P. J., CLEVELAND, D. W., KOLB, S. J. & KASPAR, B. K. 2014. Direct conversion of patient fibroblasts demonstrates non-cell autonomous toxicity of astrocytes to motor neurons in familial and sporadic ALS. *Proc Natl Acad Sci U S A,* 111**,** 829-32.

MILES, G. B., YOHN, D. C., WICHTERLE, H., JESSELL, T. M., RAFUSE, V. F. & BROWNSTONE, R. M. 2004. Functional properties of motoneurons derived from mouse embryonic stem cells. *J Neurosci,* 24**,** 7848-58.

MILLECAMPS, S. & JULIEN, J. P. 2013. Axonal transport deficits and neurodegenerative diseases. *Nat Rev Neurosci,* 14**,** 161-76.

MILLER, C. C., ACKERLEY, S., BROWNLEES, J., GRIERSON, A. J., JACOBSEN, N. J. & THORNHILL, P. 2002. Axonal transport of neurofilaments in normal and disease states. *Cell Mol Life Sci,* 59**,** 323-30.

MILLER, R. G., MITCHELL, J. D., LYON, M. & MOORE, D. H. 2003. Riluzole for amyotrophic lateral sclerosis (ALS)/motor neuron disease (MND). *Amyotroph Lateral Scler Other Motor Neuron Disord,* 4**,** 191-206.

MISGELD, T., KERSCHENSTEINER, M., BAREYRE, F. M., BURGESS, R. W. & LICHTMAN, J. W. 2007. Imaging axonal transport of mitochondria in vivo. *Nat Methods,* 4**,** 559-61.

MITCHELL, D. J., BLASIER, K. R., JEFFERY, E. D., ROSS, M. W., PULLIKUTH, A. K., SUO, D., PARK, J., SMILEY, W. R., LO, K. W., SHABANOWITZ, J., DEPPMANN, C. D., TRINIDAD, J. C., HUNT, D. F., CATLING, A. D. & PFISTER, K. K. 2012. Trk activation of the ERK1/2 kinase pathway stimulates intermediate chain phosphorylation and recruits cytoplasmic dynein to signaling endosomes for retrograde axonal transport. *J Neurosci,* 32**,** 15495-510.

MITSUMOTO, H., IKEDA, K., HOLMLUND, T., GREENE, T., CEDARBAUM, J. M., WONG, V. & LINDSAY, R. M. 1994. The effects of ciliary neurotrophic factor on motor dysfunction in wobbler mouse motor neuron disease. *Ann Neurol,* 36**,** 142-8.

MITSUMOTO, H., KURAHASHI, K., JACOB, J. M. & MCQUARRIE, I. G. 1993. Retardation of fast axonal transport in wobbler mice. *Muscle Nerve,* 16**,** 542-7.

MITSUMOTO, H., SANTELLA, R. M., LIU, X., BOGDANOV, M., ZIPPRICH, J., WU, H. C., MAHATA, J., KILTY, M., BEDNARZ, K., BELL, D., GORDON, P. H., HORNIG, M., MEHRAZIN, M., NAINI, A., FLINT BEAL, M. & FACTOR-LITVAK, P. 2008. Oxidative stress biomarkers in sporadic ALS. *Amyotroph Lateral Scler,* 9**,** 177-83.

MIZIELINSKA, S., GRONKE, S., NICCOLI, T., RIDLER, C. E., CLAYTON, E. L., DEVOY, A., MOENS, T., NORONA, F. E., WOOLLACOTT, I. O., PIETRZYK, J., CLEVERLEY, K., NICOLL, A. J., PICKERING-BROWN, S., DOLS, J., CABECINHA, M., HENDRICH, O., FRATTA, P., FISHER, E. M., PARTRIDGE, L. & ISAACS, A. M. 2014. C9orf72 repeat expansions cause neurodegeneration in Drosophila through arginine-rich proteins. *Science,* 345**,** 1192-4.

MOJSILOVIC-PETROVIC, J., NEDELSKY, N., BOCCITTO, M., MANO, I., GEORGIADES, S. N., ZHOU, W., LIU, Y., NEVE, R. L., TAYLOR, J. P., DRISCOLL, M., CLARDY, J., MERRY, D. & KALB, R. G. 2009. FOXO3a is broadly neuroprotective in vitro and in vivo against insults implicated in motor neuron diseases. *J Neurosci,* 29**,** 8236-47.

MORFINI, G., SZEBENYI, G., ELLURU, R., RATNER, N. & BRADY, S. T. 2002. Glycogen synthase kinase 3 phosphorylates kinesin light chains and negatively regulates kinesin-based motility. *Embo j,* 21**,** 281-93.

MORFINI, G. A., BOSCO, D. A., BROWN, H., GATTO, R., KAMINSKA, A., SONG, Y., MOLLA, L., BAKER, L., MARANGONI, M. N., BERTH, S., TAVASSOLI, E., BAGNATO, C., TIWARI, A., HAYWARD, L. J., PIGINO, G. F., WATTERSON, D. M., HUANG, C. F., BANKER, G., BROWN, R. H., JR. & BRADY, S. T. 2013. Inhibition of fast axonal transport by pathogenic SOD1 involves activation of p38 MAP kinase. *PLoS One,* 8**,** e65235.

MORFINI, G. A., YOU, Y.-M., POLLEMA, S. L., KAMINSKA, A., LIU, K., YOSHIOKA, K., BJ√∂RKBLOM, B., COFFEY, E. T., BAGNATO, C., HAN, D., HUANG, C.-F., BANKER, G., PIGINO, G. & BRADY, S. T. 2009. Pathogenic huntingtin inhibits fast axonal transport by activating JNK3 and phosphorylating kinesin. *Nature Neuroscience,* 12**,** 864-71.

MORRISON, B. M. & MORRISON, J. H. 1999. Amyotrophic lateral sclerosis associated with mutations in superoxide dismutase: a putative mechanism of degeneration. *Brain Res Brain Res Rev,* 29**,** 121-35.

MOSER, J. M., BIGINI, P. & SCHMITT-JOHN, T. 2013. The wobbler mouse, an ALS animal model. *Mol Genet Genomics,* 288**,** 207-29.

MOTYKA, B., KORBUTT, G., PINKOSKI, M. J., HEIBEIN, J. A., CAPUTO, A., HOBMAN, M., BARRY, M., SHOSTAK, I., SAWCHUK, T., HOLMES, C. F., GAULDIE, J. & BLEACKLEY, R. C. 2000. Mannose 6-phosphate/insulin-like growth factor II receptor is a death receptor for granzyme B during cytotoxic T cell-induced apoptosis. *Cell,* 103**,** 491-500.

MUDGETT, J. S., L. GUH-SIESEL, N.A. CHARTRAIN, L. YANG, AND M. SHEN. 1998. Targeted inactivation of the p38α gene results in midgestation embryonic lethality. *9th International Conference of the Inflammation Research Association.*

MULLIGAN, L. M. 2014. RET revisited: expanding the oncogenic portfolio. *Nat Rev Cancer,* 14**,** 173-86.

MUNCH, C., ROSENBOHM, A., SPERFELD, A. D., UTTNER, I., RESKE, S., KRAUSE, B. J., SEDLMEIER, R., MEYER, T., HANEMANN, C. O., STUMM, G. & LUDOLPH, A. C. 2005. Heterozygous R1101K mutation of the DCTN1 gene in a family with ALS and FTD. *Ann Neurol,* 58**,** 777-80.

MUNOZ, L., RALAY RANAIVO, H., ROY, S. M., HU, W., CRAFT, J. M., MCNAMARA, L. K., CHICO, L. W., VAN ELDIK, L. J. & WATTERSON, D. M. 2007. A novel p38 alpha MAPK inhibitor suppresses brain proinflammatory cytokine up-regulation and attenuates synaptic dysfunction and behavioral deficits in an Alzheimer's disease mouse model. *J Neuroinflammation,* 4**,** 21.

NEUMANN, M., SAMPATHU, D. M., KWONG, L. K., TRUAX, A. C., MICSENYI, M. C., CHOU, T. T., BRUCE, J., SCHUCK, T., GROSSMAN, M., CLARK, C. M., MCCLUSKEY, L. F., MILLER, B. L., MASLIAH, E., MACKENZIE, I. R., FELDMAN, H., FEIDEN, W., KRETZSCHMAR, H. A., TROJANOWSKI, J. Q. & LEE, V. M. 2006. Ubiquitinated TDP-43 in frontotemporal lobar degeneration and amyotrophic lateral sclerosis. *Science,* 314**,** 130-3.

NGUYEN, M. D., JULIEN, J. P. & RIVEST, S. 2001. Induction of proinflammatory molecules in mice with amyotrophic lateral sclerosis: no requirement for proapoptotic interleukin-1beta in neurodegeneration. *Ann Neurol,* 50**,** 630-9.

NISHIDA, K., YAMAGUCHI, O., HIROTANI, S., HIKOSO, S., HIGUCHI, Y., WATANABE, T., TAKEDA, T., OSUKA, S., MORITA, T., KONDOH, G., UNO, Y., KASHIWASE, K., TANIIKE, M., NAKAI, A., MATSUMURA, Y., MIYAZAKI, J., SUDO, T., HONGO, K., KUSAKARI, Y., KURIHARA, S., CHIEN, K. R., TAKEDA, J., HORI, M. & OTSU, K. 2004. p38alpha mitogen-activated protein kinase plays a critical role in cardiomyocyte survival but not in cardiac hypertrophic growth in response to pressure overload. *Mol Cell Biol,* 24**,** 10611-20.

NISHIMURA, A. L., MITNE-NETO, M., SILVA, H. C., RICHIERI-COSTA, A., MIDDLETON, S., CASCIO, D., KOK, F., OLIVEIRA, J. R., GILLINGWATER, T., WEBB, J., SKEHEL, P. & ZATZ, M. 2004. A mutation in the vesicle-trafficking protein VAPB causes late-onset spinal muscular atrophy and amyotrophic lateral sclerosis. *Am J Hum Genet,* 75**,** 822-31.

OKADA, Y., YAMAZAKI, H., SEKINE-AIZAWA, Y. & HIROKAWA, N. 1995. The neuron-specific kinesin superfamily protein KIF1A is a unique monomeric motor for anterograde axonal transport of synaptic vesicle precursors. *Cell,* 81**,** 769-80.

ORLACCHIO, A., BABALINI, C., BORRECA, A., PATRONO, C., MASSA, R., BASARAN, S., MUNHOZ, R. P., ROGAEVA, E. A., ST GEORGE-HYSLOP, P. H., BERNARDI, G. & KAWARAI, T. 2010. SPATACSIN mutations cause autosomal recessive juvenile amyotrophic lateral sclerosis. *Brain,* 133**,** 591-8.

OZSARAC, N., WEIBLE, M., 2ND, REYNOLDS, A. J. & HENDRY, I. A. 2003. Activation of protein kinase C inhibits retrograde transport of neurotrophins in mice. *J Neurosci Res,* 72**,** 203-10.

PAISAN-RUIZ, C., JAIN, S., EVANS, E. W., GILKS, W. P., SIMON, J., VAN DER BRUG, M., LOPEZ DE MUNAIN, A., APARICIO, S., GIL, A. M., KHAN, N., JOHNSON, J., MARTINEZ, J. R., NICHOLL, D., CARRERA, I. M., PENA, A. S., DE SILVA, R., LEES, A., MARTI-MASSO, J. F., PEREZ-TUR, J., WOOD, N. W. & SINGLETON, A. B. 2004. Cloning of the gene containing mutations that cause PARK8-linked Parkinson's disease. *Neuron,* 44**,** 595-600.

PANDEY, J. P. & SMITH, D. S. 2011. A Cdk5-dependent switch regulates Lis1/Ndel1/dynein-driven organelle transport in adult axons. *J Neurosci,* 31**,** 17207-19.

PARKINSON, N., INCE, P. G., SMITH, M. O., HIGHLEY, R., SKIBINSKI, G., ANDERSEN, P. M., MORRISON, K. E., PALL, H. S., HARDIMAN, O., COLLINGE, J., SHAW, P. J. & FISHER, E. M. 2006. ALS phenotypes with mutations in CHMP2B (charged multivesicular body protein 2B). *Neurology,* 67**,** 1074-7.

PATANI, R., LEWIS, P. A., TRABZUNI, D., PUDDIFOOT, C. A., WYLLIE, D. J., WALKER, R., SMITH, C., HARDINGHAM, G. E., WEALE, M., HARDY, J., CHANDRAN, S. & RYTEN, M. 2012. Investigating the utility of human embryonic stem cell-derived neurons to model ageing and neurodegenerative disease using whole-genome gene expression and splicing analysis. *J Neurochem,* 122**,** 738-51.

PENNINGROTH, S. M., CHEUNG, A., BOUCHARD, P., GAGNON, C. & BARDIN, C. W. 1982. Dynein ATPase is inhibited selectively in vitro by erythro-9-[3-2-(hydroxynonyl)]adenine. *Biochem Biophys Res Commun,* 104**,** 234-40.

PIERCE, K. L., PREMONT, R. T. & LEFKOWITZ, R. J. 2002. Seven-transmembrane receptors. *Nat Rev Mol Cell Biol,* 3**,** 639-50.

PIGINO, G., MORFINI, G., ATAGI, Y., DESHPANDE, A., YU, C., JUNGBAUER, L., LADU, M., BUSCIGLIO, J. & BRADY, S. 2009. Disruption of fast axonal transport is a pathogenic mechanism for intraneuronal amyloid beta. *Proc Natl Acad Sci U S A,* 106**,** 5907-12.

PIGINO, G., MORFINI, G., PELSMAN, A., MATTSON, M. P., BRADY, S. T. & BUSCIGLIO, J. 2003. Alzheimer's presenilin 1 mutations impair kinesin-based axonal transport. *J Neurosci,* 23**,** 4499-508.

POLLAK, M. 2008. Insulin and insulin-like growth factor signalling in neoplasia. *Nat Rev Cancer,* 8**,** 915-28.

POLLARI, E., GOLDSTEINS, G., BART, G., KOISTINAHO, J. & GINIATULLIN, R. 2014. The role of oxidative stress in degeneration of the neuromuscular junction in amyotrophic lateral sclerosis. *Front Cell Neurosci,* 8**,** 131.

POLONI, M., FACCHETTI, D., MAI, R., MICHELI, A., AGNOLETTI, L., FRANCOLINI, G., MORA, G., CAMANA, C., MAZZINI, L. & BACHETTI, T. 2000. Circulating levels of tumour necrosis factor-alpha and its soluble receptors are increased in the blood of patients with amyotrophic lateral sclerosis. *Neurosci Lett,* 287**,** 211-4.

PRATT, A. J., SHIN, D. S., MERZ, G. E., RAMBO, R. P., LANCASTER, W. A., DYER, K. N., BORBAT, P. P., POOLE, F. L., 2ND, ADAMS, M. W., FREED, J. H., CRANE, B. R., TAINER, J. A. & GETZOFF, E. D. 2014. Aggregation propensities of superoxide dismutase G93 hotspot mutants mirror ALS clinical phenotypes. *Proc Natl Acad Sci U S A,* 111**,** E4568-76.

PULS, I., JONNAKUTY, C., LAMONTE, B. H., HOLZBAUR, E. L., TOKITO, M., MANN, E., FLOETER, M. K., BIDUS, K., DRAYNA, D., OH, S. J., BROWN, R. H., JR., LUDLOW, C. L. & FISCHBECK, K. H. 2003. Mutant dynactin in motor neuron disease. *Nat Genet,* 33**,** 455-6.

QIU, H., LEE, S., SHANG, Y., WANG, W. Y., AU, K. F., KAMIYA, S., BARMADA, S. J., FINKBEINER, S., LUI, H., CARLTON, C. E., TANG, A. A., OLDHAM, M. C., WANG, H., SHORTER, J., FILIANO, A. J., ROBERSON, E. D., TOURTELLOTTE, W. G., CHEN, B., TSAI, L. H. & HUANG, E. J. 2014. ALS-associated mutation FUS-R521C causes DNA damage and RNA splicing defects. *J Clin Invest,* 124**,** 981-99.

RANGONE, H., POIZAT, G., TRONCOSO, J., ROSS, C. A., MACDONALD, M. E., SAUDOU, F. & HUMBERT, S. 2004. The serum- and glucocorticoid-induced kinase SGK inhibits mutant huntingtin-induced toxicity by phosphorylating serine 421 of huntingtin. *Eur J Neurosci,* 19**,** 273-9.

RATOVITSKI, T., CORSON, L. B., STRAIN, J., WONG, P., CLEVELAND, D. W., CULOTTA, V. C. & BORCHELT, D. R. 1999. Variation in the biochemical/biophysical properties of mutant superoxide dismutase 1 enzymes and the rate of disease progression in familial amyotrophic lateral sclerosis kindreds. *Hum Mol Genet,* 8**,** 1451-60.

REAUME, A. G., ELLIOTT, J. L., HOFFMAN, E. K., KOWALL, N. W., FERRANTE, R. J., SIWEK, D. R., WILCOX, H. M., FLOOD, D. G., BEAL, M. F., JR BROWN, R. H., SCOTT, R. W. & SNIDER, W. 1996. Motor neurons in Cu/Zn superoxide dismutase-deficient mice develop normally but exhibit enhanced cell death after axonal injury. *Nature Genetics,* 13**,** 43-47.

RENTON, A. E., CHIO, A. & TRAYNOR, B. J. 2014. State of play in amyotrophic lateral sclerosis genetics. *Nat Neurosci,* 17**,** 17-23.

RENTON, A. E., MAJOUNIE, E., WAITE, A., SIMON-SANCHEZ, J., ROLLINSON, S., GIBBS, J. R., SCHYMICK, J. C., LAAKSOVIRTA, H., VAN SWIETEN, J. C., MYLLYKANGAS, L., KALIMO, H., PAETAU, A., ABRAMZON, Y., REMES, A. M., KAGANOVICH, A., SCHOLZ, S. W., DUCKWORTH, J., DING, J., HARMER, D. W., HERNANDEZ, D. G.,

JOHNSON, J. O., MOK, K., RYTEN, M., TRABZUNI, D., GUERREIRO, R. J., ORRELL, R. W., NEAL, J., MURRAY, A., PEARSON, J., JANSEN, I. E., SONDERVAN, D., SEELAAR, H., BLAKE, D., YOUNG, K., HALLIWELL, N., CALLISTER, J. B., TOULSON, G., RICHARDSON, A., GERHARD, A., SNOWDEN, J., MANN, D., NEARY, D., NALLS, M. A., PEURALINNA, T., JANSSON, L., ISOVIITA, V. M., KAIVORINNE, A. L., HOLTTA-VUORI, M., IKONEN, E., SULKAVA, R., BENATAR, M., WUU, J., CHIO, A., RESTAGNO, G., BORGHERO, G., SABATELLI, M., HECKERMAN, D., ROGAEVA, E., ZINMAN, L., ROTHSTEIN, J. D., SENDTNER, M., DREPPER, C., EICHLER, E. E., ALKAN, C., ABDULLAEV, Z., PACK, S. D., DUTRA, A., PAK, E., HARDY, J., SINGLETON, A., WILLIAMS, N. M., HEUTINK, P., PICKERING-BROWN, S., MORRIS, H. R., TIENARI, P. J. & TRAYNOR, B. J. 2011. A hexanucleotide repeat expansion in C9ORF72 is the cause of chromosome 9p21-linked ALS-FTD. *Neuron,* 72**,** 257-68.

RESTANI, L., GIRIBALDI, F., MANICH, M., BERCSENYI, K., MENENDEZ, G., ROSSETTO, O., CALEO, M. & SCHIAVO, G. 2012. Botulinum neurotoxins A and E undergo retrograde axonal transport in primary motor neurons. *PLoS Pathog,* 8**,** e1003087.

REYNOLDS, C. H., BETTS, J. C., BLACKSTOCK, W. P., NEBREDA, A. R. & ANDERTON, B. H. 2000. Phosphorylation sites on tau identified by nanoelectrospray mass spectrometry: differences in vitro between the mitogen-activated protein kinases ERK2, c-Jun N-terminal kinase and P38, and glycogen synthase kinase-3beta. *J Neurochem,* 74**,** 1587-95.

RINGHOLZ, G. M., APPEL SH FAU - BRADSHAW, M., BRADSHAW M FAU - COOKE, N. A., COOKE NA FAU - MOSNIK, D. M., MOSNIK DM FAU - SCHULZ, P. E. & SCHULZ, P. E. 2005. Prevalence and patterns of cognitive impairment in sporadic ALS.

ROSEN, D. R., SIDDIQUE, T., PATTERSON, D., FIGLEWICZ, D. A., SAPP, P., HENTATI, A., DONALDSON, D., GOTO, J., O'REGAN, J. P., DENG, H. X. & ET AL. 1993. Mutations in Cu/Zn superoxide dismutase gene are associated with familial amyotrophic lateral sclerosis. *Nature,* 362**,** 59-62.

ROTHSTEIN, J. D., TSAI, G., KUNCL, R. W., CLAWSON, L., CORNBLATH, D. R., DRACHMAN, D. B., PESTRONK, A., STAUCH, B. L. & COYLE, J. T. 1990. Abnormal excitatory amino acid metabolism in amyotrophic lateral sclerosis. *Ann Neurol,* 28**,** 18-25.

ROTHSTEIN, J. D., VAN KAMMEN, M., LEVEY, A. I., MARTIN, L. J. & KUNCL, R. W. 1995. Selective loss of glial glutamate transporter GLT-1 in amyotrophic lateral sclerosis. *Ann Neurol,* 38**,** 73-84.

ROUX, S., SAINT CLOMENT, C., CURIE, T., GIRARD, E., MENA, F. J., BARBIER, J., OSTA, R., MOLGO, J. & BRULET, P. 2006. Brain-derived neurotrophic factor facilitates in vivo internalization of tetanus neurotoxin C-terminal fragment fusion proteins in mature mouse motor nerve terminals. *Eur J Neurosci,* 24**,** 1546-54.

ROY, S. M., GRUM-TOKARS, V. L., SCHAVOCKY, J. P., SAEED, F., STANISZEWSKI, A., TEICH, A. F., ARANCIO, O., BACHSTETTER, A. D., WEBSTER, S. J., VAN ELDIK, L. J., MINASOV, G., ANDERSON, W. F., PELLETIER, J. C. & WATTERSON, D. M. 2015. Targeting Human Central Nervous System Protein Kinases: An Isoform Selective p38alphaMAPK Inhibitor That Attenuates Disease Progression in Alzheimer's Disease Mouse Models. *ACS Chem Neurosci*.

RUMMEL, A., BADE, S., ALVES, J., BIGALKE, H. & BINZ, T. 2003. Two carbohydrate binding sites in the H(CC)-domain of tetanus neurotoxin are required for toxicity. *J Mol Biol,* 326**,** 835-47.

RUNNEGAR, M. T., WEI, X. & HAMM-ALVAREZ, S. F. 1999. Increased protein phosphorylation of cytoplasmic dynein results in impaired motor function. *Biochem J,* 342 (Pt 1)**,** 1-6.

SACCON, R. A., BUNTON-STASYSHYN, R. K., FISHER, E. M. & FRATTA, P. 2013. Is SOD1 loss of function involved in amyotrophic lateral sclerosis? *Brain,* 136**,** 2342-58.

SAREEN, D., O'ROURKE, J. G., MEERA, P., MUHAMMAD, A. K., GRANT, S., SIMPKINSON, M., BELL, S., CARMONA, S., ORNELAS, L., SAHABIAN, A., GENDRON, T., PETRUCELLI, L., BAUGHN, M., RAVITS, J., HARMS, M. B., RIGO, F., BENNETT, C. F., OTIS, T. S., SVENDSEN, C. N. & BALOH, R. H. 2013. Targeting RNA foci in iPSC-derived motor neurons from ALS patients with a C9ORF72 repeat expansion. *Sci Transl Med,* 5**,** 208ra149.

SCHEUNER, D., ECKMAN, C., JENSEN, M., SONG, X., CITRON, M., SUZUKI, N., BIRD, T. D., HARDY, J., HUTTON, M., KUKULL, W., LARSON, E., LEVY-LAHAD, E., VIITANEN, M., PESKIND, E., POORKAJ, P., SCHELLENBERG, G., TANZI, R., WASCO, W., LANNFELT, L., SELKOE, D. & YOUNKIN, S. 1996. Secreted amyloid beta-protein similar to that in the senile plaques of Alzheimer's disease is increased in vivo by the presenilin 1 and 2 and APP mutations linked to familial Alzheimer's disease. *Nat Med,* 2**,** 864-70.

SCHIAVO, G., BENFENATI, F., POULAIN, B., ROSSETTO, O., POLVERINO DE LAURETO, P., DASGUPTA, B. R. & MONTECUCCO, C. 1992a. Tetanus and botulinum-B neurotoxins block neurotransmitter release by proteolytic cleavage of synaptobrevin. *Nature,* 359**,** 832-5.

SCHIAVO, G., POULAIN, B., ROSSETTO, O., BENFENATI, F., TAUC, L. & MONTECUCCO, C. 1992b. Tetanus toxin is a zinc protein and its inhibition of neurotransmitter release and protease activity depend on zinc. *Embo j,* 11**,** 3577-83.

SCHLIWA, M., EZZELL, R. M. & EUTENEUER, U. 1984. erythro-9-[3-(2-Hydroxynonyl)]adenine is an effective inhibitor of cell motility and actin assembly. *Proc Natl Acad Sci U S A,* 81**,** 6044-8.

SCHLIWA, M. & WOEHLKE, G. 2003. Molecular motors. *Nature,* 422**,** 759-65.

SCHMIDT, H., GLEAVE, E. S. & CARTER, A. P. 2012. Insights into dynein motor domain function from a 3.3-A crystal structure. *Nat Struct Mol Biol,* 19**,** 492-7, s1.

SCHULTZ, G. S. & WYSOCKI, A. 2009. Interactions between extracellular matrix and growth factors in wound healing. *Wound Repair Regen,* 17**,** 153-62.

SENDTNER, M., SCHMALBRUCH, H., STOCKLI, K. A., CARROLL, P., KREUTZBERG, G. W. & THOENEN, H. 1992. Ciliary neurotrophic factor prevents degeneration of motor neurons in mouse mutant progressive motor neuronopathy. *Nature,* 358**,** 502-4.

SHARMA, R., BURAS, E., TERASHIMA, T., SERRANO, F., MASSAAD, C. A., HU, L., BITNER, B., INOUE, T., CHAN, L. & PAUTLER, R. G. 2010. Hyperglycemia induces oxidative stress and impairs axonal transport rates in mice. *PLoS One,* 5**,** e13463.

SHAW, J. L. & CHANG, K. T. 2013. Nebula/DSCR1 upregulation delays neurodegeneration and protects against APP-induced axonal transport defects by restoring calcineurin and GSK-3beta signaling. *PLoS Genet,* 9**,** e1003792.

SHAW, P. J., FORREST, V., INCE, P. G., RICHARDSON, J. P. & WASTELL, H. J. 1995a. CSF and plasma amino acid levels in motor neuron disease: elevation of CSF glutamate in a subset of patients. *Neurodegeneration,* 4**,** 209-16.

SHAW, P. J., INCE, P. G., FALKOUS, G. & MANTLE, D. 1995b. Oxidative damage to protein in sporadic motor neuron disease spinal cord. *Ann Neurol,* 38**,** 691-5.

SHIBATA, N., NAGAI, R., UCHIDA, K., HORIUCHI, S., YAMADA, S., HIRANO, A., KAWAGUCHI, M., YAMAMOTO, T., SASAKI, S. & KOBAYASHI, M. 2001. Morphological evidence for lipid peroxidation and protein glycoxidation in spinal cords from sporadic amyotrophic lateral sclerosis patients. *Brain Res,* 917**,** 97-104.

SIMOES-PIRES, C., ZWICK, V., NURISSO, A., SCHENKER, E., CARRUPT, P. A. & CUENDET, M. 2013. HDAC6 as a target for neurodegenerative diseases: what makes it different from the other HDACs? *Mol Neurodegener,* 8**,** 7.

SIMPSON, C. L. & AL-CHALABI, A. 2006. Amyotrophic lateral sclerosis as a complex genetic disease. *Biochim Biophys Acta,* 1762**,** 973-85.

SIMPSON, C. L., LEMMENS, R., MISKIEWICZ, K., BROOM, W. J., HANSEN, V. K., VAN VUGHT, P. W., LANDERS, J. E., SAPP, P., VAN DEN BOSCH, L., KNIGHT, J., NEALE, B. M., TURNER, M. R., VELDINK, J. H., OPHOFF, R. A., TRIPATHI, V. B., BELEZA, A., SHAH, M. N., PROITSI, P., VAN HOECKE, A., CARMELIET, P., HORVITZ, H. R., LEIGH, P. N., SHAW, C. E., VAN DEN BERG, L. H., SHAM, P. C., POWELL, J. F., VERSTREKEN, P., BROWN, R. H., JR., ROBBERECHT, W. & AL-CHALABI, A. 2009. Variants of the elongator protein 3 (ELP3) gene are associated with motor neuron degeneration. *Hum Mol Genet,* 18**,** 472-81.

SIMPSON, E. P., HENRY, Y. K., HENKEL, J. S., SMITH, R. G. & APPEL, S. H. 2004. Increased lipid peroxidation in sera of ALS patients: a potential biomarker of disease burden. *Neurology,* 62**,** 1758-65.

SINADINOS, C., BURBIDGE-KING, T., SOH, D., THOMPSON, L. M., MARSH, J. L., WYTTENBACH, A. & MUDHER, A. K. 2009. Live axonal transport disruption by mutant huntingtin fragments in Drosophila motor neuron axons. *Neurobiol Dis,* 34**,** 389-95.

SINGH, P., ALEX, J. M. & BAST, F. 2014. Insulin receptor (IR) and insulin-like growth factor receptor 1 (IGF-1R) signaling systems: novel treatment strategies for cancer. *Med Oncol,* 31**,** 805.

SMITH, B. N., TICOZZI, N., FALLINI, C., GKAZI, A. S., TOPP, S., KENNA, K. P., SCOTTER, E. L., KOST, J., KEAGLE, P., MILLER, J. W., CALINI, D., VANCE, C., DANIELSON, E. W., TROAKES, C., TILOCA, C., AL-SARRAJ, S., LEWIS, E. A., KING, A., COLOMBRITA, C., PENSATO, V., CASTELLOTTI, B., DE BELLEROCHE, J., BAAS, F., TEN ASBROEK, A. L., SAPP, P. C., MCKENNA-YASEK, D., MCLAUGHLIN, R. L., POLAK, M., ASRESS, S., ESTEBAN-PEREZ, J., MUNOZ-BLANCO, J. L., SIMPSON, M., VAN RHEENEN, W., DIEKSTRA, F. P., LAURIA, G., DUGA, S., CORTI, S., CEREDA, C., CORRADO, L., SORARU, G., MORRISON, K. E., WILLIAMS, K. L., NICHOLSON, G. A., BLAIR, I. P., DION, P. A., LEBLOND, C. S., ROULEAU, G. A., HARDIMAN, O., VELDINK, J. H., VAN DEN BERG, L. H., AL-CHALABI, A., PALL, H., SHAW, P. J., TURNER, M. R., TALBOT, K., TARONI, F., GARCIA-REDONDO, A., WU, Z., GLASS, J. D., GELLERA, C., RATTI, A., BROWN, R. H., JR., SILANI, V., SHAW, C. E. & LANDERS, J. E. 2014. Exome-wide rare variant analysis identifies TUBA4A mutations associated with familial ALS. *Neuron,* 84**,** 324-31.

SMITH, K. D., KALLHOFF, V., ZHENG, H. & PAUTLER, R. G. 2007. In vivo axonal transport rates decrease in a mouse model of Alzheimer's disease. *Neuroimage,* 35**,** 1401-8.

SMITH, R. G., HENRY, Y. K., MATTSON, M. P. & APPEL, S. H. 1998. Presence of 4-hydroxynonenal in cerebrospinal fluid of patients with sporadic amyotrophic lateral sclerosis. *Ann Neurol,* 44**,** 696-9.

SON, Y., CHEONG, Y. K., KIM, N. H., CHUNG, H. T., KANG, D. G. & PAE, H. O. 2011. Mitogen-Activated Protein Kinases and Reactive Oxygen Species: How Can ROS Activate MAPK Pathways? *J Signal Transduct,* 2011**,** 792639.

SONG, Y., NAGY, M., NI, W., TYAGI, N. K., FENTON, W. A., LOPEZ-GIRALDEZ, F., OVERTON, J. D., HORWICH, A. L. & BRADY, S. T. 2013. Molecular chaperone Hsp110 rescues a vesicle transport defect produced by an ALS-associated mutant SOD1 protein in squid axoplasm. *Proc Natl Acad Sci U S A,* 110**,** 5428-33.

SORENSON, E. J., WINDBANK, A. J., MANDREKAR, J. N., BAMLET, W. R., APPEL, S. H., ARMON, C., BARKHAUS, P. E., BOSCH, P., BOYLAN, K., DAVID, W. S., FELDMAN, E., GLASS, J., GUTMANN, L., KATZ, J., KING, W., LUCIANO, C. A., MCCLUSKEY, L. F., NASH, S., NEWMAN, D. S., PASCUZZI, R. M., PIORO, E., SAMS, L. J., SCELSA, S., SIMPSON, E. P., SUBRAMONY, S. H., TIRYAKI, E. & THORNTON, C. A. 2008. Subcutaneous IGF-1 is not beneficial in 2-year ALS trial. *Neurology,* 71**,** 1770-5.

SREEDHARAN, J., BLAIR, I. P., TRIPATHI, V. B., HU, X., VANCE, C., ROGELJ, B., ACKERLEY, S., DURNALL, J. C., WILLIAMS, K. L., BURATTI, E., BARALLE, F., DE BELLEROCHE, J., MITCHELL, J. D., LEIGH, P. N., AL-CHALABI, A., MILLER, C. C., NICHOLSON, G. & SHAW, C. E. 2008. TDP-43 mutations in familial and sporadic amyotrophic lateral sclerosis. *Science,* 319**,** 1668-72.

STAGI, M., GORLOVOY, P., LARIONOV, S., TAKAHASHI, K. & NEUMANN, H. 2006. Unloading kinesin transported cargoes from the tubulin track via the inflammatory c-Jun N-terminal kinase pathway. *Faseb j,* 20**,** 2573-5.

STEVENSON, A., YATES, D. M., MANSER, C., DE VOS, K. J., VAGNONI, A., LEIGH, P. N., MCLOUGHLIN, D. M. & MILLER, C. C. 2009. Riluzole protects against glutamate-induced slowing of neurofilament axonal transport. *Neurosci Lett,* 454**,** 161-4.

SUH, Y., ATZMON, G., CHO, M. O., HWANG, D., LIU, B., LEAHY, D. J., BARZILAI, N. & COHEN, P. 2008. Functionally significant insulin-like growth factor I receptor mutations in centenarians. *Proc Natl Acad Sci U S A,* 105**,** 3438-42.

SUNG, C. S., WEN, Z. H., CHANG, W. K., CHAN, K. H., HO, S. T., TSAI, S. K., CHANG, Y. C. & WONG, C. S. 2005. Inhibition of p38 mitogen-activated protein kinase attenuates interleukin-1beta-induced thermal hyperalgesia and inducible nitric oxide synthase expression in the spinal cord. *J Neurochem,* 94**,** 742-52.

SUNYACH, C., MICHAUD, M., ARNOUX, T., BERNARD-MARISSAL, N., AEBISCHER, J., LATYSZENOK, V., GOUARNE, C., RAOUL, C., PRUSS, R. M., BORDET, T. &

PETTMANN, B. 2012. Olesoxime delays muscle denervation, astrogliosis, microglial activation and motoneuron death in an ALS mouse model. *Neuropharmacology,* 62**,** 2346-52.

SWINNEN, B. & ROBBERECHT, W. 2014. The phenotypic variability of amyotrophic lateral sclerosis. *Nat Rev Neurol,* 10**,** 661-670.

TAES, I., GORIS, A., LEMMENS, R., VAN ES, M. A., VAN DEN BERG, L. H., CHIO, A., TRAYNOR, B. J., BIRVE, A., ANDERSEN, P., SLOWIK, A., TOMIK, B., BROWN, R. H., JR., SHAW, C. E., AL-CHALABI, A., BOONEN, S., VAN DEN BOSCH, L., DUBOIS, B., VAN DAMME, P. & ROBBERECHT, W. 2010. Tau levels do not influence human ALS or motor neuron degeneration in the SOD1G93A mouse. *Neurology,* 74**,** 1687-93.

TAES, I., TIMMERS, M., HERSMUS, N., BENTO-ABREU, A., VAN DEN BOSCH, L., VAN DAMME, P., AUWERX, J. & ROBBERECHT, W. 2013. Hdac6 deletion delays disease progression in the SOD1G93A mouse model of ALS. *Hum Mol Genet,* 22**,** 1783-90.

TAKACH, O., GILL, T. B. & SILVERMAN, M. A. 2015. Modulation of insulin signaling rescues BDNF transport defects independent of tau in amyloid-beta oligomer-treated hippocampal neurons. *Neurobiol Aging,* 36**,** 1378-82.

TERENZIO, M., GOLDING, M., RUSSELL, M. R., WICHER, K. B., ROSEWELL, I., SPENCER-DENE, B., ISH-HOROWICZ, D. & SCHIAVO, G. 2014a. Bicaudal-D1 regulates the intracellular sorting and signalling of neurotrophin receptors. *Embo j,* 33**,** 1582-98.

TERENZIO, M., GOLDING, M. & SCHIAVO, G. 2014b. siRNA screen of ES cell-derived motor neurons identifies novel regulators of tetanus toxin and neurotrophin receptor trafficking. *Front Cell Neurosci,* 8**,** 140.

TOGNON, C. E. & SORENSEN, P. H. 2012. Targeting the insulin-like growth factor 1 receptor (IGF1R) signaling pathway for cancer therapy. *Expert Opin Ther Targets,* 16**,** 33-48.

TONG, L., PAV, S., WHITE, D. M., ROGERS, S., CRANE, K. M., CYWIN, C. L., BROWN, M. L. & PARGELLIS, C. A. 1997. A highly specific inhibitor of human p38 MAP kinase binds in the ATP pocket. *Nat Struct Biol,* 4**,** 311-6.

TORTAROLO, M., VEGLIANESE, P., CALVARESI, N., BOTTURI, A., ROSSI, C., GIORGINI, A., MIGHELI, A. & BENDOTTI, C. 2003. Persistent activation of p38 mitogen-activated protein kinase in a mouse model of familial amyotrophic lateral sclerosis correlates with disease progression. *Mol Cell Neurosci,* 23**,** 180-92.

TOWNE, C., RAOUL, C., SCHNEIDER, B. L. & AEBISCHER, P. 2008. Systemic AAV6 delivery mediating RNA interference against SOD1: neuromuscular transduction does not alter disease progression in fALS mice. *Mol Ther,* 16**,** 1018-25.

TRUSHINA, E., DYER, R. B., BADGER, J. D., 2ND, URE, D., EIDE, L., TRAN, D. D., VRIEZE, B. T., LEGENDRE-GUILLEMIN, V., MCPHERSON, P. S., MANDAVILLI, B. S., VAN HOUTEN, B., ZEITLIN, S., MCNIVEN, M., AEBERSOLD, R., HAYDEN, M., PARISI, J. E., SEEBERG, E., DRAGATSIS, I., DOYLE, K., BENDER, A., CHACKO, C. & MCMURRAY, C. T. 2004. Mutant huntingtin impairs axonal trafficking in mammalian neurons in vivo and in vitro. *Mol Cell Biol,* 24**,** 8195-209.

TURNER, M. R., HARDIMAN, O., BENATAR, M., BROOKS, B. R., CHIO, A., DE CARVALHO, M., INCE, P. G., LIN, C., MILLER, R. G., MITSUMOTO, H., NICHOLSON, G., RAVITS, J., SHAW, P. J., SWASH, M., TALBOT, K., TRAYNOR, B. J., VAN DEN BERG, L. H., VELDINK, J. H., VUCIC, S. & KIERNAN, M. C. 2013. Controversies and priorities in amyotrophic lateral sclerosis. *Lancet Neurol,* 12**,** 310-22.

VALE, R. D. 2003. The molecular motor toolbox for intracellular transport. *Cell,* 112**,** 467-80.

VALE, R. D. & MILLIGAN, R. A. 2000. The way things move: looking under the hood of molecular motor proteins. *Science,* 288**,** 88-95.

VAN ES, M. A., VAN VUGHT, P. W., BLAUW, H. M., FRANKE, L., SARIS, C. G., ANDERSEN, P. M., VAN DEN BOSCH, L., DE JONG, S. W., VAN 'T SLOT, R., BIRVE, A., LEMMENS, R., DE JONG, V., BAAS, F., SCHELHAAS, H. J., SLEEGERS, K., VAN BROECKHOVEN, C., WOKKE, J. H., WIJMENGA, C., ROBBERECHT, W., VELDINK, J. H., OPHOFF, R. A. & VAN DEN BERG, L. H. 2007. ITPR2 as a susceptibility gene in sporadic amyotrophic lateral sclerosis: a genome-wide association study. *Lancet Neurol,* 6**,** 869-77.

VAN ES, M. A., VAN VUGHT, P. W., BLAUW, H. M., FRANKE, L., SARIS, C. G., VAN DEN BOSCH, L., DE JONG, S. W., DE JONG, V., BAAS, F., VAN'T SLOT, R., LEMMENS, R., SCHELHAAS, H. J., BIRVE, A., SLEEGERS, K., VAN BROECKHOVEN, C.,

SCHYMICK, J. C., TRAYNOR, B. J., WOKKE, J. H., WIJMENGA, C., ROBBERECHT, W., ANDERSEN, P. M., VELDINK, J. H., OPHOFF, R. A. & VAN DEN BERG, L. H. 2008. Genetic variation in DPP6 is associated with susceptibility to amyotrophic lateral sclerosis. *Nat Genet,* 40**,** 29-31.

VANCE, C., ROGELJ, B., HORTOBAGYI, T., DE VOS, K. J., NISHIMURA, A. L., SREEDHARAN, J., HU, X., SMITH, B., RUDDY, D., WRIGHT, P., GANESALINGAM, J., WILLIAMS, K. L., TRIPATHI, V., AL-SARAJ, S., AL-CHALABI, A., LEIGH, P. N., BLAIR, I. P., NICHOLSON, G., DE BELLEROCHE, J., GALLO, J. M., MILLER, C. C. & SHAW, C. E. 2009. Mutations in FUS, an RNA processing protein, cause familial amyotrophic lateral sclerosis type 6. *Science,* 323**,** 1208-11.

VEGLIANESE, P., LO COCO, D., BAO CUTRONA, M., MAGNONI, R., PENNACCHINI, D., POZZI, B., GOWING, G., JULIEN, J. P., TORTAROLO, M. & BENDOTTI, C. 2006. Activation of the p38MAPK cascade is associated with upregulation of TNF alpha receptors in the spinal motor neurons of mouse models of familial ALS. *Mol Cell Neurosci,* 31**,** 218-31.

VERHOEVEN, K., DE JONGHE, P., COEN, K., VERPOORTEN, N., AUER-GRUMBACH, M., KWON, J. M., FITZPATRICK, D., SCHMEDDING, E., DE VRIENDT, E., JACOBS, A., VAN GERWEN, V., WAGNER, K., HARTUNG, H. P. & TIMMERMAN, V. 2003. Mutations in the small GTP-ase late endosomal protein RAB7 cause Charcot-Marie-Tooth type 2B neuropathy. *Am J Hum Genet,* 72**,** 722-7.

VOSSEL, K. A., XU, J. C., FOMENKO, V., MIYAMOTO, T., SUBERBIELLE, E., KNOX, J. A., HO, K., KIM, D. H., YU, G. Q. & MUCKE, L. 2015. Tau reduction prevents Abeta-induced axonal transport deficits by blocking activation of GSK3beta. *J Cell Biol,* 209**,** 419-33.

VUCIC, S. & KIERNAN, M. C. 2006. Novel threshold tracking techniques suggest that cortical hyperexcitability is an early feature of motor neuron disease. *Brain,* 129**,** 2436-46.

WANG, J., XU, G. & BORCHELT, D. R. 2002. High molecular weight complexes of mutant superoxide dismutase 1: age-dependent and tissue-specific accumulation. *Neurobiol Dis,* 9**,** 139-48.

WANG, S. J., WANG, K. Y. & WANG, W. C. 2004. Mechanisms underlying the riluzole inhibition of glutamate release from rat cerebral cortex nerve terminals (synaptosomes). *Neuroscience,* 125**,** 191-201.

WEAVER, C., LEIDEL, C., SZPANKOWSKI, L., FARLEY, N. M., SHUBEITA, G. T. & GOLDSTEIN, L. S. 2013. Endogenous GSK-3/shaggy regulates bidirectional axonal transport of the amyloid precursor protein. *Traffic,* 14**,** 295-308.

WELTE, M. A. 2004. Bidirectional transport along microtubules. *Curr Biol,* 14**,** R525-37.

WICHTERLE, H., LIEBERAM, I., PORTER, J. A. & JESSELL, T. M. 2002. Directed differentiation of embryonic stem cells into motor neurons. *Cell,* 110**,** 385-97.

WILLIAMSON, T. L. & CLEVELAND, D. W. 1999. Slowing of axonal transport is a very early event in the toxicity of ALS-linked SOD1 mutants to motor neurons. *Nature Neuroscience,* 2**,** 50-6.

WONG, M. & MARTIN, L. J. 2010. Skeletal muscle-restricted expression of human SOD1 causes motor neuron degeneration in transgenic mice. *Hum Mol Genet,* 19**,** 2284-302.

WOODSON, J. C., MINOR, T. R. & JOB, R. F. 1998. Inhibition of adenosine deaminase by erythro-9-(2-hydroxy-3-nonyl)adenine (EHNA) mimics the effect of inescapable shock on escape learning in rats. *Behav Neurosci,* 112**,** 399-409.

WU, C. H., FALLINI, C., TICOZZI, N., KEAGLE, P. J., SAPP, P. C., PIOTROWSKA, K., LOWE, P., KOPPERS, M., MCKENNA-YASEK, D., BARON, D. M., KOST, J. E., GONZALEZ-PEREZ, P., FOX, A. D., ADAMS, J., TARONI, F., TILOCA, C., LECLERC, A. L., CHAFE, S. C., MANGROO, D., MOORE, M. J., ZITZEWITZ, J. A., XU, Z. S., VAN DEN BERG, L. H., GLASS, J. D., SICILIANO, G., CIRULLI, E. T., GOLDSTEIN, D. B., SALACHAS, F., MEININGER, V., ROSSOLL, W., RATTI, A., GELLERA, C., BOSCO, D. A., BASSELL, G. J., SILANI, V., DRORY, V. E., BROWN, R. H., JR. & LANDERS, J. E. 2012. Mutations in the profilin 1 gene cause familial amyotrophic lateral sclerosis. *Nature,* 488**,** 499-503.

XIE, W., ZHANG, K. & CUI, B. 2012. Functional characterization and axonal transport of quantum dot labeled BDNF. *Integr Biol (Camb),* 4**,** 953-60.

XU, Z. S. 2012. Does a loss of TDP-43 function cause neurodegeneration? *Mol Neurodegener,* 7**,** 27.

YAMANAKA, K., CHUN, S. J., BOILLEE, S., FUJIMORI-TONOU, N., YAMASHITA, H., GUTMANN, D. H., TAKAHASHI, R., MISAWA, H. & CLEVELAND, D. W. 2008. Astrocytes as determinants of disease progression in inherited amyotrophic lateral sclerosis. *Nat Neurosci,* 11**,** 251-3.

YANG, C., WANG, H., QIAO, T., YANG, B., ALIAGA, L., QIU, L., TAN, W., SALAMEH, J., MCKENNA-YASEK, D. M., SMITH, T., PENG, L., MOORE, M. J., BROWN, R. H., JR., CAI, H. & XU, Z. 2014. Partial loss of TDP-43 function causes phenotypes of amyotrophic lateral sclerosis. *Proc Natl Acad Sci U S A,* 111**,** E1121-9.

YANG, Y. M., GUPTA, S. K., KIM, K. J., POWERS, B. E., CERQUEIRA, A., WAINGER, B. J., NGO, H. D., ROSOWSKI, K. A., SCHEIN, P. A., ACKEIFI, C. A., ARVANITES, A. C., DAVIDOW, L. S., WOOLF, C. J. & RUBIN, L. L. 2013. A small molecule screen in stem-cell-derived motor neurons identifies a kinase inhibitor as a candidate therapeutic for ALS. *Cell Stem Cell,* 12**,** 713-26.

YIN, S., GIRNITA, A., STROMBERG, T., KHAN, Z., ANDERSSON, S., ZHENG, H., ERICSSON, C., AXELSON, M., NISTER, M., LARSSON, O., EKSTROM, T. J. & GIRNITA, L. 2010. Targeting the insulin-like growth factor-1 receptor by picropodophyllin as a treatment option for glioblastoma. *Neuro Oncol,* 12**,** 19-27.

YONG, H. Y., KOH, M. S. & MOON, A. 2009. The p38 MAPK inhibitors for the treatment of inflammatory diseases and cancer. *Expert Opin Investig Drugs,* 18**,** 1893-905.

YOSHIHARA, T., ISHIGAKI, S., YAMAMOTO, M., LIANG, Y., NIWA, J., TAKEUCHI, H., DOYU, M. & SOBUE, G. 2002. Differential expression of inflammation- and apoptosis-related genes in spinal cords of a mutant SOD1 transgenic mouse model of familial amyotrophic lateral sclerosis. *J Neurochem,* 80**,** 158-67.

YUAN, A., RAO, M. V., VEERANNA & NIXON, R. A. 2012. Neurofilaments at a glance. *J Cell Sci,* 125**,** 3257-63.

ZALA, D., COLIN, E., RANGONE, H., LIOT, G., HUMBERT, S. & SAUDOU, F. 2008. Phosphorylation of mutant huntingtin at S421 restores anterograde and retrograde transport in neurons. *Hum Mol Genet,* 17**,** 3837-46.

ZALA, D., HINCKELMANN, M. V., YU, H., LYRA DA CUNHA, M. M., LIOT, G., CORDELIERES, F. P., MARCO, S. & SAUDOU, F. 2013. Vesicular glycolysis provides on-board energy for fast axonal transport. *Cell,* 152**,** 479-91.

ZHANG, B., TU, P., ABTAHIAN, F., TROJANOWSKI, J. Q. & LEE, V. M. 1997. Neurofilaments and orthograde transport are reduced in ventral root axons of transgenic mice that express human SOD1 with a G93A mutation. *The Journal of Cell Biology,* 139**,** 1307-15.

ZHANG, F., STROM, A. L., FUKADA, K., LEE, S., HAYWARD, L. J. & ZHU, H. 2007. Interaction between familial amyotrophic lateral sclerosis (ALS)-linked SOD1 mutants and the dynein complex. *J Biol Chem,* 282**,** 16691-9.

ZHANG, K., OSAKADA, Y., VRLJIC, M., CHEN, L., MUDRAKOLA, H. V. & CUI, B. 2010. Single-molecule imaging of NGF axonal transport in microfluidic devices. *Lab Chip,* 10**,** 2566-73.

ZHU, Y.-B. & SHENG, Z.-H. 2011. Increased Axonal Mitochondrial Mobility Does Not Slow Amyotrophic Lateral Sclerosis (ALS)-like Disease in Mutant SOD1 Mice. *J Biol Chem,* 286**,** 23432-40.

ZIMPRICH, A., BISKUP, S., LEITNER, P., LICHTNER, P., FARRER, M., LINCOLN, S., KACHERGUS, J., HULIHAN, M., UITTI, R. J., CALNE, D. B., STOESSL, A. J., PFEIFFER, R. F., PATENGE, N., CARBAJAL, I. C., VIEREGGE, P., ASMUS, F., MULLER-MYHSOK, B., DICKSON, D. W., MEITINGER, T., STROM, T. M., WSZOLEK, Z. K. & GASSER, T. 2004. Mutations in LRRK2 cause autosomal-dominant parkinsonism with pleomorphic pathology. *Neuron,* 44**,** 601-7.

ZWANG, Y. & YARDEN, Y. 2006. p38 MAP kinase mediates stress-induced internalization of EGFR: implications for cancer chemotherapy. *Embo j,* 25**,** 4195-206.